Modification to the immunodominant loop of hepatitis B virus core protein to enhance vector properties of virus-like particles

Justin Hean

A thesis submitted to the Faculty of Health Sciences, University of the Witwatersrand, in fulfilment of the requirements for the degree

of

Doctor of Philosophy

Johannesburg, 2013

Declaration

I, Justin Hean declare that this thesis is my own work. It is being submitted for the degree of Doctor of Philosophy in the University of the Witwatersrand, Johannesburg. It has not been submitted before for any degree or examination at this or any other University.

…….

6th day of January, 2014

Dedication

To my grandparents, parents, brother, sisters, friends and Guru. Thank you for the support throughout the process of this PhD and life!

ॐ भूर् भुवः सुवहः ।
तत्सवितुर्वरेण्यं भर्गो देवस्य धीमहि ।
धियो यो नः प्रचोदयात् ॥
ॐ शान्तिः शान्तिः शान्तिः ॥

Body of all. Mind of all. Spirit of all.

May we meditate on the radiance of the inner light.

May that Self illumine our thoughts.

Let there be peace.

Publications related to thesis

1) Marimani M, Hean J, Bloom K, Ely A and Arbuthnot P. (2013) Recent advances in developing nucleic acid based hepatitis b virus therapy. Future Microbiology. In press

2) Stalder L, Heusermann W, Sokol L, Trojer D, Wirz J, Hean J, Fritzsche A, Aeschimann F, Pfanzagl V, Basselet P, Weiler J, Hintersteiner M, Morrissey DV, Meisner-Kober NC. (2013) The rough endoplasmatic reticulum is a central nucleation site of siRNA-mediated RNA silencing. EMBO J 32(8): 1115-1127.

3) Brzezinska J, D'Onofrio J, Buff MC, Hean J, Ely A, Marimani M, Arbuthnot P, Engels JW. (2012) Synthesis of 2'-O-guanidinopropyl-modified nucleoside phosphoramidites and their incorporation into siRNAs targeting hepatitis B virus. Bioorg Med Chem. 20(4): 1594-606.

4) Hean J, Crowther C, Ely A, Islam RU, Barichievy S, Bloom K, Weinberg MS, van Otterlo WAL, B. de Koning CB, Salazar F, Marion P, Roesch EB, LeMaitre M, Herdewijn P and Arbuthnot P. (2010) Inhibition of hepatitis B virus replication in vivo using lipoplexes containing altritol-modified antiviral siRNAs. Artificial DNA PNA & XNA. 1(1): 17-26.

5) Islam RU, Hean J, van Otterlo WA, de Koning CB, Arbuthnot P. (2009) Efficient nucleic acid transduction with lipoplexes containing novel piperazine- and polyamine-conjugated cholesterol derivatives. Bioorg Med Chem Lett. 19(1): 100-3

Abstract

Gene therapy has shown potential in alleviating a wide range of diseases, ranging from viral infections to autosomal diseases. One of the obstacles to gene therapy reaching its full potential is the inadequacy of methods to deliver therapeutic nucleic sequences. Current delivery of gene therapy entails use of viral and non-viral vectors. Viral vectors are however associated with drawbacks such as potential toxicity, high cost and labour-intensive production. Thus non-viral delivery alternatives are being developed in an attempt to overcome difficulties associated with nucleic acid delivery for gene therapy. Virus-like particles are potentially very useful delivery vehicles as their production is simple and cost effective, the particle surface is amenable to modification and the capsid interior can be altered to accommodate a variety of cargoes. One such particle is the recombinant HBV capsid, which comprises a single species of protein and is tolerant of amino acid substitutions on the surface exposed immunodominant loops. This study aimed to enhance the vector-like properties of the HBV virus-like particle by including amino acid substitutions on the particle surface. These substituted residues in turn provided a conjugation site for tropic and immuno evasive moieties. It was found that lysine substitutions resulted in poor conjugation to the capsid surface, whereas substituted cysteine residues resulted in almost all protein-moiety conjugates forming. In order to introduce lysine and cysteine substitutions, a novel method of cloning into the HBV was generated. In doing so, complicated procedures associated with cloning into the immunodominant loop of the HBV capsid have been alleviated. Ligands containing galactose were utilised on the surface of both the HBV capsid and liposomes to confer hepatotropism. The presence of the galactose moieties on the surface of the HBV capsid prevented indiscriminate cellular uptake in cultured cells, however did not improve hepatotropism. Galactose ligands on the surface of liposomes did improve transfection efficiency, however they required a short linker distance between liposome surface and galactose group. The inclusion of galactose in liposome formulations also provided a means to deliver siRNA to the liver of transgenic HBV mice. It is believed that with alterations to the ligand structure, it is possible to provide HBV capsids with hepatotropism in future experimentation. This study demonstrated that the exposed external surface of the HBV capsid is amenable to convenient conjugation, which potentially facilitates immune evasion and conferring of defined tropism.

Acknowledgements

1) I would like to extend my heart-felt gratitude to my supervisor, Patrick Arbuthnot, who has played a significant part in sculpting the researcher who I am today
2) Thanks go to my colleagues of AGTRU for the help and support during the course of the degree. A special thanks to Tristan Scott and Liam Thompson for providing the thought provoking conversations.
3) I would like to thank Abdullah Ely, Carol Crowther and Gladys Gagliardi for assisting with *in vivo* experimentation.
4) I would like to thank the members of the Wits Chemistry department, Charles de Koning, Willem van Otterlo, Rafique Islam and Santanu Chakraborty for the synthesis of the lipid-based compounds used in this study. I would also like to thank Prof. Injae Shin and colleagues (National Creative Research Initiative Center for Biofunctional Molecules, Department of Chemistry, Yonsei University, Korea) for the synthesis of maleimide-based carbohydrate compounds.
5) I would like to acknowledge Dr. Michael Nassal for the plasmid pCH-9/3091.
6) I would sincerely like to thank the funding bodies for support during the course of this work. The Postgraduate Merit Award, the Paul and Stella Loewenstein Charitable and Educational Trust, the Poliomyelitis Research Foundation, the National Research Foundation (Nanotechnology Flagship Program and Scarce Skills), Faculty Research Committee grant, the Sixth Research Framework Programme of the European Union, Project RIGHT (LSHB- CT-2004-005276)
7) To Goonaseelan Pillai and Nicole Meisner for organising and hosting me during an internship based within Novartis, Basel.

Table of Contents

List of Figures

List of Tables

List of Abbreviations

3D – Three dimensional

aa – Amino acid

AAV – Adeno-associated virus

Ac – Acetyl group

Ad – Adenovirus

ADA-SCID – adenosine deaminase severe combined immuno-deficiency

ALT – Alanine aminotransferase

ANA – Altritol nucleic acids

ASGPr – Asialoglycoprotein receptor

AST – Aspartate transaminase

bp – Base pair

BSA – Bovine serum albumin

c(140, 149, 160, 170, 183) – core protein variant

CK – Creatine phosphokinase

CL19 – Cationic lipid 19

cp – core protein

DC Chol - 3β-[N-(Dimethylaminoethane)carbamoyl]cholesterol

DMEM - Dulbecco's Modified Eagle's Medium

DNA – deoxyribonucleic acid

DOPE – 1,2-dioleyl-*sn*-glycero-3-phosphoethanolamine

ds – Double stranded

DTT – Dithiothreitol

e1 – epitope 1

e2 – epitope 2

eGFP – Enhanced green fluorescent protein

ELISA – Enzyme-linked immunosorbent assay

F5M – Fluorescein-5-maleimide

FCS – Foetal calf serum

FITC – Fluorescein isothiocyanate

Gal – Galactose

GalNAc – *N*-acetylgalactosamine

glu – Glucose

HBcAg – Hepatitis B core antigen

HBsAg – Hepatitis B surface antigen

HBV – Hepatitis B virus

HEK293 – Human embryonic kidney 293

HeLa – Henrietta Lacks

HIV – Human immunodeficiency virus

Huh7 – Human hepatocellular carcinoma 7

IL – Immunodominant loop

IPTG – Isopropyl β-D-1-thiogalactopyranoside

kb – kilobase

LacZ – β-galactosidase

LB – Lysogeny broth

LDH – Lactate dehydrogenase

LLC – Long linker chain

LNA – Locked nucleic acid

mal – Maleimide

MCC – Monosaccharide-cholesterol conjugates

-mer – Oligomer

min - Minute

miRNA – MicroRNA

MLC – Medium linker chain

MOI – Multiplicity of infection

NHS – N-hydroxysuccinimidyl

ORF – Open reading frame

OspA – Outer surface lipoprotein A

P-Gal – Protected galactose

PCR – Polymerase chain reaction

pDNA – Plasmid DNA

PEG – polyethylene glycol

pH – Power of hydrogen

Pol – RNA polymerase

PS – Phosphatidyl serine

pgRNA – Pregenomic RNA

RISC – RNA induced silencing complex

RNA – Ribonucleic acid

RNAi – RNA interference

sc – Succinimidyl carbonate

SEC – Size exclusion-based chromatography

SEM – standard error of the mean

SDS-PAGE – Sodium dodecyl sulphate polyacrylamide gel electrophoresis

SFDA – China's State Food and Drug Administration

siRNA – short interfering RNA

SLC – Short linker chain

TALEN – Transcription activator-like effector nucleases

TCEP – Tris(2-carboxyethyl)phosphine

UnP-Gal – Unprotected galactose

UV – Ultra violet

VLP – Virus-like particle

wt – Wild type

X-gal – 5-bromo-4-chloro-indolyl-galactopyranoside

X-SCID – X-linked severe combined immunodeficiency

List of Symbols

Å – Angstrom

α – alpha

β - beta

^{o}C – centigrade

Ci - Curie

Da – Dalton

g – local gravitational field

g – gram

H_{II} – Inverted hexagonal phase

IU – International units

L(l) – litre

μ- - micro-

k- - kilo-

m- - milli-

M- - Mega

m – meter

M – molar

mol – mole

n- – nano-

n – experimental number

p- – pico-

P – Packing parameter

T – triangulation number

w – weight

Chapter 1: Introduction

Brief overview of gene therapy

The twenty first century is an exciting age in which medicine will see the full realisation of gene therapy. Since its initial conception in the mid twentieth century the field of gene therapy has flourished into a multitude of applications. Typically gene therapy involves the introduction of exogenous nucleic acids to a cell to correct a diseased state of the host. In doing so, diseases including cancer, autosomal and viral in origin have the potential to be treated. A popular means to introduce exogenous DNA *in vivo* is through the use of recombinant viral vectors. The concept of gene transfer using viruses initiated with humble beginnings, without therapeutic objectives in mind. Viral gene transfer was first observed to occur from bacteriophages to host bacteria [1]. Although bacteriophage to bacteria gene transfer does not constitute gene therapy, it did suggest that gene transfer from one organism to another was possible. In a related experiment, gene transfer was identified to occur between Rous sarcoma virus and cultured chicken cells [2]. This observation further supported the idea that viruses could be utilised as vehicles to transfer genetic material, however the molecular biology tools required to implement gene transfer were undeveloped. The first human gene therapy experiment was performed in the 1970s using wild-type Shope papilloma virus on two individuals suffering from a urea cycle disorder [3, 4]. It was shown that the Shope papilloma virus induced arginase production in virus-induced papillomas on the skin of rabbits. It was known that the Shope papilloma virus was also capable of infecting human cells, and initial *in vitro* experiments suggested that infected cultured skin fibroblasts produced virally induced arginase. The escalated human trial was unsuccessful; the authors suggest this resulted from immune clearance of the virus or poor quality of virus administered.

It was only in the 1990s that gene therapy gained momentum, targeting a variety of diseases [5-8]. It was also required to develop vehicles/vectors for delivery of therapeutic sequences *in vivo*. Ideally the viral vectors would be non-replicative recombinant viruses with the capability to deliver therapeutic cargo to specific cell types without stimulating a significant immune response. During the 1990s it was unfortunate that one individual died of a severe immune response to the administered viral vector, and three children from leukaemia-related malignancies caused by random integration of the recombinant virus.

However this significantly contributed to the development and understanding of viral vectors for gene therapy [9]. Alternative means for delivery were also sought, employing the use of synthetic compounds and structures to deliver remedial nucleic acids. Ideally the synthetic vectors would overcome the toxicity associated with viral vectors, as well as significantly decrease the cost of vector production. Synthetic delivery systems may consist of lipids and liposomes, polymers, modified nucleic acids or virus-like particles (VLPs). For the purposes of this work a distinction between viral vectors and VLPs is required. Viral vectors are defined as bearing a large degree in similarity to their wild type counterparts. Often structure, genome size and mode of infectivity remain the same. VLPs may resemble viral structures, may not contain viral-related nucleic acids, generally are non-infectious and are often recombinantly expressed and produced.

Popular forms of gene therapy

Various forms of gene therapy have been developed, each remediating disease at the DNA, RNA or protein level. Typically the introduction of a gene cassette to a host cell is responsible for expression of the therapeutic product. Integration of the cassette into host chromosomal material may result in stable expression of the transgene; whereas episomal constructs tend toward transient expression. For the purposes of brevity, four forms of gene therapy are highlighted.

Introduction of a corrective gene to replace the effects of a dysfunctional gene

This means of correction has been used to treat several autosomal diseases such as adenosine deaminase severe combined immuno-deficiency (ADA-SCID) [10], Duchenne muscular dystrophy [11] and lysosomal storage disease [12, 13]. In each of the aforementioned states, the disease was alleviated by the introduction of a functional gene, typically delivered by a recombinant virus (Figure 1.1A). Presence of the gene could be transient or permanent, both associated with benefits and shortfalls. Transient gene expression has been demonstrated to be stable for up to two years in mice and seven years in dogs and rhesus monkeys [14-16]. Unfortunately, if the autosomal condition is not permanently corrected, multiple instances of vector re-administration will be required, which may lead to immuno-stimulatory complications. Permanent inclusion of the therapeutic sequence requires insertion into the host genetic material, which may lead to undesired mutagenesis [17].

Introduction of a gene to induce toxicity within diseased cells

Certain therapeutic approaches may introduce a gene product that induces a toxic state within targeted cells (Figure 1.1A). In doing so it is possible to destroy a particular population of cells, for example cancerous cells. Cellular death can be brought about by the conversion of a prodrug to a toxic product by the expressed therapeutic enzyme. There are several varieties of enzymes that have been assessed to induce cellular toxicity, including thymidine kinase [18-20], cytosine deaminase [21, 22] and nitroreductase [23, 24]. This form of therapy has seen successful clinical trial outcomes, and is described later in this chapter.

Introduction of a gene to down-regulate the expression of a disease causing gene

The advent of RNA interference (RNAi) has allowed for the extensive research into gene regulation, spanning from viral to host regulatory genes [25]. RNAi is a natural post-transcriptionally based regulatory system that utilises short (21-23 nucleotide) RNA sequences to target and degrade or sequester complementary RNA. This regulatory pathway can be manipulated to target specific RNA sequences at various entry points, by the introduction of therapeutic primary microRNAs, short hairpin RNAs or short interfering RNAs (Figure 1.1B). The field of RNAi contains numerous reviews, and has been thoroughly described elsewhere [26, 27].

Introduction of a corrective gene to disrupt genes causing a diseased state

Typically this form of therapy involves the introduction of a site-directed nuclease to create double stranded DNA breaks. Initially accomplished by using zinc finger nucleases [28] and meganucleases [29], recent discovery has led to the further development of designer nucleases known as transcription activator-like effector nucleases (TALENs) [30-32] and clustered regularly interspaced short palindromic repeats (CRISPR)/Cas (CRISPR associated proteins) [33-35]. Disruption of target sequences is a powerful technology, as it allows for the treatment of chronic infections caused by viruses such as hepatitis B virus, by targeting the episomal viral covalently closed circular DNA [36]. In addition, homology directed repair of the cell can be utilised to repair double stranded breaks to remediate single nucleotide polymorphisms and short regions of mutations (Figure 1.1C).

Introduction of a gene to induce a immuno-stimulatory response

Vaccinology by gene therapy requires the introduction and expression of immunogenic proteins to induce an immune response against disease causing agents (Figure 1.1A). Recently, this form of treatment made an impact within the field of HIV vaccinology [37]. Hansen and colleagues described a gene therapy vaccine capable of generating an immune

response against SIV in macaque monkeys over several months. Ideally this method of vaccinating against HIV will translate with equivalent efficacy in humans. These vaccines are not limited to viral infections but can also be applied to cancer. There are several reports indicating the potential to introduce a foreign protein to cancerous cells, causing their recognition and destruction by the immune system [38-40].

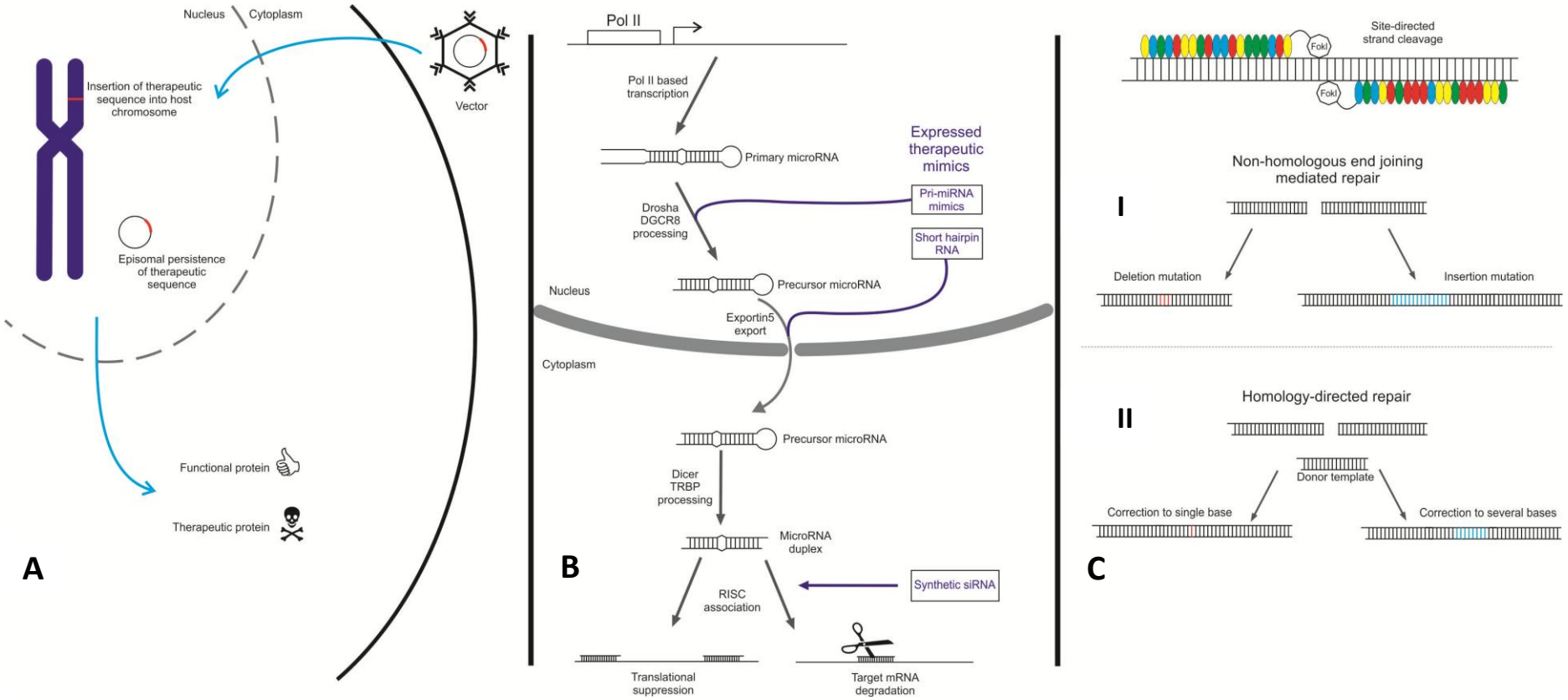

Figure 1.1: A diagrammatic comparison of gene therapy methodologies currently researched to treat various diseases. (**A**) Introduction of exogenous genes may result in dysfunctional gene correction or cellular toxicity. Typically corrective sequences are introduced by viral vectors, which deliver their cargo to the nucleus. Transient corrections are introduced by the presence of episomal structures. Stable transformations occur as a result of insertion of therapeutic sequence into host chromosome. (**B**) The natural RNA interference pathway, with entry points of potentially therapeutic mimics indicated. Mimics are introduced using viral transduction, lipid-based transfection or as naked, chemically modified siRNA structures. (**C**) TALEN mediated disruption of target sequence. After the selective binding to a target site, endonuclease *FokI*, causes a single stranded nick in the sequence. Strand breakage is caused by the binding and cleavage of dimer TALENs. I) Non-homologous end joining may result in the insertion or deletion of nucleotides at the cleaved site. II) Including a donor sequence allows for the correction of SNPs and nucleotides by homology-direct repair.

Prominent viral vectors in gene therapy

Currently there are three viral families which make up the majority of viral vectors for gene therapy: adenoviruses (Ads), adeno-associated viruses (AAVs) and retroviruses (which encompass lentiviruses). Each provides a variety of unique advantages and drawbacks. Ads were one of the few viruses to show clinical success in the early 1990s, and subsequently have been included in a large number of viral vector-based clinical trials (over 430 trials, constituting 23% of viral vector trials) [41]. These vectors have the ability to deliver transgene sizes of up to 32 kb into both dividing and non-dividing cell lines. Furthermore Ads display a large variety of serotype dependent tissue tropism, rarely integrate into host chromosomes and can be produced at high titres [42-44]. Unfortunately Ads are associated with innate and pre-existing adaptive immunity, which is especially common amongst populations of developing countries. The immune response may significantly reduce the delivery efficacy of the vector and in severe cases result in toxicity or even death. Strategies to avoid immunostimulation have been employed, such as the conjugation of polymers (e.g. PEG) to the Ad surface [45]. Treatment with recombinant Ads has resulted in variable efficacy, attributed to both virus-host interaction and therapeutic cassette expression [44, 46]. Nonetheless, successful treatment with recombinant Ads does result in prolonged therapeutic effect [47-49]. In particular, the use of third generation/gutless Ads has shown continued transgene expression of two and up to seven years (and ongoing) in primates [50]. Therapeutic Ads face certain hurdles that have to be overcome prior to their successful use as prominent gene therapy vectors. Other than the previously described immunologic hurdles, recombinant Ads are also costly and labour intensive to produce. Implementation of therapeutic Ads in developing countries may not be immediately feasible, and thus requires the development of alternative vector strategies.

Adeno-associated viruses contain a 4.7 kb single stranded DNA genome, a considerable contrast to the larger genome of Ads [51]. Despite their small genome size, recombinant AAVs (rAAVs) can be used effectively to express RNAi effector molecules, including polycistronic sequences and poly-cassette constructs [52]. Furthermore rAAVs display broad tissue tropism with low immunogenicity, episomal persistence after infecting both dividing and non-diving cells and the episomal genome/transgene construct has a low chance of integrating into the host genome [53-56]. rAAVs are also capable of combining with other

serotypes to generate chimaeras with enhanced/altered tissue tropism and immuno-evasive properties. Chen and colleagues were able to generate a pseudotyped rAAV2/8 which effectively delivered therapeutic cargo to the murine liver [57]. Pseudotyping a second variety of rAAV, AAV2/9 was able to evade to immune response generated against AAV8 and again deliver the therapeutic cargo to diseased murine hepatocytes [58]. rAAVs have several desirable properties of a gene therapy vector, however they exhibit similar difficulties to Ads in their implementation in developing countries. Production cost, scalability and labour intensity of producing rAAVs are all factors which encourage the further development of alternative delivery vectors such as non-viral vectors.

Retroviral vectors were the first described vector to be used in clinical trials [59]. Retroviral vectors have shown promise over the past two decades in the reversal of inherited diseases such as severe combined immuno-deficiency (SCID) [60], ADA-SCID [10] and X-linked chronic granulomatous disease (X-CGD) [61]. Treatments were accomplished by the stable integration of the transgene into host chromosomes which allows for the sustained expression of the therapeutic transgene. Unfortunately difficulties have been encountered in which transgene insertion may result in harmful mutagenesis, or transgene expression becomes variegated. Attempts to improve transgene expression have incorporated the use of lentiviruses, which display the capacity to transduce dividing and non-dividing cell types and readily insert into the host chromosome to provide long term transgene expression [62, 63]. Gene therapy with lentiviruses has also found application in *ex vivo* transduction, as therapeutic cells are generated *in vitro* and re-introduced to *in vivo* systems [63-65]. Retro- and lentiviruses encounter similar production difficulties as Ads and AAVs. Currently there are no clinically approved lentiviral therapeutics available, consequently implementation of these products in developing countries such as Africa does not appear to be feasible. Considering the difficulties encountered by all three viral vectors, it is imperative that attention is also given to the non-viral delivery systems.

Viral vectors are used in ±69% of the 1800 active clinical trials that use gene therapy to combat disease [41]. Approximately 60% of these trials are directed against cancer, followed by monogenetic and infectious diseases (Figure 1.2). Despite the huge number of trials being conducted, only a handful of gene therapy products have received approval for distribution, some controversial in nature. One of the first products on the market was Gendicine, a recombinant Ad used to treat head and neck squamous cell carcinoma [66, 67].

Gendicine was approved by China's State Food and Drug Administration (SFDA) for patient use prior to completion of phase III clinical trials, causing controversy surrounding its administration [68]. Two years after approval of Gendicine, the SFDA approved a second gene therapy product, Oncorine. Oncorine is a recombinant Ad developed to treat late-stage refractory nasopharyngeal cancer [69]. The only Ad vector to have completed phase III clinical trials to date and approved for administration is Cerepro [19]. An interesting chimeric vector, Cerepro consists of an Ad exterior and encodes the Herpes simplex virus thymidine kinase gene. The fourth and last approved gene therapy product is Glybera, an AAV to treat severe lipoprotein lipase deficiency by expressing lipoprotein lipase within muscle tissue [70]. There are several promising therapies being evaluated in late-stage clinical trials against Leber's congenital amaurosis [71], X-linked severe combined immunodeficiency (X-SCID) [72], Wiskott-Aldrich syndrome [73], β-thalassemia [74] and severe protein lipase deficiency [70].

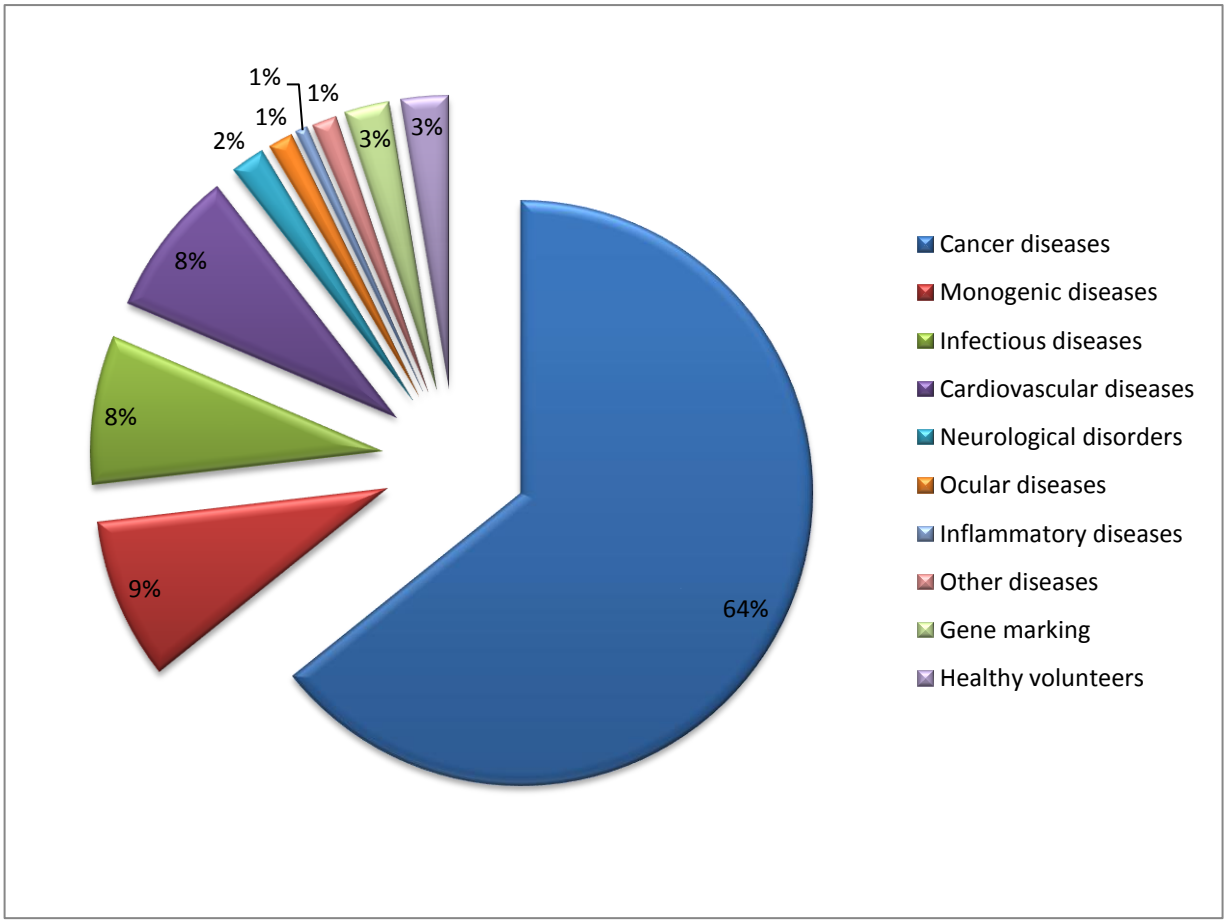

Figure 1.2: Diseases targeted by gene therapy in clinical trials. Adapted from http://www.abedia.com/wiley/indications.php [41].

Liposomes and lipoplexes as gene therapy vectors

Liposomes are synthetic constructs used to deliver a variety of molecules, such as nucleic acids and drugs. Liposomes are generally composed of lipid bilayers. The outer hydrophilic surface associates with the therapeutic cargo, and the hydrophobic intramembrane region anchors moieties and ligands displayed on the liposome surface [75]. The most successful means of delivering nucleic acids is by the use of cationic liposomes. Cationic liposomes were first utilised in 1987 by Felgner and colleagues, who demonstrated the delivery and expression of DNA to cultured cells [76]. Liposomes offer several benefits as gene therapy vectors, as their synthesis is scalable and cost effective, are potentially not as immuno-stimulatory as viral vectors and importantly have the capacity to bind and deliver RNA sequences to cells. Liposome transfection efficacy is influenced by several factors, all of which have to be designed for optimal cellular uptake, interaction and eventual cargo release. The factors include lipoplex size [77, 78], the amount of lipid required for cargo binding, lipid/nucleic acid charge ratios [79], structure of lipid species within the liposome [80, 81], the type of cell targeted [82] and whether those cells are actively dividing [83]. Liposomes do however have several short comings that need to be overcome before their successful application within a clinical setting. Liposomes display decreased levels of cellular tropism compared to viral vectors, susceptibility to cargo degradation by nucleases, may induce cellular toxicity, be negatively affected by plasma components and stimulate innate immune responses [84]. Efforts to overcome these hurdles are under continual refinement, thus enhancing liposome delivery, stability and safety.

Currently twelve liposomal based formulations have been approved for clinical use [85]. Formulations such as Doxil, Myocet and DaunoXome were used to target AIDS-related Kaposi's sarcoma, and metastatic breast cancer [86]. Others include formulations against fungal infections (AmBisome) [87], age-related macular degeneration (Visudyne) [88] and hepatitis A virus (Epaxal) [89, 90] and influenza (Inflexal V) vaccines [91]. There are several ongoing clinical trials utilising liposome-based formulations to deliver a variety of drugs to diseased tissue. Improvement on the aforementioned difficulties may provide liposomes the means to become effective therapeutic vectors. As a whole, synthetic vectors are not as effective in delivery as viruses, however are easier and cheaper to produce, may be less toxic, and can easily be manipulated to avoid immuno-stimulation.

Virus-like particles as gene therapy vectors

VLPs are considered part of the non-viral vectors. Derived from viral capsids, VLPs are biological objects such as empty viral structures, non-infectious self-assembled recombinant gene products and uncharacterised virus-like structures [92]. Furthermore, as a result of their simple nature, VLPs can be produced *en masse* in bacterial [93] or plant expression systems [94], in a scalable cost effective manner. Similarly, many synthetic vectors such as liposomes, synthetic nanoparticles and dendrimers are readily synthesised, however all are not as effective in delivering nucleic acids as viral vectors. Both viral and non-viral vectors offer benefits and drawbacks; ideally the combination of the particle properties could generate a cost effective, scalable, efficient delivery vector for application in resource poor regions like Africa.

There has been a marked increase in the amount of research performed on VLPs, increasing from 15 700 publication in 1995 to 102 000 in 2012 [92]. Initially VLPs were used as agents for vaccinology, notably utilising the hepatitis B virus and human papilloma virus capsid structures to deliver exposed epitopes. To this day, VLPs are still being developed and tested in clinical trials for vaccines [95]. VLPs may offer benefits to the field of gene therapy, as they have the capacity to deliver a variety of therapeutic agents. Additional benefits include:

1) VLPs present as a variety of nano-sized containers, in diverse shapes.
2) In comparison to viruses, VLPs are simple, scalable and cost effective to produce.
3) The VLP surface (both interior and exterior) is amenable to modifications in the forms of amino acid exchange and ligand conjugation to the capsid surface.
4) Availability of known 3D structure.
5) VLPs generally assemble with structural uniformity.

Interestingly, VLPs have seen development in a variety of fields, including chemistry, physics and engineering [96]. Since the 1980s over 100 VLPs have been characterised, the first of these structures was the HBV capsid [97]. HBV capsids are easily expressed as recombinant structures within *Escherichia coli*, which may have facilitated the early characterisation.

The HBV capsid offers several features compared to viral vectors that make it a candidate for VLP gene therapy vectorology. Production is simplified compared to viral vectors, as capsids are easily produced in recombinant *E. coli* and the production is cost

effective and scalable. The HBV capsid is amenable to amino acid changes on its surface, allowing for the introduction of functional residues. As demonstrated for the first time in this study it is possible to conjugate ligands to the HBV surface. Decoration of the capsid surface is necessary as un-enveloped viral particles lose their hepatotropism and are indiscriminately taken up by a variety of cell types [98, 99]. Indiscriminate cellular uptake is an undesirable feature for a gene therapy vector; useful properties of a vector include cellular tropism and immuno-evasion which can be introduced by the inclusion of functional ligands and chemical groups to the vector surface [45]. Lastly, a feature not always afforded to viral vectors is that capsids have the capacity to encapsidate choice therapeutic material post purification. This project aimed to contribute to the advancing field of gene therapy vectorology by developing the HBV capsid as a potential vehicle for therapeutic material. This was aided by the inclusion of liposomes within various aspects of the study. Liposomes offer an alternative platform to assess the effects of various ligands on the uptake behaviour of nanoparticles. It was established that the presence of galactose ligands on the surface of liposomes increased hepatotropic uptake *in vitro*, and permitted for hepatotropism *in vivo*. Similarly, galactose ligands were then conjugated to the surface of HBV capsids and hepatotropism was assessed *in vitro*. Despite HBV being hepatotropic, the viral capsid does not display any form of tropism. The addition of receptor-specific ligands to the capsid surface should enable targeted uptake into a variety of cell types. Galactose made for a suitable ligand as it is liver specific and could be chemically manipulated successfully to allow for inclusion on liposome and capsid surfaces. This proof of principle study was initiated by testing ligand-decorated capsid uptake into cultured liver cells. In principle, this approach could be employed with other cell types, provided a suitable tissue-tropic ligand was attached to the capsid surface. It was demonstrated in this study that:

1) The HBV capsid is amenable to amino acid substitutions on its surface.
2) The HBV capsid undergoes successful conjugation of ligands to its surface.
3) Prevention of indiscriminate cellular uptake is possible with the addition of moieties to the capsid surface.

Thus, future studies can focus on optimising the structure of the ligands conjugated to the capsid surface in order to enhance hepatotropism. In doing so it may be possible to address the deficits in current gene therapy vectorology to generate efficacious, cost effective non-viral gene therapy vectors for developing regions like Africa.

Chapter 2: The influence of galactose linker length on liposomal hepatotropic transfection efficiency

2.1. Introduction

The gene therapy field has undergone several improvements over the past decade, and continues to do so as our understanding of biological mechanisms and systems expands. One of the major challenges faced within gene therapy is delivery of therapeutic cargo, typically nucleic acids, to a target tissue/area. Development of effective viral and non-viral vectors has become paramount within the field, as the full potential of gene therapy application cannot be realised without it. Synthetic/non-viral vectors offer several advantages over viral vectors, which include ease of *in vitro* modification and manipulation, lower cost of production, scalable production, low immunogenicity and enhanced stability (reviewed in [100-105]). One of the prominent forms of non-viral vectors is liposomal-based delivery. The design and synthesis of cationic liposomes has important hurdles that must be overcome to produce a successful correlation between lipoplex structure and transfection efficiency. Lipofection *in vitro* and *in vivo* entails several potentially rate-limiting steps such as DNA lipoplexing [106], cellular binding (without cellular specificity targeting is electrostatically based), cellular uptake, endosomal escape [107], cytoplasmic transportation, nuclear entry and nucleic acid release from the lipoplex. For the purposes of this thesis, the above mentioned factors are collectively called transfection efficiency. Viral vectors experience the aforementioned rate-limiting steps to a far lesser extent, as their evolution has resulted in highly efficient nucleic acid delivery vehicles. Viral vectors have shown *in vivo* success in inducing gene therapy [59, 60], however several safety concerns have been raised. Two children treated for X-linked severe combined immunodeficiency (X-SCID) with retroviral vectors in 2002 developed leukaemia-like symptoms from random insertion events [108]. In 1999 an 18 year old patient treated for ornithine transcarbamylase deficiency with a recombinant adenovirus died as a result of a severe immune response resulting in multiple organ failure [9]. Despite the aforementioned risks, viral vectorology has seen drastic improvements over the past ten years and is still the preferred means of delivery for gene therapy as a result of enhanced tissue tropism and transgene expression [109]. Non-viral vectors have none the less made their mark in several phases of clinical

trials, summarised in Table 2.1.1. Liposomes primarily have the advantage of delivering either drugs or RNA sequences to targeted cells, a feature not available to viral-based vectors.

Table 2.1.1 Gene therapy clinical trials using lipid-based vectors

Disease	Gene treatment	Clinical phase	Clinicaltrials.gov identifier
Advanced head and neck cancer	EGFR antisense DNA	Phase I	NCT00009841
Cystic fibrosis	pGT-1 gene	Phase I	NCT00004471
Non-small-cell lung cancer	Fus-1 gene	Phase I	NCT00059605
Advanced pancreatic cancer	Bik gene	Phase I	NCT00968604
Cystic fibrosis	CFTR gene	Phase I/II	NCT00789867
Solid tumour cancers	M2 subunit of ribonucleotide reductase siRNA	Phase I	NCT00689065
Advanced solid tumours with liver involvement	VEGF and KSP siRNA	Phase I	NCT00882180
Advanced solid cancers	PKN3 siRNA	Phase I	NCT00938574
Respiratory syncytial virus infections	Nucleocapsid N gene siRNA	Phase II	NCT01065935
Transthyretin mediated amyliodosis	Transthyretin gene siRNA	Phase I	NCT01148953
Philadelphia Chromosome positive CML, AML, CLL and MDS	Growth Factor Receptor Bound Protein-2 antisense DNA	Unknown	NCT01159028
Advanced recurrent cancer	EphA2 siRNA	Not yet open	NCT01591356
Recurrent high-grade gliomas	UGT1A1 siRNA	Recruiting	NCT00734682

Adapted from Zhang *et al.* 2012 and sourced from www.chemicaltrials.gov (ALL – Acute lymphocytic leukaemia, CLL – Chronic lymphocytic leukaemia, CML – Chronic myelogenous leukaemia, EGFR – Epidermal growth factor receptor, EphA2 – Ephrin type-A receptor 2, KSP – Kinesin spindle protein, MDS – Myelodysplastic syndrome, PKN3 – Protein kinase N3, UGT1A1 – UDP glucuronosyltransferase 1 family, polypeptide A1, VEGF – Vascular endothelial growth factor)

Liposomes are generally composed of amphiphilic molecules, comprising a hydrophilic cationic head group and a hydrophobic hydrocarbon group. The cationic head group provides solubility to the liposome within an aqueous environment, whereas the hydrophobic moiety forms the basis of the micelle or lamellar membrane. The morphology of the liposome is related to the geometry of the amphiphilic molecules. This is of particular importance, as there are various morphological states of liposomes that can influence

transfection efficiency, endosomal escape and nucleic acid packing and protection [110-112]. A means to assess morphology is by the packing parameter, *P*, which is used to determine whether liposomes will tend toward micelle, cylindrical micelle, lamellar, cubic or inverted hexagonal (H_{II}) phases (Figure 2.1.1) [113, 114]. *P* is defined as the ratio of the hydrocarbon tail volume, *v*, to the product of critical length of the lipid tail, l_c, and effective head group area, *a*, as the following equation $P=v/al_c$ [115]. Thus this ratio describes the effect of the hydrophobic versus the hydrophilic volume of the amphiphilic molecule on liposome morphology. When the head group volume exceeds the hydrophobic tail group volume such that $P < 0.5$, liposomes will tend towards micellar-like structures. In particular, if $P < 0.33$ liposomes tend to form discreet micelles, whereas if $0.33 < P < 0.5$ liposomes tend toward uniform cylindrical-like structures. If $0.5 < P \leq 1$ liposomes tend towards lamellar morphology and if $P > 1$ liposomes adopt the inverted hexagonal phase (Figure 2.1.1) [115].

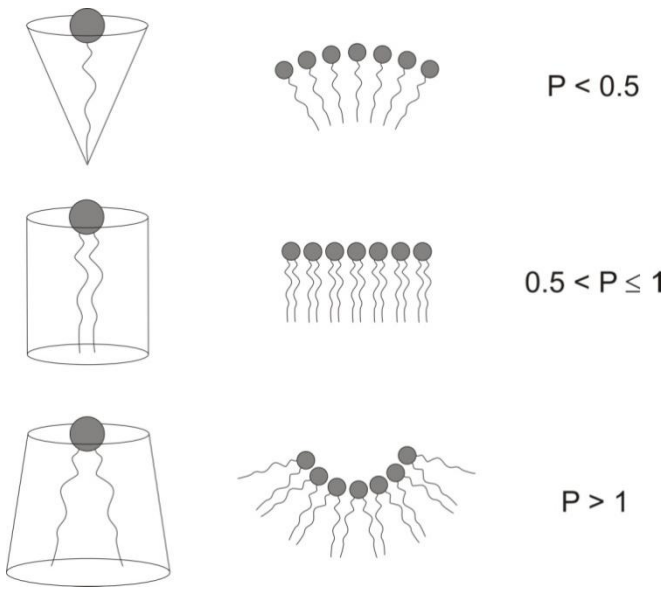

Figure 2.1.1: Diagrammatic representation of liposomal phase morphology as a result of amphiphilic lipid packing parameter (*P*). Hydrophilic head groups (grey ball) with larger volume than hydrophobic tails tend toward cone-like geometry ($P < 0.5$). Amphiphiles with packing parameters $0.5 < P \leq 1$ form lamellar bilayers. A packing parameter of $P > 1$, where the hydrophobic volume is larger than the hydrophilic, liposomes tend toward an inverted hexagonal morphology. Figure adapted from Wasungu and Hoekstra, 2006.

Salt concentration, pH and surface cationic charge play an important role in the determination of head group volume. A decrease in charge brought about by any of these factors will result in a smaller head group volume. This change promotes the conversion of liposomes from micellar/lamellar into the inverted hexagonal phase, an important step required for the release of nucleic acids from the endosomal pathway. Zwitterionic helper lipids such as 1,2-dioleyl-*sn*-glycero-3-phosphoethanolamine (DOPE) reduce the overall liposome surface potential by ionic interaction with the cationic head group [116]. This interaction facilitates the transition from micellar/lamellar to inverted hexagonal, especially

at lowered pH or physiological salt concentration. A difficulty encountered in the preparation of liposomes containing DOPE for *in vivo* application is the neutralisation of the surface potential at physiological salt concentrations. This neutralisation causes the transition from micellar/lamellar to inverted hexagonal phase, which results in the conglomeration and eventual precipitation of the liposomes [113]. DOPE also decreases the DNA binding capacity of the liposome, as a net decrease in cationic charge occurs [117]. However with a decrease in binding capacity an increase in liposome-DNA dissociation is also facilitated, allowing for the intracellular release of the liposome from bound DNA [103].

An often overlooked aspect of lipoplexing is the effect of the liposome on the structural integrity of the cargo DNA. It has been suggested that poor packaging of DNA within the liposome, such that DNA protrusions are present, potentially allows for degradation by nucleases within circulation and the cytoplasm [118]. It has also been described that effective transfections require the disassociation of the lipid vector (or its components) from the DNA cargo once within a cellular environment. Hama *et al.* reported that Lipofectamine Plus had significantly higher cellular entry, equivalent endosomal escape and slightly lower nuclear transfection compared to adenoviruses. The liposomal delivery system however required three times more DNA present within the nucleus to obtain comparable transgene expression. It was suggested by Hama and colleagues that transcription was affected by the poor dissociation of liposome and DNA within the nucleus. Supporting this finding, other instances of B-DNA structural changes have been found in which lipoplex-induced DNA compaction resulted in Z-DNA within anionic liposomes [119] and C-DNA in cationic liposomes [120]. Liposome-DNA interaction is also thought to be influenced by serum, thus affecting the overall transfection efficiency [121].

It is generally accepted that cationic liposomes interact with the cell surface in an electrostatic-based manner. The anionic cell surface charge is provided primarily by phospholipids; in addition the proteins heparin sulphate proteoglycan and integrin contribute to the anionic potential [122]. It is suggested that these proteins play an important role in lipofection, which may explain the variation in transfection efficiency seen between cell lines as a result of cell surface composition. Ligands present on the surface of liposomes provide means to bind and interact with the cell surface in a directed manner. Ligands such as antibodies/antibody fragments [123], steel factor [124], asialoglycoprotein (containing galactose or *N*-acetylgalactosamine) [125], mannose [126], lactose [127], folate

[128], integrin [129], transferrin [130] and epidermal growth factor [131] are examples used for the targeted delivery of liposomes to specific cell types. The asialoglycoprotein receptor (ASGPr) is a C-type Ca^{2+}-dependent lectin found almost exclusively on the surface of parenchymal hepatocytes [132, 133], but is also found on Kupffer cells [134]. The ASGPr binds β-D-galactose (Gal) or *N*-acetylgalactosamine (GalNAc) residues present of the surface glycoproteins, resulting in their clearance from circulation [133, 135]. The work described here made use of galactose tethered to the surface of liposomes to enhance cellular uptake and transfection efficiency in cultured hepatocytes and in a transgenic HBV murine model. The galactose affinity exhibited by the ASGPr can provide liposomes with hepatotropism by including galactose moieties within their composition.

Generally the use of ligands results in particle uptake by receptor-mediated endocytosis, as opposed to the generic ionic pairing of ligand-less liposomes [82]. Passive fusion of the lipoplex with the cell surface has been shown to cause exclusion of the cargo DNA from the cell [136]. The five major routes of endocytic uptake (reviewed in [102, 137-142]) are:

1 Phagocytosis – a process that generally occurs in neutrophils or macrophages.

2 Macropinocytosis – this form of uptake requires cell membrane ruffling and liposome fusion, that results in large endocytic vesicles which fuse with the lysosome or are recycled and released at the cell surface.

3 Clathrin-mediated endocytosis – a form of receptor mediated uptake by clathrin-coated pits which form early endosomes.

4 Caveolae-mediated endocytosis – caveolae are small sphingolipid and cholesterol-rich membrane invaginations, and are responsible for both endocytosis and signal transduction.

5 Clathrin/caveolae-independent endocytosis – these uptake pathways are not well understood and are currently being investigated. Despite the presence of targeting ligands on liposomes, there is conflicting evidence for a generalised (clathrin-mediated) mechanism of uptake [82].

Following endocytosis, lipoplexes remain enveloped within early endosomes (Illustrated in Figure 2.1.2). It is crucial that the endosome contents are released into the cytosol, as lysosomal-based degradation or release at cell surface ensues. Several mechanisms have been suggested for the successful escape of lipoplexed cargo into the cytosol. The trans-bilayer flip-flop mechanism causes anionic lipids such as phosphatidyl serine (PS) to

translocate from the outer to the inner leaflet of the endosome and interact with the lipoplex [143]. This causes destabilisation of the outer leaflet and rupture of the endosome. Alternatively PS interacts with the lipoplex surface, and the resultant ion pairing and charge neutralisation causes the liposome membrane to convert to the inverted hexagonal phase and fuse with the endosome [118, 144]. It is also possible that both mechanisms occur and contribute to endosomal instability. Helper lipids such as DOPE are said to be of importance in the conversion of lipoplexes from lamellar to inverted hexagonal phases as endosomal acidification initiates phase conversion by charge neutralisation of DOPE and the cationic lipid [116, 118]. It has been questioned whether the inverted hexagonal phase-mediated endosomal fusion is of importance to the enhancement of transfection efficiency [111, 145]. Fasbender and colleagues described helper lipids that have varying effects on both uptake and transgene expression. Furthermore the type of cationic lipid and cell type influence helper lipid behaviour, indicating a complicated uptake and release behaviour [146].

Polyethylene glycol (PEG) -like molecules have become indispensable within the field of liposome vectorology. Inclusion of PEG to liposome surfaces provides immuno-evasive properties and provides stability to the liposome structure. PEGylation of liposomes does however have a major impact on the endosomal release of lipoplexed DNA. Endosome and liposome membrane interaction responsible for membrane destabilisation and intracellular release is greatly diminished in the presence of PEG. As a result, endosome-responsive PEG in the form of exchangeable PEG-lipid analogues or pH-sensitive PEG analogues have been developed [147-149]. These PEG analogues undergo cleavage from the liposome surface within the endosome, allowing then for the ionic interaction between endosomal and liposomal membranes.

Transport and entry into the nucleus of lipoplexed DNA is a critical but poorly understood process. The nucleus has a double membrane with selective pores 10 - 25 nm in diameter [150]. The pores are far smaller than condensed plasmid DNA, constituting a major barrier to plasmid entry. As a result of cytosolic nucleases, plasmid half-life in HeLa cells was estimated at 90 minutes, making nuclear entry a critical step in the transfection process [151, 152]. It has been estimated that DNA translocation occurs for every 1 of 1000 plasmids transfected [153]. Interestingly microinjection studies have shown that lipoplex injection into the cytoplasm does not result in transfection, whereas injection into the nucleus does. Similarly naked plasmid injection into the cytoplasm does not result in transfection. Only

when lipoplexed DNA is introduced to the cytoplasm via the endosome does transfection occur, indicating an unknown intracellular transport process after endosomal uptake [154].

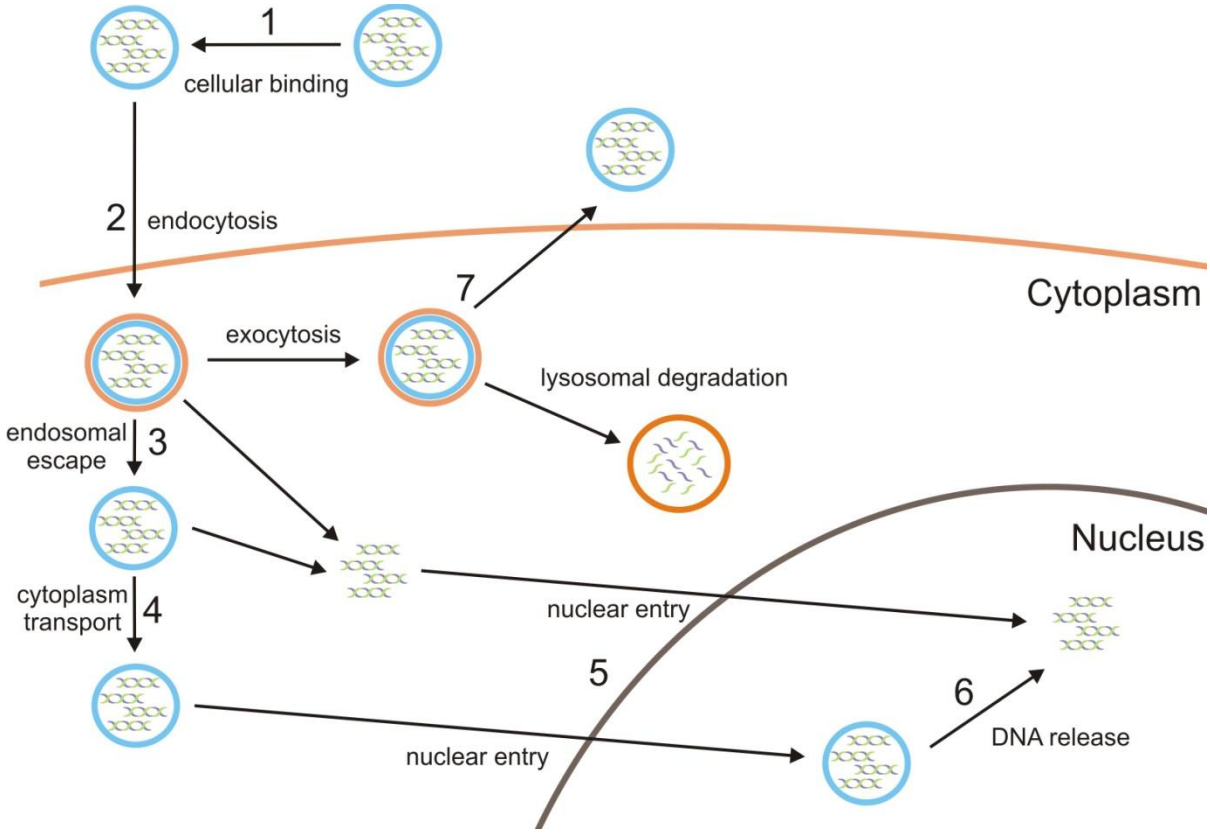

Figure 2.1.2: Summary of lipofection and barriers of gene delivery. (1) Cellular binding mediated by electrostatic or receptor interaction. (2) Endocytosis established as the main mechanism of entry. (3) Endosomal escape of lipoplexes by various mechanisms before degradation. (4) Lipoplex or nucleic acid is required to be actively transported to the nucleus. (5) Nuclear entry by active transport. (6) Lipid dissociation from cargo DNA. (7) Lipoplexes unable to escape the endosome are degraded or recycled back to the surface.

Innovative systems are under continuous development within the vectorology field. Improved receptor based targeting, immuno-evasion, improved DNA binding and release, enhanced endosomal escape are a few factors under development. In line with these factors, work described in this chapter aimed to combine hepatotropism and immuno-evasive properties into one molecule, include it within a basic liposome and assess the effect on transfection efficiency. Monosaccharide-cholesterol conjugates (MCC) were synthesised such that galactose was tethered to a cholesterol moiety by a glycol-based linker of variable length. Two versions of the galactose ligand were assessed, in which hydroxyl groups were either acetylated (protected) or unacetylated (unprotected). The acetylation status of protected galactose (P-Gal) prevented the hydroxyl species from

undergoing unwanted reactions during compound synthesis. Removal of the acetyl groups results in an unprotected galactose moiety (UnP-Gal), similar to what would reside on asialoglycoproteins (Figure 2.1.3).

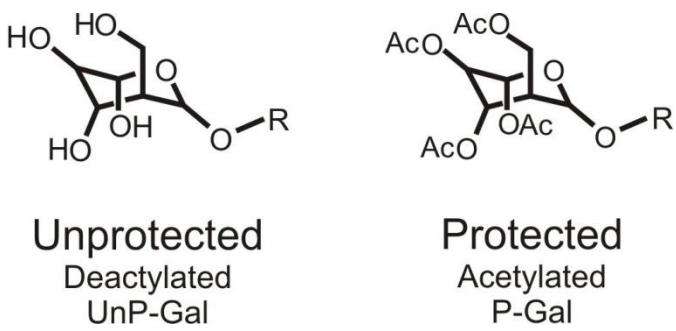

Figure 2.1.3: Illustration of galactose moieties in the unprotected state (exposed hydroxyl groups) or protected state (acetyl groups).

Three glycol-based tethers, which varied in length, were used to link the galactose and cholesterol moieties. The shortest tether, short linker chain (SLC), comprised of 1 glycol link. Similarly medium linker chain (MLC) and long linker chain (LLC) included 4 and 11 glycol links, respectively. Figure 2.1.4 illustrates the structures of DC Chol and the compounds containing P-Gal or UnP-Gal and SLC, MLC or LLC. Ideally the short PEG-like linkers would provide immuno-evasive properties to the liposomes, and not interfere with liposome morphology, cell surface interaction or endosomal escape.

Compound Name	Structure
DC Chol	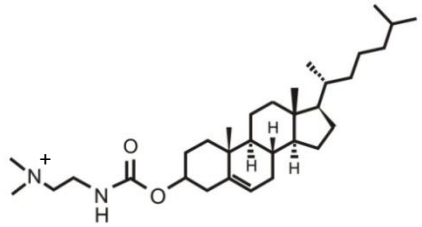
SLC UnP-Gal	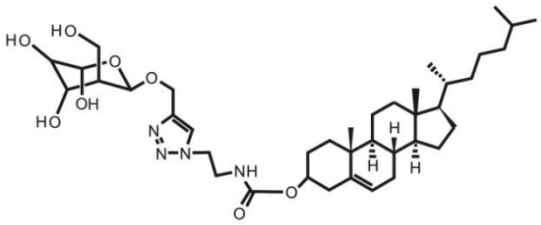
SLC P-Gal	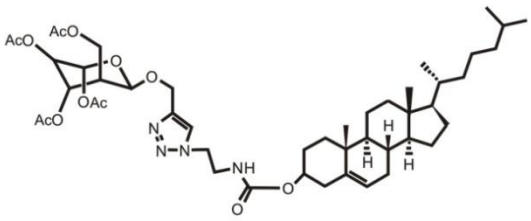
MLC UnP-Gal	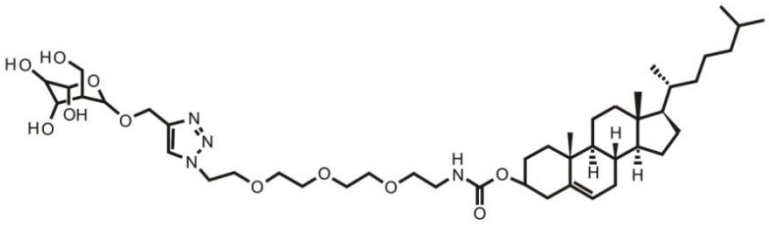
MLC P-Gal	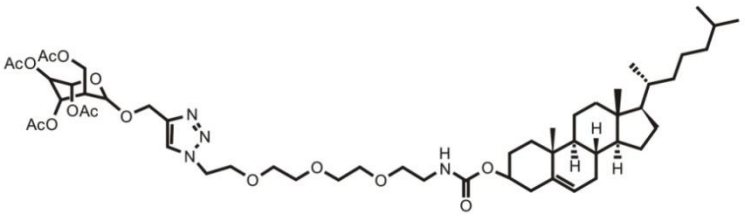
LLC P-Gal	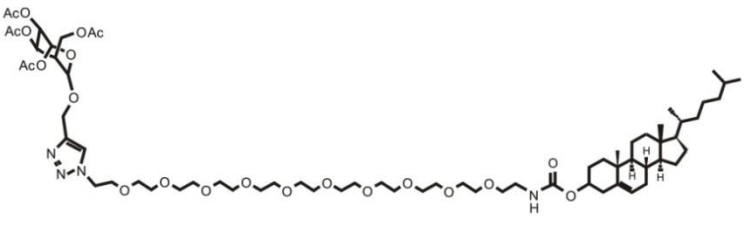

Figure 2.1.4: Illustration of the various galactose-tethered cholesterol-based moieties included in the generation of liposomes. DC Chol is a commercially available cationic lipid capable of binding to anionic DNA. The remainder of the structures contain a protected (acetylated) galactose (P-Gal) or unprotected galactose (UnP-Gal), tethered to cholesterol by a short linker chain (SLC), medium linker chain (MLC) or long linker chain (LLC).

In a collaborative effort between the Antiviral Gene Therapy Research Unit (Johannesburg, South Africa) and the Rega Institute for Medical Research (Leuven, Belgium), *in vivo* delivery of hepatotropic liposomes loaded with modified siRNAs was assessed [155]. Liposomes were generated consisting of DOPE, SLC P-Gal and the novel cationic lipid, CL19 (Figure 2.1.5). At the time of *in vivo* investigation, it was technically difficult to generate the unprotected variety of the galactose ligand, thus the protected variety was included instead. CL19 was generated during an earlier study to identify potential novel cationic lipids that allowed for *in vivo* delivery of siRNAs (data not included). Anti-HBV siRNAs included in the study contained altritol modifications (Figure 2.1.5) [156, 157]. Continual efforts to identify modifications to siRNAs which confer stability without affecting the targeting and off-targeting capacity are underway, through which the altritol nucleic acids (ANA) were identified. ANAs contain a six membered sugar ring, derived from hexitol nucleic acids. The physicochemical properties of the ANA-siRNA helix induce the A-form, a property which is thought to improve the silencing capacity. *In vitro* assessment revealed that the 3' positioning of the altritol modifications increased silencing efficacy compared to unmodified siRNAs. Together with *in vitro* transfection data, these findings prompted further investigation in an *in vivo* HBV transgenic murine model.

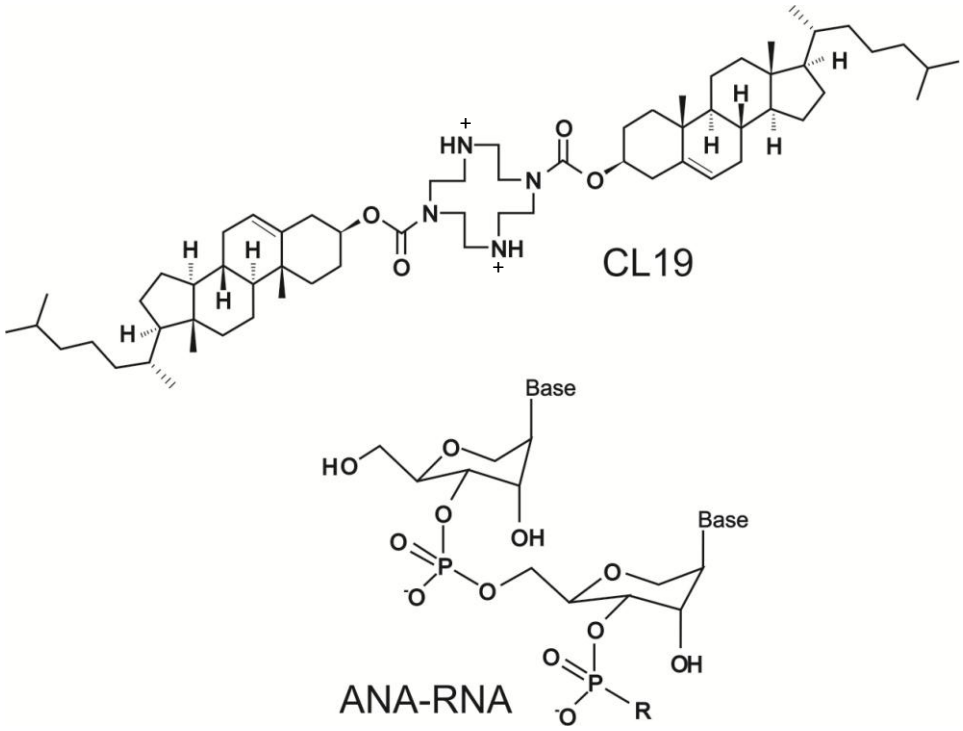

Figure 2.1.5: Structural illustration of the cationic lipid CL19 and ANA-containing RNA moieties.

It was demonstrated that increasing linker length negatively impacts on the DNA binding capacity of the liposome. Increased linker length also decreased transfection efficiency in both targeted and non-targeted cell lines. Acetylation was shown to diminish transfection efficiency in a liver derived cell line. Despite the hepatotropism provided by galactose, it was demonstrated that commercially available transfection reagents have greater transfection efficiency in hepatocytes than liposomes containing MCC structures. *In vivo* studies suggest that the P-Gal liposomes are capable of delivering siRNAs to the hepatocytes of mice. It was demonstrated that the ANA-siRNAs induced knockdown of the HBV within the transgenic mouse model, with little to no liver damage and immunostimulation.

2.2. Results

2.2.1. Initial liposome formulation with monosaccharide-cholesterol conjugates

Liposomes were formulated comprising 60% cholesterol moiety and 40% neutral helper lipid (DOPE) (mole/mole) [158]. For the purposes of this study the 60:40 ratio comprised 60 parts DC Chol and 40 parts DOPE. It was previously determined that liposomes required 16% P-Gal MCC for optimal transfection efficiency (mole/mole) [155]. This resulted in overall liposomal DC Chol content decreasing from 60% to 44%, as 36.4% of cholesterol species within the liposome were represented by MCC. Overall lipid composition of the liposomes is 44% DC Chol, 40% DOPE and 16% MCC (also expressed as a ratio of 11:10:4) unless stated otherwise.

2.2.2. Determination of DNA to lipid charge neutralising ratios by mobility shift assay

Liposome to DNA ratios required for transfection were determined by mobility shift assays (Figure 2.2.1). DNA and liposomes were combined at specific ratios (w/w), allowed to lipoplex and subjected to agarose gel electrophoresis. Lipoplexed DNA lost mobility within the agarose gel and was trapped within the loading wells. Complete plasmid DNA (pDNA) sequestration was indicative of the DNA to lipid ratio required for efficient envelopment. The control liposome consisting of DC Chol and DOPE alone completely sequestered pDNA at a DNA to lipid ratio of 1:4. The introduction of MCC species into the liposome formulation caused a decrease in DNA binding, demonstrated by the increase in liposome required to sequester pDNA completely. Liposomes containing SLC UnP-Gal, SLC P-Gal, MLC UnP-Gal and MLC P-Gal required 6 parts lipid to 1 part pDNA for complete sequestration. The protection status of galactose did not significantly influence DNA-liposome binding. As the increase of 4 to 6 parts liposome was required for complete pDNA sequestration, a correlation was noted with the associated decrease in DC Chol. The 50% increase in liposome amount required for pDNA sequestration correlates to the 36.4% decrease in DC Chol present in the liposome formulations. The highest DNA to lipid binding ratio (1:8) occurred when using LLC P-Gal in liposome formulation. A trend of increased linker length and associated decrease in DNA binding capacity was noted in which it was possible that these PEG-like moieties shield the liposome surface from pDNA access.

MCC/DC Chol	Mobility Shift Assay	Lipofection ratio (w/w)
DC Chol	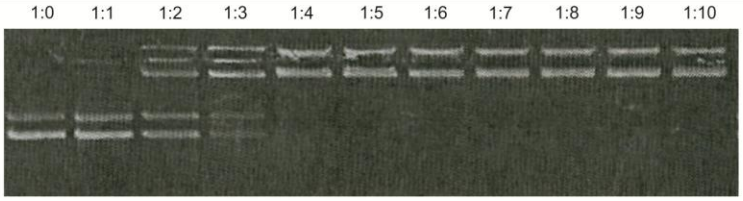	1:4
SLC, UnP-Gal	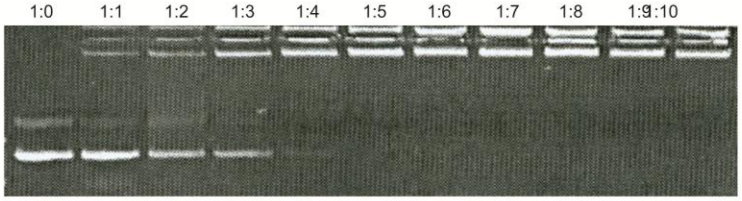	1:6
SLC, P-Gal	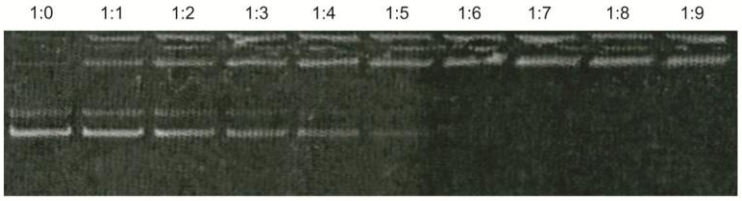	1:6
MLC, UnP-Gal	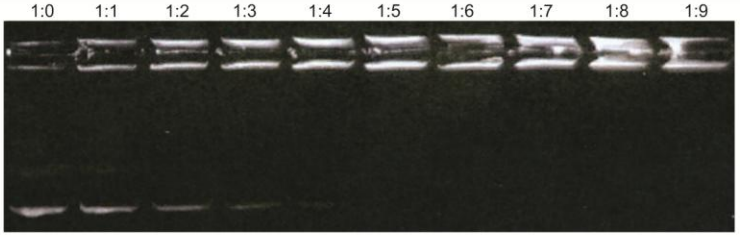	1:6
MLC, P-Gal	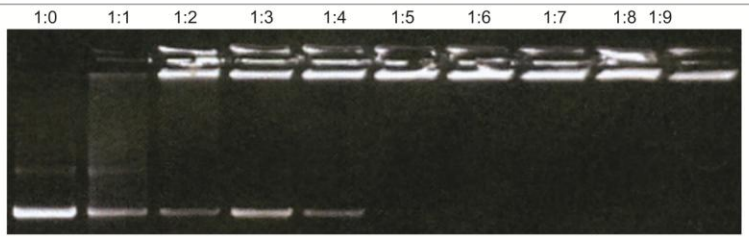	1:6
LLC, P-Gal	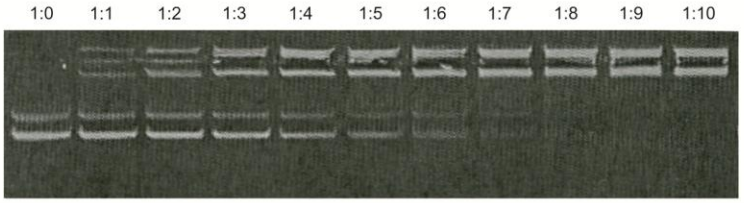	1:8

Figure 2.2.1: DNA mobility shift assay to assess the effect of MCC with varying linker lengths on liposomal DNA binding. Liposomes comprised 60% cholesterol species and 40% DOPE. MCC-containing liposomes comprised 44% DC Chol, 40% DOPE and 16% MCC (mole/mole). Increasing amounts of liposomes were lipoplexed with a constant amount of pDNA (w/w) and subjected to agarose gel electrophoresis. The lipofection ratio (DNA to liposome) was determined once charge neutralisation occurred, in which pDNA was sequestered within the gel well. (SLC – short linker chain, MLC – medium linker chain, LLC – long linker chain, UnP-Gal – unprotected galactose, P-Gal – acetyl-protected galactose).

2.2.3 Assessment of the transfection efficiency of MCC-containing liposomes

DNA to liposome ratios determined by mobility shift assay were used for transfection in two immortalised cells lines, Human hepatocellular carcinoma (Huh7) and Human embryonic kidney cells (HEK293). The Huh7 cell line has been demonstrated to express the ASGPr on the cell surface [159]. The HEK293 cell line was used as a negative control in transfection experiments, as it did not contain the ASGPr and was incapable of binding galactose. Transfection efficiency was assessed by expressed luciferase luminescence intensity, an indication of the amount of luciferase-encoding pDNA (psi-Check2.2) delivered to and released within target cells. Despite not having tested the UnP-Gal species in cell culture, the previously determined [155] ratio of 16% monosaccharide-conjugated cholesterol (mole/mole) was used as a reference starting point for MCC-containing liposomes.

Transfection efficiency was measured by the luciferase luminescence intensity, an indication of the amount of pDNA delivered and expressed in Huh7 (Figure 2.2.2A) and HEK293 (Figure 2.2.2B) cells. Inclusion of SLC UnP-Gal significantly increased the transfection efficiency by four-fold and SLC P-Gal by two-fold in Huh7 cells compared to liposomes without MCC ($p < 0.005$). It was anticipated that the protection status of the galactose would influence transfection efficiency, as the rate limiting step of acetyl group removal was required for asialoglycoprotein-receptor interaction. The MLC-containing liposomes (P-Gal and UnP-Gal) both resulted in a minor decrease in transfection efficiency, and LLC P-Gal decreased transfection efficiency by three fold in Huh7 cells. Unexpectedly SLC UnP-Gal containing liposomes resulted in an approximate 50% increase in transfection efficiency, whereas the remaining MCC-containing liposomes resulted in an equivalent or decreased transfection rate in HEK293 cells. These data suggest that protection of galactose significantly decreases transfection efficiency in Huh7 cells. Furthermore, an increase in linker length appears to correlate to a decrease in transfection efficiency.

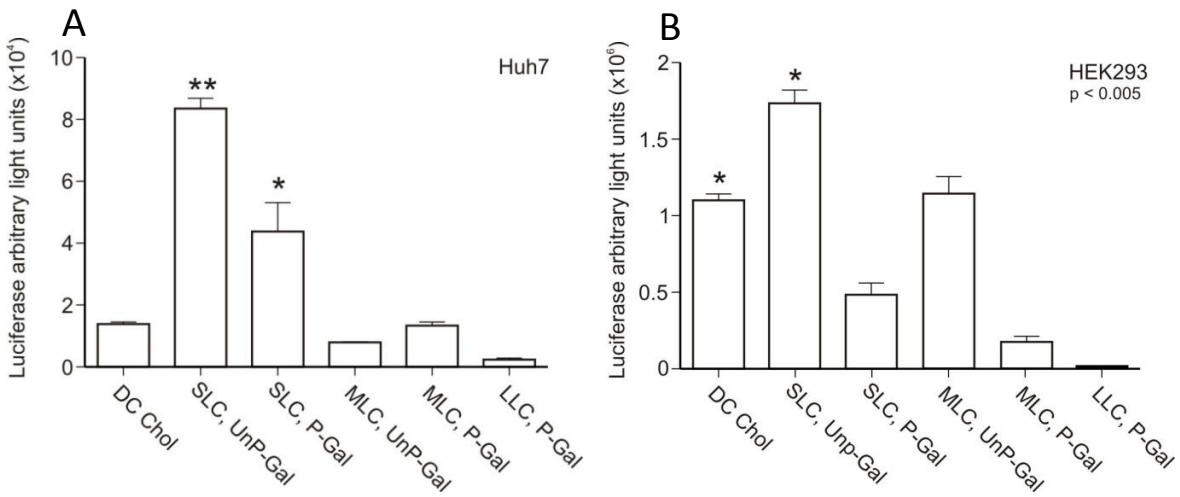

Figure 2.2.2: Luciferase assay to evaluate the transfection efficiency of lipoplexed DNA using monosaccharide-containing liposomes. The Huh7 cell line contains the ASGPr (A), and HEK293 (B) cell line is a negative control for the receptor. Liposomes contained 16% (mole/mole) MCC in a combination of SLC, MLC or LLC and either UnP-Gal or P-Gal. Transfection efficiency was compared to liposomes without galactose moieties (DC Chol). Statistical analysis done using the student t-test, number of replicates (n) = 3, SEM. **, $P < 0.0001$; *, $P < 0.05$

2.2.4 Determination of MCC concentration for optimal transfection in Huh7 cells.

Having established that SLC UnP-GAL was the best candidate for transfection in Huh7 cells, it was next determined at what MCC surface representation produces optimal transfection efficiency. Literature indicated that 2-5% of a particular targeting moiety is sufficient to produce optimal transfection *in vitro* and *in vivo* [160]. Liposomes containing 2-16% SLC UnP-Gal (mole/mole) were generated and lipoplexed at a ratio of 6 parts liposome to 1 one part psi-Check2.2 (w/w). Transfection of the Huh7 cell line (Figure 2.2.3A) indicated that the presence of 2% SLC UnP-Gal produced the best transfection efficiency, whereas 16% SLC UnP-Gal only slightly increased transfection efficiency. Liposomes containing 4-12% SLC UnP-Gal result in decreased transfection efficiency compared to liposomes without galactose (DC Chol alone). Transfection of HEK293 cells resulted in decreased transfection efficiency as the concentration of SLC UnP-Gal increased (Figure 2.2.3B). Interestingly the transfection efficiency from 12-16% SLC UnP-Gal in both Huh7 and HEK293 cell lines recovered in efficiency. Liposomes containing 3-5% PEG-2000 diminished transfection completely in Huh7 and HEK293 cells (Figure 2.2.3). It is well documented [161] that PEGylation of liposomes abrogates transfection of cultured cells, despite the surface representation of PEG only being 3-5% (mole/mole).

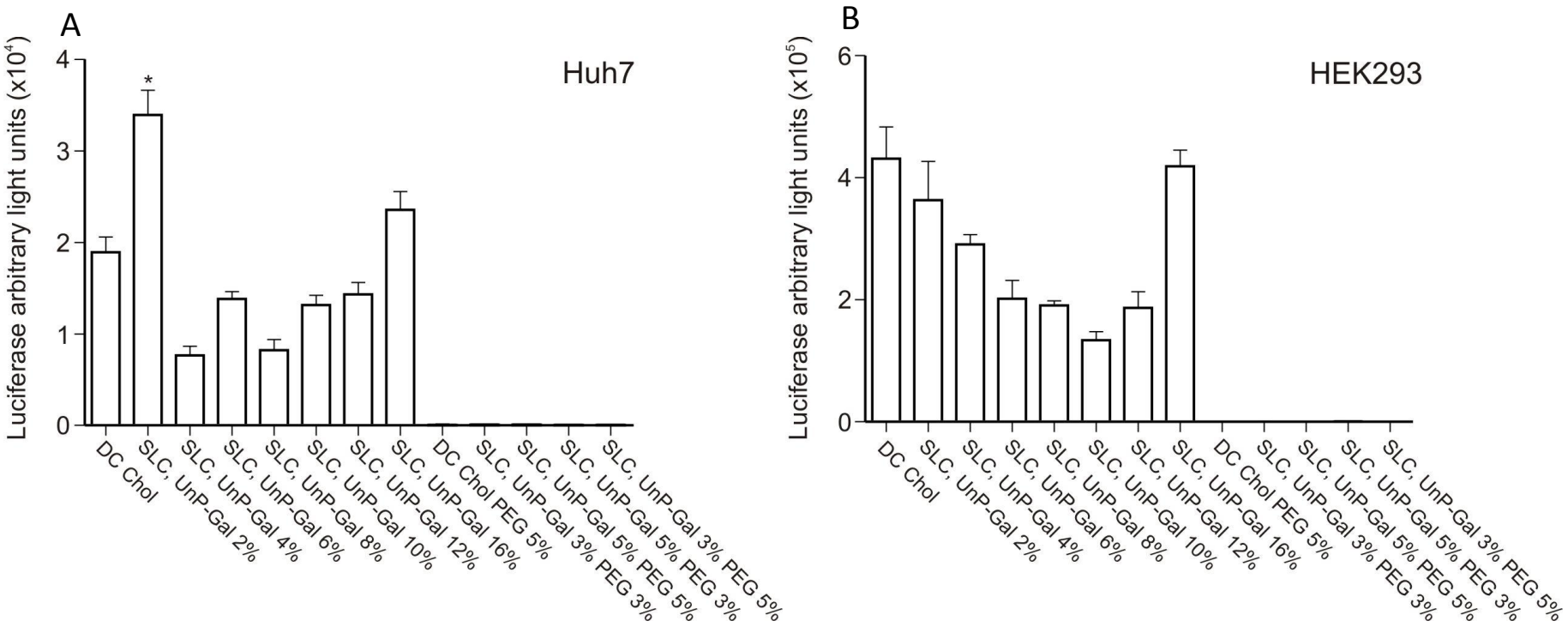

Figure 2.2.3: Luciferase assay to evaluate the transfection efficiency of liposomes with varying surface representation of SLC UnP-Gal in Huh7 (A) and HEK293 (B) cells. Liposomes were generated containing 0-16% SLC UnP-Gal or 3-5% SLC UnP-Gal and 3-5% PEG, lipoplexed with psi-Check2.2 at a DNA to lipid ratio of 1:6. Transfection efficiency was compared to liposomes without galactose moieties (DC Chol). Luciferase activity is used as a measure of reporter plasmid delivery. Statistical analyses were performed using a student t-test, n=3, SEM. *, $P < 0.05$.

2.2.5 Comparison of SLC P-Gal and Lipofectamine2000 transfection efficiency.

The presence of galactose on the surface of liposomes provided an advantage in liposomal delivery of pDNA facilitated by the interaction with the ASGPr on liver cells. It was assessed whether this transfection enhancement was comparable to Lipofectamine2000, a popular commercially available transfection reagent. Varying amounts of psi-Check2.2 were transfected into Huh7 cells using 2% SLC UnP-Gal containing liposomes at lipid to DNA ratio of 6:1 (w/w) or Lipofectamine2000, at a ratio of 1:1 (v/w). It was found that regardless of the amount of DNA transfected into Huh7 cells, using Lipofectamine2000 resulted in higher luciferase activity (Figure 2.2.4).

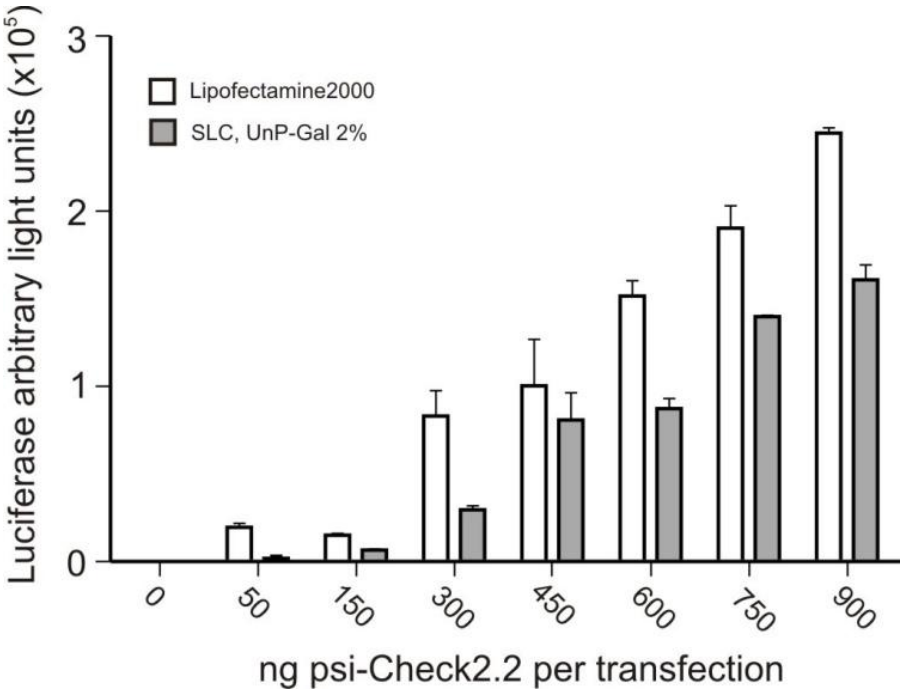

Figure 2.2.4: Luciferase based assay to compare transfection efficiency between Lipofectamine2000 and 2% SLC, UnP-Gal containing liposomes in Huh7 cells. Lipoplexing was carried out at a lipid to DNA ratio of 6:1 (w/w) using SLC UnP-Gal and 1:1 (v/w) using Lipofectamine2000. Plasmid DNA was transfected in varying amounts, ranging from 50-900 ng. Luciferase activity is an indication of liposomal based delivery of psi-Check2.2 Statistical analyses done by student t-test, n=3, SEM.

2.2.6 In vivo *delivery of anti-HBV siRNAs using hepatotropic liposomes*

The liposomes containing galactose ligands were assessed for hepatotropic behaviour *in vivo* [155]. In a previous study it was determined that CL19 from a library of cationic lipids demonstrated the best transfection efficiency. Liposomes were formulated using SLC P-Gal, DOPE and CL19 in a mole ratio of 8:20:11, respectively. The formulated liposomes were combined with ANA-siRNAs at a mass ratio of 17:1, respectively. Lipoplexed siRNAs were

administered to groups of eight HBV transgenic mice [162] at 1 mg/kg weekly, over a course of 37 days. Blood samples were collected from mice using retro-orbital puncture on days -2 (baseline), 0, 9, 21 and 37 (Illustrated in Figure 2.2.5).

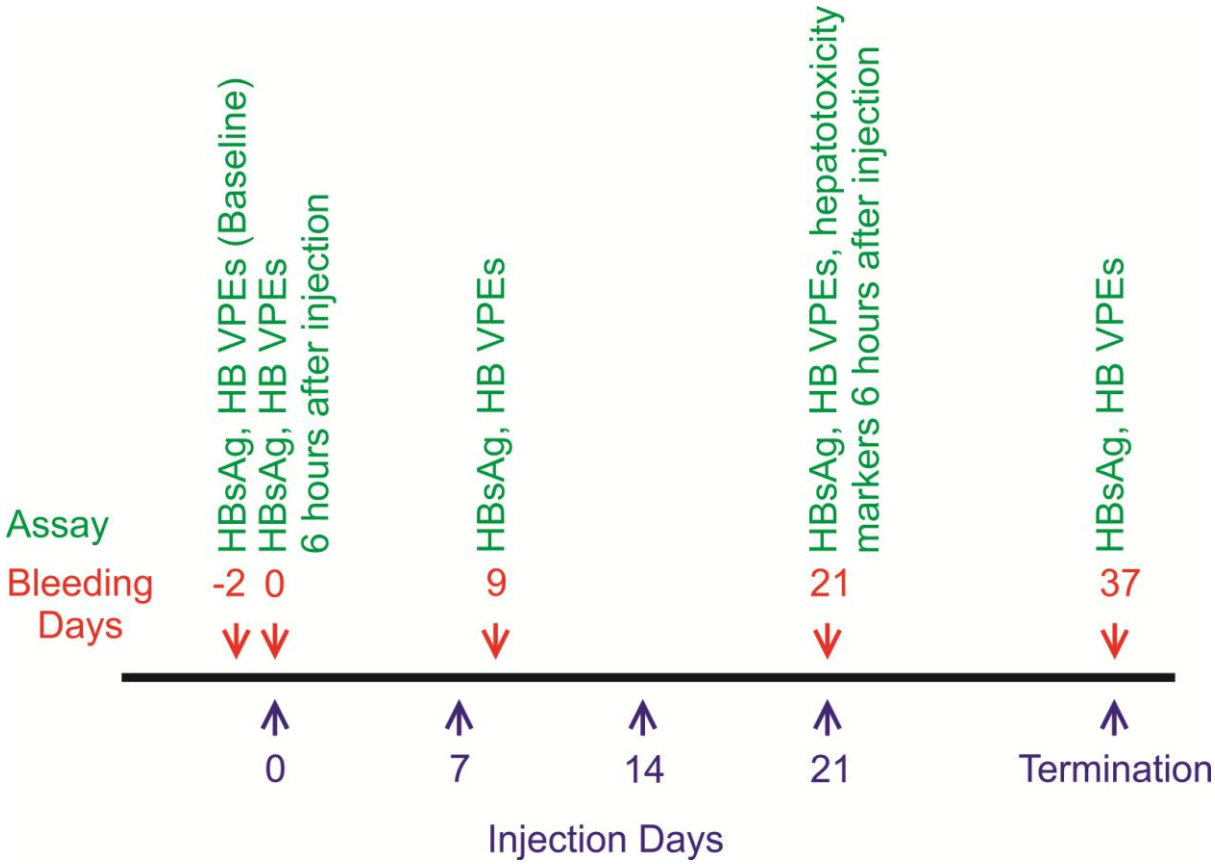

Figure 2.2.5: Illustration of the experimental program conducted on transgenic HBV mice. Groups consisted of eight mice, injected weekly over four weeks in a period of 37 days. Some groups received a single injection on day 0. Retro-orbital bleeding was used to collect blood samples on days -2, 0, 9, 21 and 37. Levels of circulating VPEs and HBsAg were assessed from each blood sample; hepatotoxicity was assessed using samples collected on day 21.

Circulating viral particle equivalents (VPEs) were determined using quantitative real time PCR (qPCR) (Figure 2.2.6A + 2.2.7A). Animals that received the anti-HBV siRNAs demonstrated a significant decrease in viral replication (Students unpaired t-test $p < 0.05$). Animals injected with a non-targeting siRNA (LacZ) also displayed viral knockdown, however knockdown was attributed to the off-target effects of the LacZ siRNA. Treatment with saline resulted in a decrease in circulating VPEs, potentially as an effect of the administration on viral replication within the liver. This observation has been made previously using transgenic HBV mice, despite no toxicity associated with saline. Systemic delivery of naked siRNAs did not result in VPE knockdown. It has been noted that the transgenic HBV mice display

increased liver sensitivity, perhaps as a consequence of constitutive viral production. This sensitivity may impact the degree of knockdown achieved using anti-HBV and control siRNAs. The alternative marker for HBV replication and knockdown is the surface antigen HBsAg. It would appear that the knockdown of HBsAg is less marked than the circulating VPEs (Figure 2.2.6B and 2.2.7B). As the HBsAg is expressed at high levels in transgenic mice, the impact on its knockdown may be less profound in comparison to circulating VPEs. Nonetheless, knockdown of the surface antigen corroborates the knockdown demonstrated for circulating VPEs.

Serum activities of aspartate transaminase (AST), alanine aminotransferase (ALT) and lactate dehydrogenase (LDH) were assessed. These enzymes are released as a consequence of hepatocyte injury, making them useful markers of hepatotoxicity. It was found that the uncomplexed liposomes and siRNA-liposome complexes result in slightly elevated liver enzyme marker levels (Figure 2.2.8). Marker levels of AST and ALT were below 100 IU/L and LDH below 1000 IU/L, which suggested liver inflammation to be minimal.

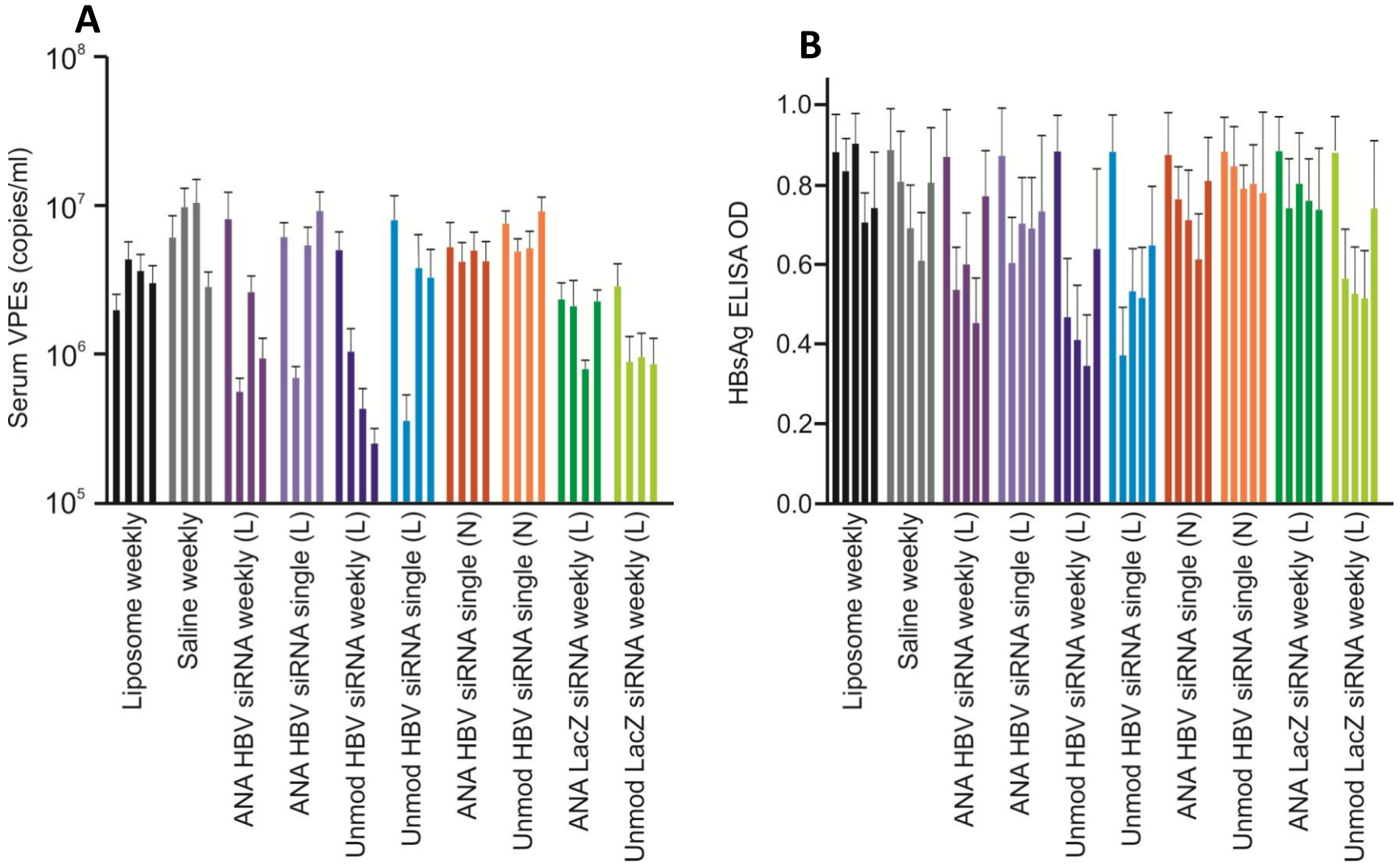

Figure 2.2.6: HBV knockdown with antiHBV siRNAs, assessed by circulating levels of viral particle equivalents (A) and viral surface anitgen (B). siRNAs were administered to mice complexed within liposomes (L) or naked (N). Each bar from left to right represents a particular time point at 0, 2, 9, 23 and 37 days after injection. Serum VPEs (A) were assesed by qPCR, and surface antigen levels by ELISA. Statistical analyses done by student t-test, n=3, SEM.

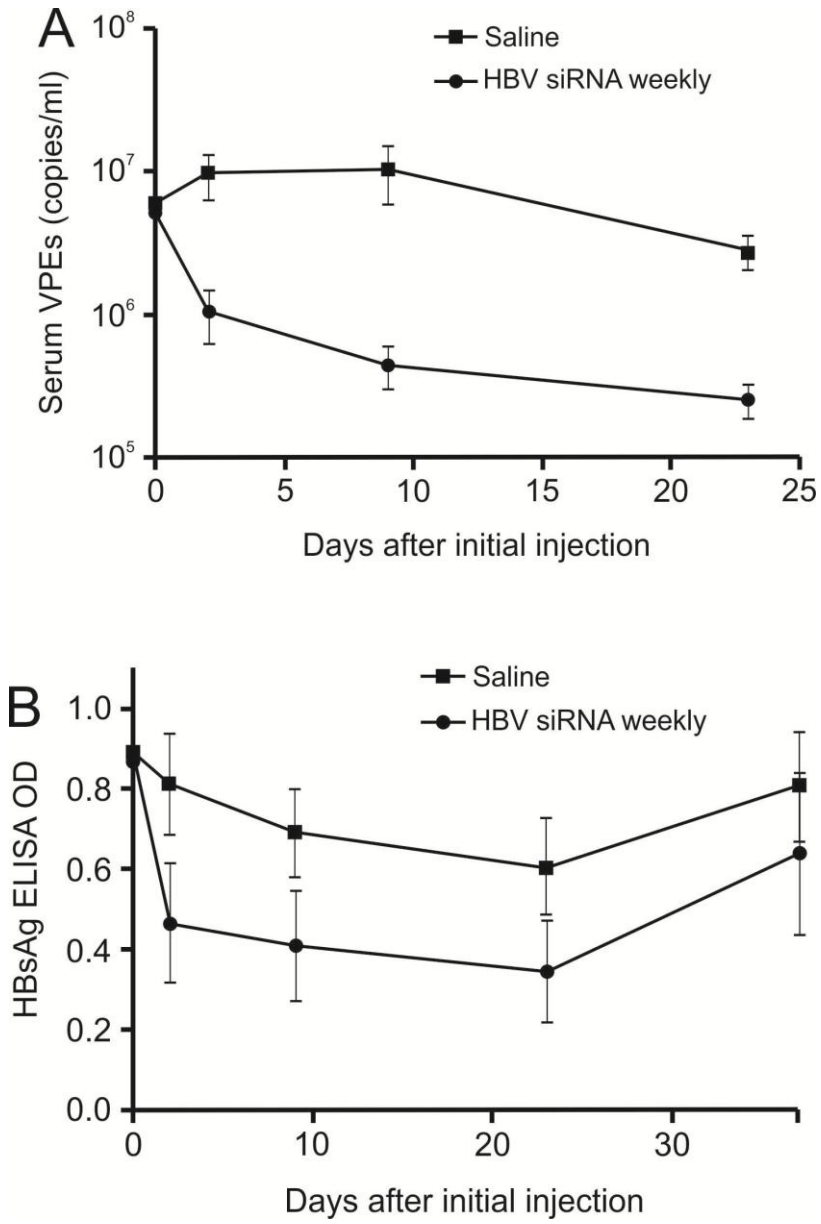

Figure 2.2.7: *In vivo* lipoplex efficiency against HBV measured by VPEs knockdown (A) and HBsAg knockdown (B). Transgenic mice constitutively expressing HBV were injected weekly with lipoplexed anti-HBV siRNAs at 1 mg per 1kg of mouse weight. Blood samples were collected by retro-orbital puncture. Statistical analyses done by student t-test, n=3, SEM.

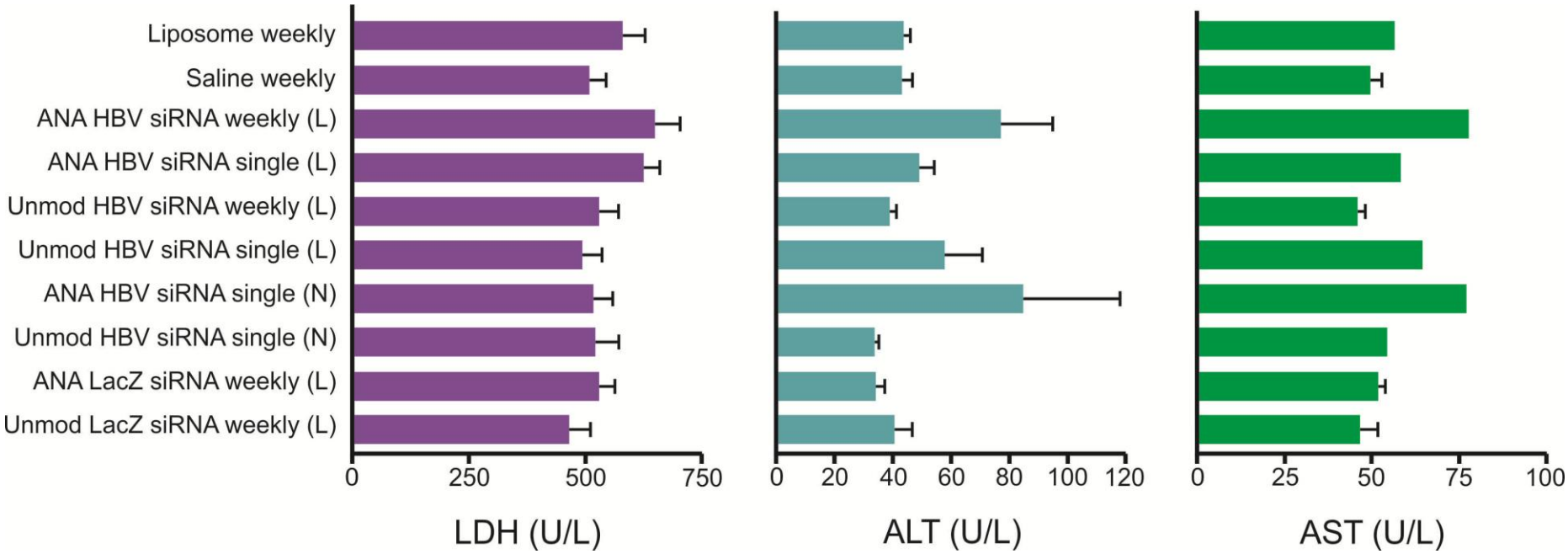

Figure 2.2.8: Assessment of hepatotoxicity by the measurement of serum liver-enzyme levels. Weekly administration of saline, liposomes, liposome-complexed ANA-siRNAs and liposome-complexed siRNAs did not increase LDH levels above 1000 IU/L and AST/ALT levels above 100 IU/L. Lipoplexed samples indicated by (L), naked (uncomplexed) siRNAs by (N). Statistical analyses done by student t-test, n=3, SEM.

2.3. Discussion

Liposome vectorology requires several considerations to produce an effective, robust and responsive nucleic acid vehicle. Every rate limiting step has to be overcome such that the DNA cargo is not cleared from circulation or within an intracellular environment. In contrast, viral based delivery systems have benefited from the effects of evolution, optimised for infection and gene transfer. Currently viral vectorology lends itself to a more efficient reliable means of therapeutic gene transfer. Despite the difficulties, the rationalised approach toward non-viral vector design and the understanding of liposome-cell interaction and trafficking will ideally produce a successful delivery candidate(s). Initially the enhancement of liposome-DNA binding could be addressed, highlighted by the stark difference between DNA binding capacity of Lipofectamine2000 and 2% SLC UnP-Gal liposomes. DC Chol is a well-established cationic lipid, however since its inception there have been more effective DNA binding lipids produced. One such example is *bis*-guanidinium-trencholesterol (BGTC), a highly cationic, compact cholesterol derivative [163]. The DNA binding capacity of liposomes must be balanced with sufficient release capacity, as DNA-bound to cationic lipid is suggested to inhibit/hinder transcription.

The data indicated that linker length of the targeting galactose ligand played an important role in DNA binding and transfection efficiency. The linker may shield the liposome surface from interaction with pDNA, thus an increasing amount of lipid was required to completely sequester pDNA. PEG polymers are known to undergo various conformations, determined by their molecular weight and concentration on the liposome surface [164, 165]. It is speculated that PEG concentrations will also affect the galactose conformation and interaction with the ASGPr, by promoting liposome surface exposure or burying it within the PEG chains (particular for LLC). It was suggested to use a short link between galactose and cholesterol (no linker as such), as it produces the most efficient transfection results in Huh7 cells (Prof. Mario Ariatti, personal communication). The inclusion of acid-labile PEG in such liposomes would improve functionality *in vivo*, however it would have to be included as a separate entity from the galactose moiety.

Transfection of HEK293 cells with MCC indicated that the presence of galactose moieties had the potential to enhance transfection efficiency. However, later studies revealed inconsistency in liposome preparation, particularly of the control liposome, DC Chol. It was noted that certain liposome preparations remained opaque after sonication. Generally the

sonication process converts the opaque lipid emulsion into a clear solution of liposomes. It was found that sonicated solutions that remained partially or slightly opaque did not transfect efficiently. These opaque solutions may not have undergone adequate sonication, resulting in a combination of liposomes and lipid emulsion. It was confirmed that the presence of galactose does indeed decrease transfection efficiency in HEK293 cells, and is not as marked as initially established in Huh7 cells (Figures 2.2.2 and 2.2.3).

The use of cell culture models to infer *in vivo* transfection efficacy of liposomal-based delivery systems is not ideal. Major contributing factors are the condition and composition of plasma that differ vastly to culture medium. This has an impact on the design of the liposome, as factors/ligands that provide function *in vivo* may hinder functionality *in vitro*. SLC UnP-Gal containing liposomes transfection efficiency is better than liposomes without galactose, however neither are as effective as Lipofectamine2000 in culture. As such, a typical *in vitro* to *in vivo* translational hurdle is highlighted. Lipofectamine2000 is known to be a poor *in vivo* transfection reagent, which does not necessarily equate to the same outcome for SLC UnP-Gal liposomes.

The field of liposome *in vivo* vectorology requires considerable improvements prior to its application being realised within a clinical setting. Nonetheless, recent research appears to have made headway in realising *in vivo* liposome-based delivery to the liver [166]. As highlighted by Wooddell *et al*, lipoplexes are able to deliver RNA to cells, a feature absent from viral-based vectors. It was demonstrated that the liposomes comprising DOPE, SLC P-Gal and the novel cationic lipid CL19 were capable of delivering siRNAs to the liver of transgenic mice. Encouragingly, lipoplex administration did not result in hepatotoxicity or immune activation despite dosage being 100-fold higher than in other studies [167]. Future improvements to the cationic head group and inclusion of the unprotected galactose ligand may result in increased RNA binding capacity of the liposomes as well as enhanced hepatotropism.

Non-viral vectors are in their infancy in development, as several cellular uptake and trafficking pathways are not completely understood. Since liposomal vector development is dependent on the elucidation of such pathways, emphasis on research of these pathways is paramount. Liposomes present with many advantages in their use as vectors for gene therapy, and will hopefully develop to a point comparable with viral vectors. The MCC compounds within liposomes show potential in increasing the transfection efficiency with

Huh7 cells compared to liposomes without. Other than liposomes, it may be possible to introduce these ligand moieties to alternative delivery particles. Virus-like particles also display potential as a nucleic acid delivery system, and could be enhanced with hepatotropic properties by including MCC compounds on their surface. Work described in chapter 3 explores the potential to modify the surface of HBV capsids (a virus-like particle) to facilitate the inclusion of MCC-like compounds on their surface. These viral structures are highly ordered and self-assemble within bacterial expression systems, making them a candidate for gene therapy vectorology.

2.4. Materials and methods

2.4.1 Formulation and lipoplexing

Lipid compounds were dissolved in chloroform as 10 mg/ml stocks and stored at -20 ^{o}C. DC Chol and all MCC compounds were synthesised by the Department of Chemistry, University of the Witwatersrand (Synthesis of compounds was performed by Dr. Rafique Islam, Prof. Charles de Koning and Prof. Willem van Otterlo). Liposomal formulations comprised 6 parts cholesterol based species and 4 parts DOPE (Avanti Polar Lipids, AL, USA) based species. Thus despite the inclusion of monosaccharide-conjugated cholesterol or DOPE-PEG, this 6 to 4 ratio remained constant. Lipids were combined to a total of 2 μmol (1.2 μmol cholesterol species : 0.8 μmol DOPE species) in a final volume of 1 ml chloroform, after which lipid films were produced in a round bottomed flask under vacuum by rotary evaporation. Lipid films were resuspended and rehydrated overnight at 4 ^{o}C in saline. Vortex mixing the subsequent morning resulted in an opaque lipid emulsion. Liposomes were generated by sonication; 50 μl of lipid emulsion was sonicated at 35 kHz for 30 minutes in a Bandolin Sonorex sonicating bath. Liposomes were used on the day generated and not stored. Plasmid DNA (refer to Appendix 3 for plasmid preparation) was lipoplexed with liposomes as a mass ratio. One microgram of plasmid DNA was incubated in 15 μl distilled water and the required amount of liposome in 15 μl saline for 10 minutes at room temperature. Both suspensions were combined and further incubated at room temperature for 20 minutes.

2.4.2 Mobility Shift Assay

One microgram of DNA was lipoplexed with increasing amounts of liposome and loaded into a 1% agarose gel containing 0.02% (w/v) ethidium bromide. Electrophoresis at 80 V in Tris-Acetate-EDTA (1 X TAE) buffer (Appendix 2) resulted in the migration of non-lipoplexed plasmids into the agarose gel. Migrated DNA was viewed using short wave ultraviolet in the G:Box gel docking system (Syngene, Cambridge, UK). A DNA to lipid ratio was determined by the complete sequestration of plasmid DNA by the liposomes.

2.4.3 Transfections and Luciferase Assays

DNA transfections were performed in the human-derived liver cell line, Huh7, and a human embryonic kidney cell line HEK293 (See Appendix 3 for culturing methods). Cells were seeded at 50% confluency in a 24 well culture dish one day prior to transfection in 10% foetal calf serum (FCS) (v/v) Dulbecco's Modified Eagle's Medium (DMEM) (Gibco, Life Technologies, CA, USA). The following morning each well received lipoplexed 100 ng pCI-eGFP [168] and 50 ng psi-Check2.2 (Promega, WI, USA) DNA in a total of 50 µl unless specified otherwise. Lipoplexing DNA to lipid ratios for transfection were determined by mobility shift assays. Lipofectamine-2000 (Invitrogen, Life Technologies, CA, USA) was used according to the manufacturer's instruction. Cells were harvested 24 hours after transfection and luciferase luminescence induced using the Dual-Luciferase Reporter Assay System (Promega, WI, USA) according to the manufacturer's instructions. Luminescence was measured in the Veritas Microplate Luminometer (Turner Biosystems, CA, USA).

2.4.4 In vivo assessment of hepatotropic delivery of liposomes in transgenic mice

All animal experimentation protocols were approved by the University of the Witwatersrand Animal Ethics Screening committee (Ethics certificate numbers 2010/10/04 and 08/24/03). Liposomes were formulated by combining SLC P-Gal, DOPE and cationic lipid 19 in a mole ratio of 8:20:11, respectively. Liposomes were generated as described in Chapter 2.4.1. Liposomes were combined with siRNAs at a mass ratio of 17:1. siRNAs were administered at a constant dose of 1 mg/kg to transgenic mice, with the volume of injectate ranging from 0.1-0.2 ml. Blood samples were collected by retro-orbital puncture. VPEs and HBsAg levels were determined by methods described previously [169].

2.4.5 Statistical analysis

All data is expressed as the mean with standard error of the mean. Statistical difference was considered significant when $p < 0.05$, determined by students two tailed unpaired t-test using the GraphPad Prism software package (GraphPad Software Inc., CA, USA).

Chapter 3: Amino acid substitutions to the immunodominant loop of the HBV capsid to generate ligand conjugation sites as a means of improving vector-like properties.

3.1. Introduction

Virus-like particles (VLPs) have shown potential as new biomaterials in fields spanning from gene therapy to metallo-organic chemistry. Appropriately, these viruses and VLPs are often termed "reactive molecular containers" within the realms of bionanotechnology. Several virus scaffolds have been developed within the field of biotechnology, derived from plant, animal, human and bacterial viruses. Included in these is a scaffold derived from the hepatitis B virus. There are several features which make the HBV capsid, VLPs and protein scaffolds attractive as catalysts and containers:

- Viruses and VLPs generally form capsid structures that are consistent in size and shape.
- Capsids can undergo engineered pleomorphism, however require chemical modification or change in amino acid composition.
- Capsids are generally amenable to amino acid modifications. Insertions and substitutions range from single amino acids up to whole protein sequences. Both the inner and outer capsid surfaces can be modified according to application.
- Certain capsids have shown stability at various environmental pHs (3-10). Recently identified thermophilic viruses have shown stability at 80 ^{o}C and pH 1. These extremophile viruses are yet to find their niche within biotechnology, however it is only a matter of time until it happens [170, 171].
- Capsids generally comprise a single/few protein species, providing a means for simple, recombinant and scalable production.
- Capsid interiors are charged to accommodate passenger nucleic acid. These cationic surfaces have also been used as catalytic metallo-nucleation sites.

The HBV capsid is associated with several of the aforementioned properties, which facilitates their generation of enhanced vector-like properties for gene therapy.

VLP applications are considerably varied; and in addition to gene therapy they vectors have been used in several interesting biochemical and biomedical applications. Protein scaffolds and VLPs present in a variety of nano-scaled shapes and sizes; icosahedron ranging from the 12 nm diameter ferritin [172] or heat shock protein cage [173, 174], to the *Paramecium bursaria* Chlorella virus type-1 of 190 nm diameter [175]. Rod-shaped virus scaffolds include the 300 nm tobacco mosaic virus (TMV) [176] and the 900 nm bacteriophage M13 [177]. Some of the virus, VLPs and protein scaffolds in development for bionanotechnology are illustrated in Figure 3.1.1. Protein scaffolds and VLPs are generally amenable to amino acid substitutions which facilitate the binding/inclusion of a large variety of molecules, such as drugs [178], antigens for vaccines [179], bioimaging markers such as nanogold or fluorophores [180, 181], immuno-evasive compounds such as PEG [45], and tropic ligands [182] (Figure 3.1.2). In addition to the internal and external surfaces, the regions between capsids subunits (such as pores) can be altered and controlled. Speir and colleagues showed that by introducing divalent metal ions to the VLPs of cowpea chlorotic mottle virus (CCMV), they could control the pores opening and closing to the environment, exposing or isolating their inner contents [183, 184]. Viruses have been manipulated and altered in a variety of ways to produce agents ranging in function from therapeutic gene delivery to catalytic nucleation sites for inorganic reactions.

This chapter focuses on the manipulation and analysis of the HBV capsid, in which particular amino acids found on the capsid surface were substituted with lysine or cysteine residues. The introduction of the new amino acid residues facilitated the attachment of functional ligands (Described in later chapters). There are several amino acid residues which have been used for ligand conjugation reactions, however this thesis focused on using lysine or cysteine as the site of functional ligand conjugation. Both lysine and cysteine are popular residues for the conjugation of functional ligands to protein surfaces. Both undergo conjugation with a reactive ligand under mild conditions, favouring protein stability. As a result of the general abundance of lysine residues within proteins, this species is often associated with multiple but random conjugation events to the protein surface. Conversely, cysteine residues occur infrequently on protein surfaces, thus are often required to be engineered in to introduce a conjugation site. In doing so a specific conjugation site is generated. Both conjugation techniques have benefits and drawbacks, discussed in detail in Chapter 4. The following sections aim to explore the functional unit of the HBV capsid,

known as the core protein or core antigen, and the potential to manipulate particular domains of the core protein in order to enhance the vector-like properties for gene therapy.

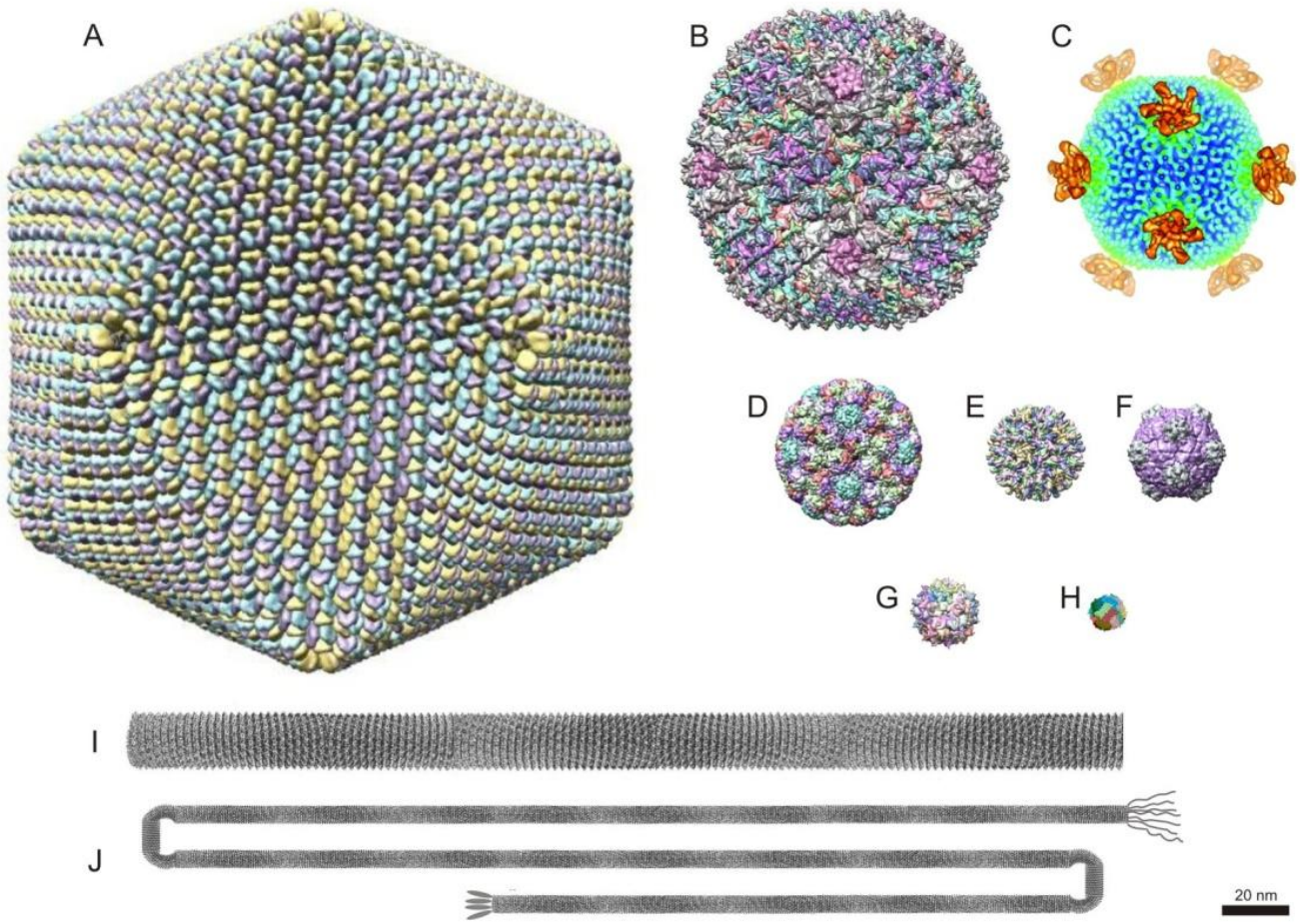

Figure 3.1.1: Structural predictions of virus/VLP/protein scaffolds with potential application in bionanotechnology. (A) *Paramecium bursaria* Chlorella virus type-1, 190 nm diameter [185]. (B) Adenovirus, 95 nm diameter [186]. (C) Sulfolobus turreted icosahedral virus, 74 nm diameter [171]. (D) Murine polyomavirus, 45 nm diameter [187]. (E) Hepatitis B virus capsid, 30 nm diameter [188]. (F) Cowpea mosaic virus, 28 nm diameter [189]. (G) Adeno-associated virus, 20 nm diameter [190] (H) Ferritin, 12 nm diameter [191] (I) Tobacco mosaic virus, 300 nm length 18 nm diameter [192]. (J) Bacteriophage M13, up to 900 nm length 7 nm diameter [177]. Figure adapted from [193].

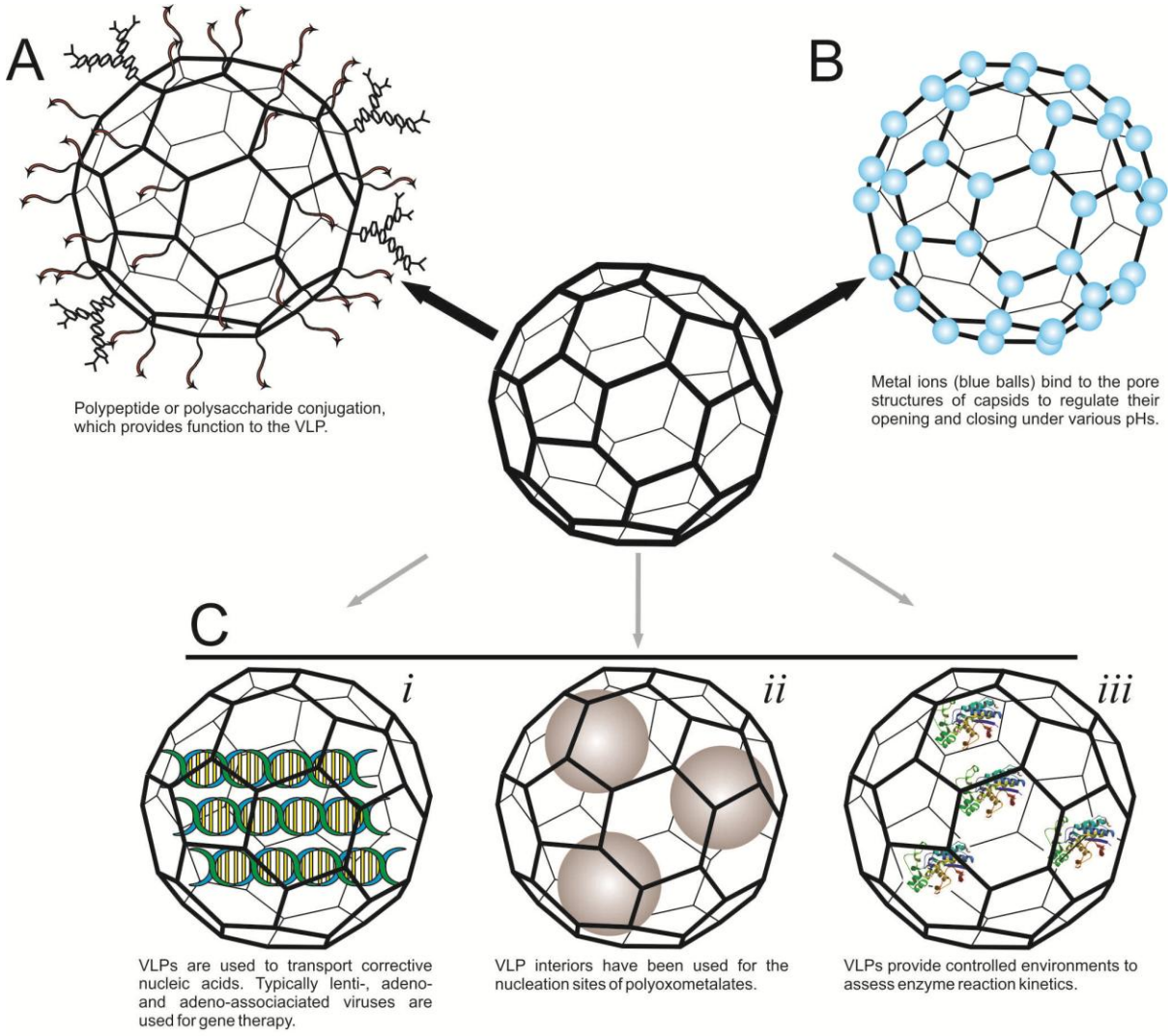

Figure 3.1.2: A schematic depiction of the VLP surfaces used for nanoplatforms and biomedicine. A) Exterior surfaces are often used for conjugation of a variety of moieties, such as peptides, polyethylene glycol or nanogold particles. B) Inter-capsid subunits form function-specific pore-like structures, which can be regulated by the presence of metal ions. C) VLP interiors have been used as molecular containers to i) transport nucleic acids ii) facilitate polyoxometalate crystal formation iii) produce isolated environments to observe enzyme reaction kinetics. Figure adapted from [193].

3.1.1 Composition of the hepatitis B virus capsid and applicability as a vector for gene therapy.

The HBV capsid has seen little development in the field of bionanotechnology as a gene therapy vector, and is perhaps better known for its use in developmental vaccines [194] and establishment of icosahedron capsid assembly kinetics [195-197]. Nonetheless, the HBV capsid does display several of the aforementioned VLP properties and also includes useful features such as:

- Simplicity of expression and construction - *E. coli* expressed recombinant core proteins auto-assemble into capsids.
- The "display" region (immunodominant loop) of the capsid is situated on the tip of tetra-α-helix bundles protruding from the capsid surface, which tolerate amino acid substitutions and insertions well. This highly exposed region is an ideal position for antigenic proteins in vaccine development and conjugation based reactions for the addition of immuno-evasive and tissue-tropic ligands.
- The capsid interior is highly cationic, however recombinant capsid formation is not dependent on the presence of these C-terminal protamine motifs.

The HBV capsid is formed by a single species of protein, hepatitis B core antigen (HBcAg). The core antigen comprises 183 amino acids, has a molecular weight of approximately 21kDa and is composed of 55-60% α-helices [198]. This was an unusual discovery, as the majority previously elucidated viral core proteins predominantly contained eight-stranded β-barrels [199]. This uncommon α-helix structure was supported by other researchers, and later confirmed by Wynne and colleagues through the analysis of the crystal structure of HBcAg/core particles [200, 201]. The various predicted and determined secondary structure distributions within the HBcAg are illustrated in Figure 3.1.3. The HBcAg is predicted to contain five major α-helices, in which helix α3 and α4 fold at a hairpin loop and form a spike-like structure, illustrated in Figure 3.1.4 [201]. Much of the HBcAg is stabilised by hydrophobic interactions. The core of the HBcAg is stabilised by highly conserved hydrophobic residue interaction between α1, the α1-α2 connecting loop, α4b and α5 [201]. Similarly, the interaction between α3 and α4 is stabilised by interhelical hydrophobic forces. The hairpin loop region formed between α3 and α4 contains a non-helical immunodominant loop (IL), which forms the distinct conformational HBcAg epitope (also

known as e1) located between residues 78-83 [202, 203]. The IL is well exposed at the capsid surface and is amenable to amino acid (aa) insertions and substitutions [202, 203] (described in detail in later sections).

The HBcAg is divided into three main domains, comprising the core (aa 1-140), linker (aa 141-149) and protamine domains (aa 150-183). The core domain forms the bulk of the HBcAg and capsid structure. It is capable of assembly into homodimers and the complete capsid without presence of the linker and protamine domains [93]. The linker domain has no apparent defined structure and is responsible for connecting the core and protamine domain, providing flexibility to the protamine domain within the capsid interior. The protamine domain contains four arginine-repeat motifs, two of which comprise three arginine residues, the other four arginine residues, resulting in a highly basic domain necessary for binding of viral DNA and RNA. Furthermore, three of the four repeat motifs comprise the sequence SPRRR, in which the serine residues are an important site for phosphorylation. It is generally accepted that the protamine domain is unstructured, and supported by the secondary structure prediction algorithm, Phyre^2 [204]. Core proteins without the arginine domain (c149) were assembled into capsids and used in several pioneering studies to observe icosahedral capsid assembly kinetics and mechanisms. The c149 capsids were morphologically similar to the wild type counterparts (which contain full length core protein, c183), however did not bind and encapsidate RNA, an additional factor which may have complicated the kinetic observations and calculations [196, 205, 206].

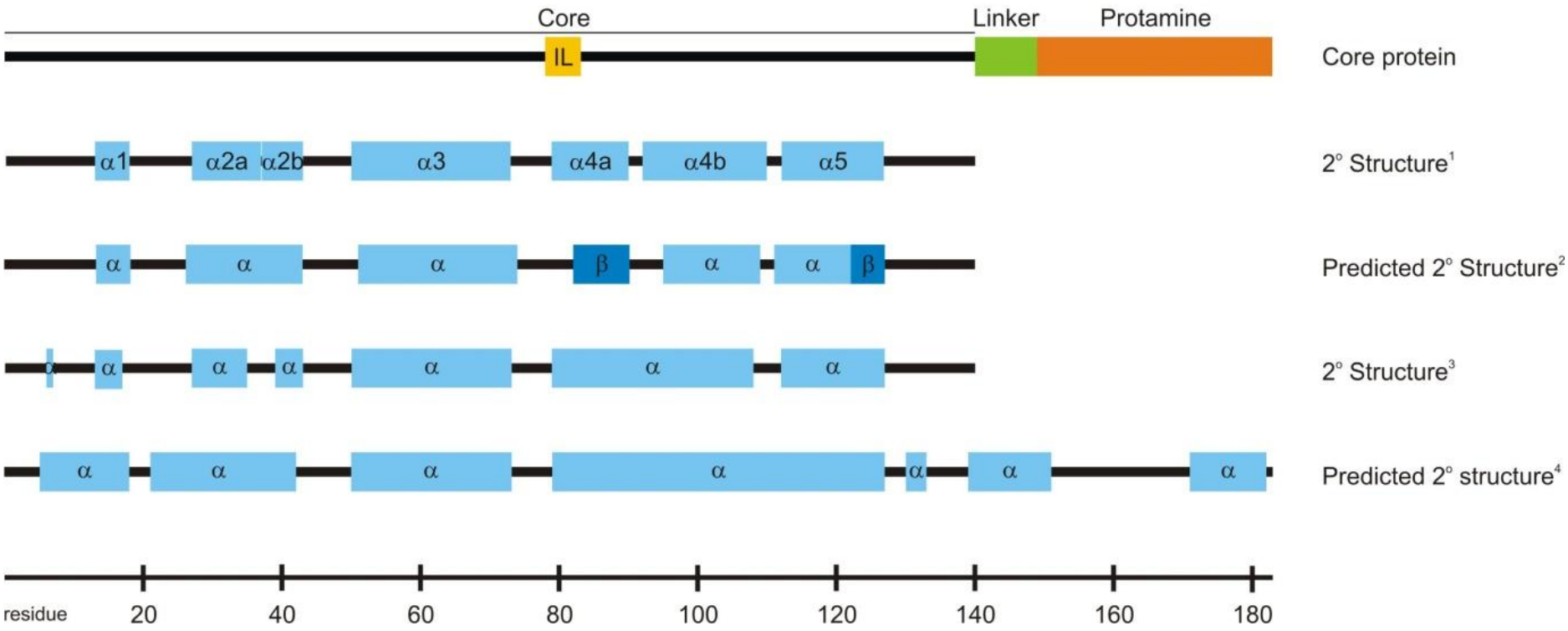

Figure 3.1.3: The predicted and determined primary and secondary structure of the hepatitis B virus core protein. The core domain (aa 1-140) forms of the bulk of the structured protein. The immunodominant loop is present from the amino acid residues 78-83 (yellow). The linker domain (aa 141-149) is highlighted in green and protamine (aa 150-183) domain in orange. Secondary structural distribution determined by crystallography by Wynne *et al.* (1) [201] and Swiss PDB entry (3) [201]. Predicted secondary structure by Bringas *et al.* (2) [200] and by the Phyre^2 algorithm (4) [204]. The α-helices from residues 140-183 determined by Phyre^2 were predicted to have a high probability of disorder. Figure adapted from [207].

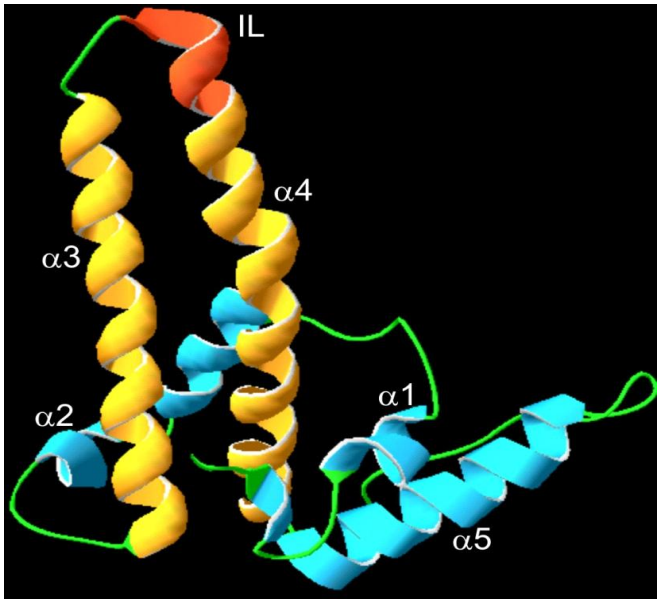

Figure 3.1.4: The predicted structure of HBV core protein. Five α-helices are present within the core protein, of which α3 and α4 associate to form a spike-like structure (yellow helices). Helices α1, α2 and α5 are involved in capsid stabilisation and inter-dimer interactions. The immuno-dominant loop (IL) is highlighted in red. Green lines represent connecting unstructured regions within the protein. Protein structure modelled in Swiss-PDB Viewer [214] using data from Wynne *et al* [201].

Core proteins naturally associate to form homodimers, and rarely exist as individual units. The homodimer is stabilised by the hydrophobic interaction of the two helical hairpins, α3 and α4, forming a four-helix bundle. Wynne and colleagues have reported that the helical hairpins are highly amphipathic, and as much as 63% of their surface is buried in a hydrophobic interaction within the four helix bundle [201]. The four-helix bundle contains a single disulphide bridge, created by the Cys61 residue from each monomer [208]. The dimer has almost two-fold symmetry, illustrated in Figure 3.1.5.

Capsids assemble from HBcAg into icosahedral particles of approximately 30 nm in diameter, with the four-helix bundles protruding 2.5 nm from the surface [201]. The capsids assemble into two conformations with triangulation numbers of *T*=3 and *T*=4. Both have been expressed *in vitro* and isolated from patients [209]. This is unusual as most viruses have a single unique *T* number that remains conserved amongst even distantly related viruses [210]. Initial studies indicated that c149 and c183 assemble into both *T*=3 and *T*=4 conformations [209], however it was later established that c183s have a propensity to form *T*=4 capsids [211]. In a *T*=3 conformation a capsid comprises 90 dimers (180 HBcAg), whereas in *T*=4 conformation 120 dimers (240 HBcAg) make up the capsid. Dimers pack

predominantly in a quasiequivalent manner around both two-fold and five-fold axes, as illustrated in Figure 3.1.6 [212, 213].

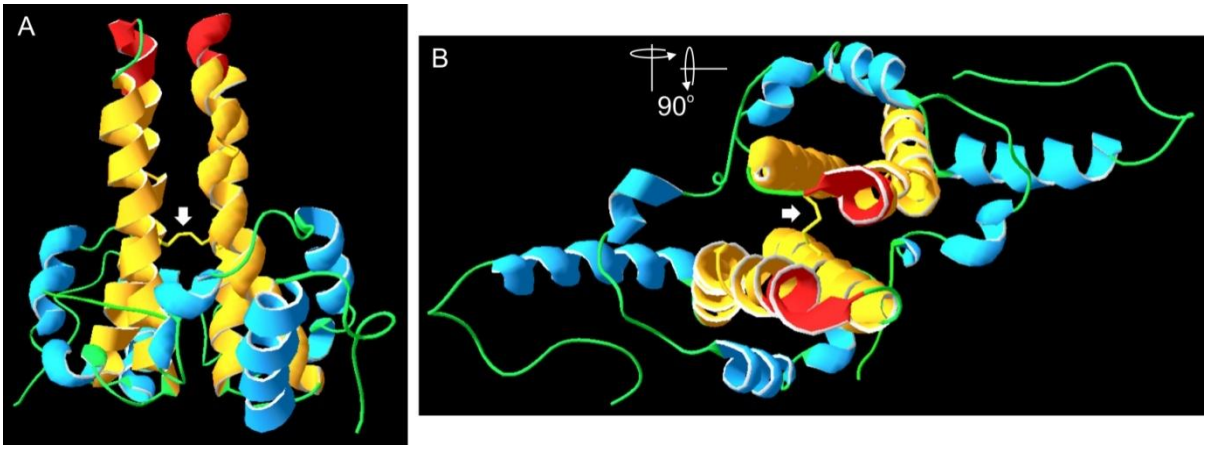

Figure 3.1.5: Homodimer of the truncated HBV core protein (c149). A single disulphide bridge is created by the Cys61 residue from each monomer indicated by the white arrow. The colour-scheme is similar to that of Figure 3.1.2. Protein structure was modelled in Swiss-PDB Viewer [214] using data from Wynne *et al* [201].

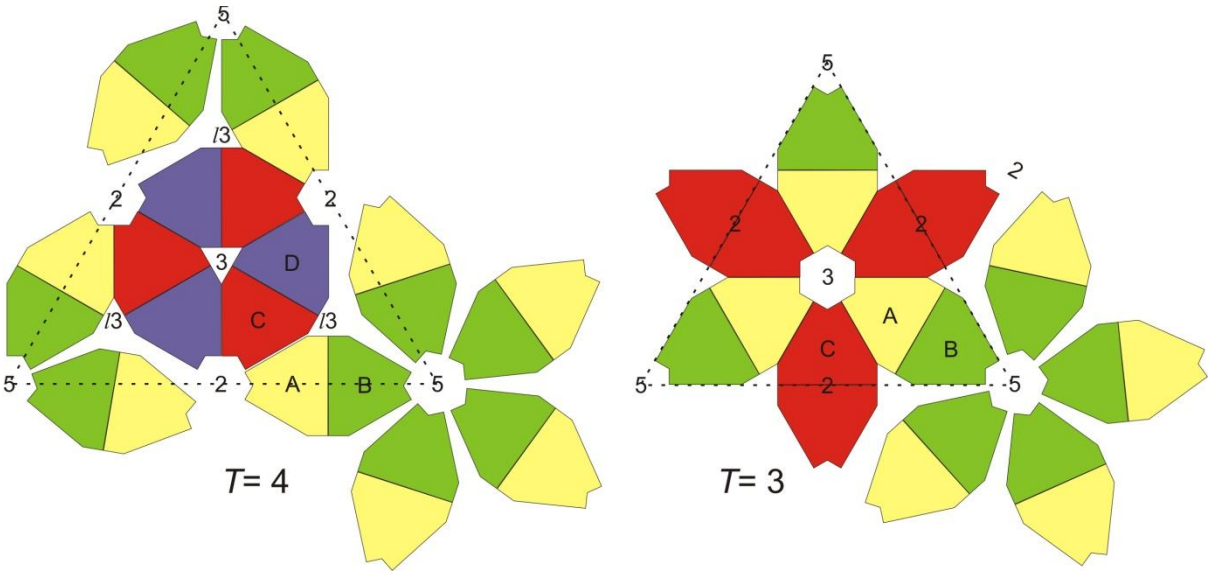

Figure 3.1.6: Schematic representation of the icosahedral symmetry of the HBV capsid in *T*=3 and *T*=4 conformation. Each independent subunit of a dimer is indicated as either A, B, C or D. Subunits are identical and associate as dimers, AB, CD or CC, depending on capsid conformation. Colour scheme of dimers indicates icosahedral faces or pentamer units on the capsid surface. One icosahedral face is represented by the dotted triangle, containing the two-, three- and five-fold symmetrical axes. Capsid pores are contained within these axes. The *T*=4 capsid contains 120 subunits, comprising 60 AB and 60 CD units. The *T*=3 capsid contains 90 subunits, comprising 60 AB and 30 CC units. Both capsid conformations have been illustrated in a two dimensional plane. When displayed in a three dimensional space (i.e. spherical), the spacing between subunits decrease significantly while pores retain their size. Figure adapted from [201, 215].

Dimer-dimer interactions mainly occur between the two- and five-fold axes of symmetry of the capsid [201]. As with the four-helix bundle, these interactions are mostly stabilised by weak hydrophobic interactions [197]. Residues from helix α5, aa 128-136 and aa 137-142/3 primarily stabilise inter-dimer interactions. The residue Tyr132 plays a crucial role in capsid formation, burying itself within a pocket formed by Pro20, Asp22, Phe23, Phe122, Trp125, Ala137, Pro138, Ile139, and Leu140 of an adjacent subunit [216]. In doing so, Tyr132 is locked into place by an adjacent dimer pocket. This arrangement occurs throughout the capsid, contributing to the stability of the structure.

The capsid contains pores around the icosahedral two-, three- and five-fold axes with diameters ranging from 12 to 15 Å [201]. The three-fold and quasi three-fold pores comprise the polar residues D2, K7, R39, E40 and E43 [201] (Figure 3.1.6). It is suggested that these pores allow for the shuttling of components required for reverse-transcription during virion maturation as well as the release of degraded RNA template monomers. Several researchers have established that the internalised protamine domain is able to protrude on the capsid surface via the pores. Residues from Glu145 to Cys183 have been identified to be exposed on the capsid surface [217]. This exposure is thought to promote phosphorylation of the C-terminus domain serine residues by cellular kinases, which play a role in nuclear uptake of the capsid and aid in dissociation from the viral nucleic acid sequence [218].

Curiously it would appear that the most exposed region of the capsid, the IL, plays no direct role in the interaction with HBV envelope surface proteins. Studies conducted in which the IL was bound by protein aptamers resulted in poor virion formation. Thus it was suggested that the IL is involved in surface protein (preS2) interaction [219]. However Koschel and colleagues report that this is a consequence of steric hindrance between surface and core proteins over direct inhibition of interaction. [220]. They suggest rather the residues between capsid spikes involving the residues A11-V13, R133-P155 and L140-S141 are responsible for interacting with the surface protein domain. Typically the surface protein domain is exposed at the endoplasmic reticulum, the initial site for HBcAg and surface protein interaction.

The HBcAg has been identified to contain two major epitope sites. These epitopes are shared with a structurally similar protein, hepatitis B e-antigen (HBeAg). The HBeAg open reading frame overlaps with the HBcAg, however the N-terminus contains an additional 10 starting amino acids. Consequently the HBeAg is unable to form capsid-like structures. The

first shared epitope of the two proteins is the IL on the tip of the protruding dimer spike (aa 78-83 – e1) which is highly exposed on both the HBcAg and HBeAg. The second antigen is within a non-helical region (aa 128-133 – e2) that becomes buried upon capsid formation, however remains exposed with HBeAg [202, 203, 221]. Several other epitopes have been mapped, of which the majority are in the region of the IL, the remainder straddle the interface of adjacent dimers [222-224]. Capitalising on the immunogenic properties, researchers in the early 1980s identified the HBV capsid as a candidate for fusion-protein-based immunostimulation. The HBcAg tolerated the insertion of peptides and exogenous proteins at the N- and C-termini, while allowing for the formation of stable core particles. It is suggested that the polymeric nature and strong immunogenic response of the capsids enhanced the immunising effect of fused/conjugated exogenous peptides/proteins [225, 226]. It was later shown that HBV capsids bind directly to naive B cells, promoting a profuse production of anti-core antibodies [227]. The capsids carrying the fusion peptide/protein sequence induced the formation of antibodies against the capsid and fusion sequence [228, 229]. Interestingly it was found that the terminal positioning of the antigens did not stimulate an immune response as prolific as the one against the core particle itself. With insertion of the peptide antigen into the predominant core epitope, e1 (within the IL), Brown and colleagues established a tenfold increase in immunogenic response when compared to terminal fusion species [225]. Subsequently, a large number of studies have incorporated a wide variety of antigens into the IL, well reviewed by Pumpens and Grens [230].

Ultimately, the display of a whole antigenic protein would produce the most comprehensive vaccine. Insertion was only possible with the elucidation of the HBV core protein structure, after which several whole proteins were inserted into the IL. Pioneering work by Kratz and colleagues indicated that whole protein insertion into the IL was tolerated by capsid formation, provided the core protein and core dimer structure were not disrupted [179]. With the inclusion of short linker sequences between the IL region and the termini of eGFP, it was possible to express capsids with functional eGFP displayed on the surface. Inclusion of whole proteins within the IL was applied to the outer surface of lipoprotein A (OspA) of *Borrelia burgdorferi*, the agent responsible for Lyme disease [231]. Recombinant particles containing OspA were produced ineffectively as a result of the poor core protein formation. The OspA protein is oblong in shape, with the N- and C-termini

located on opposite ends of the structure, preventing correct association between core helices α3 and α4. This obstruction was overcome by the introduction of a protease cleavage site near the IL region, in which cleavage removed any strain associated with HBcAg formation [232]. Alternatively, the core protein has also been expressed as two halves, either the N- or C-termini "half" (or both) with an exposed exogenous protein in place of the IL [233]. Both the IL cleavage and Splitcore systems assemble correctly, which in turn allows for correct dimer association and ultimately capsid formation. Common modifications to the core protein IL are illustrated in Figure 3.1.7.

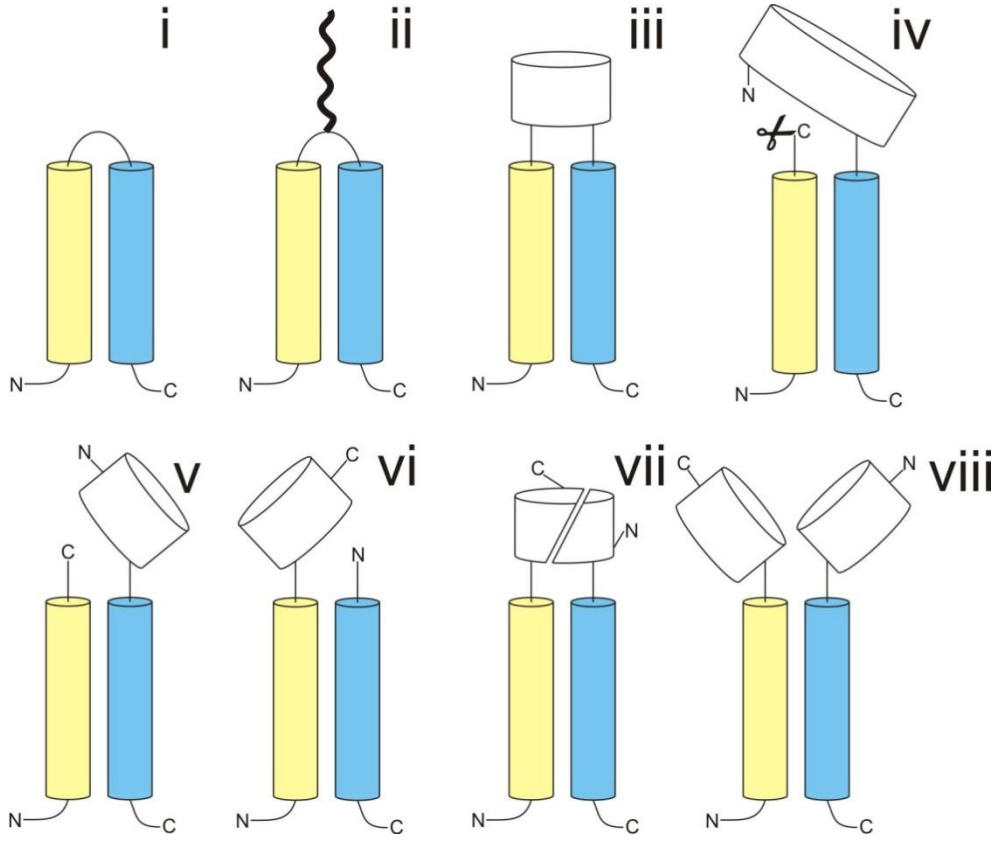

Figure 3.1.7: Schematic illustration of methods used to introduce bulky whole antigens/ligands to the spike apex (IL) of the HBV core protein. (i) Conformation of wt α3 and α4, linked by the IL. (ii) Insertion of an amino acid residue into the IL facilitating the conjugation of ligands such as PEG. (iii) Insertion of eGFP into the IL, facilitated by linker sequences [179]. (iv) Insertion of whole antigens with remote termini, facilitated by site directed protease cleavage [232]. (v, vi + viii) N and C termini expressed separately still form stable core proteins. Whole antigens can be included with the N- or C-terminal region, or both [233]. (vii) N and C termini of core protein expressed separately, each with an attached portion of protein domain. Formation of whole core protein allows for the reconstitution of attached antigen. Figure adapted from [233].

Aside from vaccine development, HBV recombinant capsids have also been used as vectors for gene therapy. Choi and colleagues developed a modified capsid vector with a RGD motif targeting integrin within the IL and replaced the cationic binding domain with p19 binding protein [98]. Despite establishing siRNA delivery to cultured B16F10 cells, Choi did not determine whether the capsid uptake was specific or indiscriminate. Furthermore, capsid uptake resulted in trafficking to the lysosome for degradation. Paradoxically, by replacing the protamine domain with a RNA binding domain, capsids lost their nuclear localisation signal [234, 235]. Despite bound siRNAs being predestined for cytoplasmic activity, avoidance of lysosomal clearance would optimise the efficacy of this modified vector. In a follow up study, Choi and colleagues tested the *in vivo* tumour targeting capacity of capsids containing the RGD motif [236]. Capsids were still significantly taken up by the liver without apparent explanation. Further investigation is required to determine the capsid uptake, intracellular fate, and effects of modification on the capsid surface with regards to cellular processing, trafficking and capsid content release. According to Cooper and Shaul, HBV capsids are indiscriminately taken up by a variety of cell lines [99]. Cellular uptake of capsids has been described to occur by various mechanisms. Cooper and Shaul found the Rab5 GTPase clathrin-mediated pathway to be responsible [237], whereas Choi and colleagues later identified clathrin-, caveolae- and macropinocytosis-mediated pathways involved in capsid uptake [98].

The HBV capsid requires tissue tropic properties to become a useful agent for nucleic acid delivery. Apart from the motif insertions done within the IL, single amino acids may also be substituted to facilitate site specific ligand conjugation. Two amino acid residues have played important roles in the conjugation of ligands, namely lysine and cysteine. Both lysine and cysteine residues have successfully been used to conjugate ligands to cowpea mosaic virus and adenovirus in *in vitro* [94, 238] and *in vivo* applications [45, 239]. This chapter compared the effects of residue substitution into the IL of HBcAg on the formation of capsids and their physicochemical properties. The IL sequence, DPASRD, displays an overall negative electrostatic charge in physiological conditions. The following work describes that disruption of the wild type IL charge with cationic residues can have an impact on capsid yield. Amino acid substitutions to the IL which had little or no impact on the electrostatic potential did not disrupt capsid formation and expressed similarly to wild type variants.

3.2. Results

3.2.1. Generation of HBV capsid library with modifications to the protamine domain.

The HBV capsid is able to withstand modifications to the protamine domain without having an impact on assembly. Two major variants are well described in the literature, c149 and c183 (wild type). c149 comprises the core domain and the linker region, and has the entire protamine domain removed. It was described that the removal of the linker region is also possible, resulting in c140 which still assembles into capsids. In addition to the aforementioned variants, this study generated two additional mutants, in which the length of the protamine domain was varied. c160 contains the first eleven amino acids of the protamine domain, in which two arginine rich motifs are present. c170 contains a further ten amino acids and an additional arginine rich motif. The various protamine domain clones are schematically described in Figure 3.2.1.

Figure 3.2.1: Protamine domain of HBV capsid variants c140, c149, c160, c170 and c183. c140 does not contain a linker or protamine domain, whereas c149 contains a linker domain. The clones c160 and c170 contain two and three arginine rich motifs, respectively (red). c183 is the full length of wild type HBV core protein.

3.2.2. Capsid yield is impacted by the position of lysine residue substitutions within the immunodominant loop

Two HBcAg IL variants were initially generated, a 15 amino acid Gly-Lys substitution, the other containing two lysine substitutions – D78K S81K, illustrated in Figure 3.2.2. The cloning procedure to generate these mutants was challenging, and several difficulties were encountered in the planning and generation of mutant clones. The first mutant, termed LinkedLys, substituted P79A80 with the amino acid sequence GGGGKGKGKGKGGGG, in which four lysine residues would be exposed at the IL tethered by flexible glycine residue linkers. Immunodominant loop flexibility provided by the glycine residues was thought to be required as the repulsive electrostatic forces brought about by the excess lysine residues may have impacted on monomer folding and dimerisation. PCR amplification to generate clonal variants produced single DNA fragments of anticipated size during agarose electrophoresis (data not shown). However, through sequence analysis of LinkedLys clones, deleterious mutations in the IL region were revealed, illustrated in Figure 3.2.3. It is possible that the repetitive nature of the LinkedLys insert (5'-GGAGGAGGAGGAAAGGGAAAGGGAAA GGGAAAGGGAGGAGGAGGAGGA-3') compromised the fidelity of the polymerase during the PCR or within host *E. coli*. Further investigation of the LinkedLys clones was not pursued. It was reasoned that varying the 15 amino acid sequence with additional or less glycine and lysine residues or interchanging their various triplet codons would be time consuming, and would not guarantee improved cloning outcomes.

Several protocols describe the purification of recombinantly expressed HBV capsids. Comparison of the protocols revealed duration and complexity had a direct effect on capsid yield. Shorter protocols were often more crude, however yielded higher levels of capsid, whereas increased stages of capsid refinement removed bacterial contaminants but also decreased overall yield. The large capsid size (±4 MDa) in comparison to other bacterial components allowed for many of the purification steps to rely on size-based exclusion. One of the first attempted protocols relied on the separation of the capsids from other bacterial contaminants using sucrose-based density centrifugation. This was the crudest attempted method, as it only utilised a single purification step after bacterial lysis. The end step capsid product often contained several additional contaminants, which would considerably complicate downstream analyses if not removed. Thus a second purification protocol was attempted (Protocol 2), which excluded the sucrose gradient however included ammonium

sulphate precipitation of the capsids followed by size exclusion-based chromatography (SEC). This protocol resulted in removal of majority of the bacterial contaminants however their levels were high enough to necessitate further investigation of alternative purification methods. The last purification protocol (Protocol 3), relied on pelleting of the capsids by centrifugation overnight, followed by two SEC steps. The final polishing step involved sucrose gradient based centrifugation of the capsids. This final protocol had the longest preparation time, however capsid purity was much improved when compared to the previous protocols described. The first protocol however, is not without use and was often employed to assess expression levels of newly cloned recombinant capsids. Capsid purity was often assessed using agarose gel and denaturing polyacrylamide gel electrophoresis. As a result of the non-denaturing environment of the agarose gel, DNA ladder markers were used to indicate the migratory position of intact capsids (up to 4 MDa). This is purely a means to reference relative migratory position as both capsid size and charge influence its electrophoretic mobility.

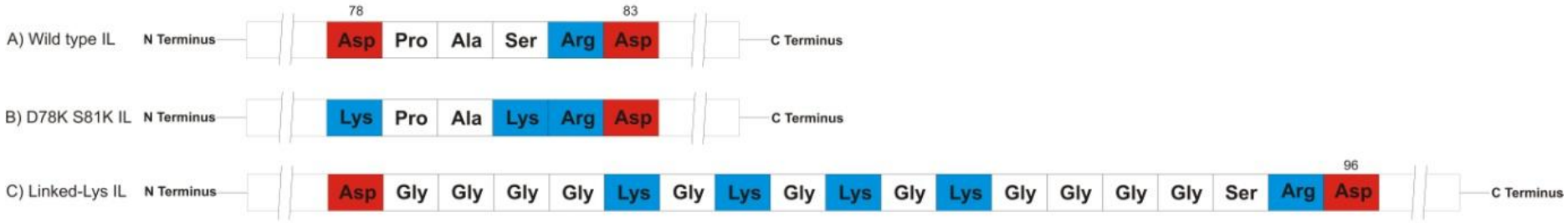

Figure 3.2.2: Amino acid sequence of (A) wild type, (B) D78K S81K core mutant and (C) LinkedLys core mutant IL. Red and blue boxes are associated with negative and positive residue charges at physiological pH, respectively.

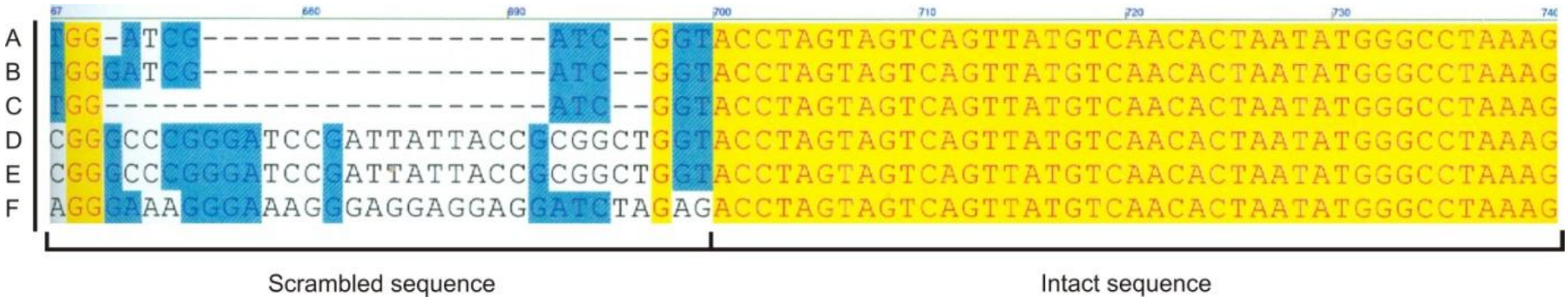

Figure 3.2.3: Sequencing results of various LinkedLys clones (A-E). All clones contained mutations to the IL region in comparison to the anticipated sequence (F).

Recombinant protein expression of a successfully cloned pET-c149 D78K S81K yielded undetectable amounts of capsid. Expressed capsids were separated from the majority of cellular debris by sucrose gradient centrifugation. Gradient fractionation and analysis by agarose gel electrophoresis and SDS-PAGE revealed no detectable expression of c149 D78K S81K protein (Figure 3.2.4 and 3.2.5). This was found to be true for all the clonal variants (pET-c149 - pET-c183) of D78K S81K. Several attempts were made to re-clone the mutant capsids, however all resulted in poor core protein expression. Introduction of basic residues into the IL may have resulted in a variety of new undetermined protein-protein interactions, perhaps resulting in core protein sequestration, degradation or precipitation. It was thus reasoned that any further substitutions into the IL should cause as little disruption as possible, without any major changes in electrostatic potential. Generation of the lysine recombinant HBcAg species was time consuming and laborious, thus to avoid future difficulties a simpler means to generate mutations within the IL was developed.

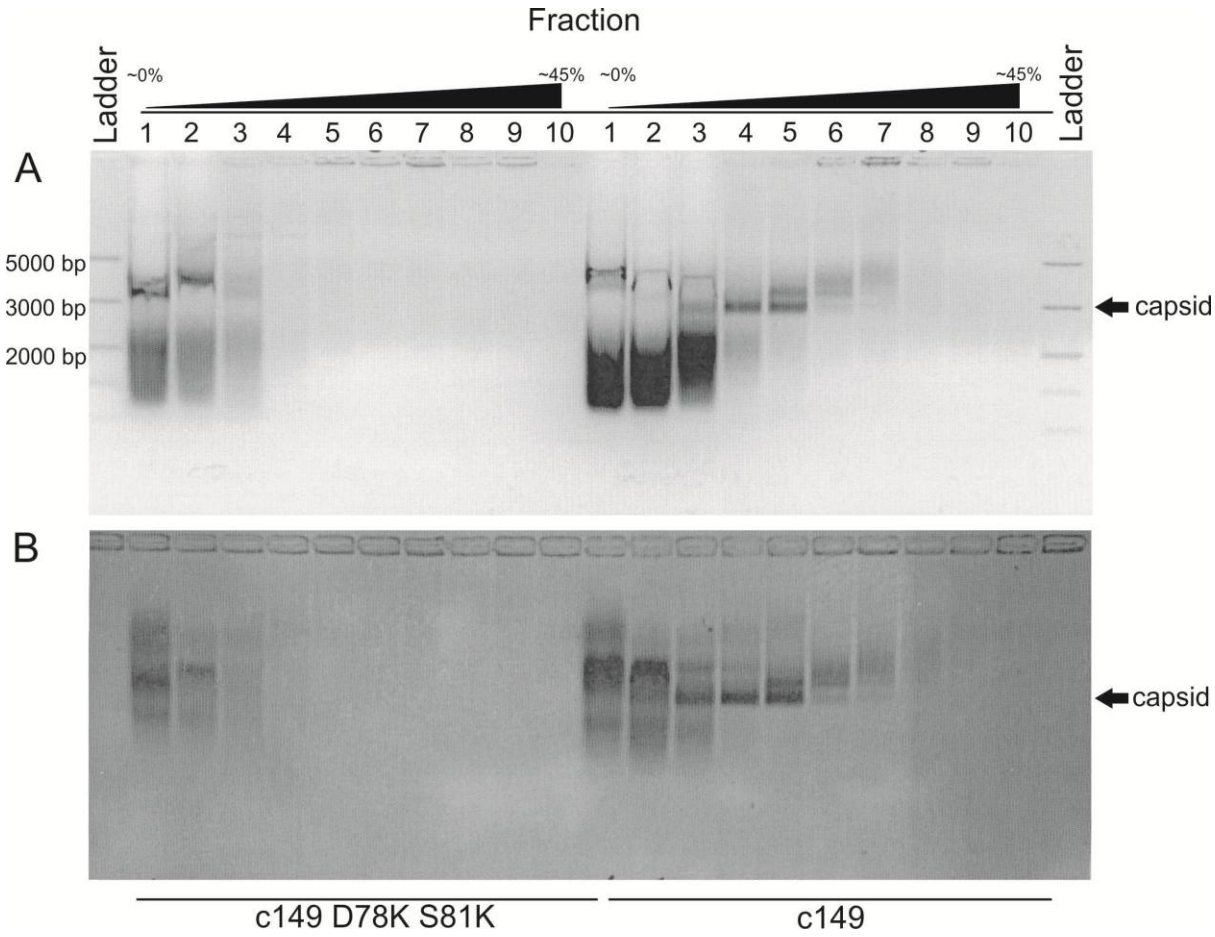

Figure 3.2.4: Preparative core protein distribution within a 10-60% sucrose gradient separated by 1% agarose gel-based electrophoresis. Sucrose gradient fractions (1 to 10) were loaded from lowest (±0%) to highest concentration (±45%). A) Ethidium bromide staining of passenger mRNA within c149 revealed capsid within fractions 3-5, just below the 3000 bp point (black arrow). No capsids appear present for the c149 D78K S81K preparation. B) Capsids stained with Coomassie Brilliant Blue-R250 similarly appear in fractions 3-5 for the c149 preparation (black arrow), however are absent from the c149 D78K S81K preparation.

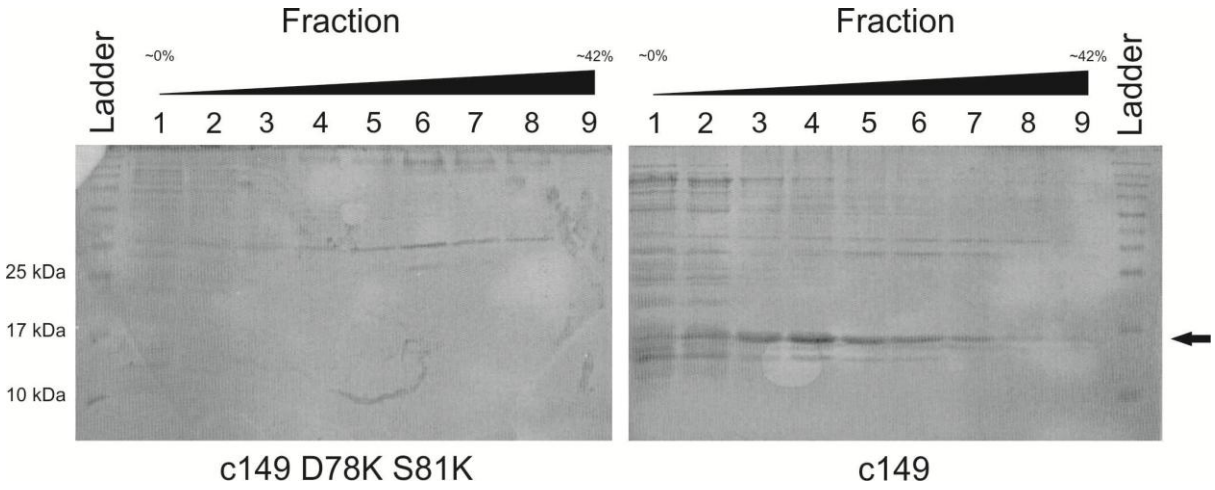

Figure 3.2.5: Core protein distribution within a 10-60% sucrose gradient assessed by 15% SDS-PAGE. Fractions (1 – 9) were loaded from lowest (±0%) to highest (±42%) sucrose concentration. Coomassie Brilliant Blue R-250 stained core proteins migrate near 17 kDa, indicated by the arrow. The c149 preparation contains core protein in fractions 3-6, whereas c149 D78K S81K contains undetectable levels of the mutant core protein.

3.2.3 Development of the core 'Snap-in' system as a means to simplify cloning into the IL region.

Specific mutations to the IL have proven difficult to engineer using canonical cloning methodologies. The IL region contains little to no conventional restriction sites, complicating the process of fragment (double stranded oligonucleotide or PCR product) insertion and ligation. Consequently an alternative, simple and universal cloning method was developed to insert any desired DNA fragment into the IL encoding region.

The cloning system relied on the use of directional non-palindromic type IIS restriction enzymes [240]. The cleavage process ensured complete removal of the type IIS restriction enzyme recognition site and generated unique overhangs facilitating fragment insertion in the correct orientation. The overall process to generate the 'Snap-in' cloning system is explained diagrammatically in Figure 3.2.6. The recognition site for the type IIS restriction enzyme *BbsI* (5'-GAAGAC-3') was introduced in two sites, each within the IL region. A single treatment with *Bbs*I would cause cleavage at sites flanking the region encoding the IL, thus result in a backbone with unique sticky overhangs which could accommodate virtually any insert. In doing so a simple and effective system to alter the region encoding the IL was generated. Type IIS restriction enzymes have been used in other studies (intron cloning [241] and TALEN generation [242]) however is the first time it has found practical use in the generation of whole HBV capsid variants. This system is applicable beyond single amino acid substitutions, and could be applied for whole antigens.

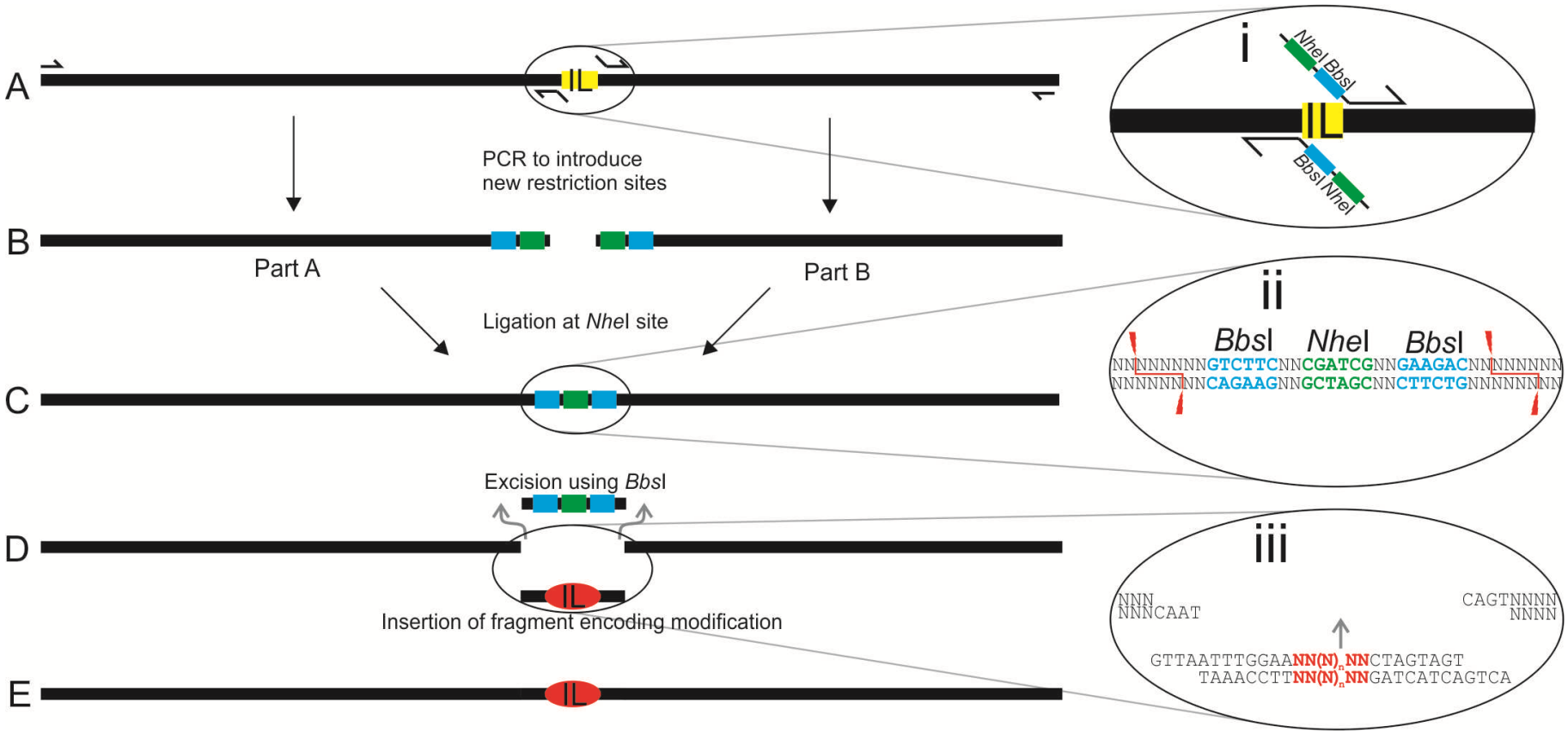

Figure 3.2.6: Schematic representation of the generation and application of the HBV core 'Snap-in' system. (A) The core ORF was amplified by PCR into part A and Part B using core specific primers in two separate reactions. Primers that directly flanked the IL encoded two additional restriction enzyme sites, *Bbs*I and *Nhe*I (i). (B) The *Nhe*I site common to both fragments was cleaved with *Nhe*I, the remaining sticky ends used to reconstitute the core "Snap In" system. (C) The 'Snap-in' cloning system contained a central reconstituted *Nhe*I binding site, flanked by two *Bbs*I binding sites. Treatment with the *Bbs*I restriction enzyme resulted in directional cleavage, which generated a unique 4 nucleotide 5' non-complementary overhang (ii and iii). (D) Any remnants of the *Bbs*I and *Nhe*I region are completely excised, and can be replaced with a double stranded oligonucleotide of approximately 40 nucleotides in length that reconstitutes the IL (which provides any required insertions/substitutions) (iii). (E) Region encodes modified IL.

3.2.4. Introduction of lysine and cysteine residues into the IL with minimal impact on electrostatic potential

Previous substitution of charged amino acids within the IL appeared to have an impact on capsid yield after expression. As such, follow up substitutions were designed to have minimal impact on capsid charge, morphology and assembly. As opposed to the cumbersome cloning methodology previously employed, the novel 'Snap-in' system allowed for quick and simplified generation of each substitutional variant of recombinant clones c149 to c183. Lysine residues were inserted into position R82 or A80 and R82, resulting in clones R82K and A80K R82K respectively. Similarly, cysteine residues were substituted into positions S81 or L76 and S81, which generated clones S81C and L76C S81C, respectively. The substitutions within the IL region are schematically represented in Figure 3.2.7. The lysine and cysteine residue substitutions into the IL did not appear to significantly impact on core protein expression. Crude extracts of bacterial lysates were subjected to sucrose-gradient based centrifugation and analysed by SDS-PAGE. A large proportion of the proteins in the lower fractions (5-8) were predominantly HBV core (Figure 3.2.8 and 3.2.9). All fractions contain capsid however the later fractions contain less bacterial protein contaminants.

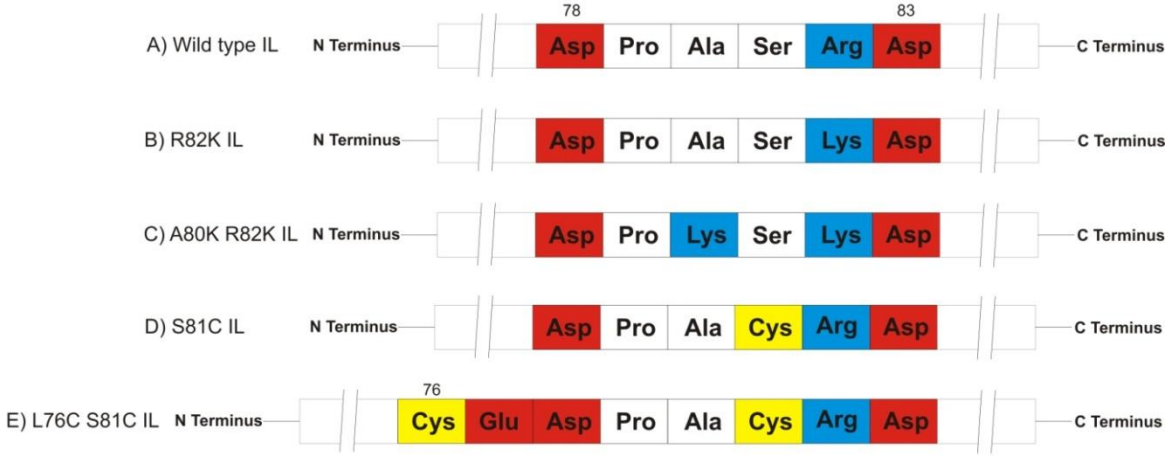

Figure 3.2.7: Illustration of the amino acid sequence of the IL region containing engineered lysine and cysteine substitutions. (A) Wild type IL amino acid sequence. (B, C) Substitution of lysine residues into positions R82 or A80 and R82. The second lysine substitution replaced a neutral with a basic residue. (D, E) Cysteine residues are substituted into positions S81 and L76 S81. Acidic residues are indicated in red, basic in blue and sulfhydryl in yellow.

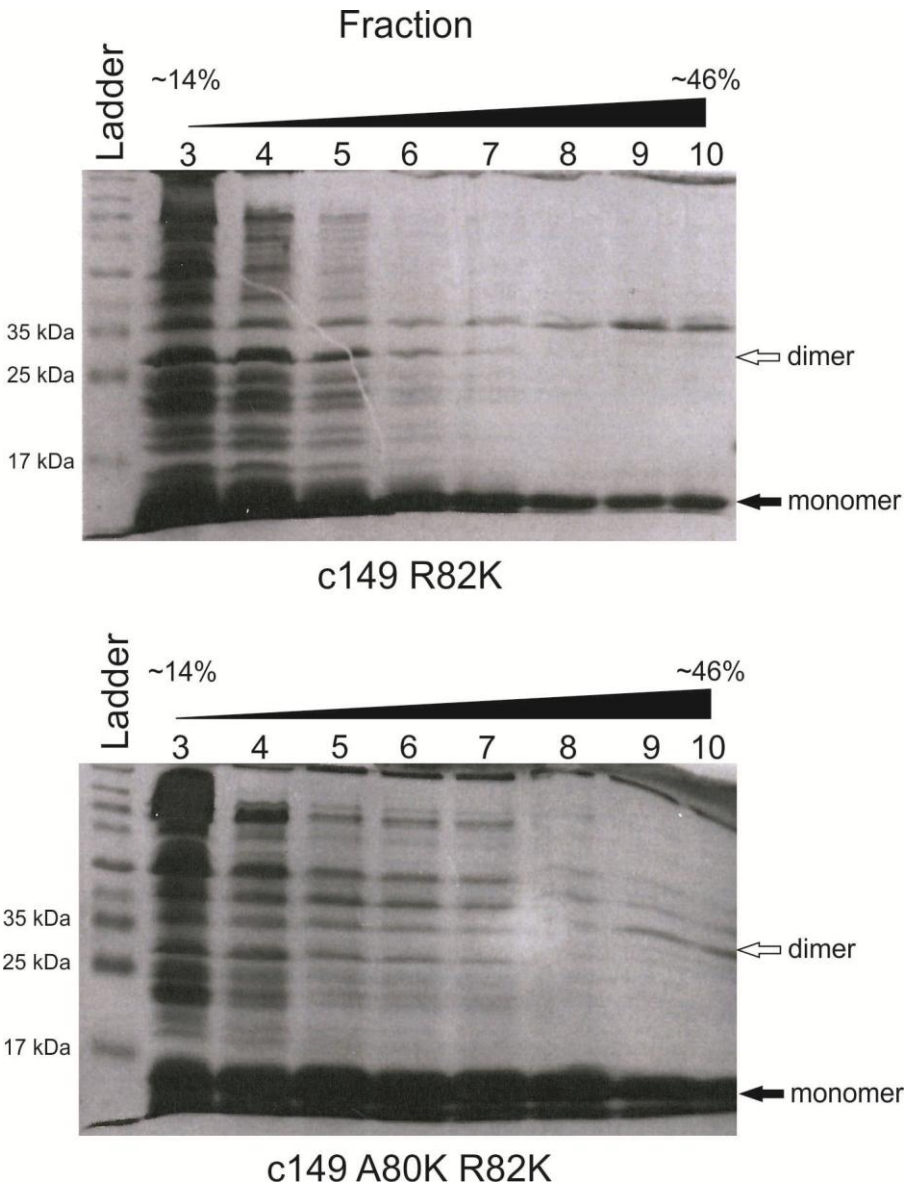

Figure 3.2.8: Core protein distribution within fractions of a 10-60% sucrose gradient. Fractions (3-10) were loaded from lowest (±14%) to highest (±46%) sucrose concentration, subjected to SDS-PAGE and stained with Coomassie Brilliant Blue R250. Crude preparation of protein contains a high expression level of both R82K and A80K R82K in c149 (black arrow). HBcAg dimers are also present in the preparation (white arrow).

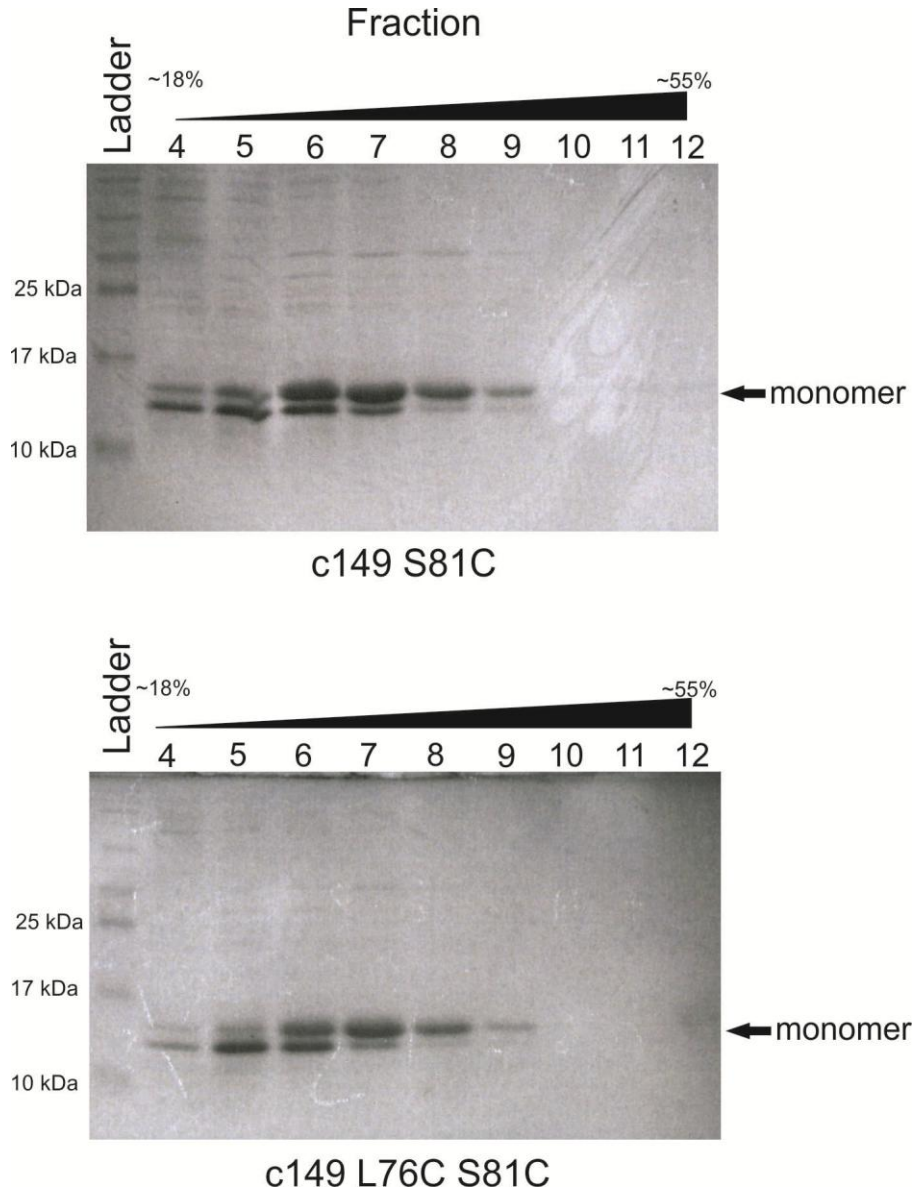

Figure 3.2.9: Core protein distribution within fractions of a 10-60% sucrose gradient. Fractions (4-12) were loaded from lowest (±18%) to highest (±55%) sucrose concentration. SDS-PAGE and Coomassie Brilliant BlueR250 staining was used to analysis protein content of each fraction. Core proteins (c149 S81C and L76C S81C (black arrow)) were the major protein species in the lower fractions.

Analysis of the electrostatic properties of the IL revealed that the substitution, R82K, had negligible effects on charge at physiological pH. Both pKa_3 values for arginine and lysine are well above physiological pH, indicating both residues remain positively charged in the IL. Anionic HBV capsids, like DNA, migrate within an agarose gel matrix by electrophoresis. Consequently, disruption of capsid charge (and size) will have a direct effect on electrophoretic mobility. Analysis of expressed recombinant anionic capsid migration by electrophoresis within an agarose gel revealed that the single lysine substitution (R82K) had

little to no effect on capsid electrophoretic mobility. This is indicative that the electrostatic potential of R82K mutants remains largely unchanged in comparison to wild type (Figure 3.2.10A). The addition of two lysine residues (A80K R82K) caused a positive shift in electrostatic potential, which resulted in these capsids migrating slower within the gel matrix, as compared to wild type and the R82K mutant (Figure 3.2.10A). Substitution of the lysine into position A80 caused an increase in overall positive electrostatic potential, thus shifting the anionic capsid charge to that of a more neutral state. The uniform nature of expressed recombinant HBV capsids (*T*=4) indicates that the electrophoretic shift occurred as a result of a change in charge and not size. As anticipated, cysteine insertions into the IL did not affect the electrophoretic nature of the capsid, and both S81C and L76C S81C mutants migrate similarly to wild type capsid (Figure 3.2.10B).

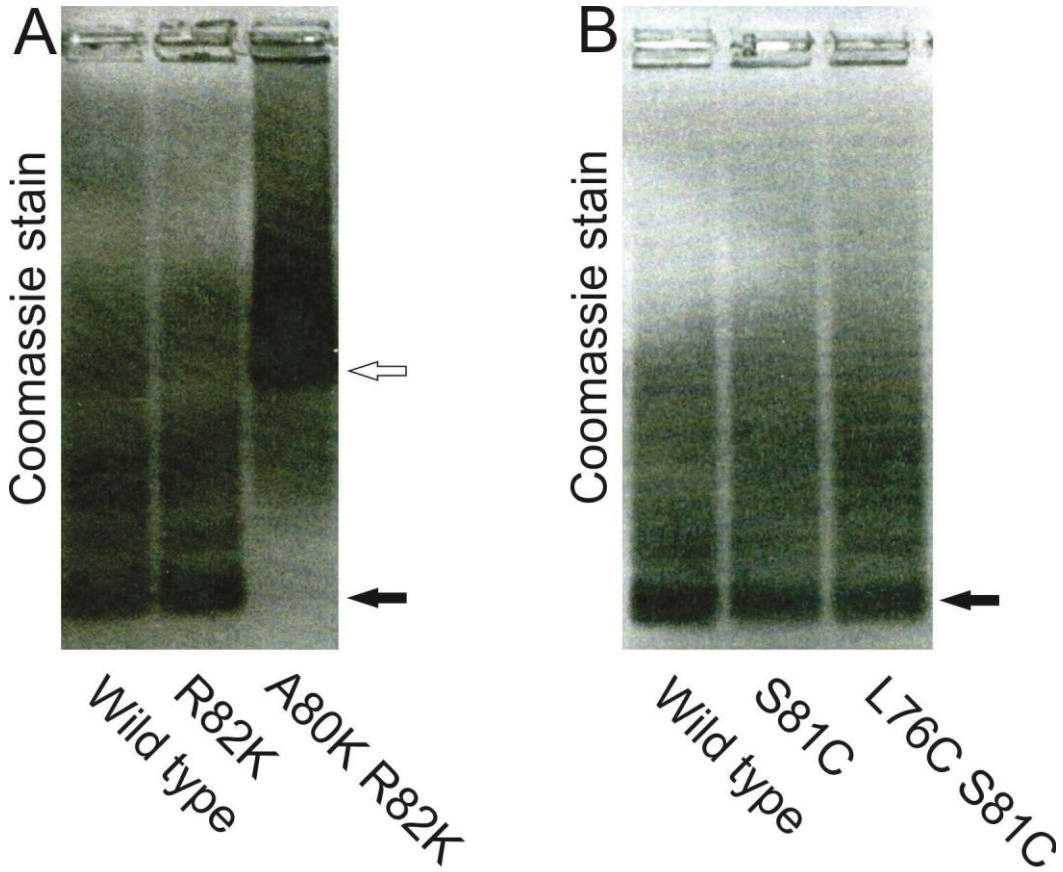

Figure 3.2.10: Effects of IL amino acid substitutions on capsid electrophoretic mobility in agarose gels. Crude preparations of *T*=4 mutant capsids were stained with Coomassie brilliant blue R250 after electrophoresis. A) Mutant R82K and wild type capsid migrate to the position of the black arrow, whereas A80K R82K migrate to the position of the white arrow. B) Cysteine substitution (S81C and L76C S81C) capsids migrate to a similar position as wild type (black arrow).

The electrostatic potential of the IL was modelled, which corroborated the mobility shift data. The electrostatic fields of the IL region were mapped using Swiss PDB Viewer [214], under the following parameters: protein and solvent dielectric constants, 4 and 80, respectively; 162 mM ionic strength (further details can be found in the materials and methods section). Comparison of the wild type and R82K mutant suggested negligible charge changes occur (Figure 3.2.11B + C). Introduction of the second lysine introduces an additional positive electrostatic region, however does not appear to influence effects of the acidic residues significantly (Figure 3.2.11A + B). The prediction software did not take into account the formation of salt bridges between acidic and basic residues, in which the formation of these bonds may impact on the extent of charged areas. Despite the exclusion of salt bridges, the predicted data of the lysine substitutions show no diminished anionic regions, rather just the introduction of a cationic region.

Similarly, the electrostatic potential of the cysteine-containing IL was predicted (Figure 3.2.12A – C). As anticipated, negligible changes in charge occur at the IL. The exchanged residues are considered to carry uncharged side chains, thus do not affect the local pKa of the IL significantly. Of interest was the change in charge of the IL of the original lysine mutant, D78K S81K (Figure 3.2.13). The predicted electrostatic potential reveals that these substitutions have a significant impact on IL charge. The replacement of an acidic with a basic residue and the introduction of an additional basic in place of the uncharged residue would appear to cause an equal distribution of both positive and negative charge at the IL. This does not imply that the IL charge became neutralised, however it may suggest that a significant change in charged residues may alter capsid behaviour within the bacteria, which caused poor yield after expression.

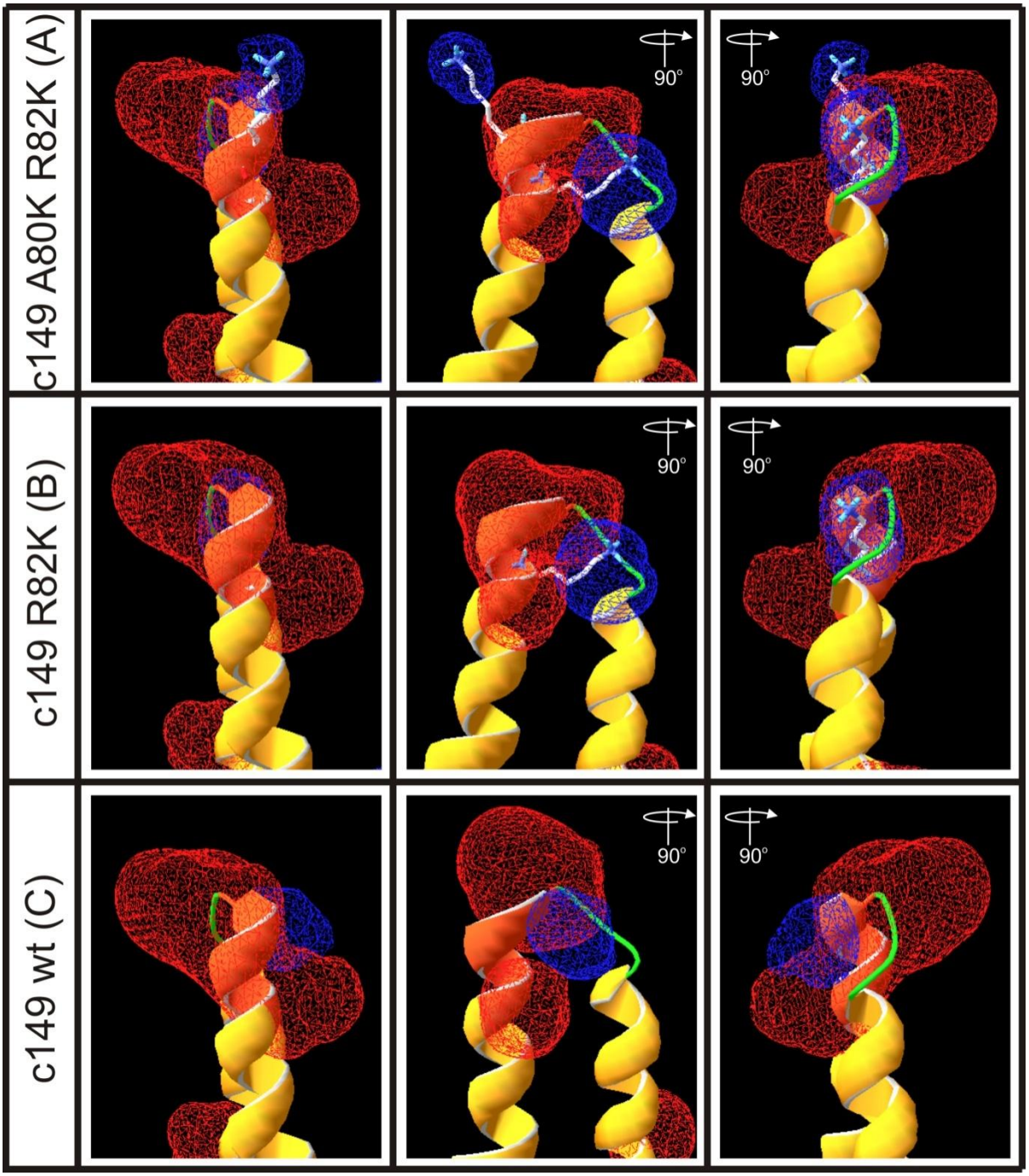

Figure 3.2.11: Electrostatic potential predictions of the monomer IL region of c149 (wild type), c149 R82K and c149 A80K R82K mutants. The apex of the hairpin is rotated 90^{o} horizontally to provide additional perspective. The side chain at position K80 and K82 are included in the illustration. Red areas map negative charge and blue represents positive charge. Protein backbone annotated as in Figure 3.1.4. Electrostatic predictions are based on Swiss-PDB Viewer of model [201].

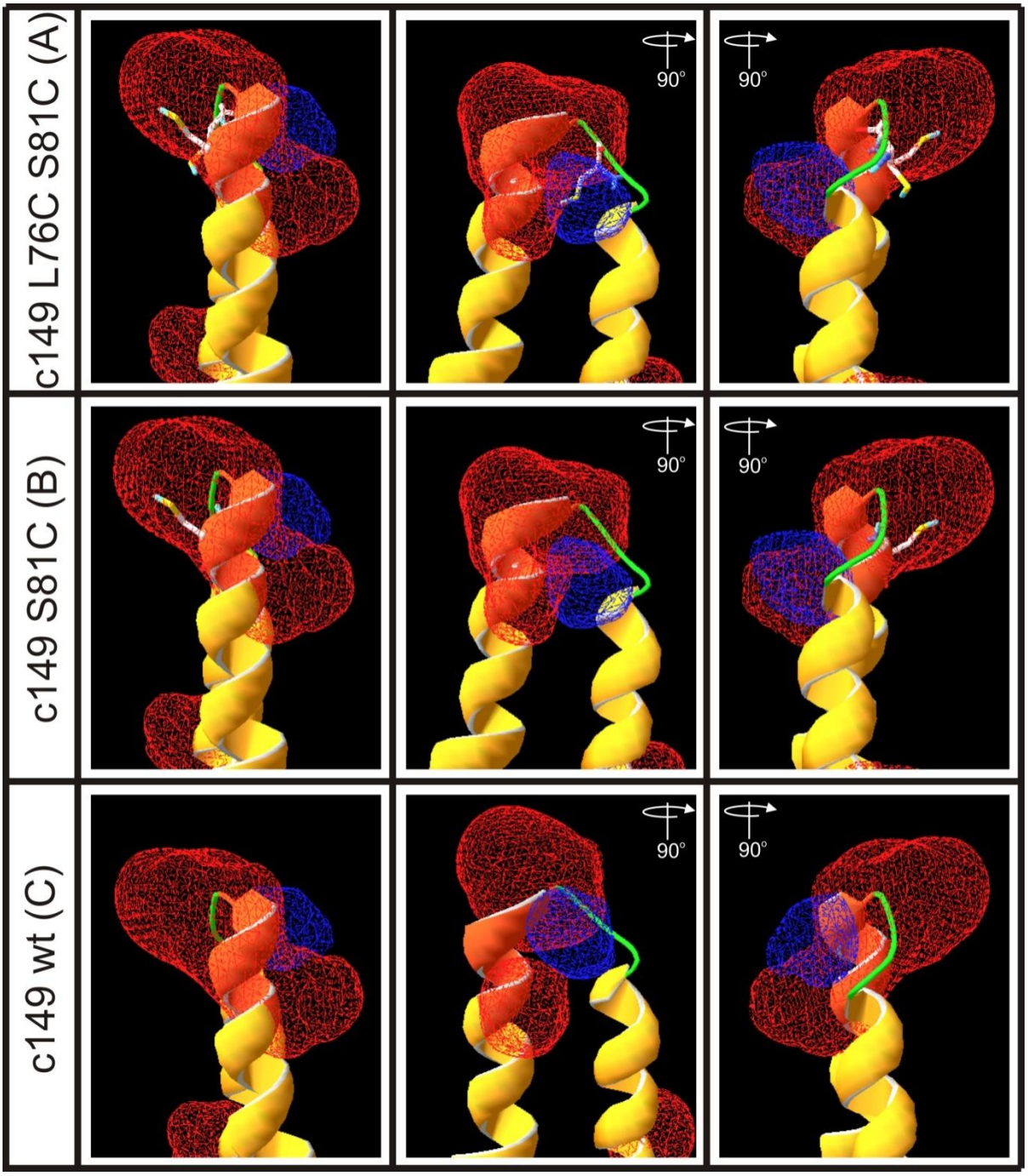

Figure 3.2.12: Electrostatic potential predictions of the monomer IL region of c149, c149 S81C and c149 L76C S81C mutants. Side chains of the cysteine residues at position S76 and S81 are included in the illustration. Red areas map negative charge and blue represents positive charge. Protein backbone annotated as in Figure 3.1.4. Electrostatic predictions are based on Swiss-PDB Viewer of model [201].

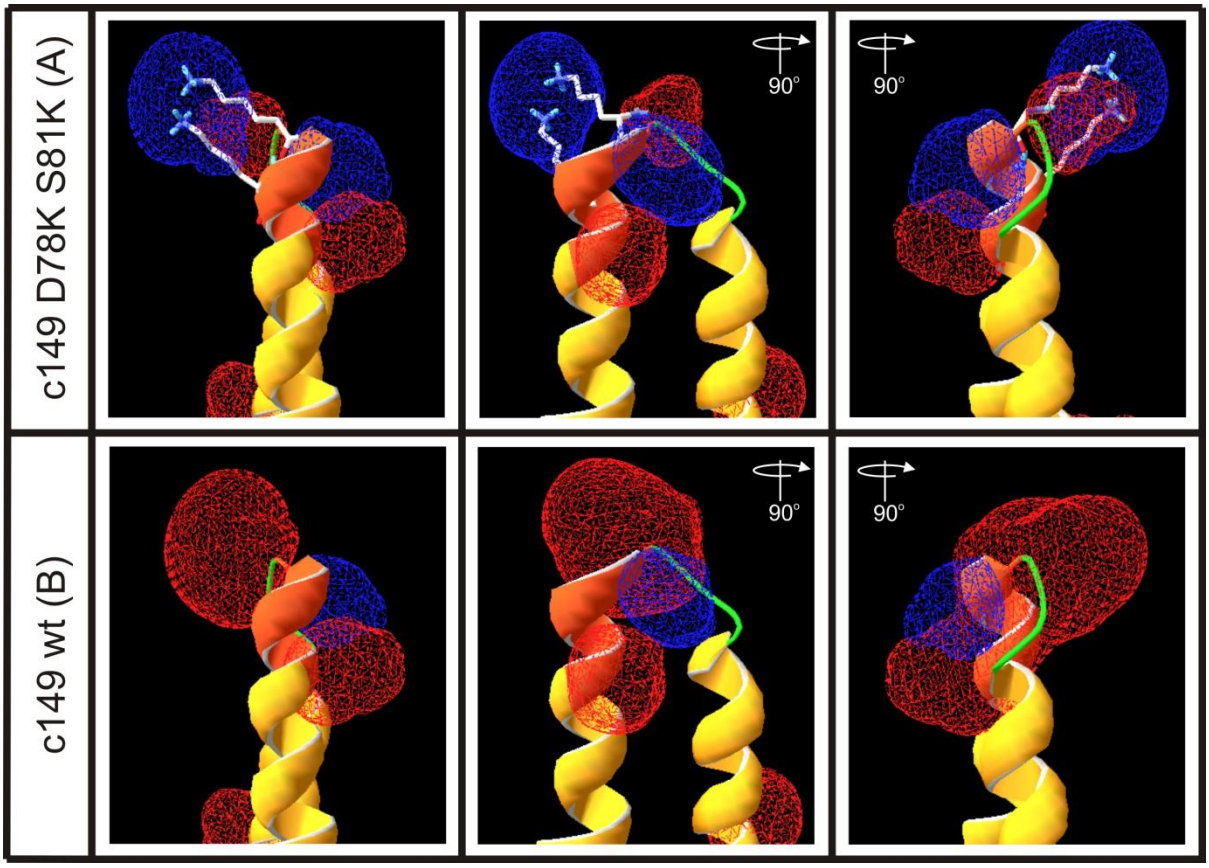

Figure 3.2.13: Electrostatic potential prediction of the monomer IL region of c149 and c149 D78K S81K mutant. The region of both monomers is shown at different perspectives. Substituted amino acid side chains of the D78K S81K mutant are included in the illustration. Red areas map negative charge and blue represents positive charge. Protein backbone annotated as in Figure 3.1.4. Electrostatic predictions are based on Swiss-PDB Viewer of model [201].

3.3. Discussion

Virus-like particles are attractive candidates for gene therapy vectors as their amenable nature allows for manipulation to introduce desired/required properties. A variety of modifications are discussed in the literature, encompassing nanowire formation to corrective-gene delivery. The HBV capsid is a suitable candidate for development, as it displays several of the required hallmark features for VLP vectorology. Previous work by other authors has demonstrated that the IL of the HBV capsid is amenable to insertions and substitutions, provided these changes do not interfere with monomer and dimer formation [179, 233]. As such, it was possible to introduce amino acid residues into the IL to provide a site for the conjugation of functional ligands. This novel study incorporated two of the more commonly used residues for conjugation chemistry, lysine and cysteine. The HBV capsid contains one exposed lysine and no exposed cysteine residues, thus substitution into the IL formed ideal specific conjugation sites.

The initial substitutions to the IL were made not taking physicochemical properties of the capsid into account. Consequently, the mutant D78K S81K displayed a significant change to the IL electrostatic potential. Further investigation regarding the poor expression of the core mutant was not pursued. It was reasoned that the drastic change in IL charge may have accounted for the almost absent yield of D78K S81K mutants, potentially as a result of capsid-protein interaction, which led to the sequestration and/or clearing of capsids during the preparation process. These data suggest that the IL is less robust than indicated in the literature, and consideration of its electrostatic nature needs to be assessed if insertions or substitutions are made.

The LinkedLys motif was planned to contain four lysine residues separated by glycine residues, and tethered to the spike tip by two linkers comprising four glycine residues. This was encoded by highly repetitive AG sequence, which is known to cause polymerase slippage and poor replication [243]. Glycine and lysine codons comprise mainly of adenine and guanine, making use of the repetitive AG sequence unavoidable. It was later demonstrated that a minimum of one target residue is sufficient in the conjugation process, consequently further development of the quadruple lysine LinkedLys-like clones were not pursued.

Modification to the region encoding the IL was found to be onerous, thus the development of a simplified cloning system was addressed. Insertion of type IIS restriction

sites flanking the region encoding the IL facilitated a convenient means to insert oligonucleotides with substituted amino acid triplet codons. This allowed for the cloning of sixteen recombinant HBV capsid clones in a short space of time. The 'Snap-in' system provides a means of cloning applicable to any VLP, simplifying generation of novel VLPs in the field of bionanotechnology and vectorology.

Walker and colleagues provided an interesting solution to the purification of capsids that may experience conformational constraints or difficulties during synthesis [233].The Splitcore technique has been demonstrated to overcome conformational constraints at the IL site when exogenous peptides were inserted. This was of particular relevance when whole or protein fragments were introduced into the immunodominant loop. The Splitcore approach may have aided in the production of mutants such as LinkedLys and D78K S81K. Division of the IL where each section contains a desired mutation may have allowed for formation and isolation of recombinant capsids, despite not containing an intact IL. It is not known what effect a dissociation-reassociation step used for therapeutic nucleotide incorporation into capsids would have on the Splitcore species during a capsid loading step. The 'Snap-in' system allowed for the generation of whole HBcAg, and simple insertion or substitution of amino acid residues into the IL. Whole HBcAg would presumably assemble more efficiently after therapeutic sequence incorporation than species that comprise two halves. Both techniques, Splitcore and 'Snap-In', provide different advantages of cloning into the HBcAg.

A lysine substitution into position R82 did not affect the overall capsid electrostatic potential, as very little change in residue charge occurred. The substitution of the second lysine at position A80 was done to further increase the chance of ligand conjugation to the IL. The amino acid position 80 was considered suitable for substitution as a change in the acidic residues (D78 or D83) was undesirable. Furthermore a change to the proline at position 79 was avoided, as proline residues are often involved in turning points within protein structures. Removal of the proline species may place additional conformational constraint within the IL (by creating a less flexible IL), hindering efficient HBcAg formation. As demonstrated in both mobility shift and electrostatic predictions, A80K R82K does decrease the overall capsid negative electrostatic potential, however did not significantly impact on capsid expression or purification. Substitution of cysteine at position S81 and L76 S81 had no observable impact on capsid expression, purification or electrostatic potential.

The second cysteine was placed in a region flanking the IL to avoid the potential cystine bridges forming within and between ILs. Double lysine and cysteine mutants were generated with the aims to potentially improve conjugation reactions. Overall the introduced substitutions that did not significantly alter the IL charge, thus capsid charge, were well tolerated by the recombinant HBV capsid.

Introduction of the lysine and cysteine residues within the IL provide a specific site for ligand conjugation. These functional ligands provide attributes such as hepatotropism and immuno-evasion. Unlike liposomes which require less than 10% surface ligand representation, the surface of the capsid required extensive decoration such that indiscriminate cellular uptake was avoided. This may require > 80% ligand conjugation to the capsid surface. The following chapter describes the conjugation of various ligands to the capsids surface, some of which were described in Chapter 2, with the aims to generate a hepatotropic vector. Furthermore, the effects of capsid envelopment within liposomes which also provide immuno-evasive and potentially hepatotropic properties were explored.

3.4. Materials and methods

3.4.1. Cloning of recombinant c140, c149, c160, c170 and c183 cassette constructs

3.4.1.1. Polymerase Chain Reaction (PCR)

The template for wild type (wt) core protein and its variants was the greater-than genome length HBV encoding plasmid pCH3091 [244]. Primers shown in Appendix 1 were used to generate the core protein cassettes and variations thereof (generic core forward, core reverse 149-183). The PCR mix consisted of the following components 1.25 U High Fidelity PCR Enzyme Mix, 5 µl 10x High Fidelity PCR Buffer (75 mM Tris-HCl (pH 8.8 at 25 °C), 20 mM $(NH_4)_2SO_4$, 0.1% (v/v) Tween 20, 1.5 mM $MgCl_2$), 10 nmol forward and reverse primer, 1 µl of 10 nM dNTPs, 1 µl of 10 nM pCH3091 up to 50 µl with H_2O (PCR reagents obtained from Fermentas, Burlington, Canada and primers obtained from IDT, IA, USA). The PCR amplification cycle was as follows: 5 minutes at 95 ^{o}C, followed by 35 cycles of 95 ^{o}C for 30 seconds 55 ^{o}C for 1 minute and 72 ^{o}C for 1 minute. The final elongation step was for 10 minutes at 72 ^{o}C.

3.4.1.2. PCR fragment isolation and purification

The completed PCR was mixed with 10 μl 6x DNA Loading Dye (Fermentas, Burlington, Canada) and loaded into a 1% (w/v) agarose gel containing 0.02% (w/v) ethidium bromide. Electrophoresis proceeded at 80 V in 1 X TAE buffer. DNA fragments were visualised using short wave ultraviolet and excised from the gel. The DNA fragments were extracted and purified using a standard phenol-chloroform protocol (Appendix 3). Briefly DNA fragments were excised then removed from the gel by centrifugation at 16000 × *g* for 10 minutes. Eluate was combined with an equal part of chloroform and salt-saturated phenol. Samples were thoroughly mixed and centrifuged at max speed (>8000 × *g*) for 90 seconds. The upper phase was retained and equal volume of chloroform added. Samples were thoroughly mixed and centrifuged at max speed (>8000 × *g*) for 90 seconds. This chloroform wash step was repeated. The upper phase was retained and an equal volume of chilled isopropanol added, to this 10% of the total volume 3 M sodium acetate was added. Samples were incubated on ice for 30 minutes and then centrifuged (>8000 × *g*) for 30 minutes at 4 ^{o}C. Supernatant was removed and DNA pellet washed with 70% ethanol. Supernatant was removed and DNA pellet dried at room temperature. The dried DNA pellet was resuspended in an appropriate volume of distilled water. DNA concentrations were determined by UV spectrometry using a Nanodrop ND-1000 (Thermo Fisher, Massachusetts, USA).

3.4.1.3. Cloning into the bacterial vector pTZ57R

All bacterial growth media was obtained from Oxoid (Thermo Scientific, MA USA). Purified PCR fragments were ligated into the T/A cloning vector pTZ57R (pTZ57R/T) according to manufacturer's instructions (Fermentas, Burlington, Canada). The completed ligation reaction was added to 100 μl of chemically competent DH5α *E. coli* bacteria (Appendix 3) and incubated on ice for 20 minutes, followed by heat shock at 42 ^{o}C for 90 seconds after which bacteria were placed back on ice for 5 minutes. Lysogeny broth (LB) agar plates containing 0.01% ampicillin (Sigma, MO, USA) and 800 μg isopropyl β-D-1-thiogalactopyranoside (IPTG) (Sigma), 800 μg 5-bromo-4-chloro-indolyl-galactopyranoside (X-gal) (Sigma) on the surface of the agar were used in the blue-white screening process. Transformed DH5α *E. coli* were plated onto IPTG-X-gal-ampicillin-enriched LB agar plates and incubated over night at 37 ^{o}C. White colonies were indicative of fragment insertion, and were selected for by two rounds of screening. The first screen was colony PCR, using primers M13 forward and M13 reverse (Appendix 1). A small portion of a positive bacterial

colony was picked and resuspended in the PCR mix. The PCR consisted of the following components 0.25 U GoTaq® DNA polymerase (Promega, WI, USA), 3 μl 5x PCR Buffer (GoTaq® Reaction Buffer (proprietary, pH 8.5)) 1.5 mM $MgCl_2$, 5 nmol forward and reverse primer, 0.5 μl of 10 nM dNTPs, up to 15 μl with H_2O. The PCR amplification conditions were as follows: 10 minutes at 95 °C, followed by 25 cycles of 95 °C for 15 seconds 55 °C for 15 seconds and 72 °C for 30 seconds. The PCR products were separated and visualised using agarose gel electrophoresis, as described in section 3.4.1.2. Selected clones were considered positive if a PCR product of 624 bp (149 core), 657 bp (160 core), 687 bp (170 core) and 726 bp (183 core) was present. The second screen was performed using restriction digestion. Positive colonies were selected and individually seeded into 5 ml LB supplemented with 0.01% ampicillin, grown overnight at 37 °C. Plasmids were extracted from DH5α using the protocol described in Appendix 3. Extracted plasmid was digested with *XhoI* and *NcoI* using the following conditions: 1 μg plasmid DNA, 10 μl Buffer Tango (66 mM Tris-acetate (pH 7.9 at 37 °C), 20 mM magnesium acetate, 132 mM potassium acetate, 0.2 mg/ml BSA - Fermentas), 0.5 U restriction enzyme, H_2O up to 50 μl, 37 °C for 60 minutes. Digested products were visualised using agarose gel electrophoresis, as described in section 3.4.1.2. A positive clone produced a digested product of 456 bp (core 149), 489 bp (core 160), 519 bp (core 170), 558 bp (core 183). Sequencing with the M13 forward primer was used to check insert sequence integrity (Inqaba Biotec, ZA).

3.4.1.4. Cloning into the bacterial expression vector pet15b

Core sequences of the species c140-c183 were excised from pTZ57R vectors using *Nco*I and *Xho*I (as per section 3.4.1.3.). The bacterial protein expression vector, pet15b, was similarly treated however 1 U Antarctic phosphatase (Fermentas) was included within the reaction. DNA fragments were isolated using agarose gel electrophoresis and phenol-chloroform extraction as described in section 3.4.1.2. Insert (core fragment) and backbone (pet15b fragment) were combined as a mole ratio of 5:1 respectively, in a ligation reaction using T4 DNA ligase (Fermentas) according to manufacturer's instructions. Chemically competent Rosetta II *E. coli* were transformed with the ligated insert and backbone (eukaryotic protein *E. coli* expression strain Rosetta II (EMD Millipore, Darmstadt, Germany)) as described in section 3.4.1.3. Transformed Rosetta II bacteria were distributed over chloramphenicol (0.0034% w/v) -ampicillin (0.01% w/v) - enriched LB agar plates and

incubated overnight at 37 ^{o}C. The following day a colony was isolated and cultured for protein expression studies.

3.4.2 Cloning of core D78K S81K mutant and core LinkedLys mutants

The aim of this cloning procedure was to introduce mutations within the IL region which substitute wild type for lysine codons. Core species 149-183 encoded within the respective pet15b backbone (Section 3.4.1.4) were used as templates in a PCR-based procedure which generated two halves of the core ORF: part A and part B. This methodology was used to generate both D78K S81K and LinkedLys clones.

Part A of the LinkedLys clone was generated using the primers Generic core forward and LinkedLys Int reverse (Appendix 1). The second half of LinkedLys was generated using a two-step PCR, in which LinkedLys Int forward 1 and respective reverse primer pertaining to core clone size (c149-c183) produced an amplicon template for the second reaction. Purified amplicon (described in Section 3.4.1.2.) was subjected to a second round of PCR using the primers LinkedLys Int forward 2 and a reverse primer pertaining to core clone size. The protocol for the above PCRs was described in Section 3.4.1.1. The cloning procedure is schematically described in Figure 3.4.1.

Part A of D78K S81K was generated using the generic core forward and Lys sub Int reverse primers. Part B of D78K S81K was generated using Lys sub Int forward and Core reverse 149 (See Appendix 1). The PCR protocol for these two reactions is described in Section 3.4.1.1). The cloning strategy for LinkedLys and mutant core D78K S81K is diagrammatically described in Figure 3.4.1.

Part A and part B amplicons were cloned into the bacterial vector, pTZ-57R, as according to the manufacturer's instruction (Fermentas). The screen for positive clones is described in Section 3.4.1.3. An unanticipated common restriction site was present in pTZ – D78K S81K part B of clones c160, c170 and c183. This resulted in an adaption in the standard cloning procedure and is addressed at the end of this section. Positive clones were cultured and plasmids isolated as described in Section 3.4.1.3. To reconstitute the IL of the mutant core clones, part A and B clones were subjected to restriction digestion and respective fragments ligated together. pTZ-c149 LinkedLys part A was treated with the restriction enzymes *Sca*I and *Stu*I; pTZ-c149 LinkedLys part B restriction enzymes *Dra*I and *Sca*I (the part B LinkedLys clones of c160, c170 and c183 clones were treated similarly); pTZ-c149 D78K S81K part A

with *Sca*I and *Ecl*136II; and pTZ-c149 D78K S81K part B with *Nla*IV and *Sca*I. All restriction digests were carried out according to manufacturer's instruction (Fermentas). Restriction digestion fragments were isolated as described in section 3.4.1.2. Part A and part B of each respective clone (which also contained a half of the pTZ57R plasmid) were ligated using T4 DNA ligase (Fermentas) according to the manufacturer's instruction. The cloning process is illustrated in Figure 3.4.1.

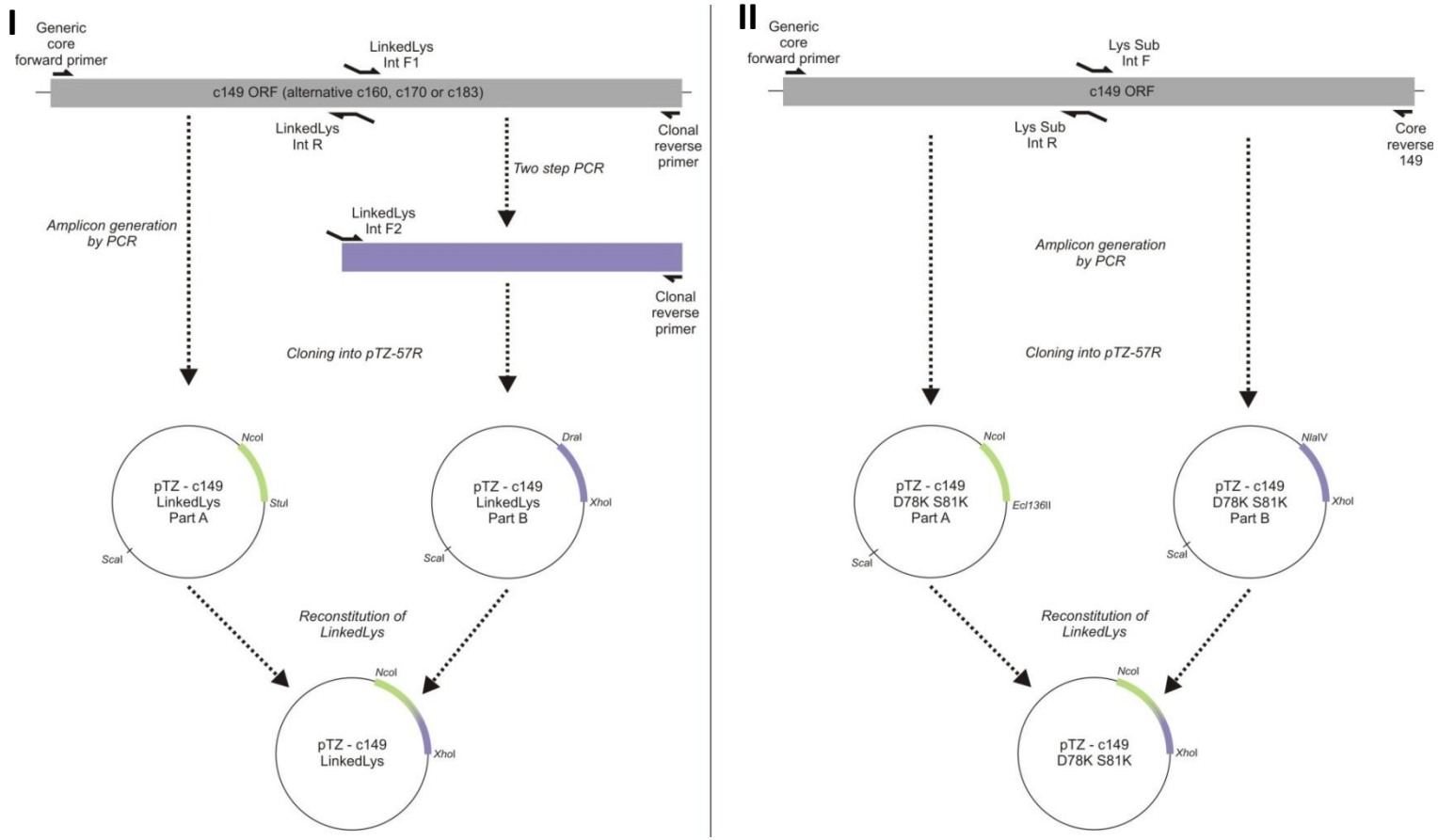

Figure 3.4.1: Schematic illustration of the cloning strategy used to generate the pTZ-LinkedLys and pTZ-c149 D78K S81K. (I) The LinkedLys species (c149-c183) were generated as two halves by PCR. The first half (Part A) was cloned directly into the cloning vector pTZ-57R, the second half (Part B) underwent a second PCR step and then cloned into pTZ-57R. Positive clones of both A and B were combined after restriction digestion and ligation, producing the recombinant pTZ-LinkedLys (for clones c149-c183). (II) The clone pTZ-c149 D78K S81K was generated in a similar manner, in that two halves of the construct were initially generated by PCR. Part A and Part B were cloned separately into pTZ-57R, screened, and a positive clone of each was treated with restriction endonucleases and ligated together, reconstituting pTZ-c149 D78K S81K.

3.4.2.1 Cloning of D78K S81K into the core species c160, c170 and c183

The part B pTZ-D78K S81K c160, c170 and c183 clones contained the blunt cutting *Nla*IV restriction site in two locations, which prevented the reconstitution of the sequence encoding core protein when digested with *Nla*IV. Thus a four-way ligation approach was used (summarised in Figure 3.4.2) which cloned directly in pET15b, circumventing the pTZ57R cloning step. Screening of colonies and plasmid preparation have been described in Sections 3.4.1.2 and 3.4.1.3. pTZ-c149 D78K S81K Part A treated with restriction enzymes *Nco*I and *Ecl*136II; pTZ-c149 D78K S81K Part B with *Nla*IV and *Bsp*EI; pTZ-c160 (or c170/c183) treated with *Bsp*EI and *Xho*I; lastly the bacterial expression vector pET-15b with *Xho*I and *Nco*I. The restriction digests were performed according to the manufacturer's instruction (Fermentas). DNA fragments were isolated as previously described (Section 3.4.1.2) and ligated together in equal mole ratios with T4 ligase (Fermentas) according to the manufacturer's instruction.

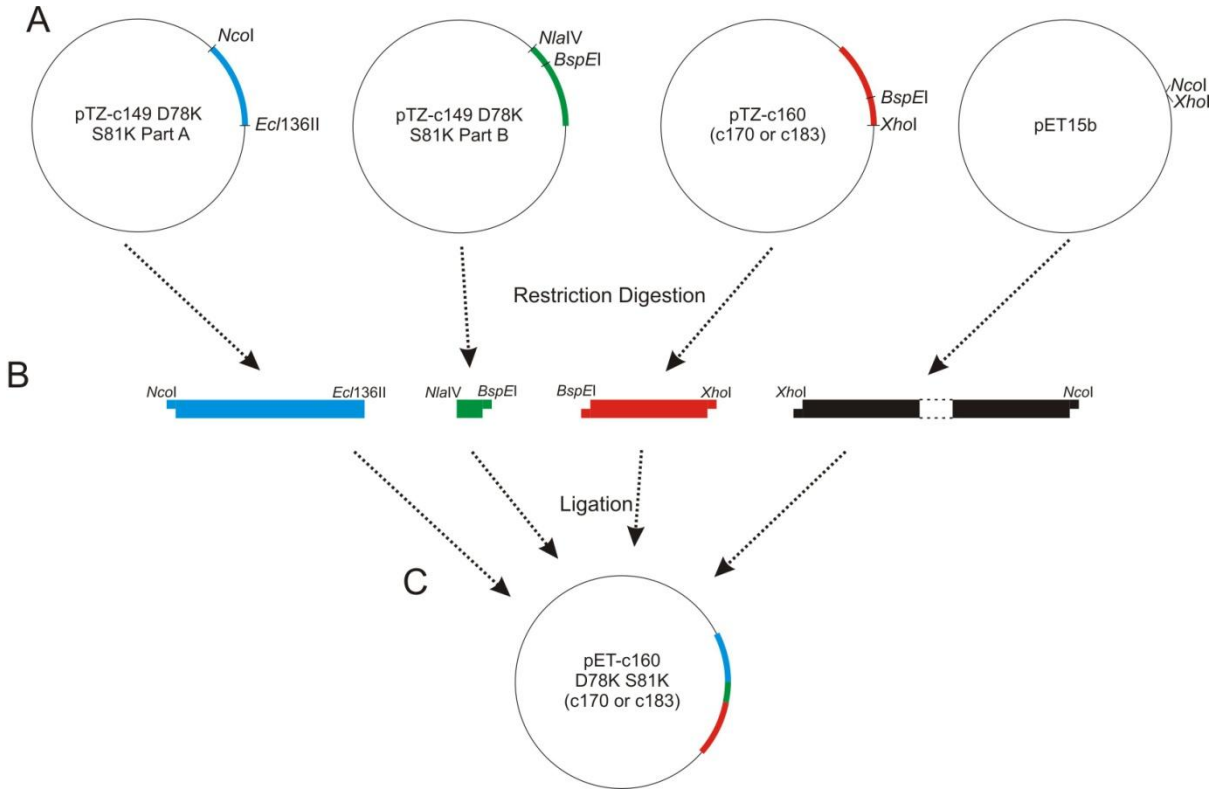

Figure 3.4.2: Schematic representation of the four-way cloning strategy used to generate the mutant clones D78K S81K directly in the bacterial expression vector pET-15b. (A) pTZ-c149 D78K S81K Part A was used to generate the first half of the cassette. The remainder of the cassette was reconstituted as follows: a fragment of pTZ-c149 D78 S81K Part B, which completes the mutated IL region; a fragment from c160, 170 or c183 to generate the various clonal sizes of core protein. (B) All fragments were generated by restriction digestion and ligated into the pET-15b backbone.

3.4.3 Generation of the IL 'Snap-in' system in pTZ57R.

A simple method for substituting triplet codons was required, as the flanking sequences to the IL contained very few useful restriction sites. A method was developed in which the IL encoding region could be excised out using type IIS restriction enzymes and replaced with a 42 bp ds oligonucleotide. The core cassette was divided in two halves using PCR: primers Generic forward core and Part A RE2 'Snap-in' reverse for Part A; Part B RE2 'Snap-in' forward with respective reverse primer pertaining to core clone size (c149-c183) for Part B (Appendix 1). PCR conditions and fragment purification were described in section 3.4.1.1 and 3.4.1.2. The expected amplicon sizes for Part A were 253 bp; 227 bp for Part B c149; 260 bp for Part B c160; 290 bp for Part B c170; and 329 bp for Part B c183. Fragments were cloned into pTZ57R/T according to manufacturer's instruction (Fermentas), which generated the clones pTZ-core 'Snap-in' part A and pTZ-core 'Snap-in' part B c149 (or c160-c183). Clone screening was as described in Section 3.4.1.2. The 'Snap-in' system was assembled by matching a Part A with a respective Part B. pTZ-core 'Snap-in' part A and pTZ-core 'Snap-in' part B were cleaved with enzymes *Sca*I and *Nhe*I (Fermentas) as follows: 1 μg plasmid DNA, 5 μl *Sca*I Buffer (10 mM *bis*-Tris Propane-HCl (pH 6.5 at 37 °C), 10 mM $MgCl_2$, 100 mM KCl, 0.1 mg/ml BSA - Fermentas), 0.5 U restriction enzyme, H_2O up to 50 μl for 2 hours at 37 ^{o}C. The restriction digest yielded fragments of 1332 bp for part A; 2032 bp for Part B c149; 2065 bp Part B c160; 2095 bp Part B c170; and 2125 bp c183, which were isolated as previously described in Section 3.4.1.2. Part A and Part B fragments were ligated together using T4 ligase according to manufacturer's instructions (Fermentas). Chemically competent *E. coli* strain DH5α was transformed with ligated product as described in Section 3.4.1.3. Selection of positive clones was described in Section 3.4.1.3. Figure 4.4.3 and schematically describes the above mentioned procedure.

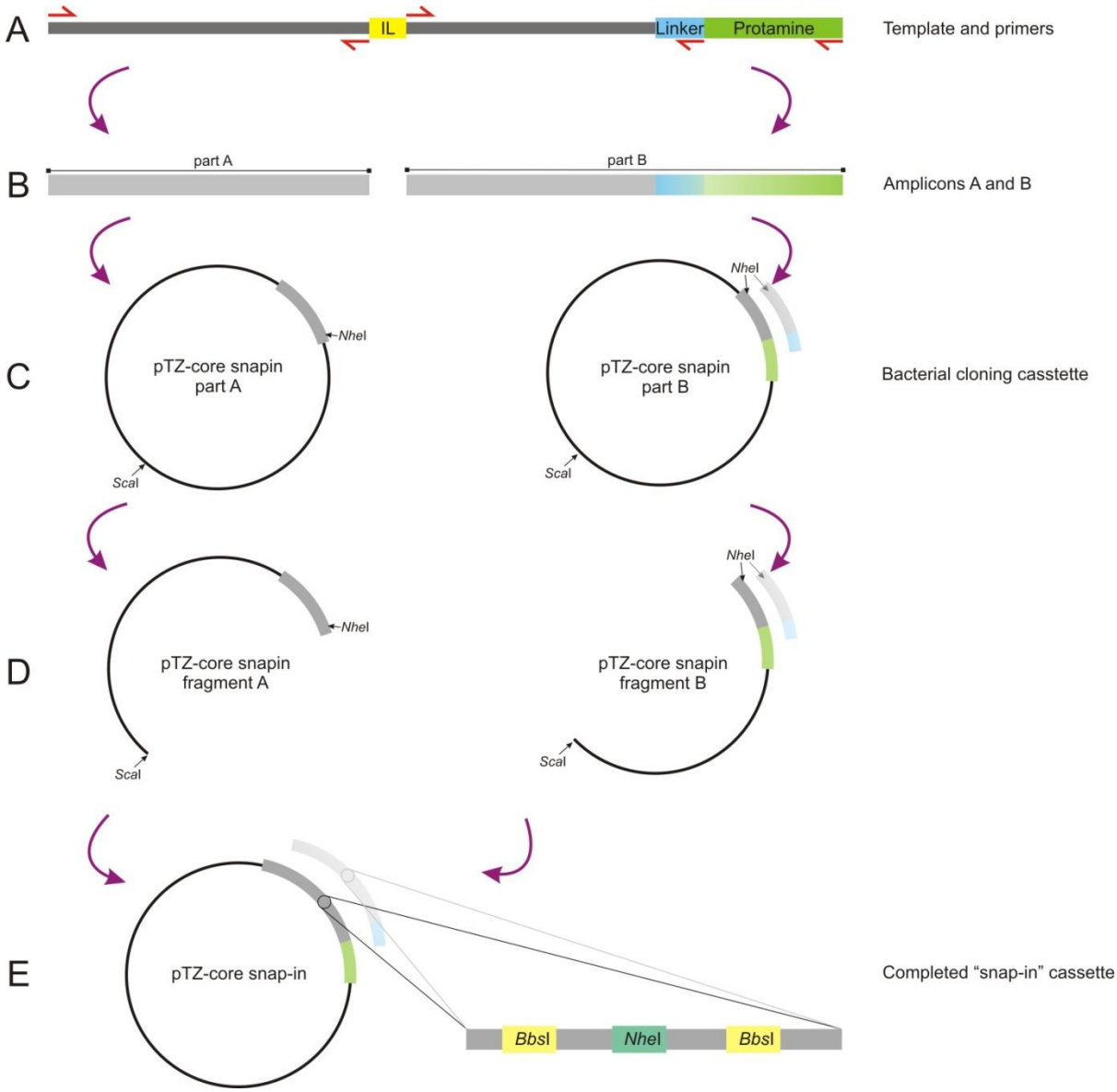

Figure 3.4.3: Summary of the 'Snap-in' cloning procedures. A PCR was used to generate 2 sequences flanking the region encoding the IL region (A-B). Amplicons were ligated into pTZ57R (C). Each respective plasmid was digested with *Nhe*I and *Sca*I and fragments ligated to reconstitute pTZ57R and generate a 'Snap-in' core cassette. The highlighted region contains the type IIS restriction enzyme, *Bbs*I (D and E).

3.4.3.1 Cloning into the 'Snap-in' system followed by insertion into the bacterial expression vector pet15b

pTZ-Snap-in clones treated with *Bbs*I generated an insertion site for an oligonucleotide encoding a modified IL region (modified sites include R82K, A80K R82K, S81C and L76C S81C – Appendix 1). The restriction digest proceeded overnight at 37 ^{o}C using 1 µg plasmid, 1 U *Bbs*I, 1 U Antarctic phosphatase, 5 µl Buffer G (10 mM Tris-HCl (pH 7.5 at 37 °C), 10 mM $MgCl_2$, 50 mM NaCl, 0.1 mg/ml BSA - Fermentas) up to 50 µl H_2O. DNA was purified as described in Section 3.4.1.2. One hundred picomol of insert oligonucleotide was treated

with T4 polynucleotide kinase (Promega), according to manufacturer's instructions. Phosphorylated oligonucleotides were purified by the phenol:chloroform extraction method (Appendix 3). Phosphorylated insert and dephosphorylated backbone were ligated as a 5:1 mole ratio respectively using T4 ligase, according to manufacturer's instructions (Fermentas). Chemically competent DH5α were transformed with the ligated product as described in section 3.4.1.3. Positive clones were selected as described in Section 3.4.1.3. The 'Snap-in' core clones (c149-c183) were inserted into the pET15b plasmid as described in Section 3.4.1.4. The above methodology is illustrated in Figure 3.4.4 and 3.2.5.

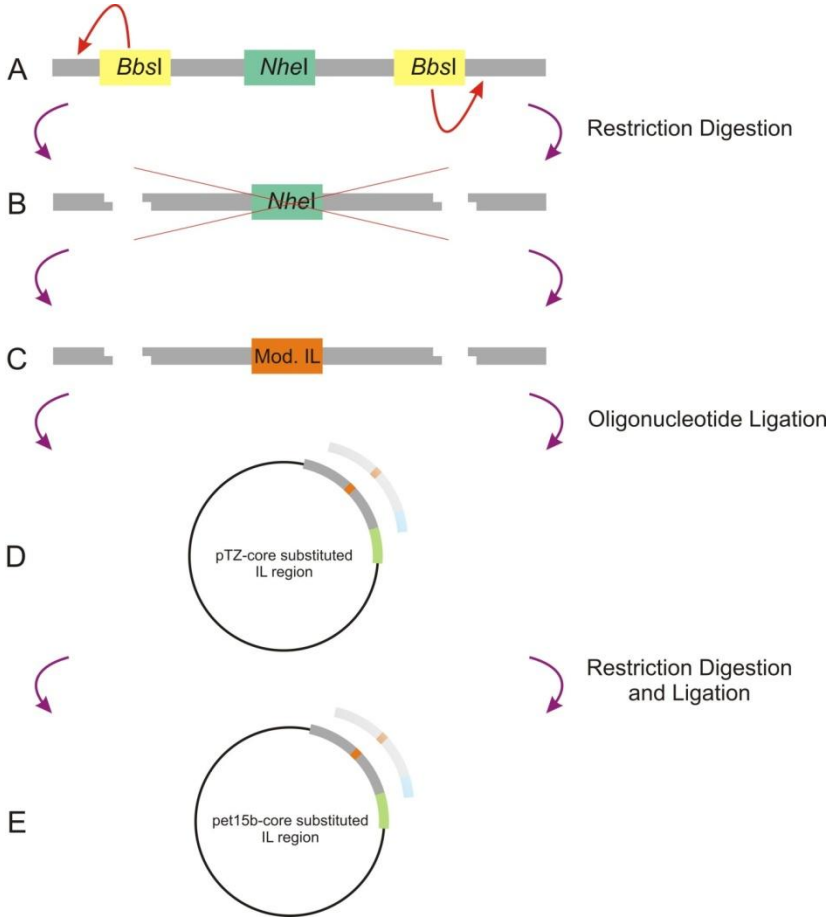

Figure 3.4.4: Schematic representation of the 'Snap-in' cloning system to generate a modified IL construct within the bacterial expression vector pET15b. pTZ-core 'Snap-in' (c149-c183) were cleaved with *Bbs*I to remove the interconnecting *Nhe*I region (A-B). A phosphorylated oligonucleotide encoding mutations to the IL was inserted (C-D).The IL-modified core cassette (c149-c183) was cleaved from pTZ backbone with *Nco*I and *Xho*I and inserted into the bacterial expression vector pET15b (E).

3.4.3. Core protein expression in Rosetta II bacteria

Three purification protocols were attempted, all varying in duration and complexity. It was found that the purification required two size exclusion steps to purify capsids to a satisfactory level. Bacterial expression broth recipe can be found in Appendix 2.

3.4.3.1. Protocol 1 – sucrose gradient-based purification.

Fifty millilitres of lysogeny broth supplemented with chloramphenicol (0.0034% w/v)-ampicillin (0.01% w/v) was inoculated with a core protein-expressing colony or bacterial glycerol stock and grown at 37 ^{o}C overnight with shaking. The following day 300 ml of protein expression broth (Appendix 2) was inoculated with 1-10 ml of seed culture grown the previous night. Variation in inoculation volume was based on culture growth rate. It was found that the cysteine modified capsids grew slower than the unmodified species. Cultures were incubated at 37 ^{o}C with vigorous shaking until the optical density of the culture had reached 0.5 at 600 nm, at which point were supplemented with IPTG to a final concentration of 1 mM (0.0238% w/v). Protein induction continued at 37 ^{o}C with vigorous shaking for 2 hours. Bacterial cells were harvested by centrifugation (5 minutes at 5000 × *g*) and resuspended in 10 ml Tris-NaCl buffer (Appendix 2) supplemented with 2 mg/ml lysozyme (Sigma) and frozen overnight at -20 ^{o}C. The following day sonication (20 seconds with 80% cycling and 80% power - performed in quadruplicate) was used to rupture the remaining bacterial cells. Lysates were stored overnight at 4 ^{o}C, following which centrifugation at 8000 × *g* for 1 hour pelleted cellular debris. Capsids within the lysate supernatant were purified on a 10-60% sucrose gradient by centrifugation at 250 000 × *g* for 2 hours at 20 ^{o}C. Distinct opaque bands formed within the sucrose gradient, most of which were bacterial contaminants. Fractions of 1 ml were taken from the gradients and analysed by SDS-PAGE for capsid content (Appendix 3). Fractions containing core protein were pooled and dialysed against TN buffer overnight, with initial buffer changes after one and two hours. Capsids were concentrated by centrifugation-based ultrafiltration with Amicon Ultracel 10k (Millipore, MA, USA). Samples were concentrated to 0.5-2 mg/ml and stored at -80 ^{o}C.

3.4.3.2 Protocol 2 - Expression and purification "Zlotnick protocol"

A second protocol was used to purify recombinant HBV capsids, based on the method described by Zlotnick *et al.* [213]. Recombinant core expressing *E. coli* was initially cultured

as described in Section 3.4.3.1, however 500 ml protein expression broth was seeded with 1-15 ml starter culture. Once cultures had reached an OD of 0.5 at 600 nm, IPTG was added to a final concentration of 2 mM (0.0475% w/v) and shaken vigorously for 3 hours at 37 ^{o}C. Bacteria were harvested by centrifugation and the pellet resuspended in 10 ml resuspension buffer A supplemented with 2 mg/ml lysozyme (Appendix 2). The bacterial suspension was frozen overnight at -20 ^{o}C. The following day the remaining bacterial cells were ruptured by sonication (20 seconds with 80% cycling and 80% power - performed in quadruplicate). Cellular debris was removed by centrifugation at 26 000 × *g* for 1 hour. Solid sucrose was added to the lysate supernatant to a final concentration of 0.15 M and further centrifuged at 100 000 × *g* for 1 hour. Solid $(NH_4)_2SO_4$ was slowly added to the supernatant to avoid permanent protein precipitation, after which the solution was gently agitated at 4 ^{o}C for 1 hour. Precipitated protein was collected by centrifugation at 26 000 × *g* for 1 hour. Protein pellets were resuspended in 5 ml column buffer A and loaded onto a pre-equilibrated Sepharose CL-6B column (GE Healthcare, NJ, USA) (22 mm x 300 mm). Majority of the capsids were eluted in the void volume using a column flow rate of 700 µl/min. Fractions containing core protein were pooled according to SDS-PAGE analysis. Capsids were concentrated to 0.5-2 mg/ml by centrifugation-based ultrafiltration using Amicon Ultracel 10k (Millipore) and stored at -80 ^{o}C.

3.4.3.3 Protocol 3 - Expression and purification "Porterfield protocol"

The final protocol used to isolate recombinant capsids was derived from Porterfield *et al.* [245]. Recombinant *E. coli* was cultured as described in Section 3.4.3.1, however 750 ml protein expression broth was seeded with 1-15 ml starter culture. Cultures were incubated at 37 ^{o}C with vigorous shaking until the optical density had reached 0.5 at 600 nm. Cultures were then supplemented with 0.238 g of IPTG (2 mM final concentration) and protein induction continued at 37 ^{o}C with vigorous shaking for 5 hours. Bacterial cells were harvested by centrifugation. The bacterial pellet was resuspended in 12 ml resuspension buffer (Appendix 2) supplemented with 2 mg/ml lysozyme (Sigma) and frozen at -20 ^{o}C overnight. Bacterial suspensions were allowed to thaw at room temperature, after which sonication (20 seconds with 80% cycling and 80% power - performed in quadruplicate) was used to disrupt the remaining intact bacteria and shred RNA and DNA. Lysate debris was collected by centrifugation at 8000 × *g* for 1 hour at 4 ^{o}C and discarded. The remaining

supernatant was subjected to further centrifugation at 120000 × *g* for 14 hours to pellet capsids. Capsid pellets were resuspended in 6 ml column buffer B (Appendix 2) and loaded onto a CL6B Sepharose (GE Healthcare) column (22 mm x 300 mm), equilibrated with column buffer B. Column flow rate was set to 500 µl/min. Fractions containing capsids were identified using SDS-PAGE analysis, pooled, and loaded onto a Blue Sepharose (GE Healthcare) column (16mm x 300mm) equilibrated with column buffer B. Column flow rate was 300 µl/min. Capsid-containing fractions were identified by SDS-PAGE analysis, pooled and loaded onto a 50 mM PBS-buffered 2 mM TCEP (pH 7.5) 40-60% sucrose gradient. Gradients were subjected to centrifugation at 120000 × *g* for 4 hours. Fractions containing capsids (determined by SDS-PAGE analysis) were pooled and dialysed overnight against column buffer B. Capsids were concentrated to 0.5-2 mg/ml with Amicon Ultracel 10k (Millipore, MA, USA) by centrifugation-based ultrafiltration and stored at -80 ^{o}C.

3.4.4 Agarose gel and polyacrylamide gel analysis and staining

3.4.5 Electrostatic modelling.

Modelling was done using the Swiss protein data base viewer (DeepView) [214] using the following parameters:

- Poisson-Boltzmann computation – A more sensitive and accurate analysis over Coulomb computation.
- Protein dielectric constant – 4. Determination of protein dielectric constant remains controversial [246], thus the software suggested value was used.
- Solvent dielectric constant – 80. This is the standard dielectric constant for water at 20 ^{o}C, the solvent used to resuspend the capsids in.

Ionic strength – 162 mM. This was the ionic strength of the PBS solution [247].

Chapter 4: Modification of recombinant HBV capsids using functional moiety-IL conjugation or liposome encapsulation.

4.1 Introduction

In Chapter 3 it was described how lysine or cysteine residues were introduced into the IL of the HBV capsid. These particular residues are frequently used for conjugation-based reactions, to facilitate the attachment of a variety of functional ligands to the protein surfaces. The ligands in turn provide the capsid with functionality suited towards gene therapy vectorology. As naked capsids are highly immunogenic and are indiscriminately taken up by a wide variety of cell types, adequate decoration of their surface with these functional ligands is useful to improve targeting and uptake efficiency. There are a few specific natural amino acids associated with ligand conjugation reactions, however unnatural amino acids have also been used for the ligand attachment. Lysine and cysteine residues are a popular choice for conjugation-based reactions; the less utilised residues include glutamic acid, aspartic acid and tyrosine. Of late, the azide-alkyne cycloaddition reaction with unnatural amino acids has seen increased use for the conjugation of ligands to protein surfaces. There are several factors which influence the choice of residue selected for the conjugation process:

- Stability of the formed conjugate, as certain conjugates (such as the ester-based reaction products) tend to be less stable.
- The prevalence of the target amino acid residue on the protein surface, as excessive surface decoration is associated with significant disadvantages such as ligand and protein inactivation.
- Location of the amino acid residue(s) on the protein surface, as ligand conjugation may influence protein stability or activity.
- Accessibility to the amino acid residue(s) by reactive ligand moieties.
- Selection of the conjugation site according to local environment. Neighbouring residues can alter the local environmental pKa, which influences the success of residue-ligand conjugation.

It has been shown possible to insert residues required for conjugation into the HBV capsid IL without affecting structural assembly or preparation yield (Chapter 3). The first substitutions to the IL of the HBV capsid utilised lysine. The lysine residue contains a primary amine which reacts with compounds containing N-hydroxysuccinimidyl esters (NHS-esters). This method of moiety to protein conjugation has successfully been employed in a multitude of studies, including the covalent linkage of polymers [248], fluorophores [249], transferrins [250], small molecules [251], PEG [252] and epitopes [253]. The presence of lysine on the protein surface offers several benefits when conjugating with functional ligands. The residue is hydrophilic in nature, which often allows for protein surface exposure. Of the 20 natural amino acids, lysine makes up 6.3% of amino acids in proteins [254], which usually makes it a readily available conjugation target. The potentially high surface representation of lysine residues can however present difficulties, as excessive decoration with ligands may result in protein or VLP instability, precipitation or ligand inactivation. The ester linkage within the ligand is also prone to hydrolysis (< 5 hour half-life), which has been shown to increase in environments above pH 7 [255]. Despite these disadvantages, NHS-esters are a popular choice for ligand conjugation, as reaction conditions are mild and a variety of ligands are commercially available.

Cysteine residues were also incorporated into the IL, facilitating an alternative conjugation reaction. A common group used to react with exposed cysteine is maleimide, however other reactive species are available [256]. Maleimide-based conjugation, like the NHS-esters, has been used in a wide variety of reactions including covalent linkage of peptides [253], small molecules [257], polymers [258] and fluorophores [259, 260]. Typically, cysteine residues represent ±1.1% of the 20 amino acid residues within proteins [254]. Consequently, externally located cysteine residues are sparse, and for conjugation purposes often require to be engineered into the target protein. It follows that cysteine residues provide site specific conjugation, preventing potential moiety conjugation to active or receptor-interacting sites. Exposed cysteine residues do pose several shortcomings, the most significant being the formation of cystine bridges with other proteins under oxidising conditions. Disulphide bond formation is also associated with protein misfolding after translation [261]. In an attempt to overcome cystine bridge formation, researchers have engineered cysteine residues within protein pockets, or within the interior of VLPs [261, 262]. A concern of generating VLPs with exposed cysteine residues was the potential

formation of cystine bridges, resulting in aggregation during the preparation or storage process. Interestingly Chapter 3 described the substitution of cysteine residues into the IL of the HBV capsid that were highly exposed to the environment. These VLPs did not aggregate significantly and were stable during storage. As with the NHS-ester reactions, maleimide reacts with cysteine under mild conditions, facilitating simple conjugation with a wide range of available (or synthesisable) ligands.

The alternative conjugation methods available are not as popular as linking to lysine or cysteine. Both aspartic and glutamic acid can be used as sites for conjugation, employing the use of carbodiimide and a primary amine-containing ligand [263]. The carbodiimide forms a reactive intermediate with the carboxylic acid group of glutamic or aspartic acid, allowing for interaction with the primary amine. This is a potential limitation, as it facilitates the conjugation of lysine residues to carboxylic acids between intra- and inter-protein residues. Tyrosine residues are also available as conjugation sites, and may provide for discreet linkage as they are represented 3.3% of the natural amino acids within proteins [254]. The conjugation reaction often involves the use of benzenediazonium to conjugate functional moieties to tyrosine residues on the protein surface [264]. Unfortunately conjugation to tyrosine residues require oxidising reagents which may cause undesired side reactions with the target protein [265].

Unnatural amino acids for ligand conjugation provide an alternative to naturally occurring amino acids. There are over 70 unnatural amino acids available [266], and techniques such as global-replacement that is residue specific (GRRS) or site specific incorporation (SSI) have been used to introduce artificial amino acids into proteins [267-269]. GGRS relies on the replacement of a natural amino acid with an analogous artificial variety during translation, and SSI utilises a stop codon as a tRNA encoding site for the unnatural amino acid. These techniques have allowed for the introduction of alkyne residues, facilitating the reaction with azide groups (Reviewed in [270, 271]). This process is known as azide alkyne cycloaddition (“click” chemistry), and is gaining popularity as a protein conjugation technique. A concern associated with the azide alkyne cycloaddition reaction is the presence of residual copper ions after the reaction and sample degradation by reactive oxygen species. The aforementioned conjugation techniques are illustrated in Figure 4.1.1.

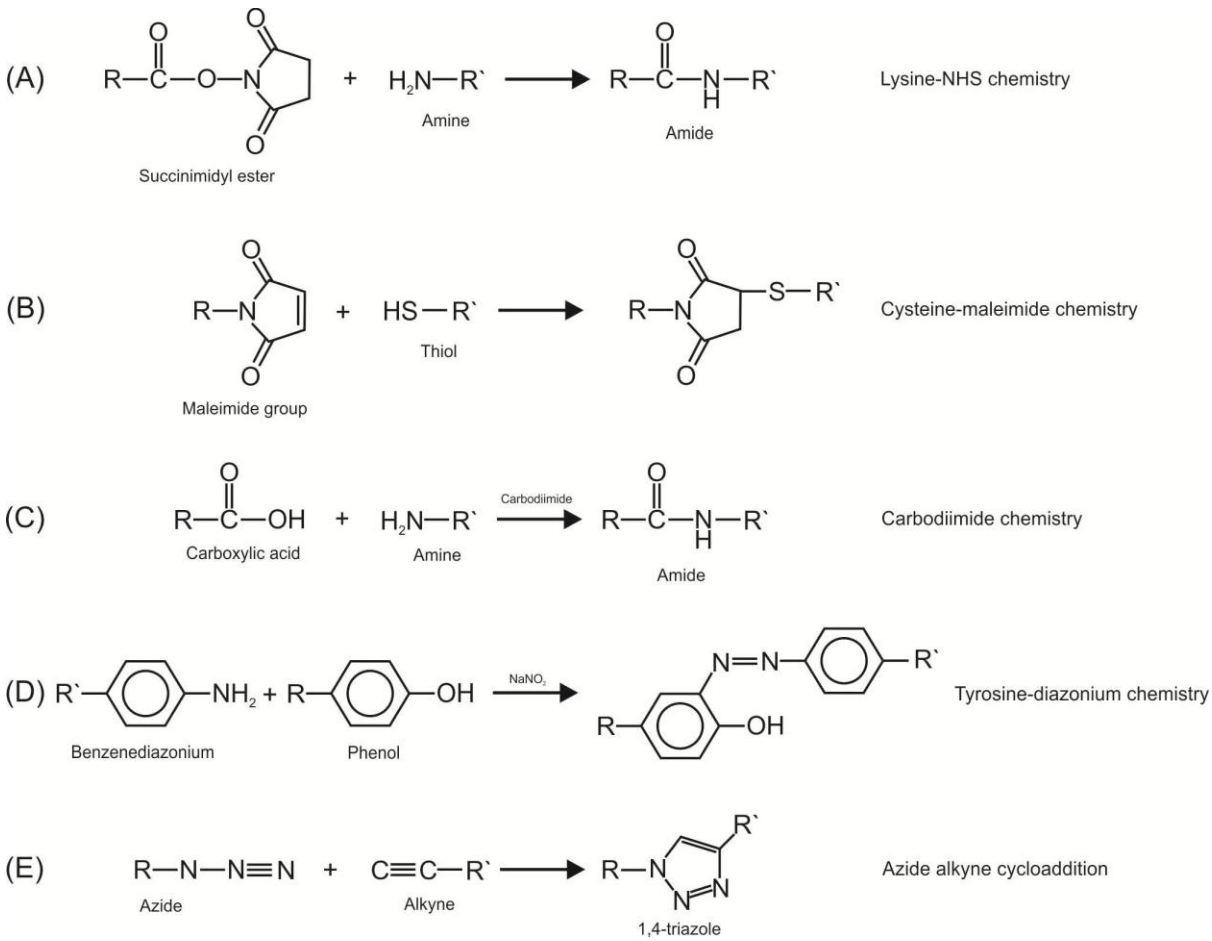

Figure 4.1.1: Illustration of various chemistries used to conjugate ligands to proteins and nanoparticles. (A) Lysine-NHS chemistry is a popular conjugation method as lysine residues are generally well represented on protein surfaces. (B) Cysteine-maleimide chemistry is another useful method, generally employed for site-specific conjugation. (C) The reaction between carboxylic acids and amines is facilitated by carbodiimide. Activated carboxylic acids may react with lysine residues. (D) Tyrosine based conjugation with diazonium. The reaction requires a strong oxidiser which may react with other protein residues. (E) Azide alkyne cycloaddition can occur at low reagent conditions in mild reaction conditions. It is noted that the triazole moiety may cause protein/VLP instability.

Several factors impact on the choice of reaction and ligand type for conjugation:

1) Prevalence and location of targeted residues affect protein stability and activity.
2) The reaction environment should not impact on protein/VLP stability or structure.
3) Availability of ligand may also influence the type of conjugation employed.

As a result of the mild and simple nature of their conjugation chemistries, as well as their infrequent occurrence on the capsid surface, both lysine and cysteine make ideal candidates for ligand conjugation. As a proof of principle starting point, initial conjugation reactions with lysine and cysteine were performed with the readily available succinimidyl carbonate

PEG5000 (scPEG) as the NHS-ester or maleimide PEG5000 (malPEG). Successful conjugation to these residues would prompt further analyses with synthesised galactose-, glucose-, polygalactose- and fluorescein-based ligands. As described in Chapter 2, the galactose ligand provides hepatotropism to the nanoparticle by interacting with the ASGPr on liver cells [132]. The glucose moiety was included as an uptake control, as hepatocytes have a far greater affinity for galactose. It was also assessed whether cellular uptake was increased when using polygalactose ligands. Decoration of the capsid surface with galactose would ideally also prevent the indiscriminate uptake of capsids by a variety of cell types. With adequate decoration using the galactose moieties, the HBV capsid may also gain immuno-evasive properties. It is anticipated that the positioning of the conjugation site and the bulky nature of the galactose compound may shield capsid surfaces which are prone to immuno-detection (such as the IL). Thus the galactose compounds may function similarly to an attached PEG molecule. The ligands conjugated to the HBV capsid surface in this study are illustrated in Figure 4.1.2.

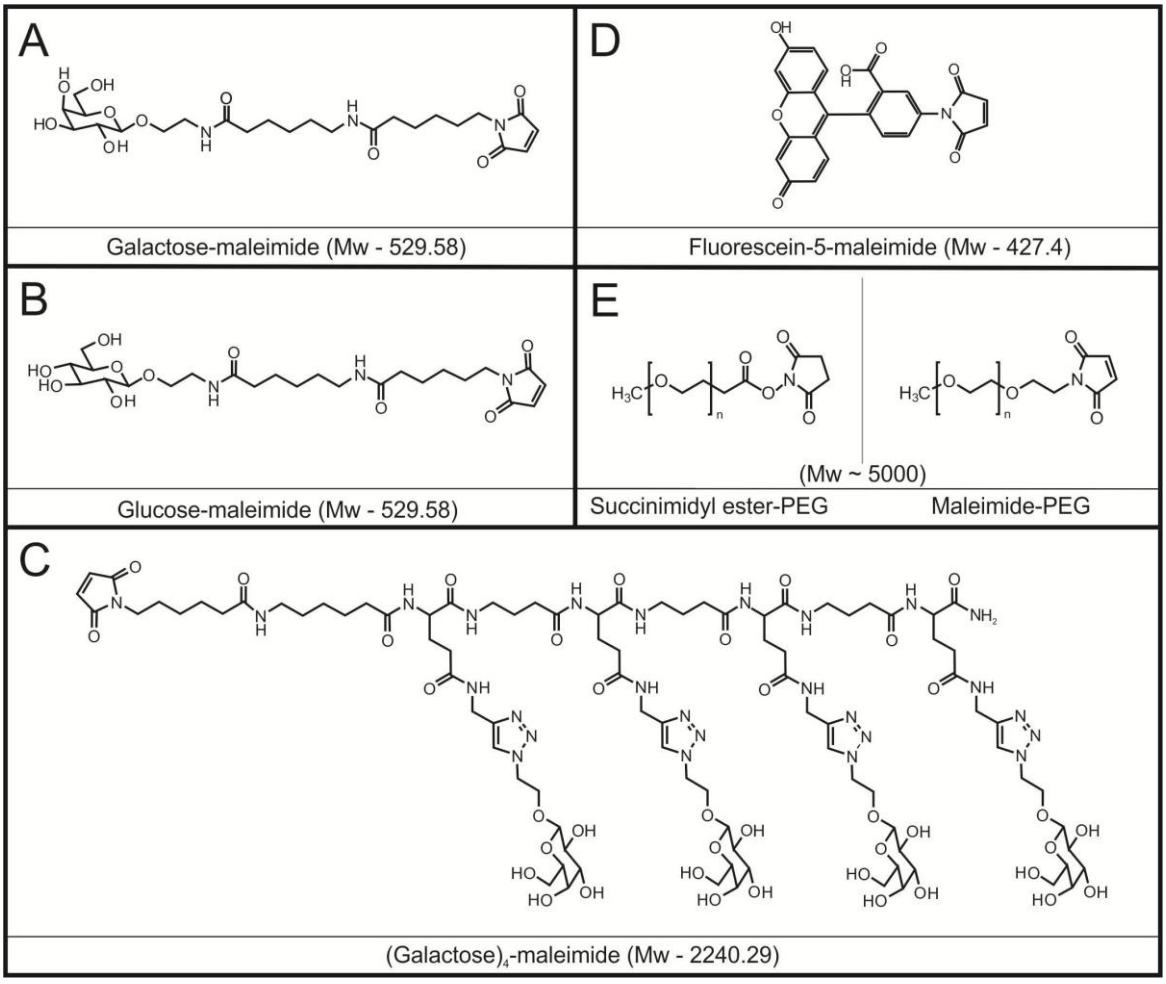

Figure 4.1.2: Diagrammatic representation of ligand moieties used to conjugate to the HBV capsid surface.

Alternative means are available to introduce functional moieties and ligands to the capsid surface. This may be required as the newly introduced residues and/or ligands change the capsid physicochemical properties in such a manner that capsids become unstable. It has been noted that excessive PEGylation to the adenovirus surface leads to VLP instability [272]. An alternative is to avoid covalent linkage to the capsid surface, thus decrease chances of capsid destabilisation. Moreover, these covalent-free methods avoid inclusion of reactive residues (such as cysteine). It has been demonstrated by a variety of researchers that it is possible to envelop VLPs in a liposomal formulation. The liposome exposes functional moieties anchored within its bilayer, avoiding the requirement of direct ligand attachment to the capsid surface. Like VLPs, liposomes have been shown to deliver a wide variety of cargoes. Innovative development has generated liposomes which are capable of drug and metal compound delivery, vaccine capacity, diagnostic imaging and delivery of proteins and peptides (reviewed in [273]). Early studies that attempted to envelop and deliver picornavirus demonstrated that cellular uptake was slow and passive [274]. The slow uptake mechanism is attributed the overall anionic charge of the picornavirus capsid, liposome membrane and cellular membrane, which reduces their association and interaction. Several years later Faller and Baltimore attempted to overcome retrovirus superinfection using anionic liposome virus-encapsulation [275]. Despite showing an improvement in superinfection with anionic liposomes, notable re-infection results were only generated once (poly)cations, such as polybrene, were included in transfections and infections [276, 277]. Similarly, the inclusion of cationic species on the liposome surface translates to significantly improved liposome-based DNA transfection over anionic liposomes [76]. The cations present on the surface of the liposomes facilitated the interaction with the anionic DNA phosphate-backbone, not only allowing for envelopment but also enhanced interaction with cellular membranes. Anionic capsids of retroviruses were also shown to interact with cationic liposomes, resulting in their envelopment and successful uptake by superinfected cells [278-282]. The cationic liposome based-envelopment principle should be applicable to any anionic VLP, including the HBV capsid.

Liposome envelopment of VLPs provides a means to display functional ligands, improve vector stability and increase immuno-evasion [278]. This is of particular importance as immune recognition of therapeutic VLPs remains a major hurdle within the field. The introduction of tissue-tropic ligands to the surface of liposomes may offer an alternative to

generating a variety of expressed motifs or conjugation-based ligands on the capsid surface. This may become necessary if the capsid preparation yields too many capsid aggregates as a result of introduced residues.

This chapter explores the optimal ligand concentration and incubation time to optimise VLP decoration with functional moieties. It was found that maleimide-cysteine based conjugation produced the most decorated capsids. The recombinant capsids of c149, c160 and c170 containing cysteine substitutions were able to undergo various degrees of conjugation. It was also assessed whether the HBV capsid can undergo envelopment using DC-Chol-DOPE-based liposomes [158]. Furthermore, it was demonstrated that liposome envelopment of HBV capsids may be possible, using cationic liposomes embedded with PEG. Both forms of modification resulted in potential improvement of the naked HBV capsid as a vector for gene therapy. It was found that the HBV capsid may be permissible to liposome envelopment, however required the presence of PEG to stabilise the new VLP structures.

4.2 Results

4.2.1 Assessment of lysine-N-hydroxysuccinimide-based conjugation of scPEG to capsids containing R82K and A80K R82K

Wild type core protein contains two lysine residues, K7 and K96 (Figure 4.2.1). Lysine 7 is located within the three-fold and quasi three-fold axes pore [201]. This location may have limited accessibility to bulky compounds such as PEG, preventing conjugation with scPEG at this site. Conversely K96 is located on the α4 helix, which is readily exposed to the environment and may undergo lysine-NHS based reactions. The lack of readily exposed lysine residues has made the HBV capsid an ideal protein to be modified with NHS-based chemistry as it favoured site-directed conjugation to the IL. A mutation such as K96R could further facilitate site-directed conjugation to the IL without impacting on capsid stability, formation and physicochemical properties.

The lysine-NHS reaction was assessed using c149 A80K R82K at a mole ratio of 1 scPEG to 1 IL lysine residue over a time course of 24 hours. In addition, a reaction consisting of the mole ratio 10 scPEG to 1 IL lysine was incubated for 8 hours at room temperature. These initial reaction conditions were assessed as the literature varied in reported ligand concentration and incubation times. SDS-PAGE analysis revealed that no significant conjugation occurred over the time course of 24 hours (Figure 4.2.2).

A series of additional reaction conditions were assessed, varying the reaction buffer, protein and ligand concentration, pH, salt concentration, incubation time and temperature. All of the varied reaction conditions did not yield a conjugate (data not included). Control proteins with significant lysine content were also assessed for conjugation to scPEG. Bovine serum album (BSA) and creatine phosphokinase (rabbit muscle) (CK) contain 59 and 33 lysine residues (Figure 4.2.1.3B), respectively, of which a large proportion are exposed to the protein surface. Similarly to reactions with c149 A80K R82K, the control proteins did not undergo scPEG conjugation (Figure 4.2.3A).

Lack of conjugation to the protein surface suggested that the reactive succinimidyl carbonate moiety may have undergone hydrolysis or oxidised with atmospheric oxygen. Dry stocks of scPEG were maintained within a desiccation chamber, thus decreasing the chances of hydrolysis. Nonetheless, chemical assessment of scPEG reactivity may reveal why the conjugation reaction to c149 A80K R82K failed. As a wide variety of reaction variables were assessed in attempting to conjugate lysine and scPEG, it was decided to investigate the alternative cysteine-maleimide reaction. Similarly to scPEG, initial reactions with maleimide-PEG were performed to determine moiety to target ratio and reaction incubation times.

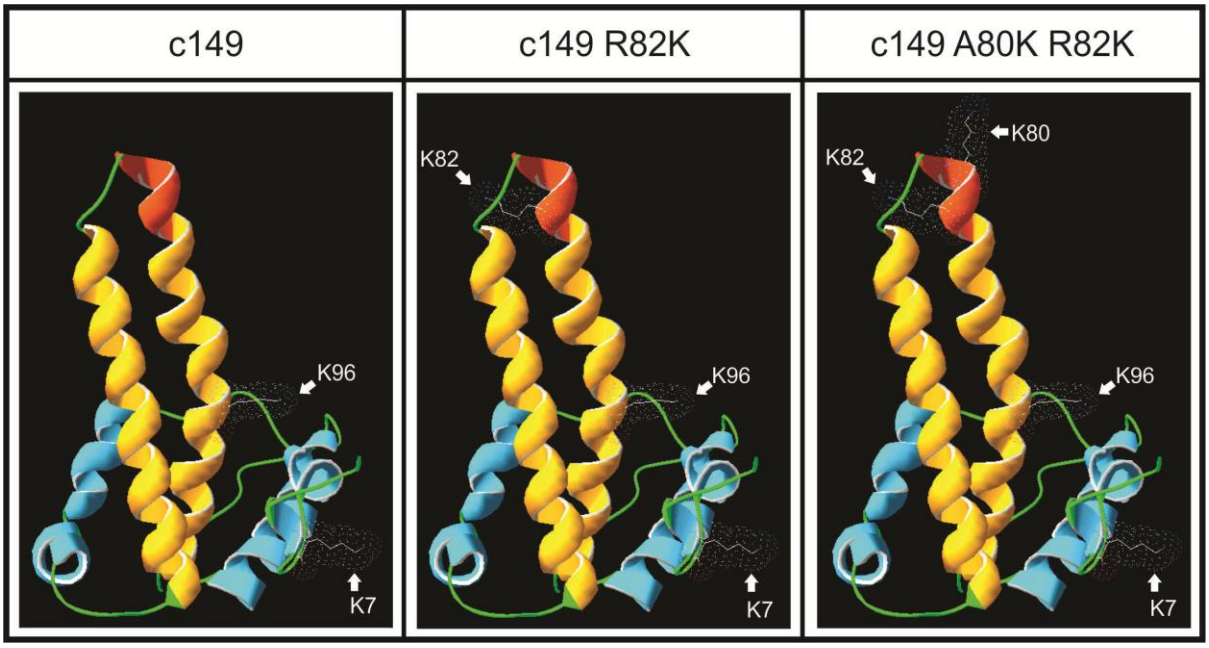

Figure 4.2.1: Distribution of lysine residues within c149, c149 R82K and c149 A80K R82K. The wild type c149 contains 2 lysine residues at position 7 and 96. The K7 residue is located within the three-fold axis pore (Figure 3.1.6) and K96 within helix α4. c149 R82K contains an additional lysine residue at position 82, and c149 A80K R82K has two additional lysine residues at position 80 and 82. The colour-scheme used is similar to that of Figure 3.1.4. Protein structure was modelled in Swiss-PDB Viewer [214] using data from Wynne *et al* [201].

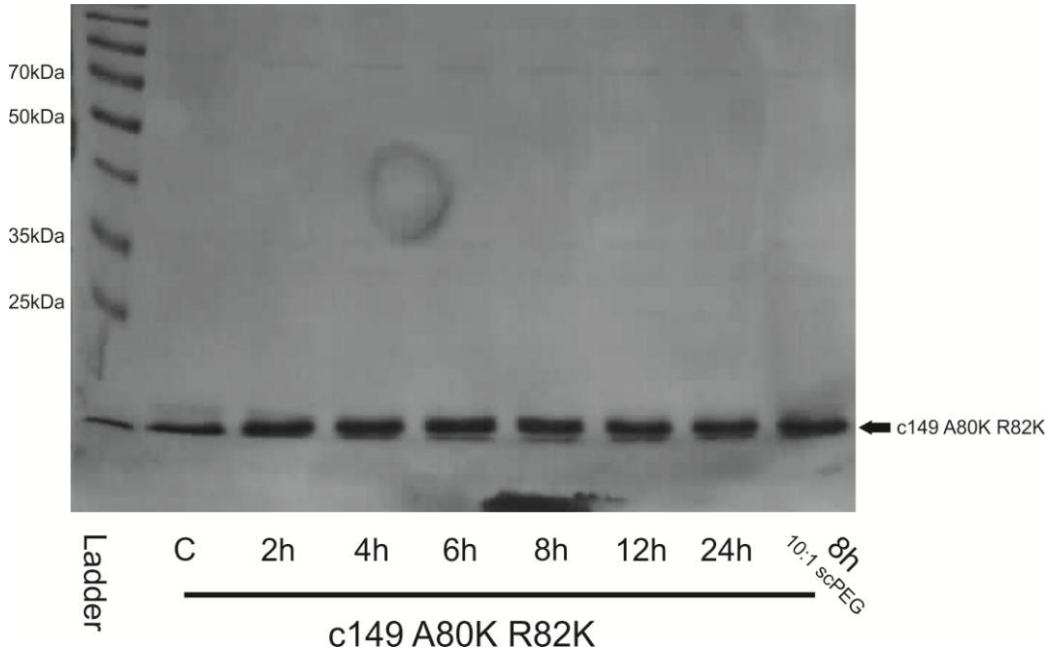

Figure 4.2.2: SDS-PAGE analysis of c149 A80K R82K reaction with scPEG over 24 hours. c149 A80K R82K, stained with Coomassie Brilliant Blue-R250, is indicated by the black arrow. The control sample (C) was treated with DMSO and contained no reactive succinimidyl groups. Samples 2h -24h were incubated at room temperature at a ratio 2 scPEG5000 to 1 core protein. The sample 8h (10:1 scPEG5000) was incubated for 8 hours with 20 scPEG5000 molecules per 1 core protein at room temperature.

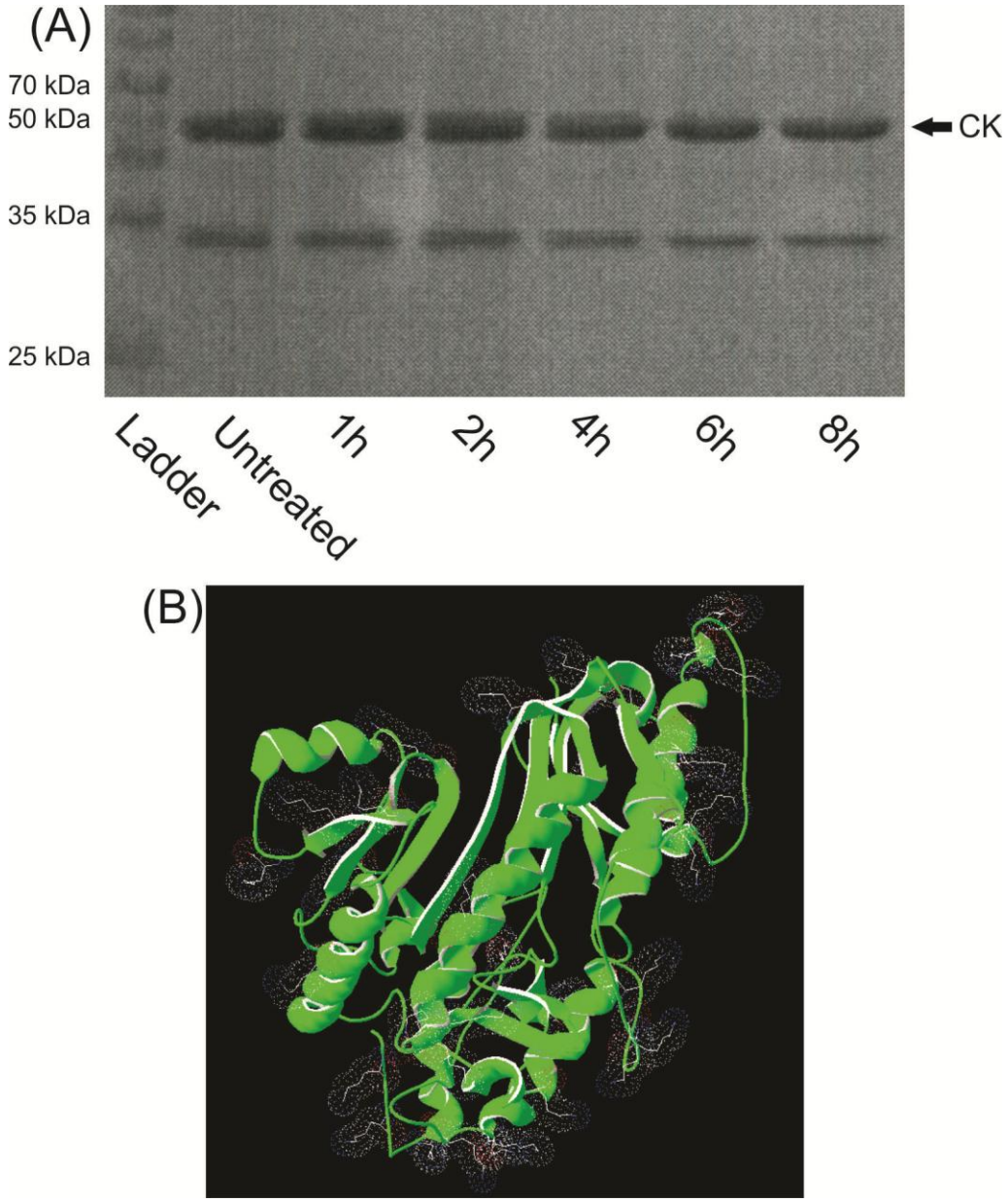

Figure 4.2.3: SDS-PAGE analysis of CK PEGylation using scPEG over an eight hour period. (A) A total of 1 μg of CK underwent a conjugation reaction, which contained 10 moles of scPEG for every 1 mole CK (black arrow). The untreated protein sample, was incubated with DMSO only. Proteins were stained with Coomassie Brilliant Blue-R250. (B) Predicted structure of CK (green), with surface exposed lysine residues highlighted (dotted regions) [283].

4.2.2 Maleimide-based ligand conjugation to inserted cysteine residues of S81C and L76C S81C

Ligand linkage to a cysteine residue provides an alternative to lysine-NHS chemistry. Generally wild type proteins have little to none exposed cysteine, allowing for site directed conjugation of introduced residues. Creatine phosphokinase contains a single exposed cysteine residue at position 254, which was used to assess conjugation of malPEG to the protein surface. As with lysine-NHS, the literature reports varied incubation times required for cysteine-maleimide conjugation. An initial time course assay was performed to determine the required duration for observable PEG-CK conjugation (Figure 4.2.4). After one hour incubation with malPEG5000 (at a mole ratio of 10 maleimide-PEG to 1 CK), a characteristic shift of ±5 kDa was observed with ±60% of the CK population. The conjugation did not appear to increase with extended incubation time. A second time course assay revealed that incubation for as little as 15 minutes at room temperature was sufficient to reach conjugation end-point between malPEG5000 and CK (data not shown).

With the aforementioned parameters in mind, the single and double cysteine mutants of c149, c160 and c170 were assessed for conjugation with malPEG5000 (Figure 4.2.5). Recombinant c183 S81C and c183 L76C S81C did not purify to accepted levels, despite a variety of preparation protocols attempted. Thus, c183 S81C and c183 L76C S81C were initially omitted from the conjugation assessment. Approximately 60% of both c149 S81C and c149 L76C S81C showed a migration-shift during SDS-PAGE analysis. Interestingly a second dominant band appeared in samples c149 S81C and c149 L76C S81C nearing 35 kDa in size. Protein in this band may have been the product of conjugation between malPEG and a dimerised core protein (±33.4 kDa). Curiously a predominant 5 kDa shift of dimer occurred, as opposed to a potential 10 kDa shift of a double PEGylated dimer. The initial conjugation of bulky PEG compounds may have significantly reduced access to the IL region of the four-helix bundle, preventing the second conjugation event. The control protein, wild type c149, did not undergo any observable migratory shift. This data suggests that the inserted cysteine residues underwent a conjugation-based reaction with malPEG, and the native cysteine residues (C48 and C61) did not interact with malPEG. No observable conjugation occurred between malPEG and the single and double cysteine substitutions of c160 and c170.

It is documented that the protamine domain is capable of protruding from capsid pores, extending outwards from residues 149-183 [217]. The cationic nature of the protamine domain has the potential to interact with the anionic IL, thus resulting in restricted access to the reactive cysteine residues. This was supported by the data in Figure 4.2.5, whereby capsid particles that contained a protamine domain (c160 and c170) displayed decreased efficiency in conjugation to ligands or moieties compared to capsid particles without protamine domains. It was reasoned that incubation periods beyond 1 hour may permit sporadic conjugation reactions to the IL, in which an observable change in protein size would occur.

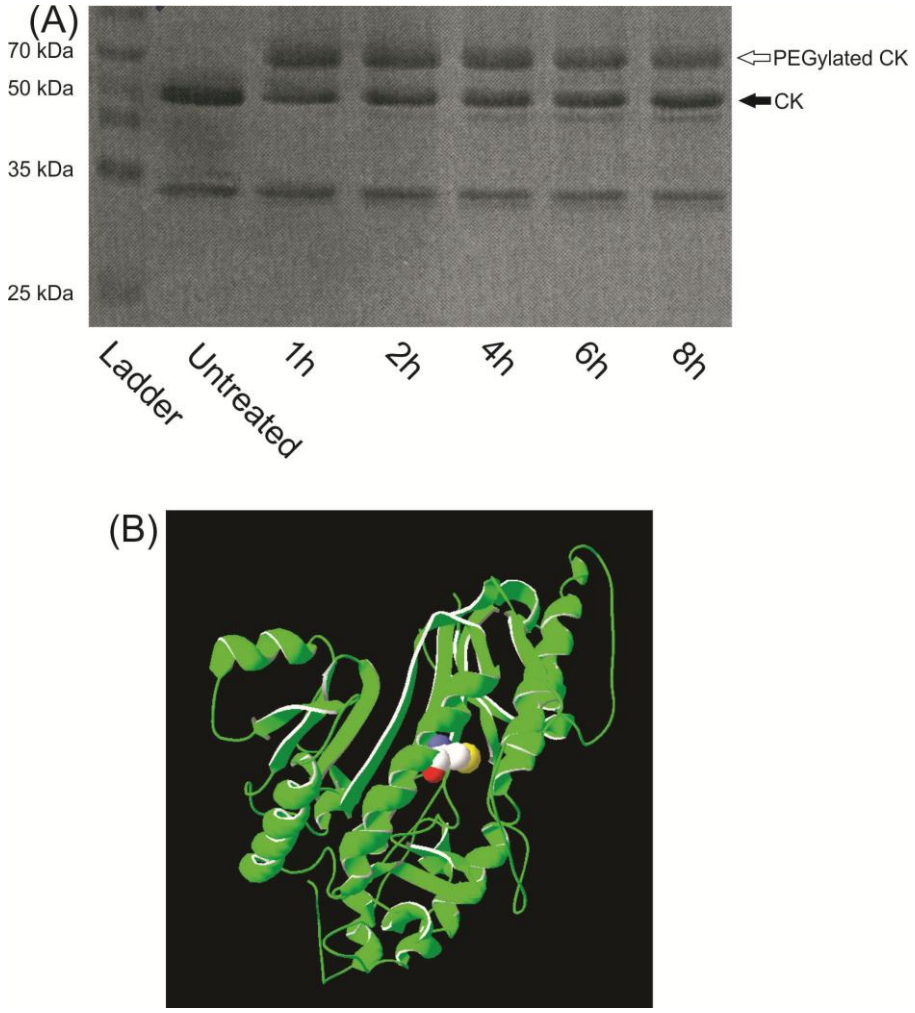

Figure 4.2.4: SDS-PAGE analysis of the conjugation reaction between CK and malPEG5000, over an 8 hour period. (A) MalPEG was combined with 1 μg CK (black arrow) at a mole ratio of 10 moles to one mole, respectively. In the presence of malPEG, an additional protein species forms (white arrow). The control sample, "untreated", did not receive malPEG treatment. (B) The predicted structure of CK, highlighting the single exposed cysteine residue (white and yellow region) [283].

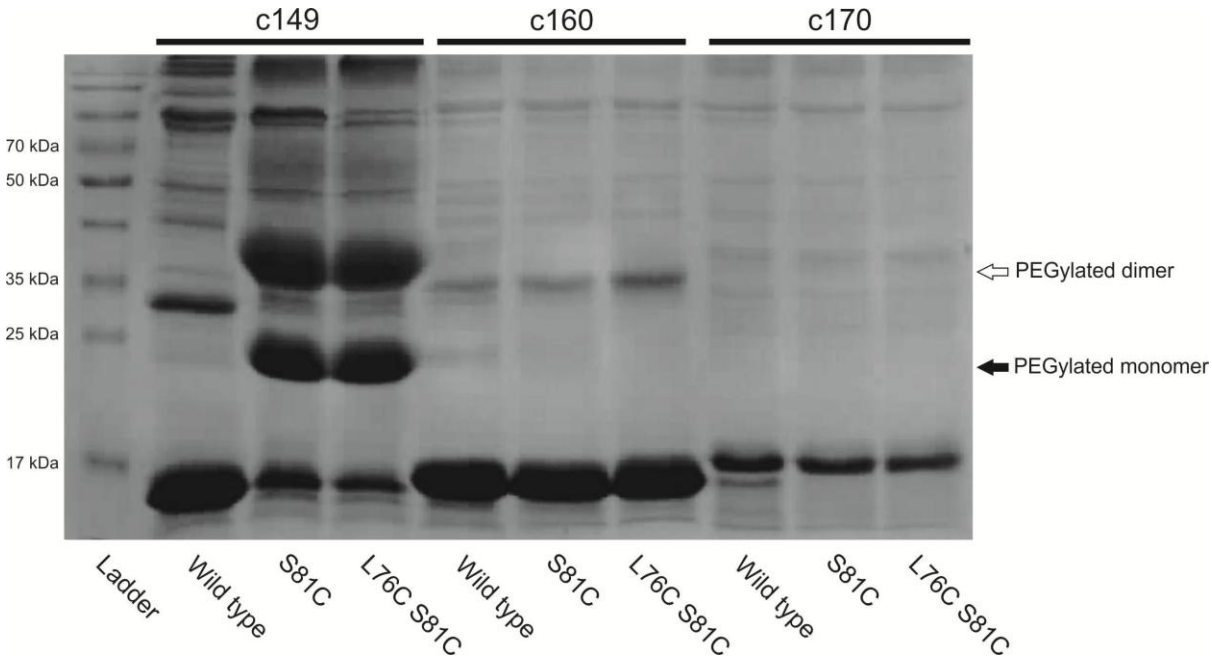

Figure 4.2.5: SDS-PAGE analysis of malPEG conjugation with core clones with/out cysteine substitutions within the IL, stained using Coomassie Brilliant Blue-R250. Preparations of c149, c160, c170 and their respective S81C or L76C S81C mutants were incubated with malPEG for 30 minutes at room temperature. One microgram of core protein was analysed, in which 10 moles malPEG molecules were present for every 1 cysteine residue at the IL. One microgram of wild type protein (control) was combined with malPEG such that 10 moles of malPEG were present for every 1 mole of core protein. The c149 S81C and c149 L76C S81C form additional distinct bands after incubation (black and white arrows). These additional bands are not present in the wild type c149, or any of the c160 and c170 clones.

4.2.3 Increased incubation time results in malPEG conjugation to c160 L76C S81C and c170 L76C S81C.

It was undetermined whether potential intermittent association of the protamine domain to the IL prevented the maleimide-cysteine conjugation reaction. However, the structurally-plastic nature of the protamine domain [218] may allow for flexibility at the IL. Without a fixed association, dissociation of the protamine domain from the IL may allow for occasional malPEG conjugation events. Subsequently c160 L76C S81C and c170 L76C S81C were incubated with malPEG5000 over a 24 hour period at room temperature (Figure 4.2.6 A and B). PEGylation of both core proteins became evident after two hours, and continued to increase up until 8 hours. Protein levels appeared to decrease after 12 hours, in which aggregation, destabilisation or degradation of core proteins may have occurred. Similarly destabilisation of CK is observed after 24 hours (Figure 4.2.6 C), in which the additional protein bands may have resulted from the PEGylation of internal cysteine residues. PEGylation of c149 capsids was considerably more efficient than the c160 and c170 species,

however the increased incubation period allowed for feasible amounts of ligand to be conjugated to their capsid surface. Having established malPEG conjugation to the capsid surface, alternative maleimide-ligands were assessed for their potential conjugation to c149 L76C S81C and c160 L76C S81C.

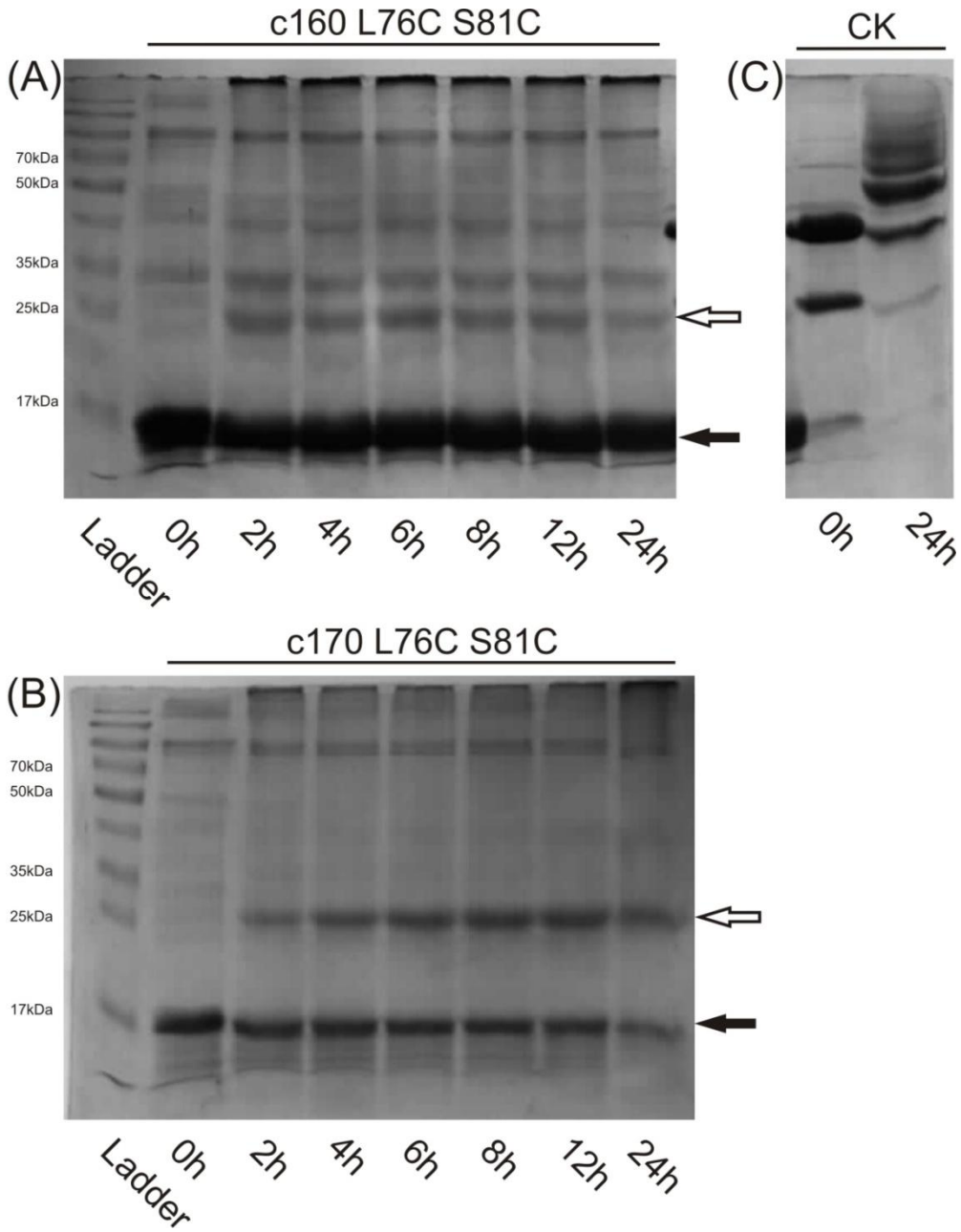

Figure 4.2.6: SDS-PAGE analysis of c160 L76C S81C and c170 L76C S81C incubation with malPEG5000 over 24 hours. (A) c160 L76C S81C (black arrow) incubation with malPEG5000 for 2 hours or longer at room temperature resulted in an additional protein band (white arrow). Similar results were found for c170 L76C S81C (B). The control protein CK also resulted in an additional band present after incubation with malPEG5000 for 24 hours (C).

4.2.4 Cysteine-maleimide conjugation of functional ligands to c149 L76C S81C and c160 L76C S81C

Capsids are indiscriminately taken up by a variety of cultured cells and decoration of the capsid surface with specific ligands may provide much required tissue-tropism [98, 99, 236]. Three maleimide-monosaccharide ligands, malPEG or F5M were independently conjugated to the surface of c149 L76C S81C. Ligand and capsid were incubated for 6 hours at room temperature at a mole ratio of 10 maleimide-ligands to 1 cysteine residue. The conjugation events resulted in an electrophoretic mobility shift, effected by the new overall charge and molecular weight (Figure 4.2.7). It was anticipated that not all core protein units will undergo conjugation (Figure 4.2.6), which would result in a heterogeneous capsid population with varying degrees of modification. Ethidium bromide incorporation revealed the position of the *T=4* capsids at approximately 3000 bp, and less so the *T=3* capsid near 1500 bp (band visibility may also be as a result of protein auto-fluorescence). Surprisingly the modified capsids showed uniform conjugation, represented by the capsid conformation *T=3*, which migrated as a distinct band, indicated in Figure 4.2.7. The *T=4* capsid band contains large amounts of capsid, in which it was difficult to differentiate varying states of modification (indicated by the black arrow). As such, it would appear that these regions contain a variety of heterogeneous ligand-conjugated capsids. Both galactose-maleimide and glucose-maleimide conjugation decreased the electrophoretic mobility of c149 L76C S81C. As galactose and glucose are 4-C epimers of each other, modified capsid migratory patterns were similar. These two monosaccharide moieties appear to increase the 'bulkiness' over altering the electrostatic potential of the capsid. As expected the compound galactose$_4$-maleimide further decreased capsid electrophoretic mobility. Galactose$_4$-maleimide displays similar physicochemical properties to the monosaccharide species, however is approximately four times larger, thus further decreasing the mobility of capsid conjugates in the agarose gel. MalPEG is the largest and bulkiest of the moieties and had the greatest effect on decreased electrophoretic mobility. Interestingly, F5M increased electrophoretic mobility, despite the molecular weight being similar to galactose-maleimide or glucose-maleimide. F5M increased the overall anionic nature of c149 L76C S81C, which resulted in increased electrophoretic mobility.

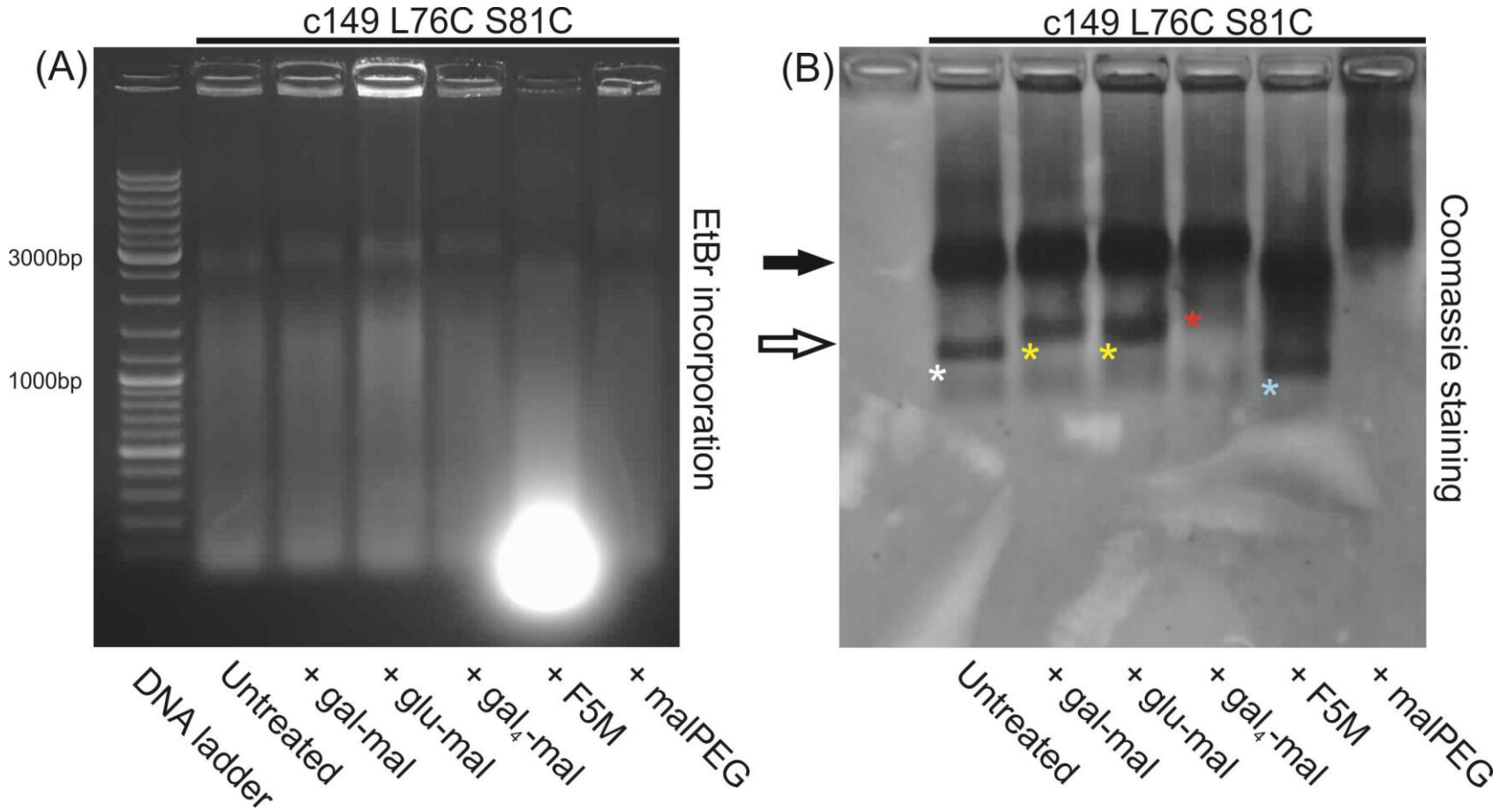

Figure 4.2.7: Effect of c149 L76C S81C mobility with surface ligand conjugation, analysed by agarose gel electrophoresis. Capsid preparations were incubated with various maleimide-ligand moieties for 2 hours, which resulted in altered electrophoretic mobility compared to unmodified c149. Ten moles of mal-ligand was combined with 1 mole exposed IL cysteine residue, in a reaction total of 1 μg core protein. Capsids produced weak auto-fluorescence, made visible under shortwave UV light (A). Two capsid conformations were present, the major *T=4* conformation (black arrow) and the minor *T=3* conformation (white arrow) (B). The shift in capsid electrophoretic mobility is more easily noticed when comparing *T=3* over *T=4* capsids indicated by the white asterisk (Untreated c149 L76C S81C), yellow asterisk (monosaccharide conjugate), red asterisk (polysaccharide conjugate) and blue asterisk (FITC conjugate).

Modified c149 L76C S81C was subjected to SDS-PAGE to determine the mobility shift of individual core proteins as a result of ligand conjugation. Overall the conjugation effect on mobility was difficult to distinguish from unmodified core protein, except for the sample conjugated with malPEG (Figure 4.2.8). The capsids conjugated with malPEG showed the anticipated ±5 kDa shift. The conjugation of galactose-maleimide, glucose-maleimide and F5M does not result in an obvious shift in core size (of approximately 0.5 kDa). This may be attributed to modified and unmodified bands being poorly distinguishable from each other. It was noted that a slight shift of mobility occurred for each of the monosaccharide-modified core proteins. Lastly, capsids modified with galactose$_4$-maleimide resulted in a faint additional band ±2 kDa above the unmodified core protein. This shift correlates to the anticipated size of galactose$_4$-maleimide (2240 Da). The additional band suggested that the sample contained both modified and unmodified core protein, and indicated that the conjugation did not occur on each protein. Once conjugated, these bulky ligands may spatially interfere with the second conjugation event to the dimer, explaining the presence of both modified and unmodified core proteins.

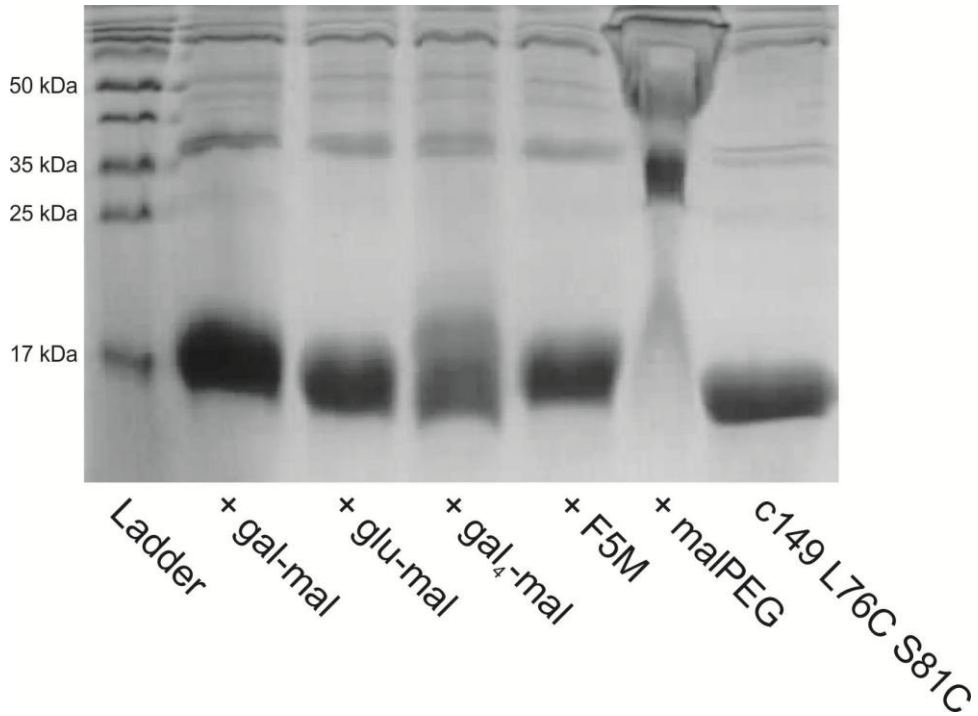

Figure 4.2.8: SDS-PAGE analysis of functional-ligand conjugation to c149 L76C S81C. One microgram of core protein was reacted with its respective ligand such that 1 mole of core protein was combined with 20 moles of mal-ligand. Conjugation with galactose-maleimide, glucose-maleimide or F5M resulted in a shift of protein migration. Two protein bands become visible after conjugation with galactose$_4$-maleimide. A predominant core species near 25 kDa becomes visible after incubation with malPEG5000.

The c149 L76C S81C recombinant protein provided a proof of concept platform in which the effects of ligand surface-conjugation were assessed. It is required of the HBV capsids to deliver a therapeutic payload to a specific cell type. As such the c149 core protein is inadequate as a nucleic acid vector as it does not contain a protamine domain which is involved in DNA/RNA binding. Both c160 L76C S81C and c170 L76C S81C contain protamine domains; and were amenable to maleimide-based ligand conjugation with increased incubation time. As a result of higher yields after induced expression in *E. coli*, c160 L76C S81C was selected for ligand conjugation analysis. Previously described ligands were independently incubated with c160 L76C S81C for 6 hours at room temperature, following which conjugates were analysed by agarose gel electrophoresis and SDS-PAGE (Figure 4.2.9 and Figure 4.2.10, respectively). A mole ratio of 10 ligand to 1 cysteine was used during the conjugation reaction. In stark contrast to the c149 L76C S81C ligand conjugation reactions, c160 L76C S81C displayed exceptional efficiency in ligand conjugation. It was observed that each of the modified capsids displayed a distinct electrophoretic mobility in comparison to the unmodified core protein. Capsids modified with galactose-maleimide and glucose-maleimide display decreased co-migration to similar positions (±4.5 kb position), while galactose$_4$-maleimide exhibited a further decreased electrophoretic mobility (±10 kb position). As previously stated this decrease in electrophoretic mobility is most likely on account of increased capsid bulk, as opposed to change in capsid electrostatic nature. Conjugation of malPEG to the capsid surface resulted in majority of the capsids aggregating near the loading well. This aggregation may be attributed to the sheer bulky nature of PEGylated capsids or precipitation of the capsids in the presence of PEG, however no flocculates were observed in solution prior to sample loading into the agarose gel. As previously described for the *T=4* capsids of c149 (and cysteine variants thereof), c160 L76 S81C without ligands migrates near 3 kb. SDS-PAGE analysis demonstrated a slight migratory shift to the majority of c160 L76C S81C conjugated with galactose-maleimide or glucose-maleimide compared to unmodified (Figure 4.2.10). Conjugation of galactose$_4$-maleimide was less efficient than the monosaccharide ligand, but a clear shift in migratory behaviour is seen. MalPEG5000 shifts the modified core protein migration to just less than 25 kDa, and is also not as efficient as the mono-sugar ligands. Curiously, it would appear that a single conjugation event occurs per protein, despite the presence of 2 cysteine residues. These

results confirm that HBV capsids are amenable to surface modification, which enable properties such as tissue-tropism and immuno-evasion to be conferred.

As described in Chapter 3, capsid integrity/viability was compromised by the exchange or addition of various amino acid residues. Furthermore, other than the 'Snap-in' cloning system, changes made to the IL can be laborious and challenging during cloning. All of these factors prompted the investigation into alternative methods of displaying functional moieties on the capsid surface without any covalent linkage. An interesting, but less utilised approach to capsid decoration with ligands is the envelopment of capsids with liposomes. As opposed to direct conjugation to the capsid surface, tissue-tropic and immuno-evasive ligands are embedded within the lipid bilayer. It may prove as an advantage to envelop capsids as the highly immunogenic IL becomes hidden within the liposomal complex, further enhancing the vector-like properties of this VLP. The following section addresses the possibility of HBV capsid-liposome envelopment.

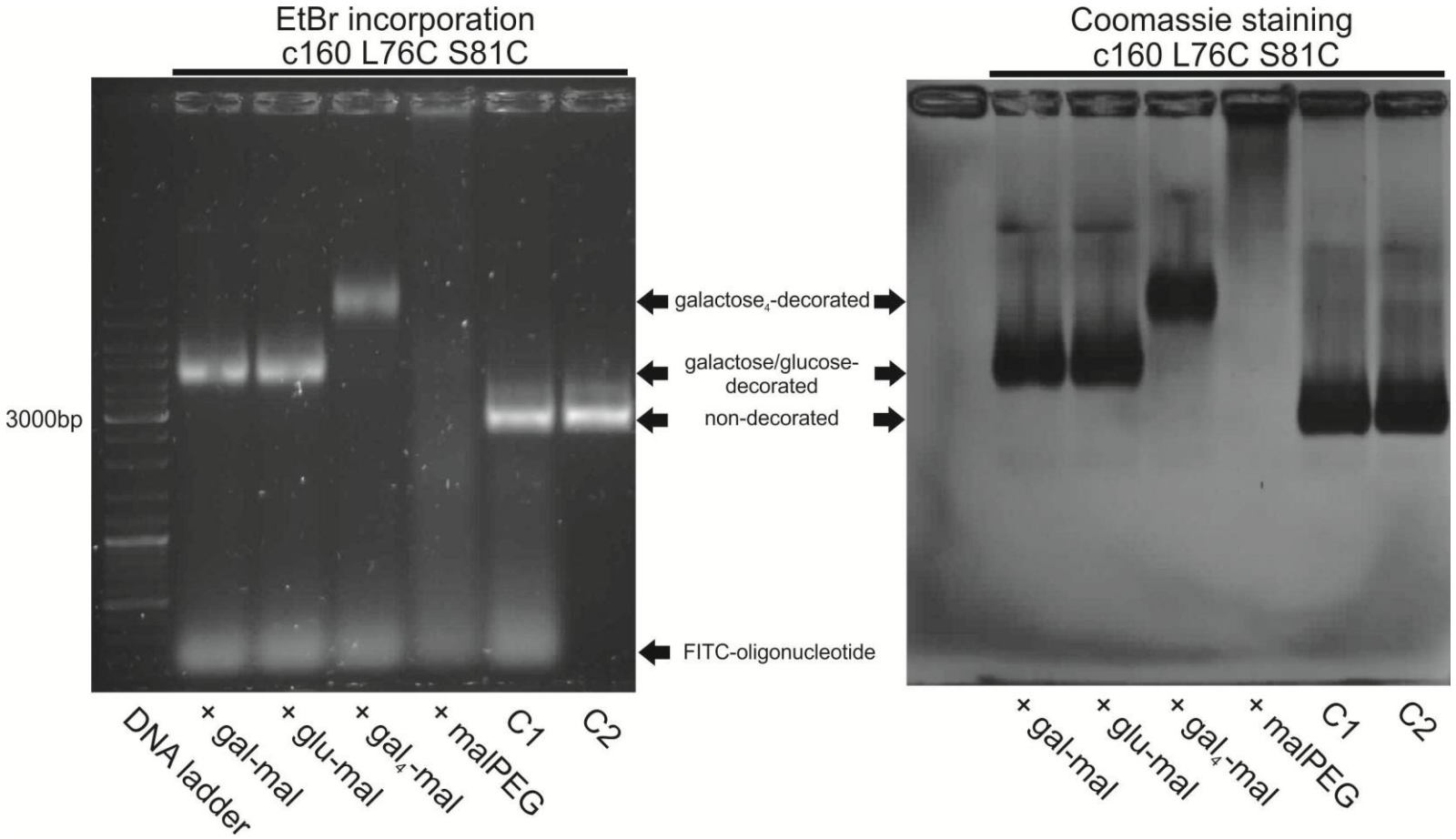

Figure 4.2.9: Effect of c160 L76C S81C electrophoretic mobility with surface moiety conjugation, analysed by agarose gel electrophoresis. Capsid preparations were incubated with various maleimide-ligands for 6 hours. One microgram of recombinant core protein was reacted with its respective mal-ligand, such that 1 mole of core protein was combined with 10 moles of mal-ligand. RNA loaded capsids incorporated EtBr, and were visible near 3000 bp (C1 and C2), 4500 bp (galactose-maleimide and glucose-maleimide) and 10 000 bp (Galactose$_4$-maleimide) under short wave UV light. Conjugation with malPEG5000 resulted in capsids not migrating from the well. Coomassie Brilliant Blue R250 staining revealed identical migratory behaviour as seen with EtBr incorporation. Control protein C1 contains a fluorescently labelled oligonucleotide, whereas C2 does not.

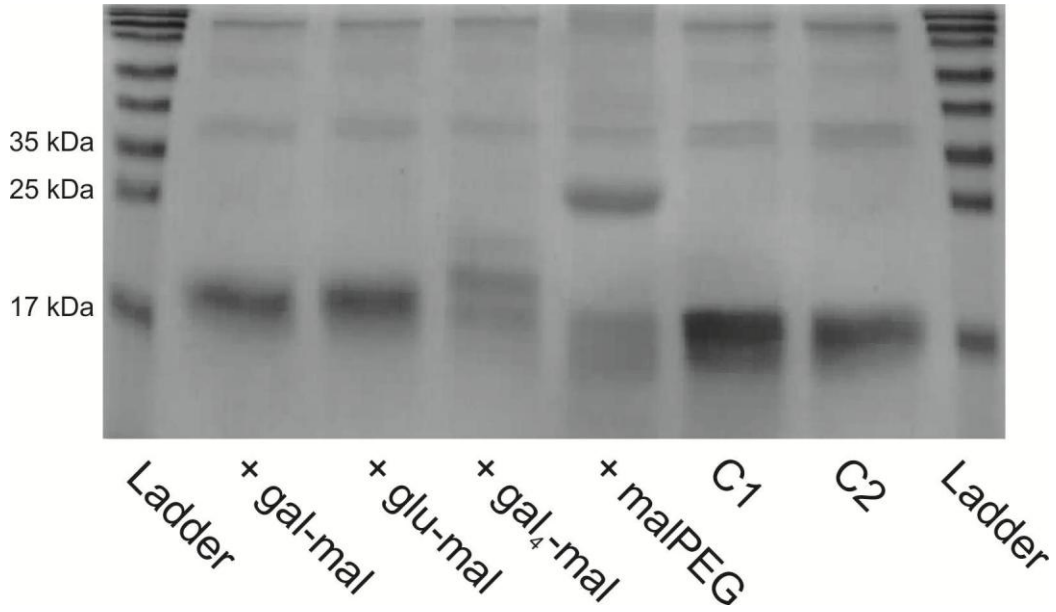

Figure 4.2.10: SDS-PAGE analysis of c160 L76C S81C conjugated with various functional ligands. One microgram of core protein was reacted with its respective ligand for 6 hours such that 1 mole of core protein was combined with 20 moles of mal-ligand. A distinct shift in core size occurs after conjugation with galactose-maleimide and glucose-maleimide. Two core protein species were evident after conjugation with galactose$_4$-maleimide. Conjugation with malPEG introduced a second protein band. Control proteins C1 and C2 do not contain any modifications to their surface.

4.2.5. Assessment of VLP liposome envelopment using mobility shift assay analysis

The anionic surface of capsids is a useful feature for electrophoresis, as capsids migrate based on size and charge through the agarose gel matrix. Capsid envelopment by liposomes nullifies the native charge and consequent electrophoretic migration was assessed by mobility shift assay in agarose gel, shown in Figure 4.2.11. Liposomes were generated by combining up to three of four lipid variants, cholesterol or DC Chol and DOPE or 5-10% DOPE-PEG. Liposomes comprising 60% cholesterol moiety and 40% DOPE moiety (mole/mole) were used as previously described [155]. In doing so four liposome varieties were generated: cholesterol with DOPE; cholesterol with DOPE and 5-10% DOPE-PEG; DC-Chol with DOPE; DC Chol with DOPE and 5-10% DOPE-PEG. Liposome and capsid were combined at various concentrations (0.25, 0.1 and 0.05 μg/μl) as to assess the effects of complex concentration on precipitation [284]. Capsid envelopment was most successful in the presence of liposomes that contained DC Chol and DOPE-PEG. Densitometric analysis revealed that in the presence of DC Chol and PEG (5 and 10%), capsids were sequestered 60% more efficiently than liposomes without either lipid species. Liposomes with an overall

anionic surface charge (DOPE-cholesterol) did not significantly sequester capsid. Interestingly DOPE-DC Chol liposomes did not sequester capsids either, despite the potential for liposome-capsid electrostatic interaction. PEGylated DOPE-cholesterol liposomes interacted poorly with the capsids suggesting that an anionic surface charge, despite improved liposome stability provided by PEG, is insufficient for capsid sequestration. These data suggest that the combination of DOPE-PEG and DC Chol in liposomes is required for the interaction, binding and sequestration of anionic HBV capsids.

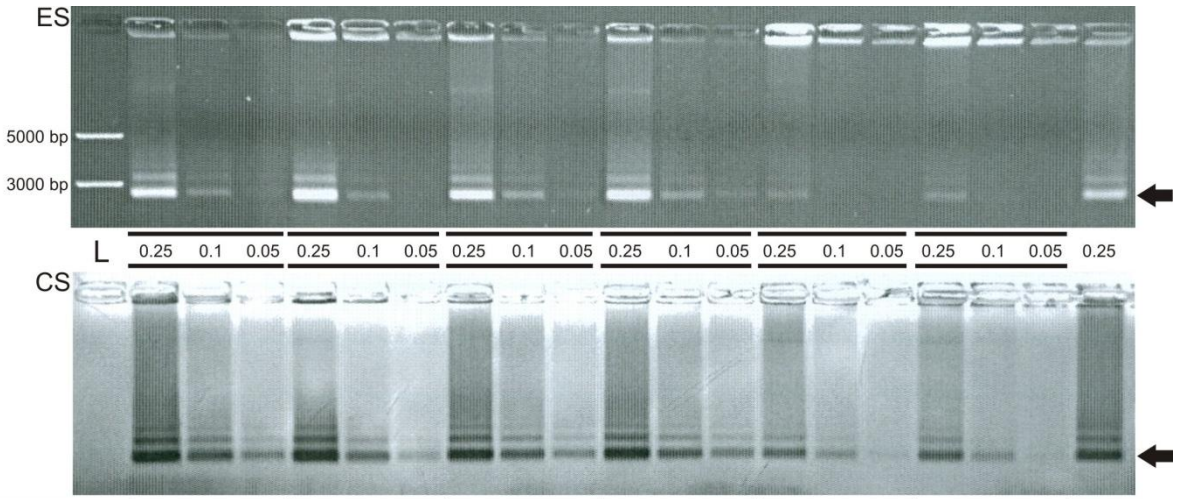

DOPE	40%	40%	30%	35%	30%	35%
DOPE-PEG			10%	5%	10%	5%
Cholesterol	60%		60%	60%		
DC Chol		60%			60%	60%

Capsid Control

Figure 4.2.11: Assessment of capsid envelopment by agarose-based mobility shift assay with ethidium bromide and Coomassie Brilliant Blue-R250 staining. Liposomes comprised 60% cholesterol (cholesterol or DC Chol) and 40% DOPE (DOPE and/or DOPE-PEG2000) moiety (mole/mole). Liposome and capsids were combined in equal amounts (w/w), at 0.25, 0.1 or 0.05 μg/μl and incubated overnight at 4 ^{o}C. Non-enveloped capsid migrated into the agarose gel by electrophoresis. The capsid control lane does not contain liposomes, Lane L is DNA ladder. The arrow indicates the position of capsid stained either with ethidium bromide (ES) or Coomassie Brilliant Blue R250 (CS).

4.2.6. Particle size analysis of capsids, liposomes and enveloped virus-like particles

To further assess HBV capsid and liposome interaction, capsids, liposomes and potential enveloped particles were analysed by particle sizing as shown in Figure 4.2.12. Liposomes comprising DC Chol and 10% DOPE-PEG were used for envelopment of capsids. Prior to complexing, 95.6% of the liposomal population were particles 153 ± 1.5 nm in diameter. The remainder of this population comprised 1.67% 22.8 nm and 2.73% 4822 nm diameter particles. These liposome sizes have consistently been generated previously (data not shown). Capsid particles were also distributed in three distinct sized populations. Interestingly the largest capsid-sample population was represented by 91.2% of 220.4 nm diameter particles. The smaller population (5.33%) were 29.9 ± 2.8 nm in diameter, which corroborate published capsid sizes [76, 198]. A small remainder of the capsid population presented as a large aggregation. Incubation of liposome with capsid yield two distinct populations, 90.6% as particles with a diameter of 740 nm and 9.4% with a 46 ± 9.2 nm diameter. The smaller unidentified particles correlate to known sizes of an enveloped HBV particle [285]. It was found that liposomes comprising DOPE and DC Chol (without DOPE-PEG) in saline appeared to form visible flocculates when incubated overnight at 4 ^{o}C. This had a direct impact on particle sizes, in that aggregates were > 5000 nm in diameter (data not shown). Consequently liposomes without PEG were excluded from sizing analysis.

These data show that the addition of liposomes to the capsid preparation containing ±30 nm particles results in particles 46 ± 9.2 nm in diameter. Both of these small particles correlate to published sizes of the HBV capsid and wild type virus.

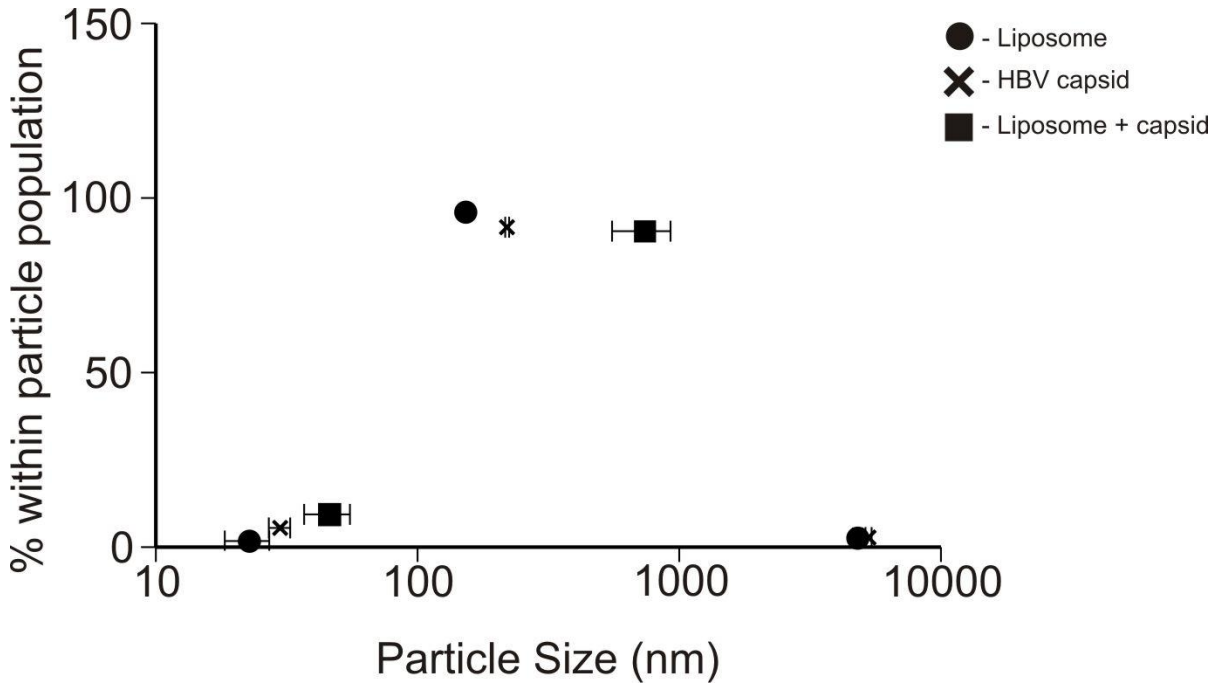

Figure 4.2.12: Particle sizing and size distribution analysis of liposomes, HBV capsids and liposomes combined with capsids. Liposomes were formulated as mole ratio of 6 parts DC Chol, 3 DOPE and 1 DOPE-PEG. Equal amounts (w/w) of capsid and liposome at 50 μg/ml were co-incubated overnight at 4 ^{o}C. DC Chol PEG liposomes (●) were predominantly represented by 153 nm diameter particles, HBV capsid (×) by 220.4 nm diameter particles and liposomes combined with capsid (■) by 740.5 nm diameter particles. X-axis plotted as logarithmic scale. Statistical analyses done by student t-test, n=3, SEM.

4.2.7. Particle analysis by electron microscopy

Capsid and capsids combined with liposomes were analysed by transmission electron microscopy, shown in Figure 4.2.13. Negatively stained capsid particles presented as individual units, small clusters of 2-5 particles or as large aggregates. Analysis of capsid-only preparations revealed the majority of particles had ± 30 nm diameter. These sizes were consistent whether the capsids were individual units or grouped in clusters. Incubation of liposomes with capsids produced two varieties of observable particles – those with and without a predominant lighter "halo". Particles without predominant halos were found to be ± 30 nm in diameter. Particles with predominant "halos" were larger (up to 46 nm in diameter) however were only present in aggregates. It was noted that the halo-like structures only occurred in association with capsids. These data do not prove capsid envelopment, however suggests that the capsids may associate with lipids, which predominantly form large capsid-liposome aggregates.

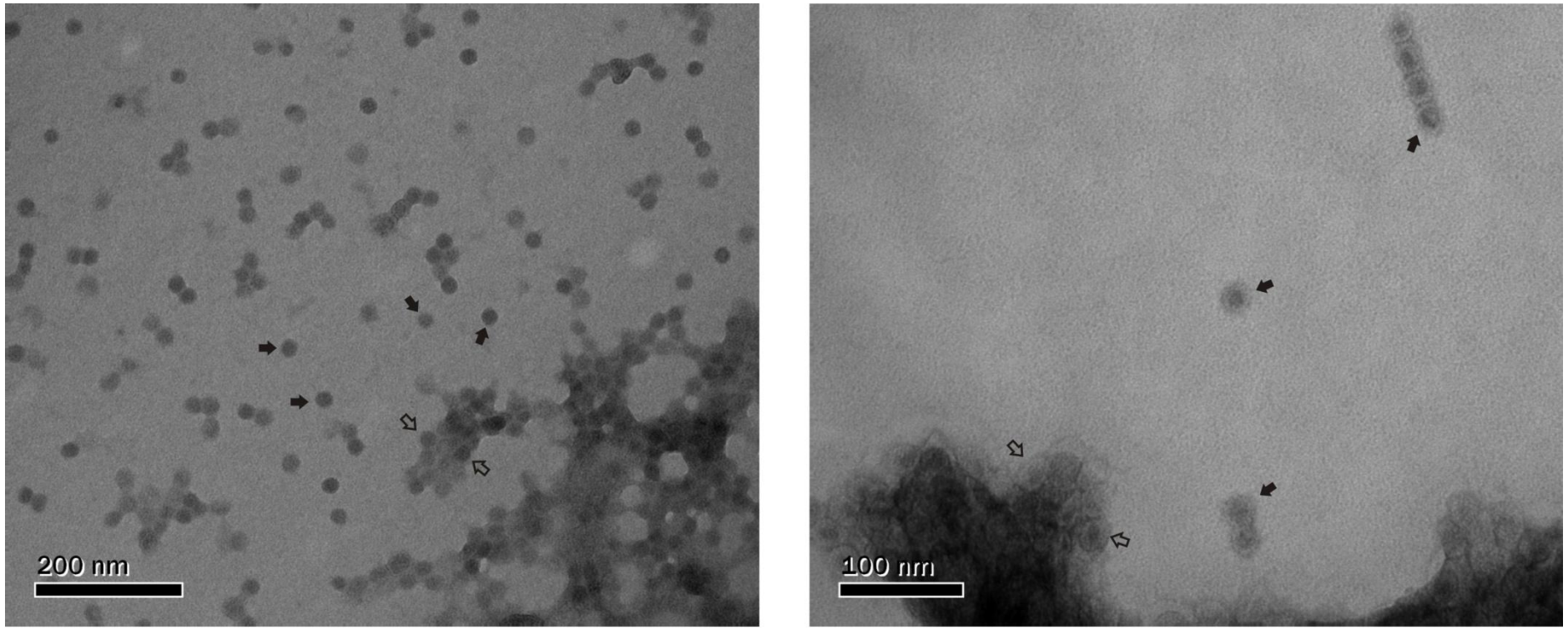

Figure 4.2.13: Electron micrograph depicting HBV capsids before and after liposome envelopment. Capsids were combined with liposomes (comprising of 60% DC Chol, 30% DOPE and 10% DOPE-PEG2000) and incubated overnight at 4 ^{o}C. Particles adhered to formvar coated grids and negatively stained with 5% uranyl acetate. Solid arrows indicate to individual capsids, hollow arrows to capsid aggregates.

4.3. Discussion

Novel delivery systems, such as VLPs, are crucial to the development of safe and effective gene therapy vectors. The manipulable nature of VLPs has seen their development in vectorology as well as chemistry and engineering. This chapter described that the HBV capsid, containing cysteine residues within the IL, was capable of conjugating with variety of functional moieties. These ligands in turn provide function to the capsid, in the form of immuno-evasion, hepatotropism, or fluorescence. Furthermore, decorating the capsid with ligands would ideally ablate the indiscriminate cellular uptake, a feature of several capsids [94, 286].

Two PEG moieties were initially assessed for conjugation to the capsid surface. The NHS-ester species did not react with IL-embedded lysine residues, while the maleimide species displayed a significant degree of conjugation to introduced cysteine residues. Generally the NHS-ester reaction is robust, and it was not established why the reaction was unsuccessful. Reagent quality was a concern, however the conjugation process had indeed been successful for PEGylating adenovirus [45]. It is feasible for the reagent to have undergone hydrolysis during storage, however this seems unlikely as several scPEG products were assessed. It was known that NHS-esters react with any anime group, thus care was taken to avoid buffers that contained tris(hydroxymethyl) aminomethane (Tris). Alternatively, the conjugation reaction may have been impacted by the potential formation of salt bridges between lysine and neighbouring acidic residues [287]. The IL contains two acidic residues, Glu77 and Asp83, both in close proximity of the inserted lysine residues. Despite potential disruption of the conjugation process, salt bridges would not completely inhibit the reaction, thus a slight degree of PEGylation would have been observed. Testing of ester viability within reactants may provide further insight to the failed lysine conjugation.

Maleimide-based conjugation was shown to occur successfully on both recombinant clones S81C and L76C S81C. The L76C S81C variety did not show an increased level of PEGylation, and may be explained by the effects of stearic hindrance. Once conjugated, the bulky nature of the PEG molecule may have prevented additional PEG molecules from accessing the IL, significantly decreasing conjugation opportunity. An alternative explanation for equivalent conjugation may be as a result of the helical nature of α3, which may have caused C76 to be buried by the helix or four-helix bundle, making it poorly accessible to bulky ligands.

PEGylation of the c160 and c170 cysteine recombinants required an increased incubation time as opposed to the c149 variant. It is established that the capsid pores allow for the exposure of the protamine to the surface of the capsid. Functionally this is required by infective virus, as it directs nuclear localisation, as well as phosphorylation of the protamine domain, which is important for capsid disassembly. It is feasible for the cationic protamine domain to reach and interact with the anionic IL. In doing so, the cysteine at position C81 may be sheltered from incoming ligands, increasing the overall reaction time required. As a result of the transient protamine domain and IL interaction, conjugation at all sites is eventually possible. It is possible that the IL-protamine domain interaction of c183 may have resulted in a disulphide bridge formation between the cysteine residue at position 183 (C183) and C76 or C81, which may account for the poor capsid yield of the c183 S81C and c183 L76C S81C species.

Ligand conjugation to the capsid surface changes the capsid physicochemical properties. This was observed by capsid and core protein electrophoresis. Capsids decorated with galactose and glucose on their surface displayed a decrease in electrophoretic mobility, as a result of the bulky neutral monosacharrides and perhaps an increase in electrostatic potential from the secondary amines within the linker chains. As to be expected, the electrophoretic mobility decreased with the addition of the galactose polymer. Fluorescein increased the electrophoretic mobility of the capsids, as both the phenolic and carboxylic groups are deprotonated at neutral pH [288].

Maleimide-based conjugation to the c160 recombinant capsids was significantly more efficient than to the c149 variety. This may be as a result of several factors, including: The initial lysis step of the bacteria uses a buffer containing dithiothreitol (DTT) to prevent potential disulphide bridge formation, and protein aggregation. This component was removed during the c160 cysteine-containing recombinants preparation and replaced with TCEP, as the thiols present in DTT react with maleimide. Despite two SEC steps and dialysis, it was possible that the DTT was not sufficiently diluted in the c149 recombinant preparation. Quality of capsid preparation will also play a role in the outcomes of conjugation. The c149 cysteine capsids were prepared several months prior to the c160 variety. With time, refinement of the purification technique occurred, perhaps producing higher quality preparations. Nonetheless, the c149 cysteine capsids served their purpose as

a proof of principle model, as further studies required capsids capable of transporting nucleic acids associated to the protamine domain.

Liposome envelopment of retroviral particles has shown to be an effective measure to superinfect cultured cells [275-277]. Viral and VLP envelopment does not appear to have made any major impact in the field of gene therapy, perhaps a result of technical challenges associated with both viral production and the envelopment process, particularly in the application to *in vivo* systems. Despite technical challenges, liposome envelopment may offer several benefits to viruses and VLPs used in gene therapy. Envelopment ensures viral particles are concealed from the immune system, increasing the half-life of circulating particles. The addition of PEG to liposome surfaces further ensures immuno-evasion and increases particle stability. Liposome envelopment may also offer a means to alter VLP tropism by including ligands on the liposome surface.

This study has shown that hepatitis B virus capsids were sequestered by liposomes provided two criteria were met. Liposomes require a cationic surface charge, which may facilitate the electrostatic based interaction with the anionic capsids. Anionic/neutral liposomes showed poor/limited interaction with capsids, a result of poor electrostatic based interaction or unstable liposome particles which switch to inverted hexagonal morphology (described in chapter 2) [113]. Consequently the capsid binding capacity of inverted hexagonal liposomes is greatly diminished, resulting in liposome/complex precipitation. The second criterion is for the addition of PEG to liposomes, as this is known to stabilise micellar/lamellar structure by decreasing inter-membrane interaction and the potential of phase conversion.

As demonstrated by particle sizing and electron microscopy, the capsids were prone to aggregate in small clusters or large masses. The preparative methodology employed to isolate capsids was fairly crude, in which additional contaminating cellular material was present amongst the capsids (Protocol 1, Chapter 3). Protein contaminants were indeed shown to be present by SDS-PAGE analysis (data not shown) and is thought to have caused capsid and liposome aggregation. The aggregation of the capsids could potentially be overcome by further purification of the HBV capsids, as described in Protocol 3, Chapter 3.

The three experiments strongly suggest that PEGylated cationic liposomes interact with HB capsids, which may form enveloped VLPs. Agarose gel electrophoresis confirmed PEGylated cationic liposomes are required to interact with and sequester capsids. Particle

sizing indicated particles 30 nm in diameter, with which the addition of liposomes to the preparation resulted particles with ±42 nm diameters. Both of these particles correlate to wild type capsids and HBV sizes. Analysis by electron microscopy confirmed that capsid preparations contained uniform 30 nm diameter particles, many of which were part of aggregations. Addition of liposomes to capsid preparations resulted in majority of the capsid particles to aggregate, each particle surrounded by a predominant halo-like structure. It is enticing to suggest the envelopment has occurred, however can only be confirmed with a more pure version of capsid preparation.

In conclusion, it has been demonstrated for the first time that the HBV capsid can be decorated with ligands attached by specific amino acids. These chemical species and ligands have shown functionality in other nanoparticles [45, 125, 128, 147], thus have the potential to provide the HBV capsid with much needed immuno-evasive and tissue tropic qualities. These findings suggest that the HBV capsid is a potential candidate for gene therapy vectorology, provided it can be loaded with a payload. Chapter 5 explores the potential to introduce foreign nucleic acids to purified HBV capsids and the potential to deliver these decorated recombinant HBV capsids in cell culture.

4.4 Materials and methods

4.4.1 Recombinant capsid preparation

Recombinant capsids involved in conjugation-based reactions were prepared using the 'Porterfield protocol' (Protocol 3 described in Section 3.4.3.3) [245]. Recombinant capsids used for liposome envelopment studies were prepared using protocol 1, described in section 3.4.3.1.

4.4.2 Conjugation of ligands to capsid surface

Prior to all conjugation reactions, protein concentration was determined by the bicinchoninic acid (BCA) assay according to manufacturer's instructions (Thermo Fischer, MA, USA). The number of IL exposed lysine or cysteine residues were subsequently calculated, using the M_w of the various recombinant clones (c149 – 16.7 kDa; c160 – 18.2 kDa; c170 – 19.8 kDa; c183 – 21.4 kDa). Reactive ligands were dissolved as stock solutions in DMSO (Sigma, Germany) at 10 mg/ml. The reactive PEG moiety was an exception and dissolved at 100 mg/ml then stored at -20 ^{o}C.

4.4.2.1 NHS-based conjugation

Recombinant capsids at 1 μg/μl were combined with the scPEG ligand stock at an appropriate mole ratio. Overall reaction volumes were typically 100 μl, the reaction buffer composed of PBS (core protein stocks contain PBS). An example calculation to determine lysine:ligand mole ratio can be found in Appendix 4. All conjugation reactions were performed at room temperature unless specified otherwise. Reactions with the capsid surface were quenched by the addition of excess L-Lysine (Sigma, Germany). Conjugated capsids were stored at -80 ^{o}C.

4.4.2.2 Maleimide-based conjugation

Recombinant capsids containing cysteine substitutions at 1 μg/μl were incubated at room temperature with a reactive ligand at the appropriate mole ratio. Reaction volumes were typically 100 μl, in PBS. As previously mentioned, an example calculation to determine cysteine:ligand mole ratio is within Appendix 4. Reactions were quenched by overnight dialysis against PBS or by the addition of 2x protein loading dye (Appendix 2). Conjugated capsids were stored at -80 ^{o}C

4.4.3 Molecular modelling

All proteins species were modelled using Swiss protein data base viewer (DeepView) [214] with parameters as described in Section 3.4.4.

4.4.4 Complexing of virus-like particles with liposomes

Generation of liposomes has been described in Chapter 2. Equal amounts (w/w) of VLP and liposome were incubated in 50 μl at 4 ^{o}C overnight.

4.4.5 Particle sizing

Particles were prepared at 0.25 μg/μl in PBS and size determined using a Zetasizer Nano ZS (Malvern, Worcestershire, UK) at 25 ^{o}C. Sizing was carried out in accordance to manufacturer's instruction.

4.4.5 Mobility shift assays

Complexed VLPs were loaded into a 1% agarose (w/v) 0.02% ethidium bromide (w/v) gel and subjected to electrophoresis at 80 V. Uncomplexed capsid particles migrated into the gel matrix and their RNA content was visible under short wave UV illumination. The capsids were made visible by soaking the agarose gel in Coomassie Brilliant Blue R250 stain for 1 hour, followed by destaining.

4.4.6 Electron Microscopy

Capsids and/or liposomes were applied to formvar-coated copper grids for 1 minute, any remaining solution was blotted from the grid surface. Capsids were negatively stained using 5% uranyl acetate solution for 1 minute, and excess stain was blotted off. Capsids were observed using a JEM-1400 transmission electron microscope (JEOL, Tokyo, Japan) under high vacuum at 100 kV.

Chapter 5: Assessment of the decorated and loaded capsid hepatotropic properties with cultured cells

5.1 Introduction

The previous chapter described the successful decoration of the recombinant capsid surface with a variety of functional moieties such as PEG or galactose. As naked capsids are indiscriminately taken up by cells [99], it was required to conjugate functional moieties to provide hepatotropism and immuno-evasion. To assess whether the newly decorated capsids exhibit tropism, the capsid cavity was loaded with reporter oligonucleotides. However, recombinantly expressed capsids contain bacterially-derived mRNA which required removal prior to the introduction of the reporter cargo [93]. In a natural infection, HBV core proteins associate with pregenomic RNA (pgRNA) and viral polymerase to assemble into capsids [289]. The viral polymerase recognises the ε loop signal on the 5' end of the pgRNA, and together with the core protein facilitate capsid formation [244, 290]. It is not known how these three components interact to ensure the encapsidation event, however it is suggested that the pgRNA interacts with the viral polymerase initially, followed by interaction with core proteins [289]. Importantly, the nucleic acid binding domain (protamine domain) of the core protein requires phosphorylation to package pgRNA [291, 292]. Three serine residues within the protamine domain (S155, S162 and S170) are thought to be involved in phosphorylation, which not only ensures specific pgRNA packaging but are also associated with reverse transcription of pgRNA and cellular trafficking of matured HBV capsids [234, 291-293]. Recombinant expression of the HBV capsid within *E. coli* does not result in the phosphorylation of the three serine residues within the protamine domain. Subsequently, the HBV capsids indiscriminately package nucleic acids during their formation. Typically packaged nucleic acids consist of those near the site of translation, such as the core protein mRNA and bacterial tRNAs [93]. This is to the advantage of this study, as it allows for removal of bacterially-associated RNA and introduction of therapeutic/reporter nucleic acids. The reporter oligonucleotides are introduced after capsid denaturation, an established process primarily accomplished by chemical denaturation [197, 245, 294].

Hepatitis B virus capsid dissociation was previously performed to model icosahedral capsid assembly kinetics [197, 206, 295]. These pioneering studies were performed using

the c149 capsid variety as it comprises a single protein species and no nucleic acid cargo. These factors helped ensure that the kinetic assembly analyses remained simple, uninfluenced by the presence of complicating factors such as protamine domain – RNA interaction. The addition of the protamine domain, generates a more stable variation of the capsid in comparison to c149, as a result of core protein - core protein interaction and core protein - RNA interaction [197, 198]. The combined effects of these interactions ensure capsid stability at both high and low ionic strength environments. It is possible however, to disrupt the loaded capsid structure with well-known protein denaturing agents. Porterfield and colleagues demonstrated that low concentrations of guanidinium hydrochloride were capable of dissociating capsids, and the addition of lithium chloride assisted in the precipitation of packaged RNA [245].

The single or double stranded nature of the packaged nucleic acid plays a major role in the efficiency of capsid formation or reassociation of disassembled capsid [245, 294]. Certain bacteriophage capsids that incorporate double stranded DNA are initially preassembled prior to packaging and require active DNA pumping into the capsid interior [296]. These capsids are robust, able to withstand the significant internal forces created by coiling double stranded DNA [297, 298]. Conversely, capsids that package single stranded DNA or RNA are typically stabilised by weak inter-core protein interactions. Following association with DNA or RNA, the capsid becomes predominately stabilised by protein-nucleic acid interaction [299, 300]. The HBV capsid initially packages single stranded pgRNA, a highly flexible substrate, which is later converted to double stranded DNA/RNA hybrid within the capsid by encapsidated viral polymerase. This conversion may have a significant impact on capsid stability, and may help drive the capsid disassembly after entering the host nucleus.

Nucleic acids in their single and double stranded formations have a particular degree of flexibility in solution, where nucleic acid length and distance between 5’ and 3’ ends describe the minimal length at which a polymer becomes inflexible (persistence length) [301]. The persistence length of double stranded DNA is approximately 50 nm (150 base pairs) [294]. This means double stranded DNA considerably larger than 50 nm does not require energy to bend, whereas strands shorter than 50 nm exhibit rod-like behaviour and require energy to bend (thus requires active pumping of DNA into viral capsids). Consequently, double stranded DNA at its persistence length will not be packaged into the

HBV capsid as a result of structural constraint. It was demonstrated that double stranded DNA of 600, 1600 and 2700 base pairs in length did not package into HBV capsids, and rather formed aberrant structures during the capsid reassembly process [294]. Conversely, single stranded DNA or RNA has a low persistence number, and allows for a strand approximately 3 kb to be packaged within HBV capsids (persistence length ±1-2 nm) [302]. Short single stranded oligonucleotides (25-mer) exhibit very low persistence length (similar to single stranded RNA) and were suitable as ^{32}P or fluorescein labelled reporter molecules to load into the HBV capsid.

It has previously been described that c183 can be loaded with short reporter oligonucleotides, followed by cellular uptake in cultured cells [99]. Naked capsids containing a fluorescently-labelled reporter oligonucleotide were indiscriminately taken up by a variety of cell lines. In an attempt to provide tropism to the HBV capsid, Choi and colleagues inserted the integrin-targeting RGD motif into the immunodominant loop [98, 236]. Unfortunately, RGD-targeting was not specific *in vitro* and *in vivo*, as modified capsids were taken up by a variety of cell types. Following these studies, HBV capsid uptake was suggested to occur by several mechanisms including clathrin-mediated endocytosis, macropinocytosis and claveolae-mediated endocytosis [98, 99, 237, 303]. It is a curious phenomenon that the HBV capsid can utilise various pathways and may suggest why indiscriminate cellular uptake occurs. Naturally, hepatotropism is conferred to the HBV by preS2 proteins embedded within the viral membrane, which interact with the sodium taurocholate co-transporting polypeptide of hepatocytes [304]. Viral binding to the hepatocyte surface allows for receptor mediated endocytosis, after which the virus escapes from the endosomal pathway without endosome vesicle acidification [305]. Interestingly it has been demonstrated that an infectious HBV capsid enveloped within a synthetic lipid membrane mimics wild type infection efficacy in cultured cells [306]. Despite the synthetic membrane utilising an alternative cellular uptake pathway, the viral capsid was still able to escape from the endosomal pathway. Once the HBV capsid has escaped from the endosomal vesicle, it is trafficked within the cytoplasm to the nucleus using the microtubule intracellular transport system [306]. Nuclear import of the capsid is an interesting process, as it requires the dissociation and reassociation while travelling from cytoplasm to nucleus. The HBV capsid docks within the nuclear pore, localised within the nuclear basket after genome maturation [307, 308]. Core proteins interact with host nucleoporin 153, and capsid

disassembly ensues. Capsids have the capacity to reassemble within the nucleus in an RNA-dependent manner once its components have passed through the nuclear pore. Viral genomic material is then released and virus production ensues. Bionanotechnology studies utilising naked HBV capsids as delivery vehicles demonstrated that their contents were released into the nucleus and cytoplasm. Cooper and colleagues demonstrated delivery of a reporter oligonucleotide to the nucleus [99], whereas Choi *et al.* showed siRNA delivery to the cytoplasm [98]. Lack of nuclear delivery may be as a consequence of replacing the protamine domain with the p19 RNA binding protein. Unfortunately it was not assessed whether the p19-modified capsids make use of the cellular trafficking machinery. Both studies did also not determine how many capsid particles were cleared through the endosomal pathway. This is an important factor for determining the efficacy of the recombinant HBV capsid as a delivery vehicle.

To assess whether galactose decoration on the capsid surface provided hepatotropism, two cell lines were compared for their capsid uptake capabilities. The human hepatocellular carcinoma cell line, Huh7, displays the cell specific ASGPr which has a high affinity for galactose [132]. The second cell line was used as an uptake control, as human embryonic kidney cells (HEK293) do not display the ASGPr [132]. As described in Chapter 2, binding and uptake by the ASGPr occurs by receptor mediated endocytosis often resulting in lysosomal degradation [132]. Endosomal escape plays a major role in the efficacy of the gene therapy vector, as it has been demonstrated that a large proportion of the delivered product is recycled out of the cell or degraded within the endosomal processing pathway [107, 309]. It is not established how wild type capsids escape from the endosomal pathway, and unknown if any protein domains on the capsid surface are responsible during the escape process. Addition of functional moieties to the capsid surface may influence the ability of the capsid to escape from the endosomal pathway, an aspect poorly examined currently.

It is described in this chapter that c183 capsids were successfully loaded with 25-mer oligonucleotides during re-association. Furthermore it was demonstrated that loaded capsids provided protection to their cargo against environmental nucleases. It was found that c160 L76C S81C also encapsidated FITC-labelled reporter oligonucleotides and underwent highly efficient surface decoration with a variety of maleimide-based compounds. *In vitro* assessment of cellular capsid-uptake revealed that decoration of the capsid surface resulted in poor uptake in both Huh7 and HEK293 cells. As previously noted

[99], naked capsids were taken up by both cell lines. It is proposed that the ligand structure is responsible for poor cellular uptake, and optimised ligands may well allow for discriminate cellular entry of loaded capsids.

5.2 Results

5.2.1 Encapsidation of radio-labelled oligonucleotides by c183

HBV capsids were assessed for their loading with short single stranded oligonucleotides. As it has previously been demonstrated by Porterfield and colleagues, the HBV capsid readily disassembles and loads with single and double stranded nucleic acid fragments varying in length [245]. It was necessary to determine whether the recombinant cysteine capsid mutants were amenable to dissociation, loading combined with re-association and finally surface decoration with functional moieties. As a point of reference, purified c183 particles were chemically dissociated in 1.5 M guanidinium chloride containing 0.5 M lithium chloride. Dissociated capsids were combined with ^{32}P-labelled 25-mer oligonucleotides and allowed to re-associate. The persistence length of the 25-mer did not affect capsid loading, and any potential secondary structure length was far shorter than the capsid diameter. Capsids containing the reporter radio-labelled oligonucleotide were separated from free oligonucleotides by agarose gel electrophoresis. The agarose gel was dried onto Whatman filter paper and analysis was conducted using a phosphorimager (Figure 5.2.1). It was shown that radio-labelled oligonucleotides were successfully encapsidated after capsid dissociation and re-association. A minimum of four hour dialysis against the dissociation buffer was required for significant oligonucleotide encapsidation, suggesting that 4 hours of dialysis was required for adequate capsid dissociation. To rule out the arbitrary association of oligonucleotides with the outer surface of capsids, samples were treated with DNase. It was found that dialysis for 4-6 hours against dissociation buffer followed by re-association was adequate to provide protection to encapsidated oligonucleotides. Inadequate dissociation (0-2 hours) did not allow for oligonucleotide uptake, resulting in their degradation. Thus these data suggest that the radio-labelled oligonucleotides are indeed housed within intact capsids, and gained protection from environmental nucleases. The dissociation/re-association process appeared to cause some of the oligonucleotides to become lodged within the agarose gel well. This was most-likely an effect of capsid aggregation between dimer-dimer units and/or potential bacterial protein contaminants. Coomassie brilliant blue

staining revealed no significant decrease in the migrated capsid concentration of dissociated and non-dissociated capsids (data not shown).

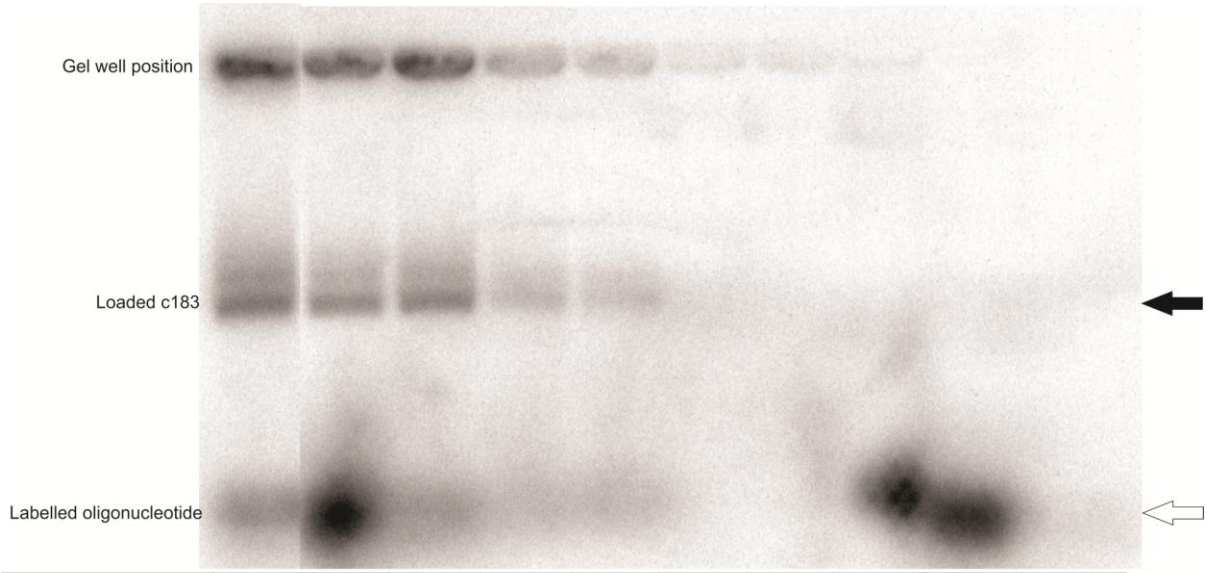

c183	X	X	X	X	X		X	X		
^{32}P-oligonucleotide	X	X	X	X	X				X	X
DNase		X	X	X	X	X		X		X
Dissociation time (h)	6	6	4	2	0					

Figure 5.2.1: Phosphorimage of c183 capsids loaded with ^{32}P- labelled oligonucleotides, separated by agarose gel electrophoresis. c183 capsids were dialysed against a dissociation buffer for 0-6 hours. DNase was included after re-association to degrade free oligonucleotides. The black arrow indicates the position of c183 capsids, while the white arrow indicates labelled 25-mer oligonucleotide.

5.2.2 In vitro *cellular uptake assessment of decorated, loaded c160 L76C S81C*

Having established that recombinant capsids were amenable to surface modification (Chapter 4), their delivery efficacy was assessed *in vitro*. The recombinant c160 L76C S81C capsid was selected to be loaded, decorated and tested in cell culture. c160 L76C S81C was able to undergo efficient conjugation with a variety of maleimide-based moieties and contains a truncated protamine domain which was capable of binding cargo nucleic acids. For the purposes of microscopy, a fluorescein-labelled oligonucleotide was encapsidated as opposed to the radio-labelled variety. It was reasoned the fluorescence would indicate subcellular localisation of the cargo during microscopy. Similarly to the c183-oligonucleotide encapsidation, c160 L76C S81C was dissociated and loaded with the fluorescent reporter. Re-associated capsids were then decorated with functional moieties described in Chapter 4.2.4. Degree of conjugation was assessed by agarose gel electrophoresis (Figure 5.2.2).

Capsids loaded with fluorescently-labelled oligonucleotides were difficult to distinguish from non-loaded, as the capsids display auto-fluorescence under short-wave UV. As successful loading was accomplished in c183, it was assumed that c160 L76C S81C contained enough reporter oligonucleotide to be visualised during microscopy.

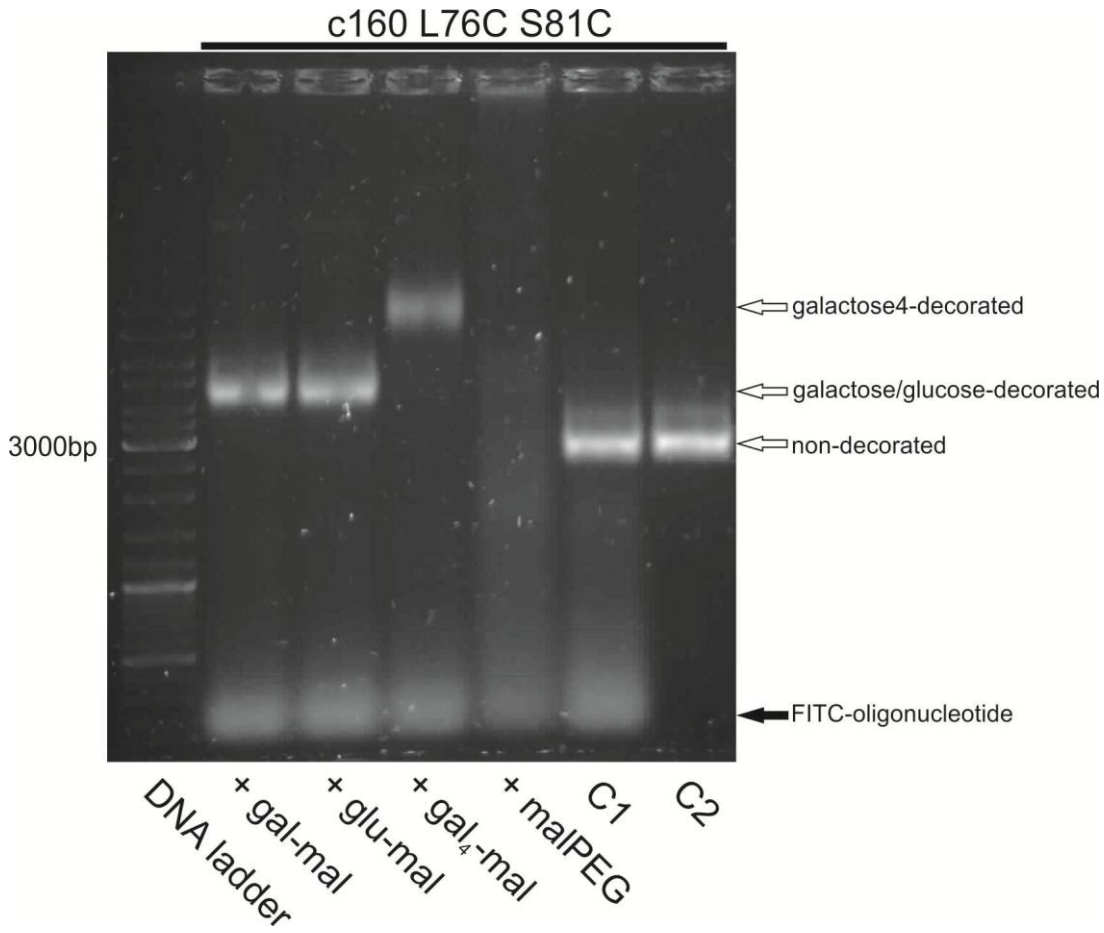

Figure 5.2.2: Loaded and decorated c160 L76C S81C analysis by agarose gel electrophoresis. Capsids were loaded with FITC-oligonucleotides followed by decoration with a functional moiety. Capsids and oligonucleotides were viewed using shortwave UV. Decorated c160 L76C S81C migrate to various positions within the gel (white arrows). Free oligonucleotides are indicated by the black arrow. Control 1 (C1) contains loaded but undecorated c160 L76C S81C capsid. Control 2 (C2) contains c160 L76C S81C without FITC oligonucleotides.

Decorated and loaded c160 L76C S81C were assessed for hepatotropism in cell culture. Approximately 70 000 Huh7 or HEK293 cells were inoculated with 4 μg of loaded capsids and incubated for 2 hours. This equated to a MOI of ±4 x10^6 which did not take into account the low levels of contaminating proteins as well as any malformed or capsid aggregates. Thus the amount of particles per cell is suggested to be lower than initial estimates. A ten-fold decrease in the amount of core protein administered did not produce visible

fluorescence (data not shown). Cellular uptake of the decorated capsids presented as localised fluorescence within the cells, assessed by fluorescence microscopy. Decoration of the capsid surface with the galactose and glucose ligands significantly decreased the cellular uptake of the loaded capsids in both cell lines (Figure 5.2.3 and 5.2.4 A + B). A low degree of localised fluorescence was present in both cell lines inoculated with the poly-galactose decorated capsids (Figure 5.2.3 and 5.2.4 C). This most-likely occurred as a result of incomplete capsid decoration, allowing for exposed capsid surface to interact with and be taken up by cells. PEGylation of the capsid surface prevented cellular uptake of the capsids (Figure 5.2.3 and 5.2.4 D). As established by previous researchers [98, 99], naked capsids are indiscriminately taken up by both cell lines (Figure 5.2.3 and 5.2.4 E), evidenced by the presence of localised fluorescence. Addition of naked oligonucleotide or naked, unloaded capsid to either cell line produced no visible fluorescence (Figure 5.2.3 and 5.2.4 F + G). Increased magnification revealed that a large degree of the oligonucleotides were localised to discrete bodies within the cells (Figure 5.2.5). These bodies are typically situated near the perimeter of the cell and are suggested to be involved in the endosomal-trafficking pathway. Currently it is not established whether the decorated capsids would escape the endosome and traffic to the nucleus.

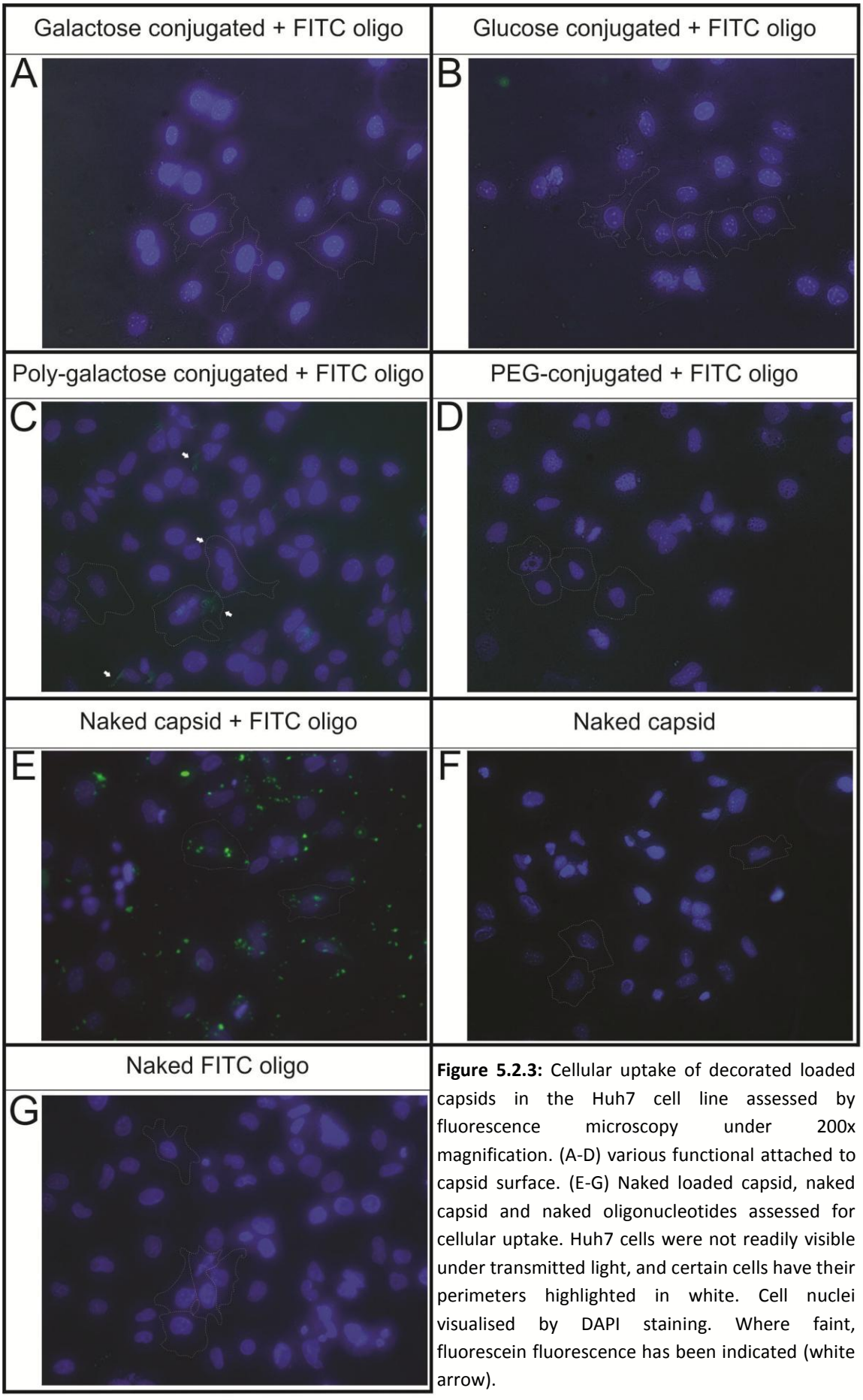

Figure 5.2.3: Cellular uptake of decorated loaded capsids in the Huh7 cell line assessed by fluorescence microscopy under 200x magnification. (A-D) various functional attached to capsid surface. (E-G) Naked loaded capsid, naked capsid and naked oligonucleotides assessed for cellular uptake. Huh7 cells were not readily visible under transmitted light, and certain cells have their perimeters highlighted in white. Cell nuclei visualised by DAPI staining. Where faint, fluorescein fluorescence has been indicated (white arrow).

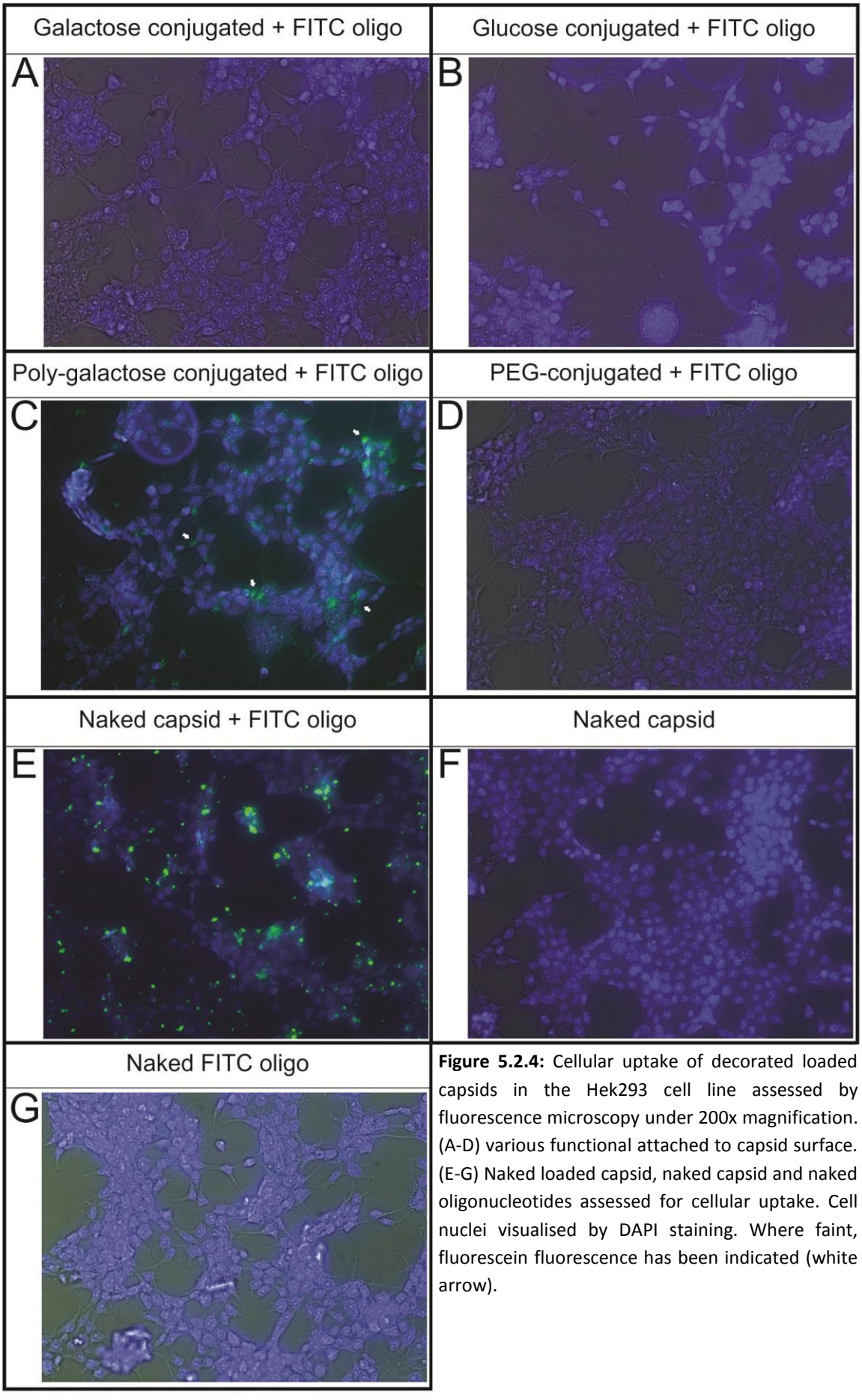

Figure 5.2.4: Cellular uptake of decorated loaded capsids in the Hek293 cell line assessed by fluorescence microscopy under 200x magnification. (A-D) various functional attached to capsid surface. (E-G) Naked loaded capsid, naked capsid and naked oligonucleotides assessed for cellular uptake. Cell nuclei visualised by DAPI staining. Where faint, fluorescein fluorescence has been indicated (white arrow).

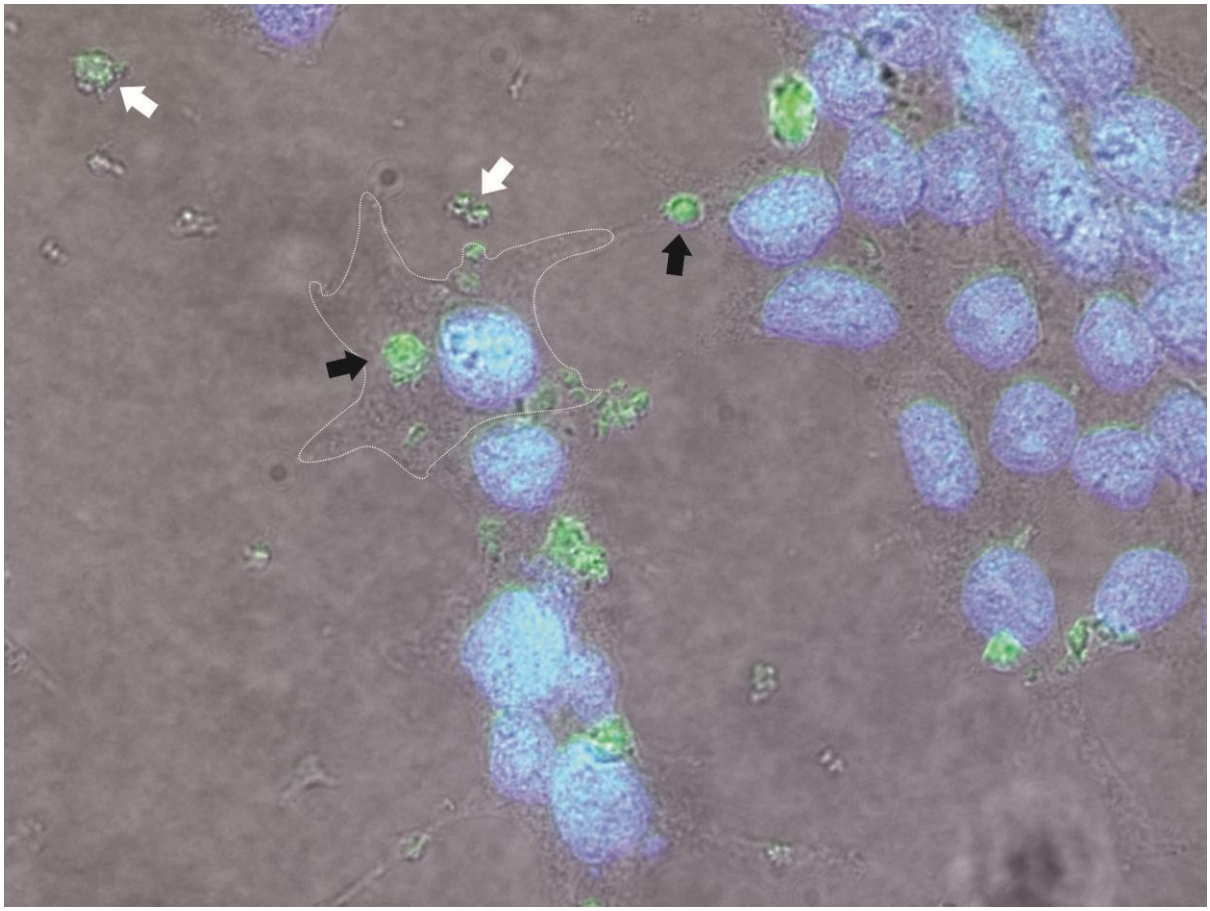

Figure 5.2.5: Visualisation of endosomal vesicles after loaded naked capsid uptake in the Hek293 cell line under 630x magnification. Endosomal vesicles indicated with a black arrow and additional extracellular vesicles indicated by the white arrow. Cell perimeter indicated with a white-lined border. Cell nuclei stained with DAPI.

5.2.4 Comparison of ligand linker lengths suggests why poor delivery occurred in cultured cells

Despite the presence of the galactose ligand on the surface of the capsid, no uptake in Huh7 cells was observed. Linker length of the ligand invariably plays an important role in determining ligand interaction with the ASGPr. A similar observation was described in Chapter 2, where linker length played an important role in transfection efficiency. Comparison of the linker length of the two galactose compounds used in the liposome and capsid decoration studies revealed that they are of similar nature (Figure 5.2.6). Including medium linker chain unprotected galactose (MLC UnP galactose) in liposomes resulted in a significant drop in transfection efficiency compared to naked and short chain equivalents (Figure 2.2.2). Both the MLC and galactose-maleimide have linker chains of comparable length, and the significant drop in cellular uptake of the decorated capsids in both cell lines may be attributed to the linker moieties behaving like PEG.

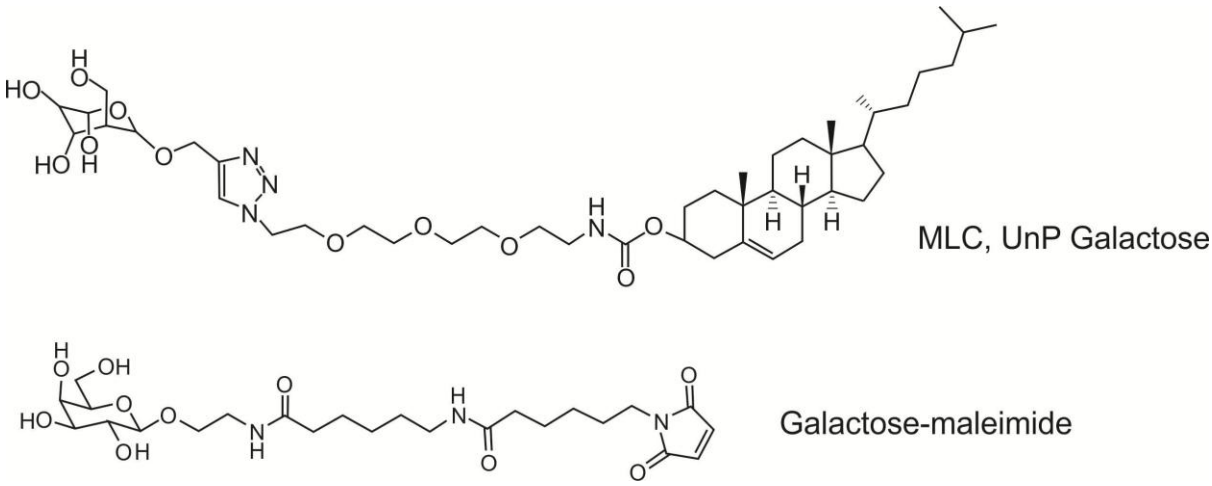

Figure 5.2.6: Comparison of the linker length of the compounds medium length chain unprotected galactose (MLC, UnP galactose) used in liposomal studies with the galactose-maleimide ligand for conjugation to capsids.

5.3 Discussion

VLPs have several attractive properties useful in the developing field of gene therapy vectorology. Generally these particles are stable, simple and easy to produce, amenable to modification and receptive to cargo loading. The work described here aimed to assess the vector-like qualities of the HBV capsid after surface modification. A general property of examined VLPs is similar cellular uptake behaviour, in that naked capsids are indiscriminately taken up by a variety of cell types [286]. Accordingly it was required for the naked HBV capsid to be decorated with moieties that would provide either tissue tropism or immuno-evasive properties. It was assessed whether HBV capsids were receptive to reporter oligonucleotide loading followed by surface decoration. These modifications would confer hepatotropic properties to the capsids, and potentially allow for delivery of reporter oligonucleotides to cultured cells.

HBV capsids were initially loaded with a radio-labelled oligonucleotide to assess whether dissociation and capsid uptake were indeed occurring. The amount of oligonucleotide loaded into each capsid was not assessed, as a result of two factors. The starting concentration of radio-labelled oligonucleotide was not determined, as a safety consideration while using communal equipment. Secondly, the drying process of the agarose gel into the filter paper does not always occur uniformly, and concentrated regions of radiolabeled oligonucleotides were seen to form. Nonetheless, this initial loading

experiment demonstrated that c183 were able to encapsidate 25-mer oligonucleotides. Loaded capsid treatment with DNase I cleared non-encapsidated oligonucleotides and demonstrated that the capsids provided a protective function against nuclease degradation. Future studies may include the incubation of loaded (and decorated) capsids within serum to assess the effect of serum proteins on capsids stability and aggregation. Once a successful loading protocol was established, c160 L76C S81C capsids were dissociated and loaded with fluorescein-labelled oligonucleotides. Again, the degree of oligonucleotide uptake was not easy to assess, as fluorescence measurements were also influenced by the auto-fluorescence of the capsids. Furthermore, ethidium bromide staining revealed that not all the RNA of bacterial origin was removed from the capsids, thus further hindering spectroscopic analysis. Capsids containing a protamine domain gain stabilisation from their nucleic acid cargo. Thus the complete removal of residual RNA may not be easily accomplished as capsids will bind nucleic acids during re-association. Perhaps if the RNA were first degraded within the capsids prior to dissociation, it may be possible to load the capsids with only therapeutic/reporter oligonucleotides.

It was assumed that the c160 L76C S81C capsids loaded a proportion of the fluorescently labelled oligonucleotides, and were then decorated with various moieties on the surface. As described in Chapter 4, a high degree of conjugation to the core protein occurred using galactose-maleimide, glucose-maleimide and maleimide-PEG. This was evidenced by the almost complete shift of core particles during agarose gel electrophoresis. Galactose$_4$-maleimide did not conjugate as successfully as the monosaccharide ligand. It was speculated that the high degree of monosaccharide ligand conjugation to the capsid may afford the vector with additional immuno-evasive properties. A basic means to assess this may be accomplished by performing an ELISA with primary antibodies targeting the IL of the HBV capsid. As described by several researchers, the IL is a predominant epitope of the HBV capsid and should elicit a reaction in the ELISA if exposed.

According to protein concentration calculations, a MOI of ±4 x 10^6 viral particles was added to cultured Huh7 and Hek293 cells. Realistically the MOI was considerably lower, as there was a low level of protein contaminants in the capsid preparations and the dissociation/reassociation process may result in capsid aggregates (Figure 5.2.1 and 5.2.2). Upon addition to cells, the capsid stock experienced a 50-fold dilution, and majority of the capsids would have remained in suspension during the 2 hour incubation process. This was a

further dilution of VLPs to cells, decreasing the MOI. Thus despite the calculated MOI of ±4 x 10^6, protein contaminants, potential core aggregation and VLPs that do not come into contact with cells, the estimated amount of capsids interacting with cells was far lower.

The ligand structure attached to the capsid surface may play a major role in determining cellular uptake. It was demonstrated in Chapter 2 that the linker length between the liposome surface and galactose moiety played an important role in transfection efficiency. The linker length of the moieties conjugated to the capsid surface was similar to the liposomal species MLC. It was demonstrated that the MLC species cause a significant drop in transfection compared to the shorter length linkers. The moiety conjugated to the capsid surface possibly behaves more PEG-like, not only preventing potential ASGPr interaction but also creating a large enough distance between the cell surface and capsid to prevent interaction and uptake. Despite the lack of cellular uptake, it is useful to know that complete capsid decoration at the IL did prevent indiscriminate uptake. This is of particular importance, considering the purpose of this research. It was indicated in Chapter 2 that shortening of the linker length of the galactose compounds increased the transfection efficiency. Thus, conjugating galactose to the capsid surface with a short as possible linker may provide hepatotropism and retain the discriminate uptake.

The HBV capsid does display potential as a vector for gene therapy. Several aspects will have to be addressed should a new ligand provide hepatotropism. One of the more problematic areas of synthetic gene delivery is the endosomal recycling of delivered cargo [107]. It will be required to determine the level of capsid uptake, release and/or degradation in cultured cells. This can be accomplished by monitoring the localisation of the capsid cargo over several time points. Over a period of 30 minutes to 2 hours, the majority of the cargo should be localised within the endosome. After 8 hours a larger proportion of the endosomal contents should be cleared, and after 24 hours even a greater degree of cargo clearance should be expected. Differential fractionation of cellular contents and analysis thereof (for example qRT-PCR) over this time period will reveal the degree of cargo delivery, especially when compared to *in situ* cellular DNA/RNA. This means of study will also give an indication of capsid disassembly and release of contents. An additional measurement to compliment localisation and recycling is the assessment of target gene knockdown induced by capsid cargo. An important aspect that many studies have overlooked is the live-cell

analysis of capsid trafficking within the cell, as modification to the outer surface of the capsid and the protamine domain may have major implications for cellular trafficking.

An aspect of HBV capsid vectorology not addressed by this study is nucleic acid cargo optimisation. It is required to optimise the type of cargo encapsidated, bearing in mind what function it is to perform, and also optimise how the new cargo is encapsidated. Studies by Choi and colleagues revealed the delivery of siRNAs to cells by replacing the protamine domain with the p19 protein. Despite achieving knockdown of their target, it was not assessed whether the capsid was trafficked to the cytoplasm or nucleus, as the protamine domain is believed to play an important role in cellular localisation. Modification of the protamine domain may play an important role in the optimisation of the HBV capsid as a vector. Aspects such as capsid cellular destination and cargo size will need to be taken into consideration prior to modifying the protamine domain. Large protamine domains, like that of the wild type virus may traffic to the nucleus effectively but not easily dissociate from the small nucleic acid strands, such as those used in this study. The type and structure of the cargo may also play an important role in the efficacy of the delivery system. Short oligonucleotides may be ineffective in generating a therapeutic effect, as RNA is susceptible to degradation and short DNA strands have not had any significant impact within the field of gene therapy. Perhaps the introduction of short stable nucleic acids such as locked nucleic acids (LNAs) would transport well within modified HBV capsids. Double stranded nucleic acids longer than 150 bp will not package into the HBV capsid as a result of persistence length. The introduction of nicks or gaps into the double-stranded sequence may provide flexibility required to load into the capsid. Alternatively, single but complementary strands could be loaded individually into capsids and administered simultaneously. However, this form of administration would require double the amount of capsids, which may impact the host response.

In conclusion, this chapter describes that the recombinant HBV capsid has the potential to be loaded with 25-mer oligonucleotides and then efficiently decorated with a variety of functional moieties. Furthermore it was found that capsids with adequate decoration to the IL did not undergo cellular uptake. This is of importance, as several of the capsids described within the literature are indiscriminately taken up *in vitro* and *in vivo*. This certainly bodes well for VLPs, as it is a matter of optimising the ligand structure to ensure hepatotropism or other cellular tropisms.

5.4 Materials and methods

5.4.1 Recombinant capsid preparation

Recombinant capsids involved in conjugation- and dissociation-based reactions were prepared using the 'Porterfield protocol' (Protocol 3 described in Section 3.4.3.3) [245].

5.4.2 Capsid dissociation and re-association

Recombinant capsids were dissociated by dialysing against dissociation buffer for 6 hours at 4 ^{o}C unless indicated otherwise. Dissociated capsids were subjected to centrifugation for 30 minutes at 20 000 × *g*, 4 ^{o}C to remove encapsidated RNA. After centrifugation the supernatant was gently collected and pellet discarded. Fluorescein-labelled oligonucleotides (25-mer, Inqaba Biotec) were added to the capsids at 25.7 pmol per 1 μg capsid, respectively (Calculation can be found in Appendix 4). Oligonucleotides were made up as 2x stocks to desired concentrations using dissociation buffer (Radio-labelled oligonucleotide concentration was not determined). Capsids were allowed to re-associate overnight by dialysing against PBS at 4 ^{o}C. The final capsid working stock concentration was 1 μg/μl. Capsids were stored at -20 ^{o}C between analyses.

5.4.3 ^{32}P-labelling of oligonucleotides

Twenty five-mer oligonucleotides were labelled with [γ-^{32}P]ATP. The reaction comprised 10 U T4 polynucleotide kinase (Fermentas), 5 μl 10x T4 polynucleotide kinase buffer (500 mM Tris-HCl pH 7.6, 100 mM $MgCl_2$, 50 mM DTT, 1 mM spermidine), 20 μCi [γ-32P]ATP (3000 Ci/mmol) and 100 pmol DNA oligonucleotide in a total volume of 50 μl, incubated at 37 ^{o}C for 2 hours. Oligonucleotides were purified by passing them through a 1 ml Sephadex G-25 column. FITC-labelled oligonucleotides were purchased from Inqaba Biotec (Pretoria, ZA)

5.4.4 Imaging with the Phosphorimager

Radio-labelled oligonucleotides were loaded into c183 capsids and subjected to agarose gel electrophoresis. A total of 30 μg of loaded capsid was loaded per well, and subjected to electrophoresis at 80 V. The agarose gel was placed on Whatman 3MM Chr paper and dried at 80 ^{o}C under vacuum. Dried gels were exposed to the BAS SR 2040 imaging plate (Fuji, Tokyo Japan) overnight, and the FLA-7000 Phosphorimager (Fuji) was used to detect signal on the imaging plate the following day.

5.4.5 Cell Culture and VLP inoculations

The cell lines Huh7 and Hek293 were maintained in DMEM (Gibco, Life Technologies, CA, USA) 10% FCS (Life Technologies, CA, USA) within a humidified incubator at 37 ^{o}C. To split Hek293 cells, medium was removed and 1 ml TripLE Express (Life Technologies, CA, USA) was added to a confluent 25 cm^2 flask and incubated at 37 ^{o}C for 1 minute. Cells were gently aspirated and added to an appropriate volume of DMEM 10% FBS. Hek293 cells were not washed during splitting as they tend to dislodge easily from the flask surface. Huh7 cells in a 25 cm^2 flask were initially washed with 10 ml saline 0.5 mM EDTA, fresh 10 ml saline 0.5 mM EDTA added and incubated at 37 ^{o}C for 5 minutes. Following the two wash steps saline was removed and cells incubated with 1 ml TripLE Express (Life Technologies, CA, USA) for 5 minutes. Cells were gently aspirated and added to an appropriate volume of DMEM 10% FCS. For VLP inoculations, cell lines were seeded at 60% confluency in 8-well glass Millicell EZ slide (Millipore, MA, USA). The following day medium was removed and replaced with 200 μl OptiMEM (Gibco, Life Technologies, CA, USA) containing 4 μg of capsid preparation. The oligonucleotide control well received 100 pmol of naked FITC-labelled 25-mer. Capsids and cells were incubated together for two hours at 37 ^{o}C in a humidified chamber. Following incubation, cells were fixed to the slide surface by gently removing the medium and immersing the glass slide in ice cold methanol for 5 minutes. Following this cells were immersed in PBS containing 14.3 mM DAPI for 3 minutes at room temperature. Slides were briefly air dried and fluorescence preserving agent, Fluorsave (Millipore, MA, USA), added prior to covering cells with a cover slip.

5.4.6 Microscopy and imaging

Microscopy was performed using the Axiovert 100M (Zeiss, Oberkochen, Germany) fitted with the Axiocam MRm camera (Zeiss). Three images were taken to capture bright field, FITC fluorescence and DAPI fluorescence images. Excitation filters for DAPI and FITC were 365/10 nm and 470/40 nm. Combined images were generated using the Axiovision 4.8 software (Zeiss).

Chapter 6: Conclusion

The field of gene therapy has made rapid progress over the past two decades in treating conditions ranging from viral infections to autosomal diseases. Typically, *in vivo* treatment utilises a recombinant viral vector to deliver the corrective therapeutic. Success has been demonstrated using this approach in treating several diseases such as adenosine deaminase deficiency severe combined immunodeficiency (ADA-SCID) and has even shown potential against Parkinson's disease [10, 310]. Despite the efficacy of the treatment itself, inefficiency of vectors remains major obstacle. Difficulties have been experienced using viral vectors, primarily involving stimulation of the immune response and a lack of immuno-evasion, toxicity, cost and scaling up of production. A variety of alternative delivery vectors are under continuous development which attempt to simplify production, decrease cost and improve biocompatibility. However, synthetic vectors often demonstrate decreased *in vivo* efficacy compared to viral vectors. In an effort to improve on the application of synthetic vectors (which may also comprise hybrid organic-synthetic vectors, such as the decorated HBV capsid), several researchers have included VLPs in the development of gene therapy vectors. One of the more developed VLPs with regard to bionanotechnology is the cowpea mosaic virus (CPMV), which has seen modifications done to its structure to enhance the delivery capacity of the particle [94, 286]. Both the HBV and CPMV capsids offer similar vector capacity; however it is felt that the HBV capsid can be more efficiently produced as it does not require a plant host for synthesis.

This study aimed to enhance the HBV capsid for delivery of a potential therapeutic cargo. The HBV capsid, like other VLPs, demonstrates indiscriminate cellular uptake *in vitro* and *in vivo*. Thus the introduction of a suitable chemical moiety to the capsid surface was required to prevent indiscriminate uptake and provide tissue tropism. Surface decoration was assessed by two means; conjugation of functional ligands to the capsids surface or envelopment of the capsids with liposomes. Maleimide-based conjugation of functional ligands to the capsid surface was accomplished by the introduction of cysteine residues into the IL of the capsid. It was shown in this study that the cysteine-maleimide reaction occurred very efficiently, attaching a functional moiety to almost all capsid proteins. In doing so, indiscriminate cellular uptake was prevented which may also function to decrease

initial immuno-stimulation *in vivo*. The HBV capsid will require tropism if it is to find use in *in vivo* application via systemic administration. This requires the development of alternative capsid ligands to provide the HBV capsid, and perhaps other VLPs, with cellular tropism.

This study generated a useful and unique form of modifying the HBV capsid at the amino acid level. The 'Snap-in' method was able to overcome difficult cloning procedures associated with introducing foreign residues or peptides into the IL. The 'Snap-in' system allowed for the generation of several cysteine and lysine substitution mutants in a short space of time. This technology has the potential to be applied to various other VLPs that may require alterations to their capsid proteins. The SplitCore approach is another means of simplifying the cloning into the IL. This approach may also provide a means to stabilise bulky peptide sequences that would otherwise destabilise the core protein. Both approaches have their merits, however the defining feature of each system is an intact core protein generated by 'Snap-in' versus the halved core components produced by Splitcore.

An aspect that will require further analysis is the type of cargo loaded into the recombinant capsid. Single stranded pgRNA (persistence length = 1-2 nm) is naturally encapsidated by the HBV capsid. Double stranded nucleic acids conversely have a fairly rigid structure (persistence length = ±50 nm), and a sequence of ±90 base pairs (30 nm) would not easily be encapsidated, nor contain viable therapeutic sequences. It is suggested that the material loaded into the capsid remains single stranded, such that both short and long sequences can be incorporated. It may be possible to administer a positive and negative strand individually, and ideally the complementary strands would combine within the cell nucleus. It may also be possible to introduce fragmented or nicked sequences, relying on the host repair machinery to reconstitute the therapeutic sequence.

With the suggested improvements to the HBV capsid, it may become feasible to deliver a therapeutic cargo (these cargo may not necessarily be nucleic acids). The delivery may not be as efficient as the current virus-based delivery vectors, however may be considerably cheaper in production. This has particular importance in resource constrained countries such as Africa, where it is vital to address the various epidemics throughout the continent. VLPs, like liposomes, may one day be a feasible form of therapy, available for simple, inexpensive production in any country.

Appendix 1

Primer sequences

Generic core forward
5’- GAT CCC ATG GAT GGA CAT CGA CCC TTA TAA -3’

Core reverse 140
5’- GAT CCT CGA GCT ATA AGA TAG GGG CAT TTG -3’

Core reverse 149
5’- GAT CCT CGA GCT AAA CAA CAG TAG TTT CCG -3’

Core reverse 160
5’- GAT CCT CGA GCT AAG TTC TTC TTC TAG GGG -3’

Core reverse 170
5’- GAT CCT CGA GCT ACG ATT GAG ACC TTC GTC -3’

Core reverse 183
5’- GAT CCT CGA GCT AAC ATT GAG ATT CCC GAG -3’

M13F
5’- GTA AAA CGA CGG CCA G -3’

M13R
5’- CAG GAA ACA GCT ATG AC -3’

Lys sub int R
5’- GAT CGA GCT CTC TTC GCT GGC TTT TCC AAA TTA ACA CCC ACC CAG G -3’

Lys sub int F
5’- GAT CGG TAC CTA GTA GTC AGT TAT GTC AAC AC -3’

LinkedLys Int F1
5’- GAT CGA TCT TTA AAG GGA AAG GGA AAG GGA AAG GGA GGA GGA GGA TCT A -3’

LinkedLys Int F2
5’- GGG AAA GGG AGG AGG AGG ATC TAG AGA CCT AGT AGT -3’

LinkedLys Int R
5’- GAT CAG GCC TCC TCC TCC ATC TTC CAA ATT AAC ACC CAC CCA GG -3’

Part A RE2 ‘Snap-in’ rev (43 bases)
5’- CTA GCG ATC GCT AGC TAG GAA GAC GTT AAC ACC CAC CCA GGT A -3’

Part B RE2 ‘Snap-in’ fwd (45 bases)
5’- GAT CGC TAG CGA TCG ATC GAA GAC GTC AGT TAT GTC AAC ACT AAT -3’

Oligonucleotides

Fwd single Lys R82K (38 bases)

5’- GTT AAT TTG GAA GAT CCA GCG TCT AAG GAC CTA GTA GT -3’

Rev single Lys R82K (38 bases)

5’- ACT GAC TAC TAG GTC CTT AGA CGC TGG ATC TTC CAA AT -3’

Fwd double A80K R82K (38 bases)

5’- GTT AAT TTG GAA GAT CCA AAG TCT AAG GAC CTA GTA GT -3’

Rev double A80K R82K (38 bases)

5’- ACT GAC TAC TAG GTC CTT AGA CTT TGG ATC TTC CAA AT -3’

Fwd single Cys S81C (38 bases)

5’- GTT AAT TTG GAA GAT CCA GCG TCT AGA GAC CTA GTA GT -3’

Rev single Cys S81C (38 bases)

5’- ACT GAC TAC TAG GTC TCT AGA CGC TGG ATC TTC CAA AT -3’

Fwd double L76C S81C (38 bases)

5’- GTT AAT TGT GAA GAT CCA GCG TCT AGA GAC CTA GTA GT -3’

Rev double L76C S81C (38 bases)

5’- ACT GAC TAC TAG GTC TCT ACA CGC TGG ATC TTC ACA AT -3’

Appendix 2

Reagent recipes

Ethidium bromide solution (100x)

100 mg ethidium bromide in 10 ml H_2O

Lysogeny broth (LB)

10 g Tryptone

5 g Yeast Extract

5 g Sodium Chloride

Make up to 1 L with H_2O – autoclave.

LB Agar

10 g Tryptone

5 g Yeast Extract

5 g Sodium Chloride

1 2g Agar

Make up to 1L with H_2O – autoclave.

Ampicillin stock (1000x)

100 mg/ml ampicillin

Dissolve in 50% (v/v) ethanol/H_2O solution

Chloramphenicol stock (1000x)

34 mg/ml chloramphenicol

Dissolve in ethanol

Transformation buffer

15 ml Glycerol

1.47 g $CaCl_2.2H_2O$

302.4 mg PIPES-HCl

80 ml H_2O

pH 7 using NaOH, make up to 100 ml with H_2O, filter sterilise

Isopropyl β-D-1-thiogalactopyranoside stock (IPTG) – blue/white screening

100 mg IPTG in 1 ml H2O

5-bromo-4-chloro-indolyl-galactopyranoside stock (X-Gal)

20 mg X-Gal in 1 ml dimethyl formamide

Protein expression broth 1 L

5 g Yeast extract

10 g tryptone

5 g glycerol

0.5 g glucose

0.7 g Na_2SO_4

2.5 g NH_4Cl

Autoclave, then add:

1 mL 2 M MgSO4

1 mL metals mix*

* Metals mix 100 mL (1000x):

50 mL 0.1 M $FeCl_3$ dissolved in 0.1 M HCl

1 mL 1 M $MnCl_2$

1 mL 1 M $ZnSO_4$

1 ml 0.2 M $CoCl_2$

1 ml 0.2 M $NiCl_2$

46 mL H_2O

Isopropyl β-D-1-thiogalactopyranoside 1000x stock (IPTG) – protein expression

0.47 g in 2 ml H_2O

PBS pH 7.4 @ room temperature 1 L

8 g NaCl

0.2 g KCl

1.44 g Na_2HPO_4

0.24 g KH_2PO_4

Resuspension Buffer A

50 mM Tris-HCl pH7.4

1 mM EDTA

5 mM DTT/TCEP (tris(2-carboxyethyl)phosphine - Sigma).

1 mM PMSF

Column Buffer A

100 mM Tris-HCl pH7.5

100 mM NaCl

50 mM sucrose

2 mM DTT/TCEP

Resuspension buffer B

0.25 mg/ml PMSF (phenylmethylsulfonyl fluoride - Sigma)

50 mM Tris pH 7.5 at 4^oC

5 mM TCEP (tris(2-carboxyethyl)phosphine - Sigma).

Column buffer B

5% w/v sucrose

5 mM EDTA

50 mM Tris pH 7.5 at 4^oC

2 mM TCEP

Tris-NaCl Buffer (TN Buffer) pH 7.6

25 mM Tris

50 mM NaCl

SDS-PAGE gel stain 2 L

1 g Coomassie Brilliant Blue

500 ml isopropanol

200 ml acetic acid

1300 ml water

malPEG5000 stock stored at -80^{o}C

100 mg malPEG5000 in 1 ml DMSO.

Transformation buffer pH 7.0 (stored at -20^{o}C)

100 mM $CaCl_2$

10 mM PIPES-HCl

15% glycerol

Make up to 50 ml with H_2O

Filter-sterilise and store

Glucose buffer (P1) pH 8.0

50 mM glucose

25 mM Tris-HCl

10 mM EDTA

Lysis buffer (P2)

0.2 M NaOH

1% SDS (w/v)

Neutralisation buffer (P3)

300 ml 5 M potassium acetate

57.5 ml glacial acetic acid

142.5 ml H_2O

Salt-saturated phenol

500 g phenol

100 ml 2M Tris-HCl, pH7.4

130 ml H_2O

Dissolve phenol, remove upper aqueous phase (sometimes it is necessary to add more Tris-HCl solution and H_2O)

Add: 100 ml 2 M Tris-HCl, pH 7.4

25 ml m-cresol

1 ml β-mercaptoethanol

500 mg 8-hydroxyquinoline

Use the upper phase from extraction purposes.

Disassociation buffer

1.5 M guanidine HCl

0.5 M LiCl

50 mM HEPES, pH 7.5

4x Running Buffer for PAGE gels

1.5 M Tris (pH 8.8) in 200 ml H_2O

4x Stacking Buffer of PAGE gels

0.5 M Tris (pH 6.8) in 50 ml H_2O

2x Protein Loading dye

2.5 ml 4x Stacking Buffer

4 ml 10% SDS

2 ml Glycerol

2 mg Bromophenol Blue

0.31 g DTT

Make up to 10 ml H_2O

50x Tris Acetate EDTA (TAE) buffer (1L)

242 g Tris

57.5 ml glacial acetic acid

100 ml 0.5M EDTA

Appendix 3 – Standard Laboratory Protocols

A3.1 Chemically competent bacteria

- Inoculate 10 ml LB with 100 µl of bacterial stock (glycerol stock or a previously prepared competent bacteria aliquot. Some bacterial strains require antibiotics during their culture to maintain important plasmids. Incubate the culture over night with shaking at 37 ^{o}C.
- Allocate 5 ml of the overnight culture into 45 ml LB. Incubate with shaking at 37 ^{o}C until the culture has reached an optical density of 0.4 @ 600 nm
- Pellet bacteria by centrifugation at 1500 × *g* for 20 minutes at 4 ^{o}C, removing the supernatant.
- Resuspend each bacterial pellet in 5 ml transformation buffer (Appendix 2), and incubate on ice for 20 minutes.
- Pellet the bacteria for 10 minutes at 500 × *g* at 4 ^{o}C, remove the supernatant and gently resuspend the collected bacteria in 2 ml transformation buffer.
- Aliquot into 100 µl stocks and store at -80 ^{o}C

A3.2 Transformation of chemically competent bacteria

- Thaw a chemically competent bacterial stock on ice.
- Add 100 ng – 1 µg of DNA to the competent bacteria and gently mix. Place on ice for 20 minutes.
- Heat shock the bacteria at 42 ^{o}C for 90 seconds and place on ice for 5 minutes
- Distribute the transformed bacteria on a LB agar plate.

A3.3 Blue-white screening

- Prior to distributing transformed bacteria on a LB agar plate, evenly spread 8 µl IPTG and 40 µl X-Gal (Appendix 2) over the agar surface and allow to dry for 20 minutes at 37 ^{o}C.
- Once the agar surface has dried distribute transformed bacteria over it. Incubate the plate at 37^{o}C overnight.

- White colonies contain the cloned gene of interest, as the β-galactosidase gene has been disrupted. Blue colonies conversely do not contain the cloned gene of interest.

A3.4 Plasmid extraction

Preparations of plasmid vary in accordance to the yield of DNA required. The main difference in both preparations is the amount of starting culture used. Mini-preps require volumes ranging between 2-10 ml of culture, and midi-preps between 100-200 ml of culture.

- Culture overnight 10 ml 200 ml of the respective clone required. Harvest the bacterial pellet by centrifugation at 5000 × *g* for 10 minutes.
- Resuspend the bacterial pellet in 200 µl 10 ml chilled glucose buffer (P1)
- Add 200 µl 10 ml lysis buffer (P2), gently mix by inversion and incubate at room temperature for 5 minutes.
- Add 200 µl 10 ml chilled neutralising buffer (P3), gently mix by inversion and incubate on ice for 10 minutes.
- Bacterial debris and precipitate is pelleted by centrifugation at 5000 × *g* for 10 minutes at 4 ^{o}C. Remove any additional debris by pouring the supernatant through a fine cloth (muslin).
- Add an equal volume of isopropanol to the filtered supernatant, mix and incubate on ice for 30 minutes.
- Centrifugation at 10000 × *g* for 30 minutes (4 ^{o}C) causes the DNA to pellet.
- Resuspend the pellet in 50 µl 600 µl H_2O, add equal volumes of chloroform and ss-phenol and briefly vortex.
- Separate the phases by centrifugation at 14000 × *g* for 1 minute.
- Carefully remove the clear upper phase (discard the lower phases) and add an equal volume of chloroform, briefly vortex and subject to centrifugation at 14000 × *g* for 1 minute. Repeat this step.
- Remove the upper phase, add an equal volume of isopropanol and 10% of the final volume of 3 M sodium acetate. Incubate on ice for 30 minutes or overnight at -20 ^{o}C.
- Pellet the DNA by centrifugation at 14000 × g, 4 ^{o}C for 30 minutes. Remove supernatant and add 500 µl 70% ethanol (v/v), incubate on ice for 10-20 minutes.

- Pellet the DNA by centrifugation at 14000 × g, 4 °C for 5 minutes. Remove supernatant and dry DNA pellet. Resuspend the pellet in 20-50 µl 200 µl-1ml sterile H_2O.

A3.4 Phenol-chloroform extraction

- Combine equal parts of DNA suspension, chloroform and salt-saturated phenol.
- Thoroughly mix samples and centrifuge at max speed (>8000 × *g*) for 90 seconds.
- Retain the upper phase and equal volume of chloroform added.
- Thoroughly mix samples and centrifuge at max speed (>8000 × *g*) for 90 seconds.
- Repeat the chloroform wash step.
- Retain the upper phase and an equal volume of chilled isopropanol added, to this add 10% of the total volume 3 M sodium acetate.
- Incubate on ice for 30 minutes and centrifuge (>8000 × *g*) for 30 minutes at 4 °C.
- Remove supernatant and wash DNA pellet with 70% ethanol.
- Remove supernatant and dry DNA pellet at room temperature.
- Resuspend the dried DNA pellet in an appropriate volume of distilled water.

A3.5 Agarose and polyacrylamide gel staining to detect recombinant HBV capsids

- After electrophoresis polyacrylamide gels were stained for two hours in Coomassie Brilliant blue stain (Appendix 2) with gentle shaking. Gels were washed in water to remove excess stain and then incubated overnight in a destaining solution (80% H_2O, 10% MeOH and 10% AcOH (v/v)). Tissue paper was included during the destaining process to aid the extraction of stain from the gel.
- Agarose gels were stained for 4 hours using a 15-fold dilution of the Coomassie Brilliant blue stain. The stain was diluted using destaining solution. Gels were washed in water to remove excess stain and then incubated overnight in a destaining solution (80% H_2O, 10% MeOH and 10% AcOH (v/v)). Tissue paper was included during the destaining process to aid the extraction of stain from the gel. The destaining process took up to 36 hours for the majority of the stain to be extracted.

Appendix 4

A4.1 Example calculation to determine lysine:ligand mole ratio for conjugation

- Recombinant c149 capsid concentration is 1 µg/µl (Mw = 16700 Da)
- Ligand stock concentration is 100 mg/ml (scPEG Mw = ±5 kDa)
- 100 µl of protein stock used
- Reaction mol ratio 10 ligand : 1 core protein

If the IL of c149 A80K R82K contains two reactive lysine species then:

$$n = \frac{m}{Mw}$$

$$n = \frac{100\ \mu g}{16700\ g.mol^{-1}}$$

$$n = \left(\frac{100\ \mu g}{16700\ g.mol^{-1}}\right) \times \frac{1 \times 10^{-4}\ g}{100\ \mu g}$$

$n = 6.25 \times 10^{-9}\ mol$ of core protein (double for the amount of lysines)

Thus 1.25 x 10^{-8} mol lysine residues per 100 µg core protein

Similarly, 1 µl of scPEG stock contains 100 µg, then

$n = 2 \times 10^{-8}\ mol$ of scPEG per 1µl of stock

Thus a reaction containing 1 part lysine to 1 part scPEG requires 100 µl core protein stock and 0.625 µl scPEG stock. Similarly a 1 part lysine to 10 parts scPEG reaction requires 100 µl core protein stock and 6.25 µl scPEG stock

A4.2 Example calculation to determine cysteine:ligand mole ratio for conjugation

- Recombinant c160 capsid concentration is 1 µg/µl (Mw = 18200 Da)
- Ligand stock concentration is 10 mg/ml (gal-mal Mw = 529.58 Da)
- 100 µl of protein stock used
- Reaction mol ratio 10 ligand : 1 core protein

If the IL of c160 L76C S81C contains two reactive cysteine species then:

$$n = \frac{m}{Mw}$$

$$n = \frac{100\ \mu g}{18200\ g.mol^{-1}}$$

$$n = \left(\frac{100\ \mu g}{18200\ g.mol^{-1}}\right) \times \frac{1 \times 10^{-4}\ g}{100\ \mu g}$$

$n = 5.5 \times 10^{-9}\ mol$ of core protein (double for the amount of lysines)

Thus 1.1 x 10^{-8} mol cysteine residues per 100 μg core protein

Similarly, 1 μl of gal-mal stock contains 10 μg gal-mal, then

$n = 1.9 \times 10^{-8}\ mol$ of gal-mal per 1μl of stock

Thus a reaction containing 1 part cysteine to 1 part gal-mal requires 100 μl core protein stock and 0.58 μl gal-mal stock. Similarly a 1 part cysteine to 10 parts gal-mal reaction requires 100 μl core protein stock and 5.8 μl gal-mal stock.

A4.3 Calculation to determine oligonucleotides (25-mer) required per μg of capsid

Porterfield *et al.* states: 0.6 Arginine residues required per 1 phosphate molecule (RNA/DNA) [245].

Thus 1 μg of c160 contains approximately:

$$n = \frac{m}{Mw}$$

$$n = \left(\frac{1\ \mu g}{18200\ g.mol^{-1}}\right) \times \frac{1 \times 10^{-6}\ g}{1\ \mu g}$$

$n = 55\ \times 10^{-12}\ mol$ of core proteins per 1 μg

c160 contains 7 arginine residues in the protamine domain, thus there are 385 pmol Arg per 1 μg protein.To determine the amount of 25-mer to add; 385 pmol Arg can bind 641.7 pmol phosphate molecules. If there are 25 phosphate per oligomer, 1 μg of capsid can bind 25.7 pmol oligomer.

References

1. Szybalska, E.H. and Szybalski, W., *Genetics of human cess line. IV. DNA-mediated heritable transformation of a biochemical trait.* Proceedings of the National Academy of Sciences, 1962. **48**(12): p. 2026-2034.
2. Temin, H.M., *Mixed infection with two types of Rous sarcoma virus.* Virology, 1961. **13**(2): p. 158-163.
3. Rogers, S., Lowenthal, A., Terheggen, H.G., and Columbo, J.P., *Induction of arginase activity with the Shope papilloma virus in tissue culture cells from an argininemic patient.* The Journal of Experimental Medicine, 1973. **137**(4): p. 1091-1096.
4. Terheggen, H.G., Lowenthal, A., Lavinha, F., Colombo, J.P., and Rogers, S., *Unsuccessful trial of gene replacement in arginase deficiency.* Zeitschrift für Kinderheilkunde, 1975. **119**(1): p. 1-3.
5. Rosenberg, S.A., Aebersold, P., Cornetta, K., Kasid, A., Morgan, R.A., Moen, R., Karson, E.M., Lotze, M.T., Yang, J.C., Topalian, S.L., Merino, M.J., Culver, K., Miller, A.D., Blaese, R.M., and Anderson, W.F., *Gene Transfer into Humans — Immunotherapy of Patients with Advanced Melanoma, Using Tumor-Infiltrating Lymphocytes Modified by Retroviral Gene Transduction.* New England Journal of Medicine, 1990. **323**(9): p. 570-578.
6. Blaese, R.M., Culver, K.W., Miller, A.D., Carter, C.S., Fleisher, T., Clerici, M., Shearer, G., Chang, L., Chiang, Y., Tolstoshev, P., Greenblatt, J.J., Rosenberg, S.A., Klein, H., Berger, M., Mullen, C.A., Ramsey, W.J., Muul, L., Morgan, R.A., and Anderson, W.F., *T Lymphocyte-Directed Gene Therapy for ADA− SCID: Initial Trial Results After 4 Years.* Science, 1995. **270**(5235): p. 475-480.
7. Bordignon, C., Notarangelo, L.D., Nobili, N., Ferrari, G., Casorati, G., Panina, P., Mazzolari, E., Maggioni, D., Rossi, C., Servida, P., Ugazio, A.G., and Mavilio, F., *Gene Therapy in Peripheral Blood Lymphocytes and Bone Marrow for ADA− Immunodeficient Patients.* Science, 1995. **270**(5235): p. 470-475.
8. Puumalainen, A.M., Vapalahti, M., Agrawal, R.S., Kossila, M., Laukkanen, J., Lehtolainen, P., Viita, H., Paljarvi, L., Vanninen, R., and Yla-Herttuala, S., *Beta-galactosidase gene transfer to human malignant glioma in vivo using replication-deficient retroviruses and adenoviruses.* Human gene therapy, 1998. **9**: p. 1769-1774.
9. *Assessment of adenoviral vector safety and toxicity: report of the National Institutes of Health Recombinant DNA Advisory Committee.* Human gene therapy, 2002. **13**: p. 3-13.
10. Aiuti, A., Cattaneo, F., Galimberti, S., Benninghoff, U., Cassani, B., Callegaro, L., Scaramuzza, S., Andolfi, G., Mirolo, M., Brigida, I., Tabucchi, A., Carlucci, F., Eibl, M., Aker, M., Slavin, S., Al-Mousa, H., Al Ghonaium, A., Ferster, A., Duppenthaler, A., Notarangelo, L., Wintergerst, U., Buckley, R.H., Bregni, M., Marktel, S., Valsecchi, M.G., Rossi, P., Ciceri, F., Miniero, R., Bordignon, C., and Roncarolo, M.-G., *Gene Therapy for Immunodeficiency Due to Adenosine Deaminase Deficiency.* New England Journal of Medicine, 2009. **360**(5): p. 447-458.
11. Goyenvalle, A., Seto, J.T., Davies, K.E., and Chamberlain, J., *Therapeutic approaches to muscular dystrophy.* Human Molecular Genetics, 2011. **20**(R1): p. R69-R78.
12. Hawkins-Salsbury, J.A., Reddy, A.S., and Sands, M.S., *Combination therapies for lysosomal storage disease: is the whole greater than the sum of its parts?* Human Molecular Genetics, 2011. **20**(R1): p. R54-R60.
13. Byrne, B.J., Falk, D.J., Pacak, C.A., Nayak, S., Herzog, R.W., Elder, M.E., Collins, S.W., Conlon, T.J., Clement, N., Cleaver, B.D., Cloutier, D.A., Porvasnik, S.L., Islam, S., Elmallah, M.K., Martin, A., Smith, B.K., Fuller, D.D., Lawson, L.A., and Mah, C.S., *Pompe disease gene therapy.* Human Molecular Genetics, 2011. **20**(R1): p. R61-R68.
14. Herzog, R., Yang, E., Couto, L., Hagstrom, J., Elwell, D., Fields, P., Burton, M., Bellinger, D., Read, M., Brinkhaus, K., Podsakoff, G., Nichols, T., Kurtzman, G., and High, K., *Long-term correction of canine hemophilia B by gene transfer of blood coagulation factor IX mediated by adeno-associated viral vector.* Nature medicine, 1999. **5**: p. 56-63.

15. Manno, C.S., Chew, A.J., Hutchison, S., Larson, P.J., Herzog, R.W., Arruda, V.R., Tai, S.J., Ragni, M.V., Thompson, A., Ozelo, M., Couto, L.B., Leonard, D.G.B., Johnson, F.A., McClelland, A., Scallan, C., Skarsgard, E., Flake, A.W., Kay, M.A., High, K.A., and Glader, B., *AAV-mediated factor IX gene transfer to skeletal muscle in patients with severe hemophilia B.* Blood, 2003. **101**(8): p. 2963-2972.
16. Rabinowitz, J.E. and Samulski, J., *Adeno-associated virus expression systems for gene transfer.* Current Opinion in Biotechnology, 1998. **9**(5): p. 470-475.
17. Beard, B., Keyser, K., Trobridge, G., Peterson, L., Miller, D., Jacobs, M., Kaul, R., and Kiem, H.M., *Unique Integration Profiles in a Canine Model of Long-Term Repopulating Cells Transduced with Gammaretrovirus, Lentivirus, or Foamy Virus.* Human gene therapy, 2007. **18**(5): p. 423-434.
18. Degreve, B., Andrei, G., Izquierdo, M., Piette, J., Morin, K., Knaus, E.E., Wiebe, L.I., Basrah, I., Walker, R.T., De Clercq, E., and Balzarini, J., *Varicella-zoster virus thymidine kinase gene and antiherpetic pyrimidine nucleoside analogues in a combined gene/chemotherapy treatment for cancer.* Gene Ther, 1997. **4**(10): p. 1107-1114.
19. Immonen, A., Vapalahti, M., Tyynela, K., Hurskainen, H., Sandmair, A., Vanninen, R., Langford, G., Murray, N., and Yla-Herttuala, S., *AdvHSV-tk Gene Therapy with Intravenous Ganciclovir Improves Survival in Human Malignant Glioma: A Randomised, Controlled Study.* Mol Ther, 2004. **10**(5): p. 967-972.
20. Fillat, C., Carrio, M., Cascante, A., and Sangro, B., *Suicide gene therapy mediated by the Herpes Simplex virus thymidine kinase gene/Ganciclovir system: fifteen years of application.* Current Gene Therapy, 2003. **3**(1): p. 13-26.
21. Kievit, E., Bershad, E., Ng, E., Sethna, P., Dev, I., Lawrence, T.S., and Rehemtulla, A., *Superiority of Yeast over Bacterial Cytosine Deaminase for Enzyme/Prodrug Gene Therapy in Colon Cancer Xenografts.* Cancer Research, 1999. **59**(7): p. 1417-1421.
22. Mullen, C.A., Kilstrup, M., and Blaese, R.M., *Transfer of the bacterial gene for cytosine deaminase to mammalian cells confers lethal sensitivity to 5-fluorocytosine: a negative selection system.* Proceedings of the National Academy of Sciences, 1992. **89**(1): p. 33-37.
23. Knox, R.J., Burke, P.J., Chen, S., and Kerr, D.J., *CB 1954: from the Walker tumor to NQO2 and VDEPT.* Current Pharmaceutical Design, 2003. **9**(26): p. 2091-2104.
24. Denny, W.A., *Nitroreductase-based GDEPT.* Curr. Pharm. Des, 2002. **8** (15): p. 1349–1361.
25. Fire, A., Xu, S., Montgomery, M., Kostas, S., Driver, S., and Mello, C., *Potent and specific genetic interference by double-stranded RNA in Caenorhabditis elegans.* Nature, 1998: p. 806-810.
26. Wilson, R.C. and Doudna, J.A., *Molecular Mechanisms of RNA Interference.* Annual Review of Biophysics, 2013. **42**(1): p. 217-239.
27. Sibley, C.R., Seow, Y., and Wood, M.J.A., *Novel RNA-based Strategies for Therapeutic Gene Silencing.* Mol Ther, 2010. **18**(3): p. 466-476.
28. Urnov, F., Rebar, E., Holmes, M., Zhang, S., and Gregory, P., *Genome editing with engineered zinc finger nucleases.* Nature Reviews Genetics, 2010. **11**: p. 636-646.
29. Stoddard, B.L., *Homing Endonucleases: From Microbial Genetic Invaders to Reagents for Targeted DNA Modification.* Structure (London, England : 1993), 2011. **19**(1): p. 7-15.
30. Wood, A.J., Lo, T.-W., Zeitler, B., Pickle, C.S., Ralston, E.J., Lee, A.H., Amora, R., Miller, J.C., Leung, E., Meng, X., Zhang, L., Rebar, E.J., Gregory, P.D., Urnov, F.D., and Meyer, B.J., *Targeted Genome Editing Across Species Using ZFNs and TALENs.* Science, 2011. **333**(6040): p. 307.
31. Tesson, L., Usal, C., Menoret, S., Leung, E., Niles, B.J., Remy, S., Santiago, Y., Vincent, A.I., Meng, X., Zhang, L., Gregory, P.D., Anegon, I., and Cost, G.J., *Knockout rats generated by embryo microinjection of TALENs.* Nat Biotech, 2011. **29**(8): p. 695-696.
32. Hockemeyer, D., Wang, H., Kiani, S., Lai, C.S., Gao, Q., Cassady, J.P., Cost, G.J., Zhang, L., Santiago, Y., Miller, J.C., Zeitler, B., Cherone, J.M., Meng, X., Hinkley, S.J., Rebar, E.J.,

Gregory, P.D., Urnov, F.D., and Jaenisch, R., *Genetic engineering of human pluripotent cells using TALE nucleases.* Nat Biotech, 2011. **29**(8): p. 731-734.
33. Horvath, P. and Barrangou, R., *CRISPR/Cas, the Immune System of Bacteria and Archaea.* Science, 2010. **327**(5962): p. 167-170.
34. Jinek, M., Chylinski, K., Fonfara, I., Hauer, M., Doudna, J.A., and Charpentier, E., *A Programmable Dual-RNA–Guided DNA Endonuclease in Adaptive Bacterial Immunity.* Science, 2012. **337**(6096): p. 816-821.
35. Cong, L., Ran, F.A., Cox, D., Lin, S., Barretto, R., Habib, N., Hsu, P.D., Wu, X., Jiang, W., Marraffini, L.A., and Zhang, F., *Multiplex Genome Engineering Using CRISPR/Cas Systems.* Science, 2013. **339**(6121): p. 819-823.
36. Bloom, K., Ely, A., Mussolino, C., Cathomen, T., and Arbuthnot, P., *Inactivation of Hepatitis B Virus Replication in Cultured Cells and In Vivo with Engineered Transcription Activator-Like Effector Nucleases.* Mol Ther, 2013.
37. Hansen, S.G., Jr, M.P., Ventura, A.B., Hughes, C.M., Gilbride, R.M., Ford, J.C., Oswald, K., Shoemaker, R., Li, Y., Lewis, M.S., Gilliam, A.N., Xu, G., Whizin, N., Burwitz, B.J., Planer, S.L., Turner, J.M., Legasse, A.W., Axthelm, M.K., Nelson, J.A., Fruh, K., Sacha, J.B., Estes, J.D., Keele, B.F., Edlefsen, P.T., Lifson, J.D., and Picker, L.J., *Immune clearance of highly pathogenic SIV infection.* Nature, 2013. **advance online publication**.
38. Isomura, H. and Stinski, M., *Coordination of late gene transcription of human cytomegalovirus with viral DNA synthesis: recombinant viruses as potential therapeutic vaccine candidates.* Expert Opinion on Therapeutic Targets, 2012. **17**(2): p. 157-166.
39. Nemunaitis, J., Senzer, N., Olivares, J., Kumar, P., Barve, M., Kuhn, J., Nemunaitis, T., Magee, M., Yu, Y., Wallraven, G., Pappen, B.O., and Maples, P.B., *Immune response and survival of refractory cancer patients who received TGF-[beta]2 antisense/GM-CSF gene modified autologous tumor cell (TAG) vaccine.* Gene Ther, 2013. **20**(9): p. 875-879.
40. Gavazza, A., Lubas, G., Fridman, A., Reruzzi, D., Impellizeri, J., Luberto, L., Marra, E., Roscilli, G., Ciliberto, G., and Aurisicchio, L., *Safety and Efficacy of a Genetic Vaccine Targeting Telomerase Plus Chemotherapy for the Therapy of Canine B-Cell Lymphoma.* Human gene therapy, 2013. **24**(8): p. 728-738.
41. Edelstein, M., *Gene Therapy Trial Worldwide.* http://www.abedia.com/wiley/vectors.php, 2012.
42. Ehrhardt, A., Xu, H., and Kay, M.A., *Episomal Persistence of Recombinant Adenoviral Vector Genomes during the Cell Cycle In Vivo.* Journal of Virology, 2003. **77**(13): p. 7689-7695.
43. Khare, R., Chen, C.Y., Weaver, E.A., and Barry, M.A., *Advances and Future Challenges in Adenoviral Vector Pharmacology and Targeting.* Current Gene Therapy. **11**(4): p. 241-258.
44. Rauschhuber, C., Noske, N., and Ehrhardt, A., *New insights into stability of recombinant adenovirus vector genomes in mammalian cells.* European Journal of Cell Biology, 2012. **91**(1): p. 2-9.
45. Crowther, C., Ely, A., Hornby, J., Mufamadi, S., Salazar, F., Marion, P., and Arbuthnot, P., *Efficient Inhibition of Hepatitis B Virus Replication In Vivo, Using Polyethylene Glycol-Modified Adenovirus Vectors.* Human gene therapy, 2008. **19**(11): p. 1325-1332.
46. Rauschhuber, C., Xu, H., Salazar, F.H., Marion, P.L., and Ehrhardt, A., *Exploring gene-deleted adenoviral vectors for delivery of short hairpin RNAs and reduction of hepatitis B virus infection in mice.* The Journal of Gene Medicine, 2008. **10**(8): p. 878-889.
47. Wang, L., HernÁndez-Alcoceba, R., Shankar, V., Zabala, M., Kochanek, S., Sangro, B., Kramer, M.G., Prieto, J., and Qian, C., *Prolonged and inducible transgene expression in the liver using gutless adenovirus: A potential therapy for liver cancer.* Gastroenterology, 2004. **126**(1): p. 278-289.
48. Du, L., Dronadula, N., Tanaka, S., and Dichek, D., *Helper-Dependent Adenoviral Vector Achieves Prolonged, Stable Expression of Interleukin-10 in Rabbit Carotid Arteries but Does Not Limit Early Atherogenesis.* Human gene therapy, 2011. **22**(8): p. 959-968.

49. Morsy, M.A., Gu, M., Motzel, S., Zhao, J., Lin, J., Su, Q., Allen, H., Franlin, L., Parks, R.J., Graham, F.L., Kochanek, S., Bett, A.J., and Caskey, C.T., *An adenoviral vector deleted for all viral coding sequences results in enhanced safety and extended expression of a leptin transgene.* Proceedings of the National Academy of Sciences, 1998. **95**(14): p. 7866-7871.
50. N, B.-P., T, N., D, I., W, C., G, S., M, L., J, B., D, P., N, G., K, R., C, B., M, F., A, B., C, M., and P, N., *Transgene Expression up to 7 Years in Nonhuman Primates Following Hepatic Transduction with Helper-Dependent Adenoviral Vectors.* Human gene therapy, 2013. **24**(8): p. 761-765.
51. Srivastava, A., Lusby, E.W., and Berns, K.I., *Nucleotide sequence and organization of the adeno-associated virus 2 genome.* Journal of Virology, 1983. **45**(2): p. 555-564.
52. Rothe, D., Wajant, G., Grunert, H., Zeichhardt, H., Fechner, H., and Kurreck, J., *Rapid Construction of Adeno-Associated Virus Vectors Expressing Multiple Short Hairpin RNAs with High Antiviral Activity Against Echovirus 30.* Oligonucleotides, 2010. **20**(4): p. 191-198.
53. Afione, S.A., Conrad, C.K., Kearns, W.G., Chunduru, S., Adams, R., Reynolds, T.C., Guggino, W.B., Cutting, G.R., Carter, B.J., and Flotte, T.R., *In vivo model of adeno-associated virus vector persistence and rescue.* Journal of Virology, 1996. **70**(5): p. 3235-41.
54. Hauck, B., Zhao, W., High, K., and Xiao, W., *Intracellular Viral Processing, Not Single-Stranded DNA Accumulation, Is Crucial for Recombinant Adeno-Associated Virus Transduction.* Journal of Virology, 2004. **78**(24): p. 13678-13686.
55. Zaiss, A.-K., Liu, Q., Bowen, G.P., Wong, N.C.W., Bartlett, J.S., and Muruve, D.A., *Differential Activation of Innate Immune Responses by Adenovirus and Adeno-Associated Virus Vectors.* Journal of Virology, 2002. **76**(9): p. 4580-4590.
56. Schnepp, B.C., Jensen, R.L., Chen, C.-L., Johnson, P.R., and Clark, K.R., *Characterization of Adeno-Associated Virus Genomes Isolated from Human Tissues.* Journal of Virology, 2005. **79**(23): p. 14793-14803.
57. Chen, C.C., Ko, T.M., Ma, H.I., Wu, H.L., Xiao, X., Li, J., Chang, C.M., Wu, P.Y., Chen, C.H., Han, J.M., Yu, C.P., Jeng, K.S., Hu, C.P., and Tao, M.H., *Long-term inhibition of hepatitis B virus in transgenic mice by double-stranded adeno-associated virus 8-delivered short hairpin RNA.* Gene Ther, 2006. **14**(1): p. 11-19.
58. Chen, C.-C., Sun, C.-P., Ma, H.-I., Fang, C.-C., Wu, P.-Y., Xiao, X., and Tao, M.-H., *Comparative Study of Anti-hepatitis B Virus RNA Interference by Double-stranded Adeno-associated Virus Serotypes 7, 8, and 9.* Mol Ther, 2008. **17**(2): p. 352-359.
59. Hacein-Bey-Abina, S., Le Deist, F., Carlier, F., Bouneaud, C., Hue, C., De Villartay, J.-P., Thrasher, A.J., Wulffraat, N., Sorensen, R., Dupuis-Girod, S., Fischer, A., Davies, E.G., Kuis, W., Leiva, L., and Cavazzana-Calvo, M., *Sustained Correction of X-Linked Severe Combined Immunodeficiency by ex Vivo Gene Therapy.* New England Journal of Medicine, 2002. **346**(16): p. 1185-1193.
60. Cavazzana-Calvo, M., Hacein-Bey, S., Basile, G.v.d.S., Gross, F., Yvon, E., Nusbaum, P., Selz, F.o., Hue, C., Certain, S.p., Casanova, J.-L., Bousso, P., Deist, F.o.L., and Fischer, A., *Gene Therapy of Human Severe Combined Immunodeficiency (SCID)-X1 Disease.* Science, 2000. **288**(5466): p. 669-672.
61. Naumann, N., De Ravin, S.S., Choi, U., Moayeri, M., Whiting-Theobald, N., Linton, G.F., Ikeda, Y., and Malech, H.L., *Simian immunodeficiency virus lentivector corrects human X-linked chronic granulomatous disease in the NOD//SCID mouse xenograft.* Gene Ther, 2007. **14**(21): p. 1513-1524.
62. Verma, I.M. and Weitzman, M.D., *Gene Therapy: Twenty-First Century Medicine.* Annu Rev Biochem, 2005. **74**: p. 711-738.
63. Naldini, L., Blömer, U., Gallay, P., Ory, D., Mulligan, R., Gage, F.H., Verma, I.M., and Trono, D., *In Vivo Gene Delivery and Stable Transduction of Nondividing Cells by a Lentiviral Vector.* Science, 1996. **272**(5259): p. 263-267.

64. Oertel, M., Rosencrantz, R., Chen, Y.-Q., Thota, P.N., Sandhu, J.S., Dabeva, M.D., Pacchia, A.L., Adelson, M.E., Dougherty, J.P., and Shafritz, D.A., *Repopulation of rat liver by fetal hepatoblasts and adult hepatocytes transduced ex vivo with lentiviral vectors.* Hepatology, 2003. **37**(5): p. 994-1005.
65. Swainson, L., Mongellaz, C., Adjali, O., Vicente, R., and Taylor, N., *Lentiviral Transduction of Immune Cells*, in *Innate Immunity*, J. Ewbank and E. Vivier, Editors. 2008, Humana Press. p. 301-320.
66. Peng, Z., *Current status of gendicine in China: recombinant human Ad-p53 agent for treatment of cancers. .* Human gene therapy, 2005. **16**: p. 1016-1027.
67. Wilson, J.M., *Gendicine: the first commercial gene therapy product.* Human gene therapy, 2005. **16**: p. 1014-1015.
68. Xin, H., *Gendicine's Efficacy: Hard to Translate.* Science, 2006. **314**(5803): p. 1233.
69. Garber, K., *China Approves World's First Oncolytic Virus Therapy For Cancer Treatment.* Journal of the National Cancer Institute, 2006. **98**(5): p. 298-300.
70. Yla-Herttuala, S., *Endgame: Glybera Finally Recommended for Approval as the First Gene Therapy Drug in the European Union.* Mol Ther, 2012. **20**(10): p. 1831-1832.
71. Maguire, A.M., High, K.A., Auricchio, A., Wright, J.F., Pierce, E.A., Testa, F., Mingozzi, F., Bennicelli, J.L., Ying, G.-s., Rossi, S., Fulton, A., Marshall, K.A., Banfi, S., Chung, D.C., Morgan, J.I.W., Hauck, B., Zelenaia, O., Zhu, X., Raffini, L., Coppieters, F., De Baere, E., Shindler, K.S., Volpe, N.J., Surace, E.M., Acerra, C., Lyubarsky, A., Redmond, T.M., Stone, E., Sun, J., McDonnell, J.W., Leroy, B.P., Simonelli, F., and Bennett, J., *Age-dependent effects of RPE65 gene therapy for Leber's congenital amaurosis: a phase 1 dose-escalation trial.* The Lancet. **374**(9701): p. 1597-1605.
72. Hacein-Bey-Abina, S., Hauer, J., Lim, A., Picard, C., Wang, G.P., Berry, C.C., Martinache, C., Rieux-Laucat, F., Latour, S., Belohradsky, B.H., Leiva, L., Sorensen, R., Debré, M., Casanova, J.L., Blanche, S., Durandy, A., Bushman, F.D., Fischer, A., and Cavazzana-Calvo, M., *Efficacy of Gene Therapy for X-Linked Severe Combined Immunodeficiency.* New England Journal of Medicine, 2010. **363**(4): p. 355-364.
73. Boztug, K., Schmidt, M., Schwarzer, A., Banerjee, P.P., Díez, I.A., Dewey, R.A., Böhm, M., Nowrouzi, A., Ball, C.R., Glimm, H., Naundorf, S., Kühlcke, K., Blasczyk, R., Kondratenko, I., Maródi, L., Orange, J.S., von Kalle, C., and Klein, C., *Stem-Cell Gene Therapy for the Wiskott–Aldrich Syndrome.* New England Journal of Medicine, 2010. **363**(20): p. 1918-1927.
74. Cavazzana-Calvo, M., Payen, E., Negre, O., Wang, G., Hehir, K., Fusil, F., Down, J., Denaro, M., Brady, T., Westerman, K., Cavallesco, R., Gillet-Legrand, B., Caccavelli, L., Sgarra, R., Maouche-Chretien, L., Bernaudin, F., Girot, R., Dorazio, R., Mulder, G.-J., Polack, A., Bank, A., Soulier, J., Larghero, J., Kabbara, N., Dalle, B., Gourmel, B., Socie, G., Chretien, S., Cartier, N., Aubourg, P., Fischer, A., Cornetta, K., Galacteros, F., Beuzard, Y., Gluckman, E., Bushman, F., Hacein-Bey-Abina, S., and Leboulch, P., *Transfusion independence and HMGA2 activation after gene therapy of human [bgr]-thalassaemia.* Nature, 2010. **467**(7313): p. 318-322.
75. Chesnoy, S. and Huang, L., *Structure and function of lipid-DNA complexes for gene delivery.* Annual Review of Biophysics and Biomolecular Structure, 2000. **29**(1): p. 27-47.
76. Felgner, P.L., Gadek, T.R., Holm, M., Roman, R., Chan, H.W., Wenz, M., Northrop, J.P., Ringold, G.M., and Danielsen, M., *Lipofection: a highly efficient, lipid-mediated DNA-transfection procedure.* Proceedings of the National Academy of Sciences, 1987. **84**(21): p. 7413-7417.
77. Almofti, M., Harashima, H., Shinohara, Y., Almofti, A., Li, W., and Kiwada, H., *Lipoplex size determines lipofection efficiency with or without serum.* Molecular Membrane Biology, 2003. **20**(1): p. 35-43.
78. Ross, P. and Hui, S., *Lipoplex size is a major determinant of in vitro lipofection efficiency.* Gene Ther, 1999. **6**(4): p. 651-659.

79. Hirko, A., Tang, F., and Hughes, J.L., *Cationic lipid vectors for plasmid DNA delivery.* Curr. Med. Chem., 2003. **10**(14): p. 1185-1193.
80. Ferrari, M.E., Rusalov, D., Enas, J., and Wheeler, C.J., *Synergy between cationic lipid and co-lipid determines the macroscopic structure and transfection activity of lipoplexes.* Nucleic Acids Research, 2002. **30**(8): p. 1808-1816.
81. Congiu, A., Pozzi, D., Esposito, C., Castellano, C., and Mossa, G., *Correlation between structure and transfection efficiency: a study of DC-Chol–DOPE/DNA complexes.* Colloids and Surfaces B: Biointerfaces, 2004. **36**(1): p. 43-48.
82. Elouahabi, A. and Ruysschaert, J.-M., *Formation and Intracellular Trafficking of Lipoplexes and Polyplexes.* Mol Ther, 2005. **11**(3): p. 336-347.
83. Brunner, S., Sauer, T., Carotta, S., Cotten, M., Saltik, M., and Wagner, E., *Cell cycle dependence of gene transfer by lipoplx, polyplex and recombinant adenovirus.* Gene Therapy, 2000. **7**(5): p. 401-407.
84. Wang, W., Wenzhong, L., Ma, N., and Steinhoff, G., *Non-viral gene delivery methods.* Current Pharmaceutical Biotechnology, 2013. **14**: p. 46-60.
85. Chang, H. and Yeh, M., *Clinical development of liposome-based drugs: formulation, characterization and therapeutic efficacy.* Int. J. Nanomedicine, 2012. **7**: p. 49-60.
86. Parks, J., *Liposome-based drug delivery in breast cancer treatment.* Breast Cancer Res., 2002. **4**: p. 95-99.
87. Meunier, F., Prentice, H.G., and Ringdén, O., *Liposomal amphotericin B (AmBisome): safety data from a phase II/III clinical trial.* Journal of Antimicrobial Chemotherapy, 1991. **28**(suppl B): p. 83-91.
88. Augustin, A., Puls, S., and Offermann, I., *Triple therapy for choroidal neovascularization due to age-related macular degeneration: Verteporfin PDT, Bevacizumab, and Dexamethasone.* RETINA, 2007. **27**(2): p. 133-140 10.1097/IAE.0b013e3180323de7.
89. Usonis, V., Bakasénas, V., Valentelis, R., Katiliene, G., Vidzeniene, D., and Herzog, C., *Antibody titres after primary and booster vaccination of infants and young children with a virosomal hepatitis A vaccine (Epaxal®).* Vaccine, 2003. **21**(31): p. 4588-4592.
90. D'Acremont, V., Herzog, C., and Genton, B., *Immunogenicity and Safety of a Virosomal Hepatitis A Vaccine (Epaxal®) in the Elderly.* Journal of Travel Medicine, 2006. **13**(2): p. 78-83.
91. Herzog, C., Hartmann, K., Künzi, V., Kürsteiner, O., Mischler, R., Lazar, H., and Glück, R., *Eleven years of Inflexal® V—a virosomal adjuvanted influenza vaccine.* Vaccine, 2009. **27**(33): p. 4381-4387.
92. Zeltins, A., *Construction and Characterization of Virus-Like Particles: A Review.* Molecular Biotechnology, 2013. **53**(1): p. 92-107.
93. Birnbaum, F. and Nassal, M., *Hepatitis B virus nucleocapsid assembly: primary structure requirements in the core protein.* J. Virol., 1990. **64**(7): p. 3319-3330.
94. Wang, Q., Kaltgrad, E., Lin, T., Johnson, J.E., and Finn, M.G., *Natural Supramolecular Building Blocks: Wild-Type Cowpea Mosaic Virus.* Chemistry & Biology, 2002. **9**(7): p. 805-811.
95. Roldão, A., Mellado, M.C.M., Castilho, L.R., Carrondo, M.J.T., and Alves, P.M., *Virus-like particles in vaccine development.* Expert Review of Vaccines, 2010. **9**(10): p. 1149-1176.
96. Soto, C.M. and Ratna, B.R., *Virus hybrids as nanomaterials for biotechnology.* Current Opinion in Biotechnology, 2010. **21**(4): p. 426-438.
97. Burrell, C.J., Mackay, P., Greenaway, P.J., Hofschneider, P.H., and Murray, K., *Expression in Escherichia coli of hepatitis B virus DNA sequences cloned in plasmid pBR322.* Nature, 1979. **279**(5708): p. 43-47.
98. Choi, K.-m., Choi, S.-H., Jeon, H., Kim, I.-S., and Ahn, H.J., *Chimeric Capsid Protein as a Nanocarrier for siRNA Delivery: Stability and Cellular Uptake of Encapsulated siRNA.* ACS Nano, 2011. **5**(11): p. 8690-8699.

99. Cooper, A. and Shaul, Y., *Recombinant viral capsids as an efficient vehicle of oligonucleotide delivery into cells.* Biochemical and Biophysical Research Communications, 2005. **327**(4): p. 1094-1099.
100. Mintzer, M.A. and Simanek, E.E., *Nonviral Vectors for Gene Delivery.* Chemical Reviews, 2008. **109**(2): p. 259-302.
101. Ewert, K., Ahmad, A., Bouxsein, N., Evans, H., and Safinya, C., *Non-Viral Gene Delivery with Cationic Liposome-DNA Complexes*, in *Gene Therapy Protocols*. 2008, Humana Press. p. 159-175.
102. Zhang, X.-X., McIntosh, T.J., and Grinstaff, M.W., *Functional lipids and lipoplexes for improved gene delivery.* Biochimie, 2012. **94**(1): p. 42-58.
103. Wasungu, L. and Hoekstra, D., *Cationic lipids, lipoplexes and intracellular delivery of genes.* Journal of Controlled Release, 2006. **116**(2): p. 255-264.
104. Wolff, J.A. and Rozema, D.B., *Breaking the Bonds: Non-viral Vectors Become Chemically Dynamic.* Mol Ther, 2007. **16**(1): p. 8-15.
105. Zhi, D., Zhang, S., Wang, B., Zhao, Y., Yang, B., and Yu, S., *Transfection Efficiency of Cationic Lipids with Different Hydrophobic Domains in Gene Delivery.* Bioconjugate Chemistry, 2010. **21**(4): p. 563-577.
106. Eastman, S.J., Siegel, C., Tousignant, J., Smith, A.E., Cheng, S.H., and Scheule, R.K., *Biophysical characterization of cationic lipid:DNA complexes.* Biochimica et Biophysica Acta (BBA) - Biomembranes, 1997. **1325**(1): p. 41-62.
107. Stalder, L., Heusermann, W., Sokol, L., Trojer, D., Wirz, J., Hean, J., Fritzsche, A., Aeschimann, F., Pfanzagl, V., Basselet, P., Weiler, J., Hintersteiner, M., Morrissey, D.V., and Meisner-Kober, N.C., *The rough endoplasmatic reticulum is a central nucleation site of siRNA-mediated RNA silencing.* EMBO J, 2013. **32**(8): p. 1115-1127.
108. Hacein-Bey-Abina, S., von Kalle, C., Schmidt, M., Le Deist, F.o., Wulffraat, N., McIntyre, E., Radford, I., Villeval, J.-L., Fraser, C.C., Cavazzana-Calvo, M., and Fischer, A., *A Serious Adverse Event after Successful Gene Therapy for X-Linked Severe Combined Immunodeficiency.* New England Journal of Medicine, 2003. **348**(3): p. 255-256.
109. Hama, S., Akita, H., Iida, S., Mizuguchi, H., and Harashima, H., *Quantitative and mechanism-based investigation of post-nuclear delivery events between adenovirus and lipoplex.* Nucleic Acids Research, 2007. **35**(5): p. 1533-1543.
110. Koltover, I., Salditt, T., Rädler, J.O., and Safinya, C.R., *An Inverted Hexagonal Phase of Cationic Liposome-DNA Complexes Related to DNA Release and Delivery.* Science, 1998. **281**(5373): p. 78-81.
111. Stegmann, T. and Legendre, J.-Y., *Gene transfer mediated by cationic lipids: lack of a correlation between lipid mixing and transfection.* Biochimica et Biophysica Acta (BBA) - Biomembranes, 1997. **1325**(1): p. 71-79.
112. Pires, P., Simões, S., Nir, S., Gaspar, R., Düzgünes, N., and Pedroso de Lima, M.C., *Interaction of cationic liposomes and their DNA complexes with monocytic leukemia cells.* Biochimica et Biophysica Acta (BBA) - Biomembranes, 1999. **1418**(1): p. 71-84.
113. Smisterova, J., Wagenaar, A., Stuart, M.C.A., Polushkin, E., ten Brinke, G., Hulst, R., Engberts, J.B.F.N., and Hoekstra, D., *Molecular Shape of the Cationic Lipid Controls the Structure of Cationic Lipid/Dioleylphosphatidylethanolamine-DNA Complexes and the Efficiency of Gene Delivery.* Journal of Biological Chemistry, 2001. **276**(50): p. 47615-47622.
114. Koltover, I., Salditt, T., RÃ¤dler, J.O., and Safinya, C.R., *An Inverted Hexagonal Phase of Cationic Liposome-DNA Complexes Related to DNA Release and Delivery.* Science, 1998. **281**(5373): p. 78-81.
115. Hsu, W.-L., Chen, H.-L., Liou, W., Lin, H.-K., and Liu, W.-L., *Mesomorphic Complexes of DNA with the Mixtures of a Cationic Surfactant and a Neutral Lipid.* Langmuir, 2005. **21**(21): p. 9426-9431.

116. Hirsch-Lerner, D., Zhang, M., Eliyahu, H., Ferrari, M.E., Wheeler, C.J., and Barenholz, Y., *Effect of "helper lipid" on lipoplex electrostatics.* Biochimica et Biophysica Acta (BBA) - Biomembranes, 2005. **1714**(2): p. 71-84.
117. Scarzello, M., Wagenaar, A., Stuart, M.C.A., Hoekstra, D., Engberts, J.B.F.N., and Hulst, R., *Sunfish Cationic Amphiphiles: Toward an Adaptative Lipoplex Morphology.* Journal of the American Chemical Society, 2005. **127**(29): p. 10420-10429.
118. Zuhorn, I.S., Bakowsky, U., Polushkin, E., Visser, W.H., Stuart, M.C.A., Engberts, J.B.F.N., and Hoekstra, D., *Nonbilayer phase of lipoplex-membrane mixture determines endosomal escape of genetic cargo and transfection efficiency.* Mol Ther, 2005. **11**(5): p. 801-810.
119. Patil, S.D., Rhodes, D.G., and Burgess, D.J., *Biophysical characterization of anionic lipoplexes.* Biochimica et Biophysica Acta (BBA) - Biomembranes, 2005. **1711**(1): p. 1-11.
120. Zuidam, N.J., Barenholz, Y., and Minsky, A., *Chiral DNA packaging in DNA-cationic liposome assemblies.* FEBS Letters, 1999. **457**(3): p. 419-422.
121. Boukhnikachvili, T., Aguerre-Chariol, O., Airiau, M., Lesieur, S., Ollivon, M., and Vacus, J., *Structure of in-serum transfecting DNA-cationic lipid complexes.* FEBS Letters, 1997. **409**(2): p. 188-194.
122. Mislick, K.A. and Baldeschwieler, J.D., *Evidence for the role of proteoglycans in cation-mediated gene transfer.* Proceedings of the National Academy of Sciences, 1996. **93**(22): p. 12349-12354.
123. Ferkol, T., Perales, J.C., Eckman, E., Kaetzel, C.S., Hanson, R.W., and Davis, P.B., *Gene transfer into the airway epithelium of animals by targeting the polymeric immunoglobulin receptor.* The Journal of Clinical Investigation, 1995. **95**(2): p. 493-502.
124. Schwarzenberger, P., Spence, S.E., Gooya, J.M., Michiel, D., Curiel, D.T., Ruscetti, F.W., and Keller, J.R., *Targeted gene transfer to human hematopoietic progenitor cell lines through the c-kit receptor.* Blood, 1996. **87**(2): p. 472-478.
125. Wu, G.Y. and Wu, C.H., *Receptor-mediated in vitro gene transformation by a soluble DNA carrier system.* Journal of Biological Chemistry, 1987. **262**(10): p. 4429-4432.
126. Diebold, S.S., Lehrmann, H., Kursa, M., Wagner, E., Cotten, M., and Zenke, M., *Efficient Gene Delivery into Human Dendritic Cells by Adenovirus Polyethylenimine and Mannose Polyethylenimine Transfection* Human gene therapy, 1999. **10**(5): p. 775-786.
127. Choi, Y.H., Liu, F., Park, J.S., and Kim, S.W., *Lactose-Poly(ethylene Glycol)-Grafted Poly-l-Lysine as Hepatoma Cell-Targeted Gene Carrier.* Bioconjugate Chemistry, 1998. **9**(6): p. 708-718.
128. Wang, S., Lee, R.J., Cauchon, G., Gorenstein, D.G., and Low, P.S., *Delivery of antisense oligodeoxyribonucleotides against the human epidermal growth factor receptor into cultured KB cells with liposomes conjugated to folate via polyethylene glycol.* Proceedings of the National Academy of Sciences, 1995. **92**(8): p. 3318-3322.
129. Erbacher, P., Remy, J.-S., and Behr, J.-P., *Gene transfer with synthetic virus-like particles via the integrin-mediated endocytosis pathway.* Gene Therapy, 1999. **6**(138-145).
130. Cotten, M., Längle-Rouault, F., Kirlappos, H., Wagner, E., Mechtler, K., Zenke, M., Beug, H., and Birnstiel, M.L., *Transferrin-polycation-mediated introduction of DNA into human leukemic cells: stimulation by agents that affect the survival of transfected DNA or modulate transferrin receptor levels.* Proceedings of the National Academy of Sciences, 1990. **87**(11): p. 4033-4037.
131. Schaffer, D.V. and Lauffenburger, D.A., *Optimization of Cell Surface Binding Enhances Efficiency and Specificity of Molecular Conjugate Gene Delivery.* Journal of Biological Chemistry, 1998. **273**(43): p. 28004-28009.
132. Ashwell, G. and Harford, J., *Carbohydrate-Specific Receptors of the Liver.* Annual Review of Biochemistry, 1982. **51**: p. 531-554.
133. Spiess, M., *The asialoglycoprotein receptor: a model for endocytic transport receptors.* Biochemistry, 1990. **29**(43): p. 10009-10018.

134. Kolb-Bachofen, V., Schlepper-Schäfer, J., Vogell, W., and Kolb, H., *Electron microscopic evidence for an asialoglycoprotein receptor on kupffer cells: Localization of lectin-mediated endocytosis.* Cell, 1982. **29**(3): p. 859-866.
135. Morell, A.G., Irvine, R.A., Sternlieb, I., Scheinberg, I.H., and Ashwell, G., *Physical and Chemical Studies on Ceruloplasmin: V. Metabolic studies on sialic acid-free ceruloplasmin in vivo.* Journal of Biological Chemistry, 1968. **243**(1): p. 155-159.
136. Elouahabi, A., Thiry, M., Pector, V.r., Ruysschaert, J.-M., Vandenbranden, M., and Nejat, D., *Calorimetry of Cationic Liposome-DNA Complex and Intracellular Visualization of the Complexes*, in *Methods in Enzymology*. 2003, Academic Press. p. 312-332.
137. Nabi, I.R. and Le, P.U., *Caveolae/raft-dependent endocytosis.* The Journal of Cell Biology, 2003. **161**(4): p. 673-677.
138. Swanson, J.A. and Watts, C., *Macropinocytosis.* Trends in Cell Biology, 1995. **5**(11): p. 424-428.
139. Conner, S.D. and Schmid, S.L., *Regulated portals of entry into the cell.* Nature, 2003. **422**(6927): p. 37-44.
140. Damm, E.-M., Pelkmans, L., Kartenbeck, J., Mezzacasa, A., Kurzchalia, T., and Helenius, A., *Clathrin- and caveolin-1-independent endocytosis: entry of simian virus 40 into cells devoid of caveolae.* The Journal of Cell Biology, 2005. **168**(3): p. 477-488.
141. Takei, K. and Haucke, V., *Clathrin-mediated endocytosis: membrane factors pull the trigger.* Trends in Cell Biology, 2001. **11**(9): p. 385-391.
142. Anderson, R.G.W., *The Caveolae Membrane System.* Annual Reviews, 1998. **67**: p. 199-225.
143. Xu, Y. and Szoka, F.C., *Mechanism of DNA Release from Cationic Liposome/DNA Complexes Used in Cell Transfection.* Biochemistry, 1996. **35**(18): p. 5616-5623.
144. Hafez, I.M., Maurer, N., and Cullis, P.R., *On the mechanism whereby cationic lipids promote intracellular delivery of polynucleic acids.* Gene Therapy, 2001. **8**: p. 1188-1196.
145. Pires, P., SimÃµes, S.r., Nir, S., Gaspar, R.r., DÃ¼zgÃ¼nes, N., and Pedroso de Lima, M.C., *Interaction of cationic liposomes and their DNA complexes with monocytic leukemia cells.* Biochimica et Biophysica Acta (BBA) - Biomembranes, 1999. **1418**(1): p. 71-84.
146. Fasbender, A., Marshall, J., Moninger, T.O., Grunst, T., Cheng, S., and M.J., W., *Effect of co-lipids in enhancing cationic lipid-mediated gene transfer in vitro and in vivo.* Gene Therapy, 1997. **4**: p. 716-725.
147. Rejman, J., Wagenaar, A., Engberts, J.B.F.N., and Hoekstra, D., *Characterization and transfection properties of lipoplexes stabilized with novel exchangeable polyethylene glycol-lipid conjugates.* Biochimica et Biophysica Acta (BBA) - Biomembranes, 2004. **1660**(1): p. 41-52.
148. Shi, F., Wasungu, L., Nomden, A., Stuart, M.C.A., Polushkin, E., Engberts, J.B.F.N., and Hoekstra, D., *Interference of poly(ethylene glycol)-lipid analogues with cationic-lipid-mediated delivery of oligonucleotides; role of lipid exchangeability and non-lamellar transitions.* Biochemical Journal, 2002. **366**: p. 333-341.
149. Guo, X. and Szoka, F.C., *Steric Stabilization of Fusogenic Liposomes by a Low-pH Sensitive PEG--Diortho Ester--Lipid Conjugate.* Bioconjugate Chemistry, 2001. **12**(2): p. 291-300.
150. Melchior, F. and Gerace, L., *Mechanisms of nuclear protein import.* Current Opinion in Cell Biology, 1995. **7**(3): p. 310-318.
151. Lechardeur, D., Sohn, K.-J., Haardt, M., Joshi, P.B., Monck, M., Graham, R.W., Beatty, B., Squire, J., O'Brodovich, H., and Lukacs, G.L., *Metabolic instability of plasmid DNA in the cytosol: a potential barrier to gene transfer.* Gene Therapy, 1999. **6**(4): p. 482-497.
152. Pollard, H., Toumaniantz, G., Amos, J.L., Avet-Loiseau, H., Guihard, G., Behr, J.-P., and Escande, D., *Ca2+-sensitive cytosolic nucleases prevent efficient delivery to the nucleus of injected plasmids.* Journal of Gene Medicine, 2001. **3**(2): p. 153-164.

153. Pollard, H.l.n., Remy, J.-S., Loussouarn, G., Demolombe, S., Behr, J.-P., and Escande, D., *Polyethylenimine but Not Cationic Lipids Promotes Transgene Delivery to the Nucleus in Mammalian Cells.* Journal of Biological Chemistry, 1998. **273**(13): p. 7507-7511.
154. Neves, C., Escriou, V., Byk, G., Scherman, D., and Wils, P., *Intracellular fate and nuclear targeting of plasmid DNA.* Cell Biology and Toxicology, 1999. **15**(3): p. 193-202.
155. Hean, J., Crowther, C., Ely, A., ul Islam, R., Barichievy, S., Bloom, K., Weinberg, M.S., van Otterlo, W.A.L., de Koning, C.B., Salazar, F., Marion, P., Roesch, E.B., LeMaitre, M., Herdewijn, P., and Arbuthnot, P., *Inhibition of hepatitis B virus replication in vivo using lipoplexes containing altritol-modified antiviral siRNAs.* Artificial DNA: PNA & XNA, 2010. **1**(1): p. 17-26.
156. Bramsen, J.B., Laursen, M.B., Nielsen, A.F., Hansen, T.B., Bus, C., Langkjær, N., Babu, B.R., Højland, T., Abramov, M., Van Aerschot, A., Odadzic, D., Smicius, R., Haas, J., Andree, C., Barman, J., Wenska, M., Srivastava, P., Zhou, C., Honcharenko, D., Hess, S., Müller, E., Bobkov, G.V., Mikhailov, S.N., Fava, E., Meyer, T.F., Chattopadhyaya, J., Zerial, M., Engels, J.W., Herdewijn, P., Wengel, J., and Kjems, J., *A large-scale chemical modification screen identifies design rules to generate siRNAs with high activity, high stability and low toxicity.* Nucleic Acids Research, 2009. **37**(9): p. 2867-2881.
157. Fisher, M., Abramov, M., Van Aerschot, A., Xu, D., Juliano, R.L., and Herdewijn, P., *Inhibition of MDR1 expression with altritol-modified siRNAs.* Nucleic Acids Research, 2007. **35**(4): p. 1064-1074.
158. Gao, X. and Huang, L., *A novel cationic liposome reagent for efficient transfection of mammalian cells.* Biochemical and Biophysical Research Communications, 1991. **179**(1): p. 280-285.
159. Treichel, U., Meyer zum Büschenfelde, K.-H., Stockert, R.J., Poralla, T., and Gerken, G., *The Asialoglycoprotein Receptor Mediates Hepatic Binding and Uptake of Natural Hepatitis B Virus Particles Derived From Viraemic Carriers.* Journal of General Virology, 1994. **75**(11): p. 3021-3029.
160. Singh, M., Hawtrey, A., and Ariatti, M., *Lipoplexes with biotinylated transferrin accessories: Novel, targeted, serum-tolerant gene carriers.* International Journal of Pharmaceutics, 2006. **321**(1): p. 124-137.
161. Mishra, S., Webster, P., and Davis, M.E., *PEGylation significantly affects cellular uptake and intracellular trafficking of non-viral gene delivery particles.* European Journal of Cell Biology, 2004. **83**(3): p. 97-111.
162. Marion, P.L., Salazar, F.H., Liittschwager, K., Bordier, B.B., Seeger, C., Winters, M.A., Cooper, A.D., and Cullen, J.M., *Chapter 18 - A transgenic mouse lineage useful for testing antivirals targeting hepatitis B virus*, in *Frontiers in Viral Hepatitis*, F.S. Raymond, et al., Editors. 2003, Elsevier: Amsterdam. p. 197-210.
163. Vigneron, J.P., Oudrhiri, N., Fauquet, M., Vergely, L., Bradley, J.C., Basseville, M., Lehn, P., and Lehn, J.M., *Guanidinium-cholesterol cationic lipids: efficient vectors for the transfection of eukaryotic cells.* Proceedings of the National Academy of Sciences, 1996. **93**(18): p. 9682-9686.
164. Needham, D., Stoicheva, N., and Zhelev, D.V., *Exchange of monooleoylphosphatidylcholine as monomer and micelle with membranes containing poly(ethylene glycol)-lipid.* Biophysical Journal, 1997. **73**(5): p. 2615-2629.
165. de Gennes, P.G., *Conformations of Polymers Attached to an Interface.* Macromolecules, 1980. **13**(5): p. 1069-1075.
166. Wooddell, C.I., Rozema, D.B., Hossbach, M., John, M., Hamilton, H.L., Chu, Q., Hegge, J.O., Klein, J.J., Wakefield, D.H., Oropeza, C.E., Deckert, J., Roehl, I., Jahn-Hofmann, K., Hadwiger, P., Vornlocher, H.-P., McLachlan, A., and Lewis, D.L., *Hepatocyte-targeted RNAi Therapeutics for the Treatment of Chronic Hepatitis B Virus Infection.* Mol Ther, 2013. **21**(5): p. 973-985.

167. Semple, S.C., Akinc, A., Chen, J., Sandhu, A.P., Mui, B.L., Cho, C.K., Sah, D.W.Y., Stebbing, D., Crosley, E.J., Yaworski, E., Hafez, I.M., Dorkin, J.R., Qin, J., Lam, K., Rajeev, K.G., Wong, K.F., Jeffs, L.B., Nechev, L., Eisenhardt, M.L., Jayaraman, M., Kazem, M., Maier, M.A., Srinivasulu, M., Weinstein, M.J., Chen, Q., Alvarez, R., Barros, S.A., De, S., Klimuk, S.K., Borland, T., Kosovrasti, V., Cantley, W.L., Tam, Y.K., Manoharan, M., Ciufolini, M.A., Tracy, M.A., de Fougerolles, A., MacLachlan, I., Cullis, P.R., Madden, T.D., and Hope, M.J., *Rational design of cationic lipids for siRNA delivery.* Nat Biotech, 2010. **28**(2): p. 172-176.
168. Passman, M., Weinberg, M., Kew, M., and Arbuthnot, P., *In Situ Demonstration of Inhibitory Effects of Hammerhead Ribozymes That Are Targeted to the Hepatitis Bx Sequence in Cultured Cells.* Biochemical and Biophysical Research Communications, 2000. **268**(3): p. 728-733.
169. Carmona, S., Ely, A., Crowther, C., Moolla, N., Salazar, F.H., Marion, P.L., Ferry, N., Weinberg, M.S., and Arbuthnot, P., *Effective Inhibition of HBV Replication in Vivo by Anti-HBx Short Hairpin RNAs.* Mol Ther, 2006. **13**(2): p. 411-421.
170. Rachel, R., Bettstetter, M., Hedlund, B.P., Häring, M., Kessler, A., Stetter, K.O., and Prangishvili, D., *Remarkable morphological diversity of viruses and virus-like particles in hot terrestrial environments.* Archives of Virology, 2002. **147**(12): p. 2419-2429.
171. Rice, G., Tang, L., Stedman, K., Roberto, F., Spuhler, J., Gillitzer, E., Johnson, J.E., Douglas, T., and Young, M., *The structure of a thermophilic archaeal virus shows a double-stranded DNA viral capsid type that spans all domains of life.* Proceedings of the National Academy of Sciences of the United States of America, 2004. **101**(20): p. 7716-7720.
172. Harrison, P.M. and Arosio, P., *The ferritins: molecular properties, iron storage function and cellular regulation.* Biochimica et Biophysica Acta (BBA) - Bioenergetics, 1996. **1275**(3): p. 161-203.
173. Haslbeck, M., Kastenmüller, A., Buchner, J., Weinkauf, S., and Braun, N., *Structural Dynamics of Archaeal Small Heat Shock Proteins.* Journal of Molecular Biology, 2008. **378**(2): p. 362-374.
174. White, H.E., Orlova, E.V., Chen, S., Wang, L., Ignatiou, A., Gowen, B., Stromer, T., Franzmann, T.M., Haslbeck, M., Buchner, J., and Saibil, H.R., *Multiple Distinct Assemblies Reveal Conformational Flexibility in the Small Heat Shock Protein Hsp26.* Structure, 2006. **14**(7): p. 1197-1204.
175. Yan, X., Olson, N.H., Van Etten, J.L., Bergoin, M., Rossmann, M.G., and Baker, T.S., *Structure and assembly of large lipid-containing dsDNA viruses.* Nat Struct Mol Biol, 2000. **7**(2): p. 101-103.
176. Knez, M., Kadri, A., Wege, C., Gösele, U., Jeske, H., and Nielsch, K., *Atomic Layer Deposition on Biological Macromolecules: Metal Oxide Coating of Tobacco Mosaic Virus and Ferritin.* Nano Letters, 2006. **6**(6): p. 1172-1177.
177. Newman, J., Swinney, H.L., and Day, L.A., *Hydrodynamic properties and structure of fd virus.* Journal of Molecular Biology, 1977. **116**(3): p. 593-603.
178. Flenniken, M.L., Liepold, L.O., Crowley, B.E., Willits, D.A., Young, M.J., and Douglas, T., *Selective attachment and release of a chemotherapeutic agent from the interior of a protein cage architecture.* Chemical Communications, 2005. **0**(4): p. 447-449.
179. Kratz, P., Böttcher, B., and Nassal, M., *Native display of complete foreign protein domains on the surface of hepatitis B virus capsids.* Proceedings of the National Academy of Sciences, 1999. **96**(5): p. 1915.
180. Wang, Q., Lin, T., Tang, L., Johnson, J.E., and Finn, M.G., *Icosahedral Virus Particles as Addressable Nanoscale Building Blocks.* Angewandte Chemie International Edition, 2002. **41**(3): p. 459-462.
181. Lewis, J.D., Destito, G., Zijlstra, A., Gonzalez, M.J., Quigley, J.P., Manchester, M., and Stuhlmann, H., *Viral nanoparticles as tools for intravital vascular imaging.* Nat Med, 2006. **12**(3): p. 354-360.

182. Flenniken, M.L., Willits, D.A., Harmsen, A.L., Liepold, L.O., Harmsen, A.G., Young, M.J., and Douglas, T., *Melanoma and Lymphocyte Cell-Specific Targeting Incorporated into a Heat Shock Protein Cage Architecture.* Chemistry & Biology, 2006. **13**(2): p. 161-170.
183. Speir, J.A., Munshi, S., Wang, G., Baker, T.S., and Johnson, J.E., *Structures of the native and swollen forms of cowpea chlorotic mottle virus determined by X-ray crystallography and cryo-electron microscopy.* Structure (London, England : 1993), 1995. **3**(1): p. 63-78.
184. Tama, F. and Brooks Iii, C.L., *The Mechanism and Pathway of pH Induced Swelling in Cowpea Chlorotic Mottle Virus.* Journal of Molecular Biology, 2002. **318**(3): p. 733-747.
185. Nandhagopal, N., Simpson, A.A., Gurnon, J.R., Yan, X., Baker, T.S., Graves, M.V., Van Etten, J.L., and Rossmann, M.G., *The structure and evolution of the major capsid protein of a large, lipid-containing DNA virus.* Proceedings of the National Academy of Sciences, 2002. **99**(23): p. 14758-14763.
186. Liu, H., Jin, L., Koh, S.B.S., Atanasov, I., Schein, S., Wu, L., and Zhou, Z.H., *Atomic Structure of Human Adenovirus by Cryo-EM Reveals Interactions Among Protein Networks.* Science, 2010. **329**(5995): p. 1038-1043.
187. Stehle, T. and Harrison, S.C., *Crystal structures of murine polyomavirus in complex with straight-chain and branched-chain sialyloligosaccharide receptor fragments.* Structure, 1996. **4**(2): p. 183-194.
188. Bourne, C.R., Finn, M.G., and Zlotnick, A., *Global Structural Changes in Hepatitis B Virus Capsids Induced by the Assembly Effector HAP1.* J. Virol., 2006. **80**(22): p. 11055-11061.
189. Ochoa, W.F., Chatterji, A., Lin, T., and Johnson, J.E., *Generation and Structural Analysis of Reactive Empty Particles Derived from an Icosahedral Virus.* Chemistry & Biology, 2006. **13**(7): p. 771-778.
190. Xie, Q., Lerch, T.F., Meyer, N.L., and Chapman, M.S., *Structure–function analysis of receptor-binding in adeno-associated virus serotype 6 (AAV-6).* Virology, 2011. **420**(1): p. 10-19.
191. Baraibar, M.A., Muhoberac, B.B., Garringer, H.J., Hurley, T.D., and Vidal, R., *Unraveling of the E-helices and Disruption of 4-Fold Pores Are Associated with Iron Mishandling in a Mutant Ferritin Causing Neurodegeneration.* Journal of Biological Chemistry, 2010. **285**(3): p. 1950-1956.
192. Sachse, C., Chen, J.Z., Coureux, P.-D., Stroupe, M.E., Fändrich, M., and Grigorieff, N., *High-resolution Electron Microscopy of Helical Specimens: A Fresh Look at Tobacco Mosaic Virus.* Journal of Molecular Biology, 2007. **371**(3): p. 812-835.
193. Douglas, T. and Young, M., *Viruses: Making Friends with Old Foes.* Science, 2006. **312**(5775): p. 873-875.
194. Nassal, M., Skamel, C., Vogel, M., Kratz, P.A., Stehle, T., Wallich, R., and Simon, M.M., *Development of hepatitis B virus capsids into a whole-chain protein antigen display platform: New particulate Lyme disease vaccines.* International Journal of Medical Microbiology, 2008. **298**(1-2): p. 135-142.
195. Zlotnick, A., *To Build a Virus Capsid : An Equilibrium Model of the Self Assembly of Polyhedral Protein Complexes.* Journal of Molecular Biology, 1994. **241**(1): p. 59-67.
196. Zlotnick, A., Johnson, J.M., Wingfield, P.W., Stahl, S.J., and Endres, D., *A Theoretical Model Successfully Identifies Features of Hepatitis B Virus Capsid Assembly* Biochemistry, 1999. **38**(44): p. 14644-14652.
197. Ceres, P. and Zlotnick, A., *Weak Protein-Protein Interactions Are Sufficient To Drive Assembly of Hepatitis B Virus Capsids.* Biochemistry, 2002. **41**(39): p. 11525-11531.
198. Wingfield, P.T., Stahl, S.J., Williams, R.W., and Steven, A.C., *Hepatitis Core Antigen Produced in Escherichia coli: Subunit Composition, Conformation Analysis, and in Vitro Capsid Assembly.* Biochemistry, 1995. **34**(15): p. 4919-4932.
199. Chapman, M.S., Liljas, L., and Wah Chiu and John, E.J., *Structural Folds of Viral Proteins*, in *Advances in Protein Chemistry*. 2003, Academic Press. p. 125-196.

200. Bringas, R., *Folding and Assembly of Hepatitis B Virus Core Protein: A New Model Proposal.* Journal of Structural Biology, 1997. **118**(3): p. 189-196.
201. Wynne, S.A., Crowther, R.A., and Leslie, A.G.W., *The Crystal Structure of the Human Hepatitis B Virus Capsid.* Molecular Cell, 1999. **3**(6): p. 771-780.
202. Salfeld, J., Pfaff, E., Noah, M., and Schaller, H., *Antigenic determinants and functional domains in core antigen and e antigen from hepatitis B virus.* Journal of virology, 1989. **63**(2): p. 798.
203. Sällberg, M., Rudén, U., Magnius, L., Harthus, H., Noah, M., and Wahren, B., *Characterisation of a linear binding site for a monoclonal antibody to hepatitis B core antigen.* J Med Virol, 1991. **33**(4): p. 248-252.
204. Kelley, L.A. and Sternberg, M.J.E., *Protein structure prediction on the Web: a case study using the Phyre server.* Nat. Protocols, 2009. **4**(3): p. 363-371.
205. Singh, S. and Zlotnick, A., *Observed Hysteresis of Virus Capsid Disassembly Is Implicit in Kinetic Models of Assembly.* Journal of Biological Chemistry, 2003. **278**(20): p. 18249-18255.
206. Endres, D. and Zlotnick, A., *Model-Based Analysis of Assembly Kinetics for Virus Capsids or Other Spherical Polymers.* Biophysical Journal, 2002. **83**(2): p. 1217-1230.
207. Steven, A.C., Conway, J.F., Cheng, N., Watts, N.R., Belnap, D.M., Harris, A., Stahl, S.J., Wingfield, P.T., and Polly, R., *Structure, Assembly, and Antigenicity of Hepatitis B Virus Capsid Proteins*, in *Advances in Virus Research*. 2005, Academic Press. p. 125-164.
208. Nassal, M., Rieger, A., and Steinau, O., *Topological analysis of the hepatitis B virus core particle by cysteine-cysteine cross-linking.* Journal of Molecular Biology, 1992. **225**(4): p. 1013-1025.
209. Crowther, R., Kiselev, N., Bottcher, B., Berriman, J., Borisova, G., Ose, V., and Pumpens, P., *Three-dimensional structure of hepatitis B virus core particles determined by electron cryomicroscopy.* Cell, 1994. **77**(6): p. 943.
210. Booy, F.P., Trus, B.L., Davison, A.J., and Steven, A.C., *The Capsid Architecture of Channel Catfish Virus, an Evolutionarily Distant Herpesvirus, Is Largely Conserved in the Absence of Discernible Sequence Homology with Herpes Simplex Virus.* Virology, 1996. **215**(2): p. 134-141.
211. Kenney, J., Bonsdorff, C., Nassal, M., and Fuller, S., *Evolutionary conservation in the hepatitis B virus core structure: comparison of human and duck cores.* Structure, 1995. **3**(10): p. 1009-1019.
212. Caspar, D.L.D. and Klug, A., *Physical principles in the construction of regular viruses.* Cold Spring Harb. Symp. Quant. Biol., 1962. **XXVII**: p. 1-24.
213. Zlotnick, A., Cheng, N., Conway, J.F., Booy, F.P., Steven, A.C., Stahl, S.J., and Wingfield, P.T., *Dimorphism of Hepatitis B Virus Capsids Is Strongly Influenced by the C-Terminus of the Capsid Protein.* Biochemistry, 1996. **35**(23): p. 7412-7421.
214. Guex, N. and Peitsch, M.C., *SWISS-MODEL and the Swiss-PdbViewer: An environment for comparative protein modeling.* Electrophoresis, 1997. **18**: p. 2714-2723.
215. Böttcher, B., Vogel, M., Ploss, M., and Nassal, M., *High Plasticity of the Hepatitis B Virus Capsid Revealed by Conformational Stress.* Journal of Molecular Biology, 2006. **356**(3): p. 812-822.
216. Bourne, C.R., Katen, S.P., Fulz, M.R., Packianathan, C., and Zlotnick, A., *A Mutant Hepatitis B Virus Core Protein Mimics Inhibitors of Icosahedral Capsid Self-Assembly* Biochemistry, 2009. **48**(8): p. 1736-1742.
217. Seifer, M. and Standring, D.N., *A protease-sensitive hinge linking the two domains of the hepatitis B virus core protein is exposed on the viral capsid surface.* Journal of Virology, 1994. **68**(9): p. 5548-5555.
218. Wang, J.-Y., Dhason, M.S., and Zlotnick, A., *Structural Organization of Pregenomic RNA and the Carboxy-Terminal Domain of the Capsid Protein of Hepatitis B Virus.* PLoS Pathog, 2012. **8**(9): p. e1002919.

219. Dyson, M.R. and Murray, K., *Selection of peptide inhibitors of interactions involved in complex protein assemblies: association of the core and surface antigens of hepatitis B virus.* Proceedings of the National Academy of Sciences, 1995. **92**(6): p. 2194-2198.
220. Koschel, M., Oed, D., Gerelsaikhan, T., Thomssen, R., and Bruss, V., *Hepatitis B Virus Core Gene Mutations Which Block Nucleocapsid Envelopment.* Journal of virology, 2000. **74**(1): p. 1-7.
221. Seifer, M. and Standring, D., *Assembly and antigenicity of hepatitis B virus core particles.* Intervirology, 1995. **38**(1-2): p. 47-62.
222. Takahashi, K., Machida, A., Funatsu, G., Nomura, M., Usuda, S., Aoyagi, S., Tachibana, K., Miyamoto, H., Imai, M., and Nakamura, T., *Immunochemical structure of hepatitis B e antigen in the serum.* The Journal of Immunology, 1983. **130**(6): p. 2903.
223. Belnap, D.M., Watts, N.R., Conway, J.F., Cheng, N., Stahl, S.J., Wingfield, P.T., and Steven, A.C., *Diversity of core antigen epitopes of hepatitis B virus.* Proceedings of the National Academy of Sciences of the United States of America, 2003. **100**(19): p. 10884-10889.
224. Conway, J., Watts, N., Belnap, D., Cheng, N., Stahl, S., Wingfield, P., and Steven, A., *Characterization of a conformational epitope on hepatitis B virus core antigen and quasiequivalent variations in antibody binding.* Journal of virology, 2003. **77**(11): p. 6466.
225. Brown, A.L., Francis, M.J., Hastings, G.Z., Parry, N.R., Barnett, P.V., Rowlands, D.J., and Clarke, B.E., *Foreign epitopes in immunodominant regions of hepatitis B core particles are highly immunogenic and conformationally restricted.* Vaccine, 1991. **9**(8): p. 595-601.
226. Clarke, B.E., Newton, S.E., Carroll, A.R., Francis, M.J., Appleyard, G., Syred, A.D., Highfield, P.E., Rowlands, D.J., and Brown, F., *Improved immunogenicity of a peptide epitope after fusion to hepatitis B core protein.* Nature, 1987. **330**(6146): p. 381-384.
227. Milich, D.R., Chen, M., Schödel, F., Peterson, D.L., Jones, J.E., and Hughes, J.L., *Role of B cells in antigen presentation of the hepatitis B core.* Proceedings of the National Academy of Sciences, 1997. **94**(26): p. 14648-14653.
228. Francis, M.J., Hastings, G.Z., Brown, A.L., Grace, K.G., Rowlands, D.J., Brown, F., and Clarke, B.E., *Immunological properties of hepatitis B core antigen fusion proteins.* Proceedings of the National Academy of Sciences, 1990. **87**(7): p. 2545-2549.
229. Stahl, S.J. and Murray, K., *Immunogenicity of peptide fusions to hepatitis B virus core antigen.* Proceedings of the National Academy of Sciences, 1989. **86**(16): p. 6283-6287.
230. Pumpens, P. and Grens, E., *HBV Core Particles as a Carrier for B Cell/T Cell Epitopes.* Intervirology, 2001. **44**(2-3): p. 98-114.
231. Nassal, M., Skamel, C., Kratz, P.A., Wallich, R., Stehle, T., and Simon, M.M., *A fusion product of the complete Borrelia burgdorferi outer surface protein A (OspA) and the hepatitis B virus capsid protein is highly immunogenic and induces protective immunity similar to that seen with an effective lipidated OspA vaccine formula.* European Journal of Immunology, 2005. **35**(2): p. 655-665.
232. Walker, A., Skamel, C., Vorreiter, J., and Nassal, M., *Internal Core Protein Cleavage Leaves the Hepatitis B Virus Capsid Intact and Enhances Its Capacity for Surface Display of Heterologous Whole Chain Proteins.* Journal of Biological Chemistry, 2008. **283**(48): p. 33508-33515.
233. Walker, A., Skamel, C., and Nassal, M., *SplitCore: An exceptionally versatile viral nanoparticle for native whole protein display regardless of 3D structure.* Sci. Rep., 2011. **1**.
234. Liao, W. and Ou, J.H., *Phosphorylation and nuclear localization of the hepatitis B virus core protein: significance of serine in the three repeated SPRRR motifs.* Journal of virology, 1995. **69**(2): p. 1025-9.
235. Eckhardt, S.G., Milich, D.R., and McLachlan, A., *Hepatitis B virus core antigen has two nuclear localization sequences in the arginine-rich carboxyl terminus.* Journal of virology, 1991. **65**(2): p. 575-582.

236. Choi, K.-m., Kim, K., Kwon, I.C., Kim, I.-S., and Ahn, H.J., *Systemic Delivery of siRNA by Chimeric Capsid Protein: Tumor Targeting and RNAi Activity in Vivo.* Molecular Pharmaceutics, 2012. **10**(1): p. 18-25.
237. Cooper, A. and Shaul, Y., *Clathrin-mediated Endocytosis and Lysosomal Cleavage of Hepatitis B Virus Capsid-like Core Particles.* Journal of Biological Chemistry, 2006. **281**(24): p. 16563-16569.
238. Klem, M.T., Willits, D., Young, M., and Douglas, T., *2-D Array Formation of Genetically Engineered Viral Cages on Au Surfaces and Imaging by Atomic Force Microscopy.* Journal of the American Chemical Society, 2003. **125**(36): p. 10806-10807.
239. Prill, J.-M., Espenlaub, S., Samen, U., Engler, T., Schmidt, E., Vetrini, F., Rosewell, A., Grove, N., Palmer, D., Ng, P., Kochanek, S., and Kreppel, F., *Modifications of Adenovirus Hexon Allow for Either Hepatocyte Detargeting or Targeting With Potential Evasion From Kupffer Cells.* Mol Ther, 2011. **19**(1): p. 83-92.
240. Pingoud, A. and Jeltsch, A., *Structure and function of type II restriction endonucleases.* Nucleic Acids Research, 2001. **29**(18): p. 3705-3727.
241. Sibley, C.R., Seow, Y., Saayman, S., Dijkstra, K.K., El Andaloussi, S., Weinberg, M.S., and Wood, M.J.A., *The biogenesis and characterization of mammalian microRNAs of mirtron origin.* Nucleic Acids Research, 2012. **40**(1): p. 438-448.
242. Cermak, T., Doyle, E.L., Christian, M., Wang, L., Zhang, Y., Schmidt, C., Baller, J.A., Somia, N.V., Bogdanove, A.J., and Voytas, D.F., *Efficient design and assembly of custom TALEN and other TAL effector-based constructs for DNA targeting.* Nucleic Acids Research, 2011. **39**(12): p. e82.
243. Viguera, E., Canceill, D., and Ehrlich, S.D., *Replication slippage involves DNA polymerase pausing and dissociation.* EMBO J, 2001. **20**(10): p. 2587-2595.
244. Nassal, M., *The arginine-rich domain of the hepatitis B virus core protein is required for pregenome encapsidation and productive viral positive-strand DNA synthesis but not for virus assembly.* Journal of virology, 1992. **66**(7): p. 4107-4116.
245. Porterfield, J.Z., Dhason, M.S., Loeb, D.D., Nassal, M., Stray, S.J., and Zlotnick, A., *Full-Length Hepatitis B Virus Core Protein Packages Viral and Heterologous RNA with Similarly High Levels of Cooperativity.* Journal of virology, 2010. **84**(14): p. 7174-7184.
246. Li, L., Li, C., Zhang, Z., and Alexov, E., *On the Dielectric "Constant" of Proteins: Smooth Dielectric Function for Macromolecular Modeling and Its Implementation in DelPhi.* Journal of Chemical Theory and Computation, 2013. **9**(4): p. 2126-2136.
247. Noémie, L., Rune, S.F., Thor, C.M., Nathalie, I.R., Shivendra, U., Luca De, V., Jan, H.J., Jesper, N., and Karen, L.M., *Effects of buffer composition and dilution on nanowire field-effect biosensors.* Nanotechnology, 2013. **24**(3): p. 035501.
248. Manzenrieder, F., Luxenhofer, R., Retslaff, M., Jordan, R., and Finn, M.G., *Stabilization of virus-like particles with poly(2-oxazoline)s.* Angewandte Chemie International Edition, 2001. **50**(11): p. 2601-2605.
249. Pokorski, J.K., Hovlid, M.L., and Finn, M.G., *Cell Targeting with Hybrid Qβ Virus-Like Particles Displaying Epidermal Growth Factor.* ChemBioChem, 2011. **12**(16): p. 2441-2447.
250. Galaway, F.A. and Stockley, P.G., *MS2 Viruslike Particles: A Robust, Semisynthetic Targeted Drug Delivery Platform.* Molecular Pharmaceutics, 2012. **10**(1): p. 59-68.
251. Running, W.E., Ni, P., Kao, C.C., and Reilly, J.P., *Chemical Reactivity of Brome Mosaic Virus Capsid Protein.* Journal of Molecular Biology, 2012. **423**(1): p. 79-95.
252. Carrico, Z.M., Farkas, M.E., Zhou, Y., Hsiao, S.C., Marks, J.D., Chokhawala, H., Clark, D.S., and Francis, M.B., *N-Terminal Labeling of Filamentous Phage To Create Cancer Marker Imaging Agents.* ACS Nano, 2012. **6**(8): p. 6675-6680.
253. Cantin, G., Resnick, S., Jin, H., O'Hanlon, R., Espinosa, O., Stevens, A., Payne, J., Glenn, N., Rasochova, L., and Allen, J., *Comparison of Methods for Chemical Conjugation of an Influenza Peptide to Wild-Type and Cysteine-Mutant Virus-Like Particles Expressed in Pseudomonas*

fluorescens. International Journal of Peptide Research and Therapeutics, 2011. **17**(3): p. 217-224.
254. Gilis, D., Massar, S., Cerf, N., and Rooman, M., *Optimality of the genetic code with respect to protein stability and amino-acid frequencies.* Genome Biology, 2001. **2**(11): p. research0049.1–0049.12.
255. Mattson, G., Conklin, E., Desai, S., Nielander, G., Savage, M.D., and Morgensen, S., *A practical approach to crosslinking.* Molecular Biology Reports, 1993. **17**(3): p. 167-183.
256. Roberts, M.J., Bentley, M.D., and Harris, J.M., *Chemistry for peptide and protein PEGylation.* Advanced Drug Delivery Reviews, 2002. **54**(4): p. 459-476.
257. Lockney, D.M., Guenther, R.N., Loo, L., Overton, W., Antonelli, R., Clark, J., Hu, M., Luft, C., Lommel, S.A., and Franzen, S., *The Red clover necrotic mosaic virus Capsid as a Multifunctional Cell Targeting Plant Viral Nanoparticle.* Bioconjugate Chemistry, 2010. **22**(1): p. 67-73.
258. Lucon, J., Qazi, S., Uchida, M., Bedwell, G.J., LaFrance, B., Prevelige, P.E., and Douglas, T., *Use of the interior cavity of the P22 capsid for site-specific initiation of atom-transfer radical polymerization with high-density cargo loading.* Nat Chem, 2012. **4**(10): p. 781-788.
259. Stephanopoulos, N., Liu, M., Tong, G.J., Li, Z., Liu, Y., Yan, H., and Francis, M.B., *Immobilization and One-Dimensional Arrangement of Virus Capsids with Nanoscale Precision Using DNA Origami.* Nano Letters, 2010. **10**(7): p. 2714-2720.
260. Natilla, A. and Hammond, R.W., *Maize rayado fino virus virus-like particles expressed in tobacco plants: A new platform for cysteine selective bioconjugation peptide display.* Journal of Virological Methods, 2011. **178**(1–2): p. 209-215.
261. Steinmetz, N.F., Lin, T., Lomonossoff, G.P., and Johnson, J.E., *Structure-Based Engineering of an Icosahedral Virus for Nanomedicine and Nanotechnology*, in *Viruses and Nanotechnology*, M. Manchester and N. Steinmetz, Editors. 2009, Springer Berlin Heidelberg. p. 23-58.
262. Stephanopoulos, N., Tong, G.J., Hsiao, S.C., and Francis, M.B., *Dual-Surface Modified Virus Capsids for Targeted Delivery of Photodynamic Agents to Cancer Cells.* ACS Nano, 2010. **4**(10): p. 6014-6020.
263. Smith, M.T., Hawes, A.K., and Bundy, B.C., *Reengineering viruses and virus-like particles through chemical functionalization strategies.* Current Opinion in Biotechnology, 2013. **24**(4): p. 620-626.
264. Horowitz, E.D., Finn, M.G., and Asokan, A., *Tyrosine Cross-Linking Reveals Interfacial Dynamics in Adeno-Associated Viral Capsids during Infection.* ACS Chemical Biology, 2012. **7**(6): p. 1059-1066.
265. Deng, H., *Nitrite anions induce nitrosative deamination of peptides and proteins.* Rapid Communications in Mass Spectrometry, 2006. **20**(24): p. 3634-3638.
266. Liu, C.C. and P.G., S., *Adding New Chemistries to the Genetic Code.* Annual Review of Biochemistry, 2010. **79**: p. 413-444.
267. Loscha, K.V., Herlt, A.J., Qi, R., Huber, T., Ozawa, K., and Otting, G., *Multiple-Site Labeling of Proteins with Unnatural Amino Acids.* Angewandte Chemie International Edition, 2012. **51**(9): p. 2243-2246.
268. Johnson, J.A., Lu, Y.Y., Van Deventer, J.A., and Tirrell, D.A., *Residue-specific incorporation of non-canonical amino acids into proteins: recent developments and applications.* Current Opinion in Chemical Biology, 2010. **14**(6): p. 774-780.
269. Ozawa, K., Loscha, K.V., Kuppan, K.V., Loh, C.T., Dixon, N.E., and Otting, G., *High-yield cell-free protein synthesis for site-specific incorporation of unnatural amino acids at two sites.* Biochemical and Biophysical Research Communications, 2012. **418**(4): p. 652-656.
270. Lallana, E., Riguera, R., and Fernandez-Megia, E., *Reliable and Efficient Procedures for the Conjugation of Biomolecules through Huisgen Azide–Alkyne Cycloadditions.* Angewandte Chemie International Edition, 2011. **50**(38): p. 8794-8804.

271. Millward, S.W., Agnew, H.D., Lai, B., Lee, S.S., Lim, J., Nag, A., Pitram, S., Rohde, R., and Heath, J.R., *In situ click chemistry: from small molecule discovery to synthetic antibodies.* Integrative Biology, 2013. **5**(1): p. 87-95.
272. Wonganan, P. and Croyle, M.A., *PEGylated Adenoviruses: From Mice to Monkeys.* Viruses, 2010. **2**(2): p. 468-502.
273. Torchilin, V.P., *Recent advances with liposomes as pharmaceutical carriers.* Nat Rev Drug Discov, 2005. **4**(2): p. 145-160.
274. Wilson, T., Papahadjopoulos, D., and Taber, R., *The introduction of poliovirus RNA into cells via lipid vesicles (liposomes).* Cell, 1979. **17**(1): p. 77-84.
275. Faller, D.V. and Baltimore, D., *Liposome encapsulation of retrovirus allows efficient superinfection of resistant cell lines.* Journal of virology, 1984. **49**(1): p. 269.
276. Toyoshima, K. and Vogt, P.K., *Enhancement and inhibition of avian sarcoma viruses by polycations and polyanions.* Virology, 1969. **38**(3): p. 414-426.
277. Davis, H.E., Rosinski, M., Morgan, J.R., and Yarmush, M.L., *Charged Polymers Modulate Retrovirus Transduction via Membrane Charge Neutralization and Virus Aggregation.* Biophysical Journal, 2004. **86**(2): p. 1234-1242.
278. Porter, C.D., Lukacs, K.V., Box, G., Takeuchi, Y., and Collins, M.K.L., *Cationic Liposomes Enhance the Rate of Transduction by a Recombinant Retroviral Vector In Vitro and In Vivo.* Journal of Virology, 1998. **72**(6): p. 4832-4840.
279. Themis, M., Forbes, S.J., Chan, L., Cooper, R.G., Etheridge, C.J., Miller, A.D., Hodgson, H.J.F., and Coutelle, C., *Enhanced in vitro and in vivo gene delivery using cationic agent complexed retrovirus vectors.* Gene Therapy, 1998. **5**: p. 1180-1186.
280. Swaney, W.P., Sorgi, F.L., Bahnson, A.B., and Barranger, J.A., *The effect of cationic liposome pretreatment and centrifugation on retrovirus-mediated gene transfer.* Gene Therapy, 1997. **4**: p. 1379-1386.
281. Porter, C.D., *Rescue of retroviral envelope fusion deficiencies by cationic liposomes.* The Journal of Gene Medicine, 2002. **4**(6): p. 622-633.
282. Jiang, J. and Coombs, K.M., *Infectious entry of reovirus cores into mammalian cells enhanced by transfection.* Journal of Virological Methods, 2005. **128**(1-2): p. 88-92.
283. Mohana Rao, J.K., Bujacz, G., and Wlodawer, A., *Crystal structure of rabbit muscle creatine kinase.* FEBS Letters, 1998. **439**(1–2): p. 133-137.
284. Fasbender, A., Zabner, J., Chillón, M., Moninger, T.O., Puga, A.P., Davidson, B.L., and Welsh, M.J., *Complexes of Adenovirus with Polycationic Polymers and Cationic Lipids Increase the Efficiency of Gene Transfer in Vitro and in Vivo.* Journal of Biological Chemistry, 1997. **272**(10): p. 6479-6489.
285. Howard, C.R., *The Biology of Hepadnaviruses.* Journal of General Virology, 1986. **67**(7): p. 1215-1235.
286. Wang, Q., Lin, T., Johnson, J.E., and Finn, M.G., *Natural Supramolecular Building Blocks: Cysteine-Added Mutants of Cowpea Mosaic Virus.* Chemistry & Biology, 2002. **9**(7): p. 813-819.
287. Milunović, T., Kunstelj, M., Fidler, K., Anderluh, G., and Gaberc Porekar, V., *Coupling purification and on-column PEGylation of tumor necrosis factor alpha analogue.* Analytical Biochemistry, 2012. **430**(2): p. 105-107.
288. Leonhardt, H., Gordon, L., and Livingston, R., *Acid-base equilibriums of fluorescein and 2',7'-dichlorofluorescein in their ground and fluorescent states.* The Journal of Physical Chemistry, 1971. **75**(2): p. 245-249.
289. Hirsch, R.C., Lavine, J.E., Chang, L.-j., Varmus, H.E., and Ganem, D., *Polymerase gene products of hepatitis B viruses are required for genomic RNA packaging as well as for reverse transcription.* Nature, 1990. **344**(6266): p. 552-555.

290. Junker-Niepman, M., Bartenschlager, R., and Schaller, H., *A short cis-acting sequence is required for hepatitis B virus pregenome encapsidation and sufficient for packaging of foreign RNA.* EMBO J, 1990. **9**: p. 3389-3396.
291. Gazina, E.V., Fielding, J.E., Lin, B., and Anderson, D.A., *Core Protein Phosphorylation Modulates Pregenomic RNA Encapsidation to Different Extents in Human and Duck Hepatitis B Viruses.* Journal of virology, 2000. **74**(10): p. 4721-4728.
292. Kann, M. and Gerlich, W.H., *Effect of core protein phosphorylation by protein kinase C on encapsidation of RNA within core particles of hepatitis B virus.* Journal of virology, 1994. **68**(12): p. 7993-8000.
293. Lan, Y.T., Li, J., Liao, W.-y., and Ou, J.-h., *Roles of the Three Major Phosphorylation Sites of Hepatitis B Virus Core Protein in Viral Replication.* Virology, 1999. **259**(2): p. 342-348.
294. Dhason, M.S., Wang, J.C.Y., Hagan, M.F., and Zlotnick, A., *Differential assembly of Hepatitis B Virus core protein on single- and double-stranded nucleic acid suggest the dsDNA-filled core is spring-loaded.* Virology, 2012. **430**(1): p. 20-29.
295. Endres, D., Miyahara, M., Moisant, P., and Zlotnick, A., *A reaction landscape identifies the intermediates critical for self-assembly of virus capsids and other polyhedral structures.* Protein Science, 2005. **14**(6): p. 1518-1525.
296. Smith, D.E., Tans, S.J., Smith, S.B., Grimes, S., Anderson, D.L., and Bustamante, C., *The bacteriophage [phis]29 portal motor can package DNA against a large internal force.* Nature, 2001. **413**(6857): p. 748-752.
297. Evilevitch, A., Lavelle, L., Knobler, C.M., Raspaud, E., and Gelbart, W.M., *Osmotic pressure inhibition of DNA ejection from phage.* Proceedings of the National Academy of Sciences, 2003. **100**(16): p. 9292-9295.
298. Grayson, P., Evilevitch, A., Inamdar, M.M., Purohit, P.K., Gelbart, W.M., Knobler, C.M., and Phillips, R., *The effect of genome length on ejection forces in bacteriophage lambda.* Virology, 2006. **348**(2): p. 430-436.
299. Oren, M.E. and Michael, F.H., *Encapsulation of a polymer by an icosahedral virus.* Physical Biology, 2010. **7**(4): p. 045003.
300. Johnson, J.M., Willits, D.A., Young, M.J., and Zlotnick, A., *Interaction with Capsid Protein Alters RNA Structure and the Pathway for In Vitro Assembly of Cowpea Chlorotic Mottle Virus.* Journal of Molecular Biology, 2004. **335**(2): p. 455-464.
301. Grosberg, A., Izrailev, S., and Nechaev, S., *Phase transition in a heteropolymer chain at a selective interface.* Physical Review E, 1994. **50**(3): p. 1912-1921.
302. Chen, H., Meisburger, S.P., Pabit, S.A., Sutton, J.L., Webb, W.W., and Pollack, L., *Ionic strength-dependent persistence lengths of single-stranded RNA and DNA.* Proceedings of the National Academy of Sciences, 2012. **109**(3): p. 799-804.
303. Macovei, A., Radulescu, C., Lazar, C., Petrescu, S., Durantel, D., Dwek, R.A., Zitzmann, N., and Nichita, N.B., *Hepatitis B Virus Requires Intact Caveolin-1 Function for Productive Infection in HepaRG Cells.* Journal of virology, 2010. **84**(1): p. 243-253.
304. Yan, H., Zhong, G., Xu, G., He, W., Jing, Z., Gao, Z., Huang, Y., Qi, Y., Peng, B., Wang, H., Fu, L., Song, M., Chen, P., Gao, W., Ren, B., Sun, T., Feng, X., Sui, J., and Li, W., *Sodium taurocholate cotransporting polypeptide is a functional receptor for human hepatitis B and D virus.* Elife, 2012. **1**: p. e00049.
305. Köck, J., Borst, E.M., and Schlicht, H.J., *Uptake of duck hepatitis B virus into hepatocytes occurs by endocytosis but does not require passage of the virus through an acidic intracellular compartment.* Journal of virology, 1996. **70**(9): p. 5827-31.
306. Rabe, B., Glebe, D., and Kann, M., *Lipid-mediated introduction of hepatitis B virus capsids into nonsusceptible cells allows highly efficient replication and facilitates the study of early infection events.* Journal of virology, 2006. **80**(11): p. 5465-5473.
307. Rabe, B., Delaleau, M., Bischof, A., Foss, M., Sominskaya, I., Pumpens, P., Cazenave, C., Castroviejo, M., and Kann, M., *Nuclear entry of hepatitis B virus capsids involves*

disintegration to protein dimers followed by nuclear reassociation to capsids. PLoS Pathog, 2009. **5**(8): p. e1000563.
308. Schmitz, A., Foss, M., Zhou, L., Rabe, B., Hoellenriegel, J., Stoeber, M., Panté, N., and Kann, M., *Nucleoporin 153 Arrests the Nuclear Import of Hepatitis B Virus Capsids in the Nuclear Basket.* PLoS Pathog, 2010. **6**(1): p. e1000741.
309. Sahay, G., Querbes, W., Alabi, C., Eltoukhy, A., Sarkar, S., Zurenko, C., Karagiannis, E., Love, K., Chen, D., Zoncu, R., Buganim, Y., Schroeder, A., Langer, R., and Anderson, D.G., *Efficiency of siRNA delivery by lipid nanoparticles is limited by endocytic recycling.* Nat Biotech, 2013. **31**(7): p. 653-658.
310. Coune, P.G., Schneider, B.L., and Aebischer, P., *Parkinson's Disease: Gene Therapies.* Cold Spring Harbor Perspectives in Medicine, 2012. **2**(4).